A Mechanism Based Probe for Visualising Chromatin-modifying Enzyme Lysine-Specific Histone Demethylase 1

Philip Edward Lane

A thesis submitted in partial fulfilment of the requirements of
Sheffield Hallam University
for the degree of Doctor of Philosophy

January 2021

Candidate Declaration

I hereby declare that:

1. I have not been enrolled for another award of the University, or other academic or professional organisation, whilst undertaking my research degree
2. The following material contained in the thesis formed part of a submission for the following award

   Name of award: Doctor of Philosophy

   Awarding Body: University of Sheffield

   Material submitted for that award: Treatment and visualisation of click fluorophor peptide and non-clicked peptide in HCT 116 colorectal cancers.
3. I am aware of and understand the University's policy on plagiarism and certify that this thesis is my own work. The use of all published or other sources of material have been properly and fully acknowledged.

   Some of the data presented in this thesis was obtained in an experiment carried out by the Andrews group in the Centre for Stem Cell Biology, University of Sheffield. I played a major role in the preparation and execution of the experiment, and the data analysis and interpretation are entirely my own work. Any contributions from colleagues in the collaboration, such as diagrams or calibrations, are explicitly attributed in the text.
4. The work undertaken towards the thesis has been conducted in accordance with the SHU Principles of Integrity in Research and the SHU Research Ethics Policy
5. The word count for this thesis is 37950

Name	Mr Philip Edward Lane
Date	January 2021
Award	Doctor of Philosophy
Faculty	Health and Wellbeing
Directors of Studies	Dr Simon M. Turega, Dr Alexander J. Hamilton, Dr Caroline F. Dalton

Abstract

Lysine-specific demethylase 1 (LSD1), the first histone demethylase to be identified, catalyses specifically the demethylation of the mono and dimethyl groups of histone 3 (H3) lysine 4 (K4), and its dysregulation is thought to contribute to the development of cancer. GlaxoSmithKline (GSK) and Oryzon Genomics (ORY) have submitted numerous N-alkylated phenylcyclopropylamine (PCPA) molecules to phase II clinical trials against several different cancers. Eight probes have been designed and synthesised with alkyne and azide tags from PCPA. Their inhibitory values have been investigated towards Monoamine Oxidase (MAO) and LSD1, showing over two times the increase in selectivity towards LSD1. **Probe 1** has been subject to cell treatment and its ability to inhibit LSD1 confirmed using NTERA2 cells. Furthermore, these synthesised probes are conjugated to a peptide to successfully guide the probes into the cell. The addition of the peptide causes an increase in the inhibitory values towards LSD1 by on average seven fold. Chiral separation was undertaken on **probe 7** to explore the potential inhibition differences of the two enantiomers. Single Crystal X-Ray Diffraction analysis and ^{1}H NMR Nuclear Overhauser effect (nOe) confirmed the chiral separation, with inhibitory data showing **(1 *R* – 2 *S*)-probe 7** is a more potent inhibitor of LSD1 than its enantiomer. In addition to this, N-alkylation of **probe 4** achieved a successfully increase of potency towards LSD1 over PCPA. The mechanistic inhibition pathway for PCPA inhibiting LSD1 is currently unknown. Here, DFT is used on cluster models of Flavin Adenine Dinucleotide (FAD) and the active site of LSD1 (135 atoms and 218 atoms) to investigate the mechanistic inhibition pathway for PCPA inhibiting the FAD cofactor. The calculated energy of the potential rate determining step was 45.3 kcal mol^{-1} which is 23.5 kcal mol^{-1} greater than the experimental activation energy for the inhibition of LSD1.

Acknowledgements

Firstly, I would like to express my sincere gratitude to Dr Simon M. Turega, for offering me the opportunity to work in this fascinating, multidisciplined field of research.

I would equally like to thank my fantastic supervisory team, Dr Simon M. Turega, Dr Alexander J. Hamilton, Dr Caroline F. Dalton, for their support, guidance and knowledge during my research, without which I would have been unable to grow and become the diligent researcher I am today.

I would also like to thank Sheffield Hallam University, Vice Chancellors Fellowship for providing funding throughout my PhD.

Finally, I would like to thank everyone who has supported me during my research, but especially my partner, for her continued support, love and patience.

Contents

Table of Figures

Acronyms

AD	Alzheimer's Disease
ADHD	adult attention deficit hyperactivity disorder
AdoHcy	S-adenosyl-L-homocysteine
AdoMet	S-adenosyl-L-Methionine
AL	Acute Leukemia
AML	Acute Myeloid Leukemia
ASD	autism spectrum disorder
CoA	Coenzyme A
CpG	Cytosine – phosphate – Guanine
CuAAC	Cu(I) Catalysed azide-alkyne cycloaddition
DFT	Density Functional Theory
DIPA	diffuse intrinsic pontine glioma
DNMT	DNA methyltransferase
dsDNA	Double Stranded DNA
ESD	Estimated standard deviation
FAD	Flavin Adenine Dinucleotide
F.U.	Fluorescence unit
GGA	Generalized Gradient Approximation
GNAT	Gcn5-related N-acetyltransferases
GSK	GlaxoSmithKline
H2A	Histone 2A
H2B	Histone 2B
H3	Histone 3
H4	Histone 4
H1K26	Histone 1 Lysine 26
H3K4	Histone 3 Lysine 4
H3K9	Histone 3 Lysine 9
H3K27	Histone 3 Lysine 27
H3K36	Histone 3 Lysine 36
H3K79	Histone 3 Lysine 79
H3K4m1	Histone 3 Lysine 4 mono-methylation
H3K4me2	Histone 3 Lysine 4 di-methylation
H3K4me3	Histone 3 Lysine 4 tri-methylation
HAT	Histone acetyltransferase

HDAC	Histone Deacetylase
HMBC	Heteronuclear Multiple Bond Correlation
HPLC	High performance liquid chromatography
ICC	Immunocytochemistry
JMJD	Jumonji domain-containing protein
K4	Lysine 4
LBD	Lewy body dementia
LSD1	Lysine Specific Demethylase 1
MALDI-TOF	Matrix-Assisted Laser Desorption/Ionization-Time Of Flight
MAO	Monoamine Oxidase
MAOA	Monoamine Oxidase A
MAOB	Monoamine Oxidase B
MDS	Myelodysplastic syndromes
MM	Michaelis Menten
MOMCl	Chloromethyl methyl ether
MOM	Methyl methyl ether
MS	multiple sclerosis
mRNA	messenger RNA
NAD+	Nicotinamide Adenine Dinucleotide
NMR	Nuclear Magnetic Resonance
nOe	Nuclear Overhauser effect
ORY	Oryzon Genomins
PCPA	phenylcyclopropylamine
PCET	Proton coupled electron transfer
PK	pharmacokinetics
QM/MM	Quantum Mechanics/Molecular Mechanics
qPCR	quantitative polymerase chain reaction
ROS	reactive oxygen species
SET	Single Electron Transfer

Chapter 1 Introduction

1.1 Introduction

The MAO inhibitor PCPA scaffold has been developed to selectively inhibit FAD cofactor of LSD1. In many diseases, including myeloid leukaemia,[1] and cancers,[1] LSD1 is over expressed,[2] causing changes in the expression of genes that control regulation of cellular functions, this aberration leads to the uncontrolled replication and repair of these cells. Therefore, it is possible to envision that LSD1 inhibition could be used as a therapeutic agent, as well as a tool to reveal the biological functions of enzymes. Histone modifying enzymes have been found to be important in the pathology and treatment of diseases[3] such as cancers,[4] infectious diseases,[5] myeloid Leukaemia,[1] neurological diseases[6] and play a key role in the pluripotent stem cell renewal cycle.[7–9] The MAO inhibitor, PCPA was one of the first identified drugs for the inhibition of LSD1, from this, NCL-1 was developed as the first cell active LSD1 inhibitor,[10,11] which has been shown to cause the accumulation of the H3K4me2 epigenetic mark and repress cancer cell growth.[12]

1.2 Histone Modifications

The human genome must accomplish multiple functions with two main roles. Specifically; Compaction of 3 billion bp genomes into the nucleus, and the regulation of the physical accessibility for gene transcription, repair and replication. This enables the DNA to be transcribed to messenger RNA (mRNA), this is decoded to produce specific amino acid chains, which fold into active protein.[13,14]

The chromatin complex is wrapped between double stranded DNA (dsDNA) which forms the nucleosome which is composed of around 148 base pairs of dsDNA.[15] The nucleosome complex includes two copies each of protein from the histone classes, H2A, H2B, H3, H4, which forms the histone core of the nucleosome. The histone core is folded into heterodimer pairs, H2A/H2B and H3/H4.[16] The bulk of the histone post translational modifications are upon the histone tails that protrude from then central histone core, with H2A, H2B being the C-terminals, and the H3, H4 being the N-terminals of each histone (**Figure.1**).[17]

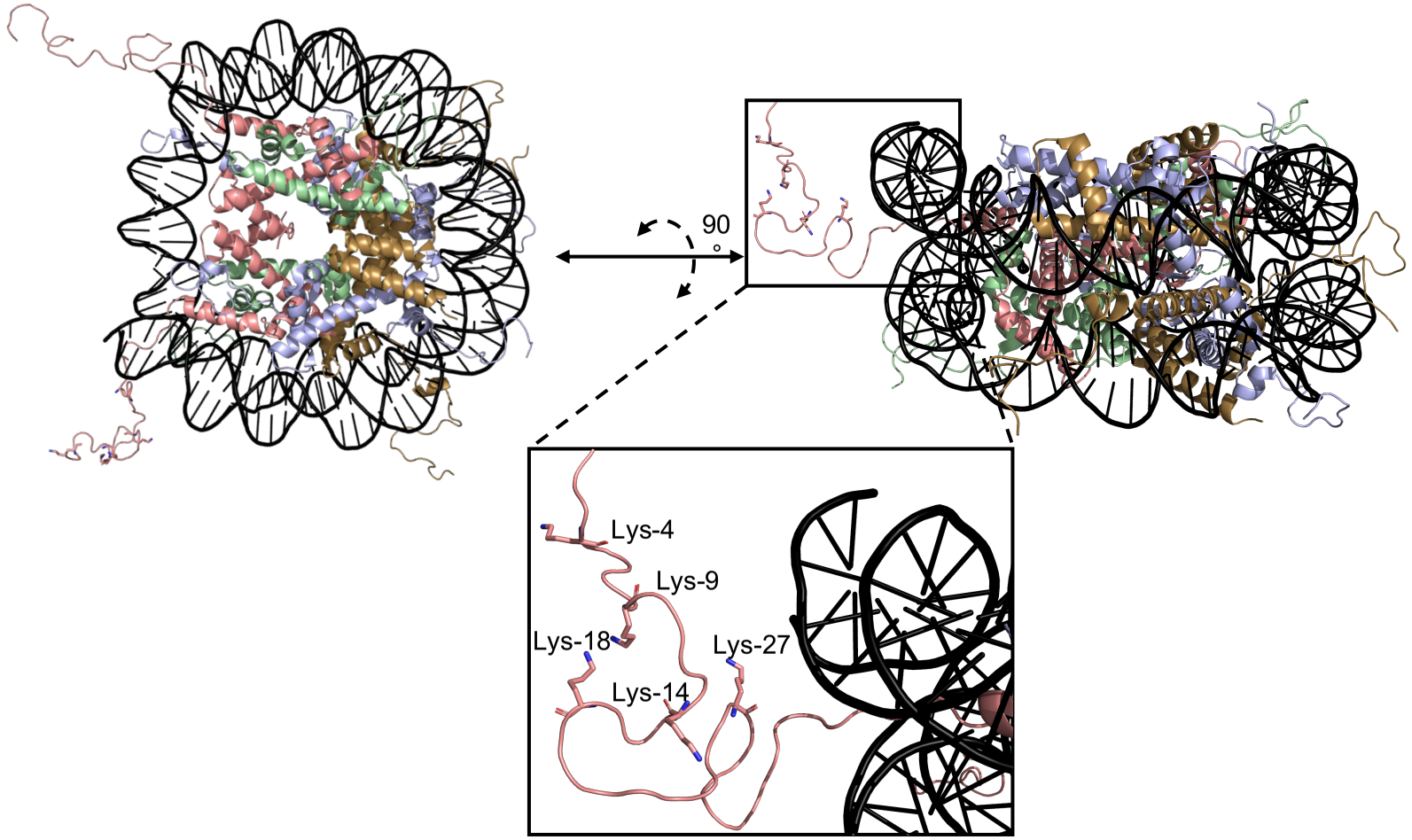

Figure.1 Chromatin crystal structure (PDB code 1AOI). The DNA coil is represented by black ribbon. The H2A core protein is represented by light-blue cartoon. The H2B core protein is represented by sand cartoon. The H4 core protein is represented by pale-green cartoon. The H3 core protein is represented by salmon cartoon, with Lysine 4 (Lys-4), Lysine 9 (Lys-9), Lysine 14 (Lys-14), Lysine 18 (Lys-18) and Lysine 27 (Lys-27) shown as salmon sticks with blue (nitrogen) and red (oxygen).[166]

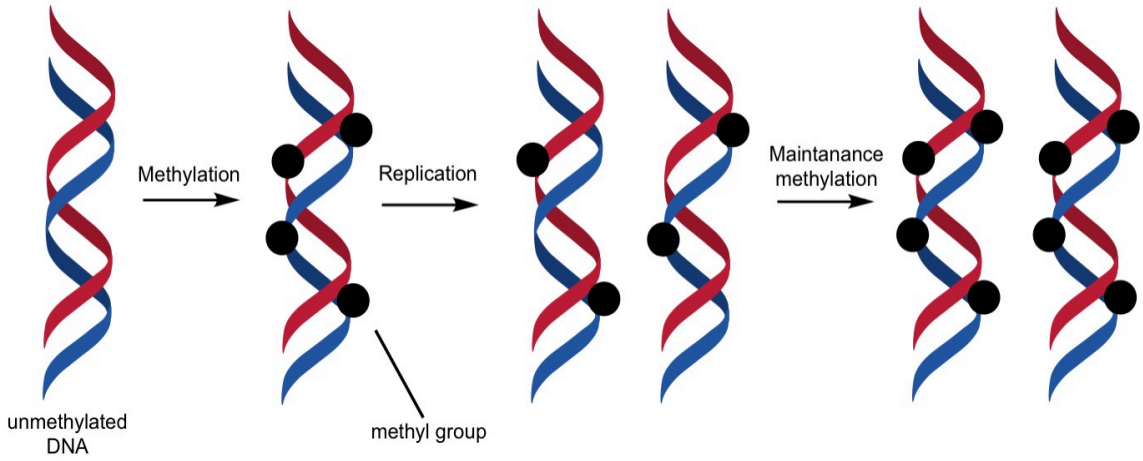

Figure.2 Schematic representation of methylation and maintenance methylation of DNA.

The chromatin structure is modified by methylation to allow proteins and complexes to bind and interact with the DNA enabling transcription, repair[18] and replication (**Figure.2**).[14,19]

Eukaryotic chromatin is in equilibrium between two distinct structures: heterochromatin and euchromatin. Heterochromatin is a tightly packed chromatin structure, which is transcriptionally silent. In contrast, euchromatin is a less condensed structure, which is transcriptionally active. Acetylation of the N-terminal histone tails enables the equilibrium to shift towards the euchromatin structure, increasing the ability for chromatin modifications by the enzymes to allow transcription, repair and replication to occur.[20–22]

1.2.1 Epigenetic markers for the covalent modifications of chromatin that influence gene regulation

An overall representation of the histone covalent modifications that will be discussed in depth is shown in **Figure.3a**. Post translation modifications to the chromatin on structures shown in **Figure.3b,** such as acetylation and methylation can alter the cell to be either translationally active, or silent. Methylation of lysine residues in histone proteins is a post-translation modification that occurs on various histone sites, H1K26, H3K4, H3K9, H3K27, H3K36, H3K79 and H3K27, these have been shown to demonstrate transcriptional activation or silencing.[23] For example, H3K4 is associated with actively transcribing gene loci, whereas methylation at H3K9 and H3K27 leads to transcriptional silencing.[24] Methylation can also occur on arginine residues on the histone.[25]

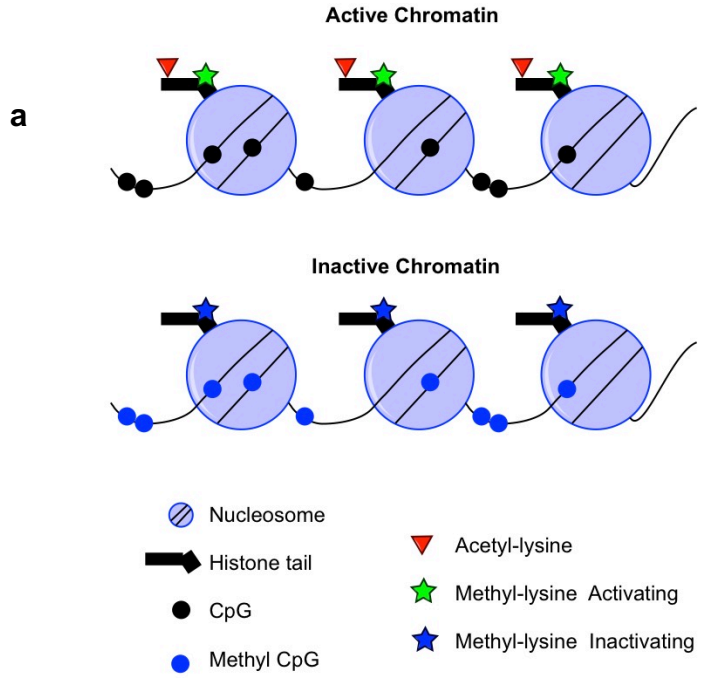

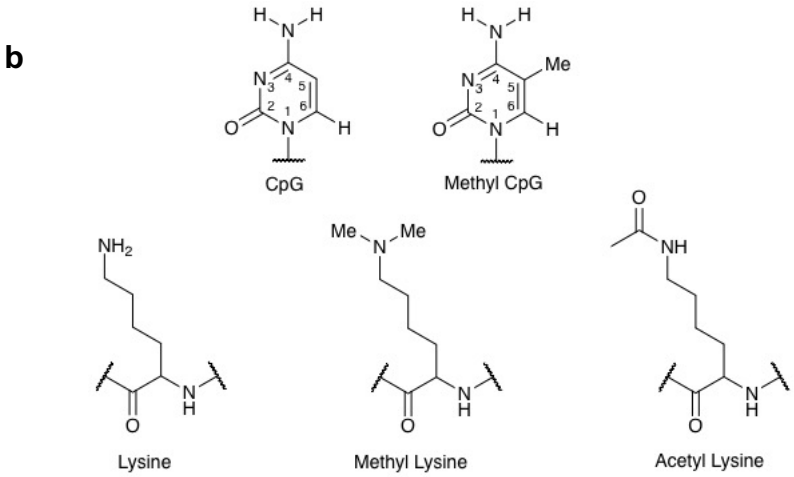

Figure.3a. Epigenetic markers that initiate covalent modifications to direct gene regulation on the chromatin **b.** Structural representation of chromatin modification that direct gene regulation

1.2.2 Cytosine methylation

The methylation of cytosine in Cytosine – phosphate – Guanine (CpG) nucleotide motifs is catalysed by DNA methyltransferase (DNMT) the carbon on position no. 5 of the cytosine is not particularly nucleophilic requiring the energy barrier for the reaction to be lowered by the enzyme.[26,27] In the CpG methylation mechanism described in **Figure.4**, the cysteine thiolate attacks the 6 carbon of the cytosine in a conjugate addition reaction, forming a covalent bond. This addition is then balanced by the rearrangement of electronic structure, stabilized by protonation

of the 3-nitrogen by a glutamate residue. The glutamate then regains its proton, allowing the nucleophilic attack on the methyl of the AdoMet, converting this to AdoHcy and methylating the 5-carbon position. The reaction is completed by a β-elimination, losing a proton and the cysteine enzyme, forming a carbon-carbon double bond.

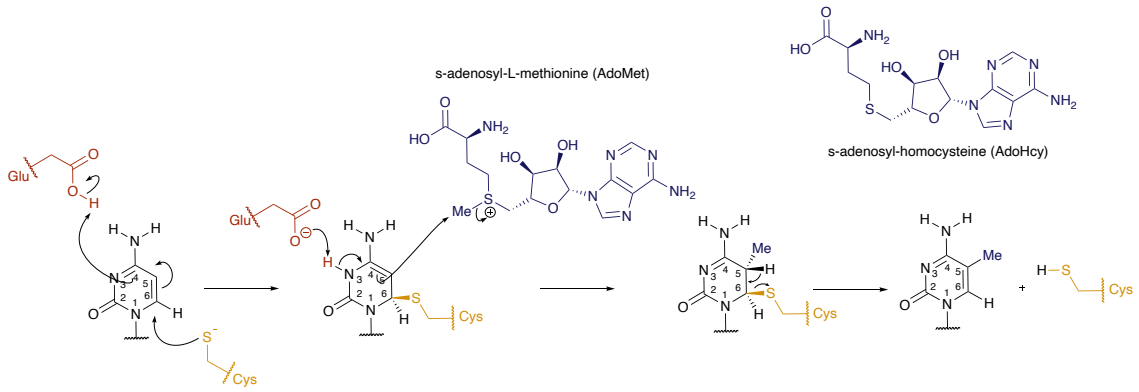

Figure.4 Mechanism of the methylation of cytosine in DNA, catalysed by DNA methyltransferases

1.2.3 Histone Acetylation

In the mechanism of the acetylation (**Figure.5**), the glutamate acts as a base, activating the lysine amino group for a nucleophilic attack onto the carbonyl of the Coenzyme A (CoA) forming a tetrahedral intermediate.[28] This is eliminated, reforming the carbonyl group and losing the CoA species leaving the acetylated lysine residue. This is the general mechanism for the acetylation of the histone residue that occurs in the human genome. There are different families of enzymes that undertake this process, The Gcn5-related N-acetyltransferase (GNAT) occurs in humans, whereas MYST and Rtt109 occur in yeast.[29–31] Further to the acetylation, there are changes to the structure of the chromatin (as previously described) enabling other histone modifications to be undertaken.

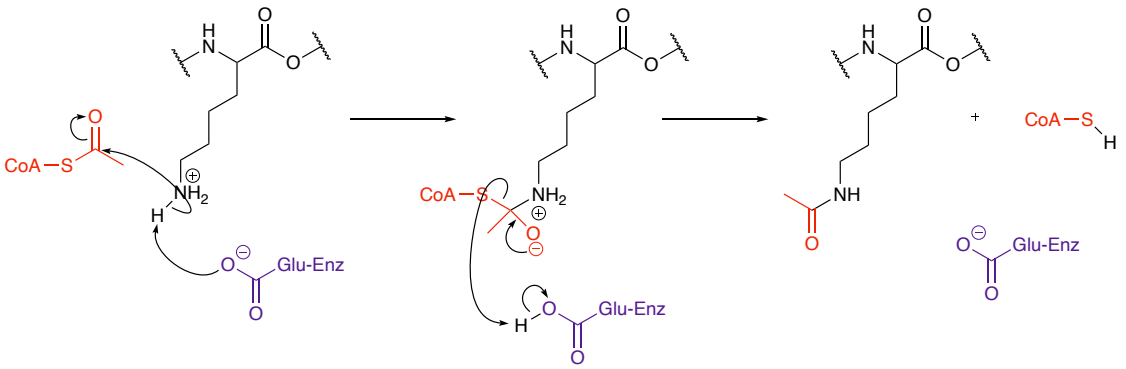

Figure.5 Mechanism for the acetylation of the Histone Lysine residue

1.2.4 Histone deacetylation

The acetyl group can be removed by histone deacetylase (HDACs) enzymes. There are 4 types of this enzyme. Type I, II, IV use Zn^{2+} dependent active sites for their mechanism (**Figure.6**)[32–34] and are usually found in the nucleus and cytoplasm, whereas Type III uses a nicotinamide adenine dinucleotide (NAD+) dependent catalytic mechanism (**Figure.7**) and is usually found in the nucleus, cytoplasm and mitchondria.[35,36]

1.2.4.1 Mechanism I

For the Zn^{2+} dependent enzymes (**Figure.6**), the reaction requires the nucleophilic attack of water on the carbonyl of the acetyl. Histidine acts as a base, taking a proton from the water. This then attacks the acetyl carbonyl which is activated through hydrogen bonding to the HDAC Zn^{2+} cofactor tyrosine residue. This forms an intermediate tetrahedral species, where the anionic oxygen reforms a carbonyl compound eliminating itself from the lysine residue, which takes a proton from the histidine, reforming its neutral charged state and acetate as a side product.[36–38]

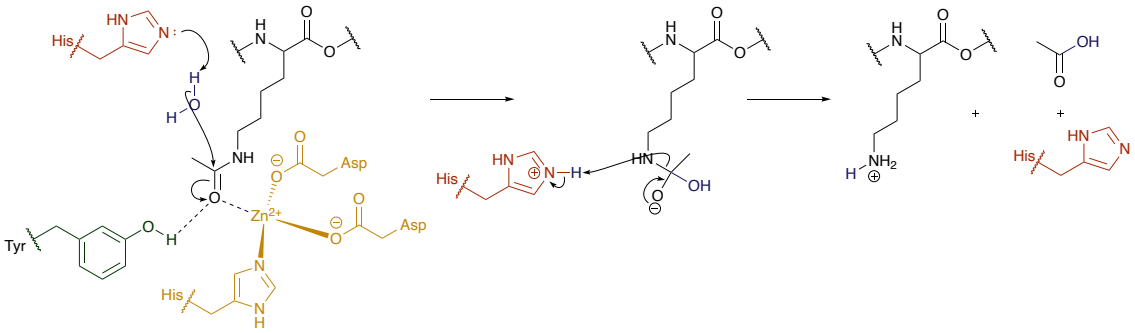

Figure.6 Mechanism for the de-acetylation of histone lysine residue using I, II, IV classes for HDAC's

1.2.4.2 Mechanism II

In these enzymes the carbonyl of the acetyl is activated by covalently bonding to the acetyl, rather than complexing with it. The formation of the positive nitrogen is driven by the NAD+, with the acetyl carbonyl π bond breaking and its electrons attacking the NAD+, releasing the nicotinamide from it (**Figure.7**). Histidine is used as a base, allowing the O-alkylamidate intermediate to cyclize forming a cyclic intermediate.

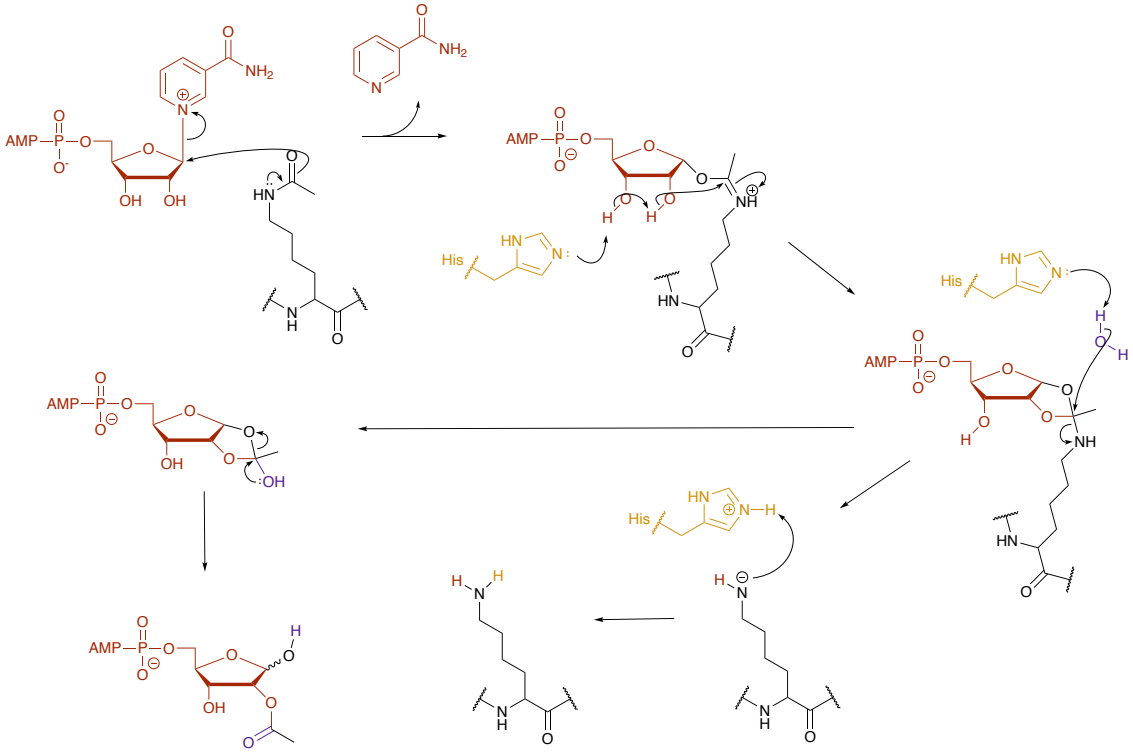

Figure.7 Mechanism for the de-acetylation of histone lysine residues using III class HDAC

Water acts as a nucleophile to attack the tetrahedral carbon, releasing the de-acetylated histone lysine residue, leaving an acetylated cofactor.[39–41]

Less than 20 years ago was the first discovery of histone modifying enzymes, with histone acetyltransferase (HAT) being the first.[42] This HAT catalyses the acetylation of the ε-amine of the histone lysine unit.[28]

Subsequent histone modifying enzymes have been discovered; histone phosphorylation enzymes,[18] and the most researched translational enzymes, histone methylation (which was identified in 2003)[23], demethylation enzymes (lysine specific demethylase 1 (LSD1)[43,44] and Jumonji domain-containing protein (JMJD)[45,46]).[47,48]

1.2.5 Histone Methylation

Histone methyltransferase (HMT) catalyses the methylation of these units from, H3K4 to, mono-methylated species, di-methylated species and tri-methylated species (H3K4me, H3K4me2 and H3K4me3) (**Scheme.1**).[49]

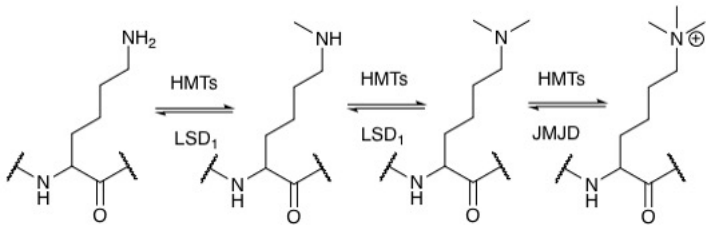

Scheme.1 Methylation and demethylation of lysine residues using chromatin modifying enzymes

The methylation of the lysine residues uses the same AdoMet cofactor as DNA methylation, and proceeds through the mechanism in (**Figure.8**). The nitrogen lone pair attacks the methyl group of the AdoMet, transferring a methyl group to the its positive charge to the lysine forming a positively charged quaternary ammonium group resulting in AdoMet converting to AdoHcy.[50,51]

It was originally thought that these mono, di and tri-methylated lysine units were unable to be de-methylated,[52,53] until in 2004, when two classes of enzymes were discovered for the demethylation of methylated lysine residues. The first class of demethylase was Lysine specific demethylase 1 (LSD1), which demethylates the mono and di methylated lysine units though a flavin adenine dinucleotide (FAD)-dependent Monoamine Oxidase (MAO) domain.[43] The second class is the Jumonji C domain (JMJD) demethylase which has a catalytic Fe^{2+} cofactor at its active site.

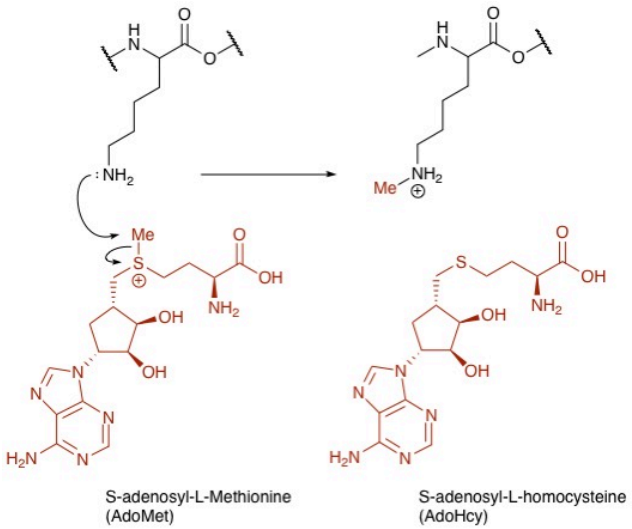

Figure.8 Mechanism for the methylation of histone lysine residues.

1.2.6 Histone Demethylation

1.2.6.1 Mechanism I (LSD)

LSD1 cleaves methyl groups from mono and di-methylated lysine residues through a catalytic oxidative reaction using the FAD cofactor.[54–57] The methyl group is converted to an iminium cation, through a two single electron oxidation by the FAD co-factor. Next the addition of water to the cation forms an intermediate, which spontaneously reacts to form formaldehyde and a histone lysine unit with one less methyl group.

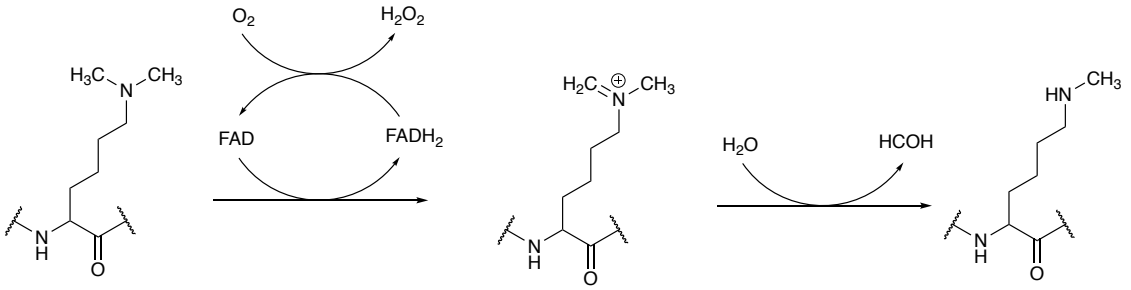

Scheme.2 Coupled oxidative mechanism for the demethylation of the lysine residue through the FAD Cofactor

The $FADH_2$ generated in the first stage, is oxidised by O_2 to form the original catalytic FAD molecule. With the regeneration of the FAD catalyst, the O_2 is converted to hydrogen peroxide as a side product (**Scheme.2**).[58,59]

1.2.6.2 Mechanism II (JMJD)

The second class of demethylation enzymes are the Jumonji C domain-containing proteins (JMJD) which demethylate the tri-methylated lysine unit through a α-ketoglutarate and Fe^{2+} complex.[60] The mechanism by which demethylation occurs by the JMJD enzyme, (**Figure.9**) commences through the complexation of the α-ketoglutarate with the Fe^{2+} complex, this then binds the tri-methyled lysine residue, releasing 3 H_2O molecules from its original structure. A single electron is transferred from the oxygen to the Fe metal atom, reducing to Fe^{3+}, simultaneously forming an oxygen radical. The Fe is further reduced forming a Fe^{4+} and superoxide species.

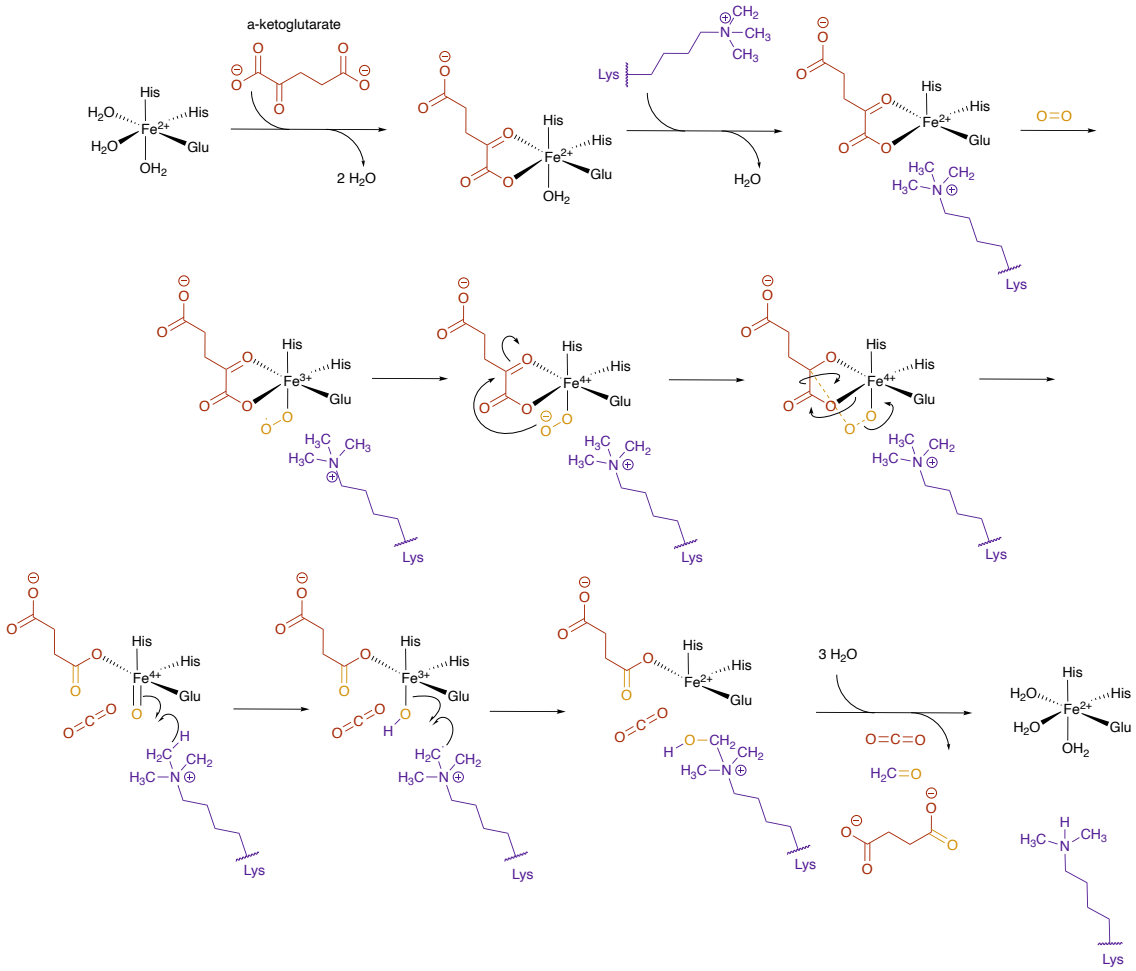

Figure.9 Mechanism for the demethylation of trimethylated histone lysine residue through JMJD

The superoxide acts as a nucleophile and attacks the second carbonyl of the α-ketoglutarate, causing de-carboxylation of the α-ketoglutarate, forming carbon dioxide, $Fe^{4+}O$ species and succinate. This $Fe^{4+}O$ extracts a hydrogen atom from the methylated lysine, oxidating the Fe to $Fe^{3+}OH$ species, and forming a radical upon the carbon on the methylene. The radical reaction between the $Fe^{3+}OH$ and methylene species forms a temporary hemiaminal intermediate which spontaneously forms formaldehyde and the dimethylated lysine residue, the Fe^{3+} is oxidised to its original Fe^{2+} form and with the addition of what the catalyst is reformed, forming side products of carbon dioxide and succinate.[61–64]

1.3 LSD1 inhibition Theory

1.3.1 LSD & Flavin Adenine Dinucleotide (FAD) Cofactor domain

LSD1 enzyme (**Figure.10**) is comprised of a central catalytic MAO domain (in Red in the **Figure.10**), which is shared with the MAO family. This contains the FAD cofactor which catalyses the removal of methyl groups. Connected to the MAO domain are; SWIRM domain (Purple), Tower domain (Green), and CoREST linker (Blue). To the CoREST linker is connected SANT2 (Orange).[65]

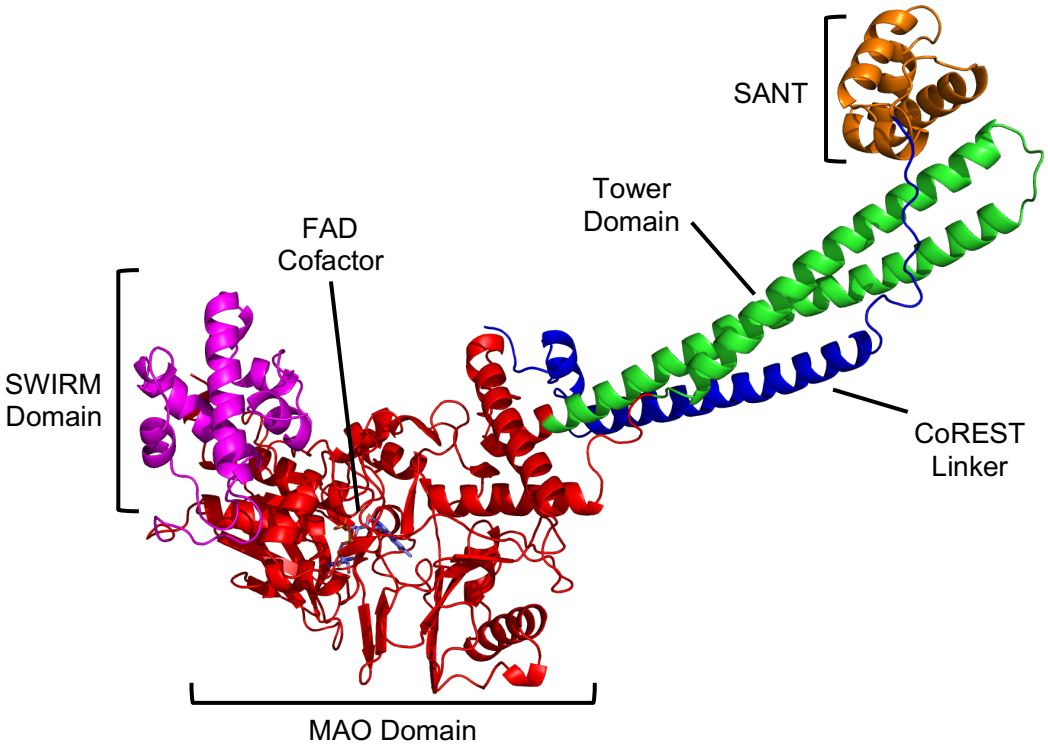

Figure.10 LSD1 crystal structure interaction with CoREST (PDB code 5L3D). The FAD Cofactor is shown as light blue sticks while the substrate is represented as blue (nitrogen), red (oxygen) and orange (phosphorus). The MAO Domain is represented by red cartoon. The SWIRM Domain is represented by magenta cartoon. The SANT2 is represented by orange cartoon. The CoREST Linker is represented by blue cartoon. The Tower Domain is represented by green cartoon.

These additional domains are not essential for the removal of the methyl groups. However, they make it more efficient for the MAO domain to interact with the histone core complex, by clamping onto the chromosome enabling the MAO domain to remove the methyl groups.[66]

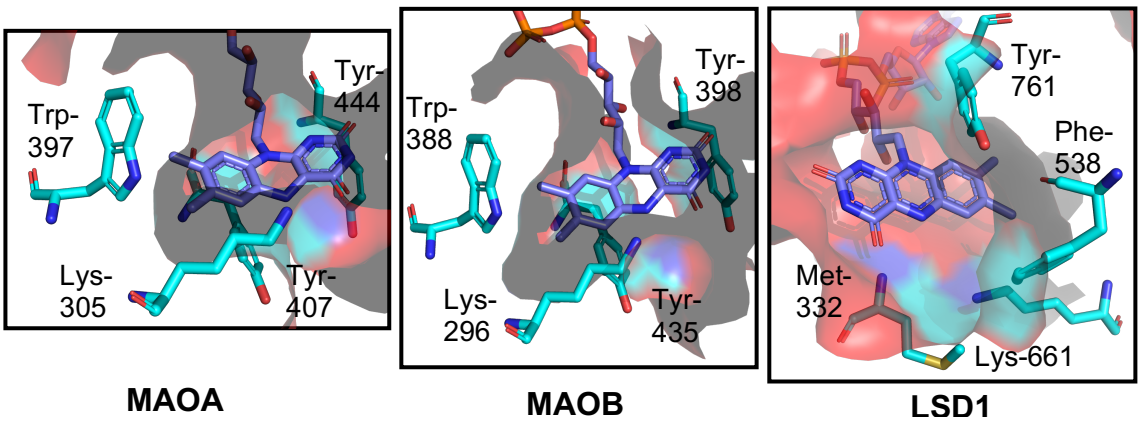

Figure.11 Crystal Structures for MAO domain containing enzymes, **MAOA** (PDB code 2Z5Y), **MAOB** (PDB code 1GOS), **LSD1** (PDB code 2HKO). The surface of the active site is shown to 40% transparency. The FAD cofactor is shown as purple sticks with blue (nitrogen), red (oxygen) and orange (phosphorus). Individual amino acid restudies are highlighted as light blue sticks with blue (nitrogen) and red (oxygen). **MAOA**: Trp-397, Tyr-444, Lys-305, Tyr-407. **MAOB**: Trp-388, Tyr-398, Lys-305, Tyr 435. **LSD1**: Tyr-761, Phe-538, Lys-661, Met332.

Comparison of the active sites of the different MAO enzymes[67–69] **Figure.11** shows the structural differences between MAOs enzymes and LSD1. This is highlighted by the active pocket surface and situation of individual amino acid residues. For the MAO, the amino acids highlighted are in a similar position around the FAD cofactor, with the pocket being compact, as these interact with small molecules (dopamine, serotonin, phenylethylamine). LSD1 is the reverse of this, containing a large opening to interact with the H3 core protein, with additional space (**Figure.12**) which MAOs are lacking.[10,55,56,70]

This space has been exploited by drug companies to synthesise molecules which are highly selective towards LSD1.

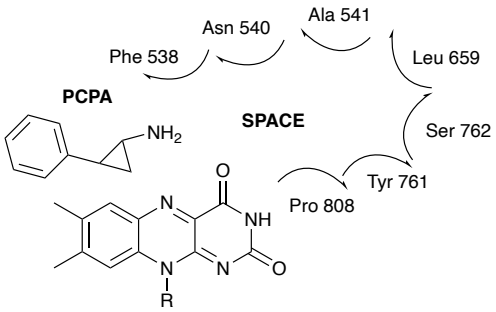

Figure.12 Identification of free “space” for developing PCPAs selectivity towards LSD1

LSD1 contains the MAO domain and shares the same FAD cofactor as MAOA/B. Therefore, proposed MAO inhibitors that could inhibit LSD1. Phenelzine **1**, Pargyline **2** and trans-2-phenylcyclopropylamine (PCPA) **3** have all been tested with **3** being intensively researched (**Figure.13**), due to its irreversible covalent binding to the FAD cofactor (See section 1.3.2.2), based on kinetics and MS.[71] The inhibition of LSD1 by PCPA is covered in section 1.3.2.2.

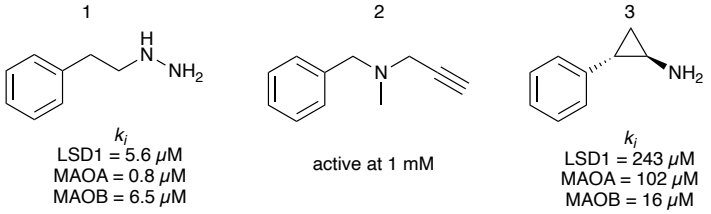

Figure.13 Initial MAO inhibitor used to inhibit LSD1. **1** Phenelzine, **2** Pargyline, **3** PCPA

1.3.2 LSD1 theoretical inhibition by PCPA

1.3.2.1 Proposed reaction mechanisms for MAO catalytic cycle

MAO catalyses the first stage in the oxidative deamination of primary and secondary amines (**Scheme.2**). Three different mechanisms have been proposed[72,73] **Scheme.3a**. a Single Electron Transfer (SET) mechanism, where the hydrogen is transferred as a neutral hydrogen, **Scheme.3b**. the hydrogen is transferred as a hydride (H^-), **Scheme.3c**. a polar nucleophilic mechanism, where the lone pair of electrons on the amine group is transferred to the FAD and the hydrogen is transferred as a proton (H^+).

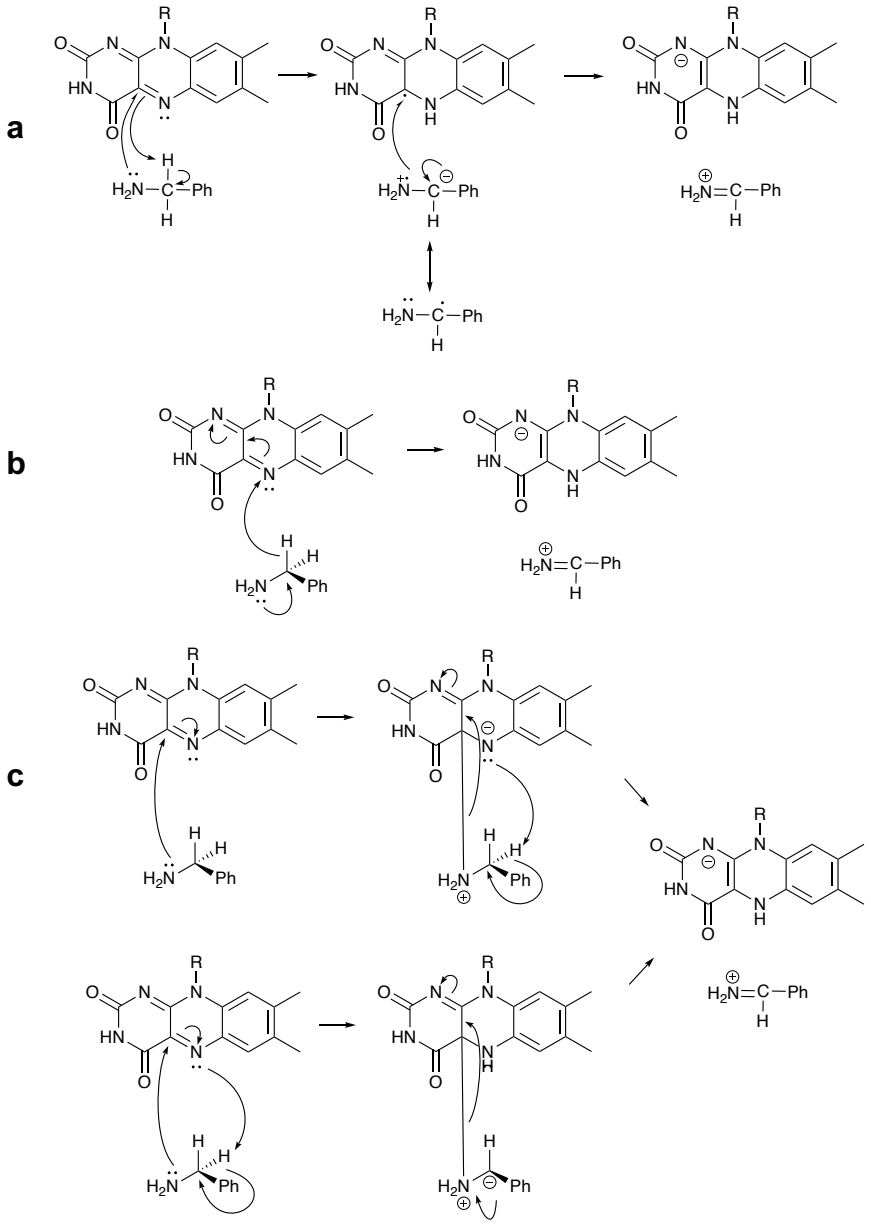

Scheme.3 Proposed Reaction mechanisms for MAO Domain. **a.** SET mechanism, **b.** hydride mechanism**, c.** polar nucleophilic mechanism.

1.3.2.2 Proposed Mechanism for LSD1 inhibition by PCPA

LSD1 inhibition by **PCPA** (**Figure.10**) occurs by the formation of a covalent adduct with the flavin ring. Three possible inhibition products have been theorised based on their crystal structures. One structure is the formation of a five-member ring,[58] which can be followed by the removal of water, forming a double bond. Two other products are linear chains where the steric hindrance of **3** causes different products to be formed. With (*1 R - 2 S*)-**3** forming N(5) product **A**, whereas (*1 S – 2 R*)-**3** forms N(5) product **B** (**Figure.14**).[74] There is some speculation as to how PCPA inhibits FAD, with 2 different theoretical methods; SET and Hydride Mechanisms.

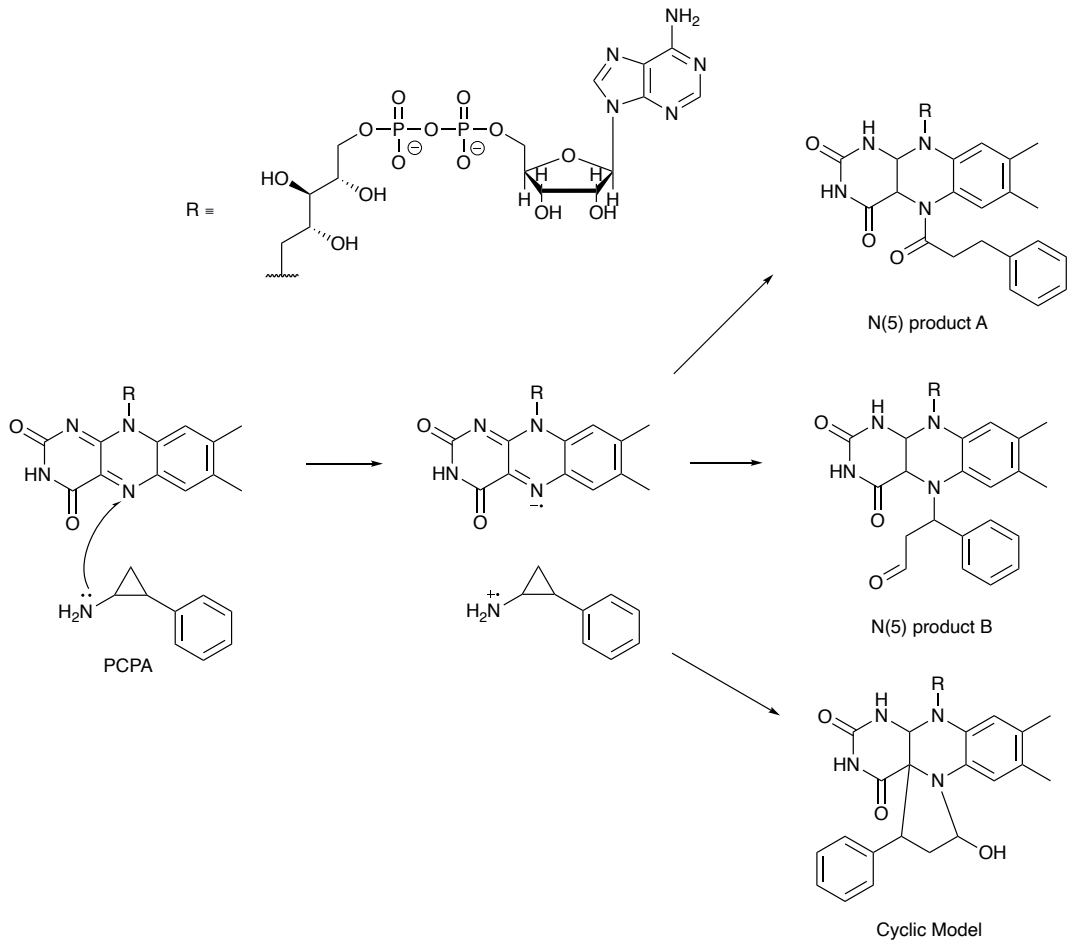

Figure.14 Covalent inhibition of FAD through PCPA, N(5) product A (PDB code 2AXJ), N(5) product B (PDB code 2XAH), Five-membered ring product (PDB code 2Z5U)

1.4 PCPA Synthesis

1.4.1.1 General Synthesis

The PCPA core has been widely developed for inhibitors of LSD1 with substitution on the *meta* and *para* positions of the ring[75,10,11,76] and N-alkylation[77] producing novel inhibition of the FAD cofactor in the LSD1 enzyme.

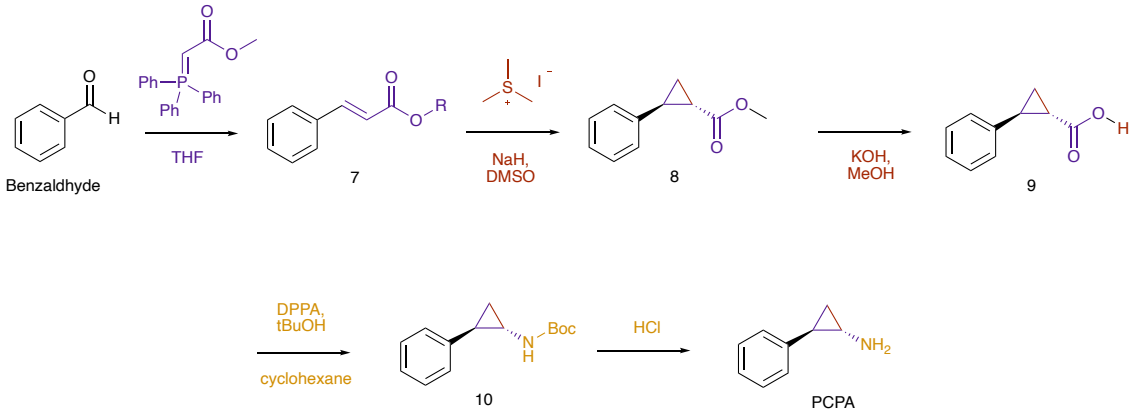

Scheme.4 General syntheses for PCPA through a Wittig reaction, Corey Chaykovsky, and Curtis rearrangement reaction.

A synthetic route for PCPA proceeds through the synthetic route shown in **Scheme.4**. Starting with benzaldehyde, this is reacted through the Wittig reaction to afford compound **7**. The cyclopropane is then formed using the Corey Chaykovsky reaction to give compound **8**.[78] This reaction in general produces poor yields ranging between 18% and 30%. Furthermore, starting with only *trans alkene* **7 t**his reaction pathway produces only two desired isomers, whereas using a racemic mixture of alkene 7, produces four isomers of the PCPA. This cyclopropane is de-protected to produce compound **9**. Finally, ending with the Curtis Rearrangement to receive the protection amine PCPA **(10)**, which is de-protected to give the PCPA through a five step wise synthesis mechanism.[11,76]

1.4.1.2 Enzyme Synthesis of olefin cyclopropanation

As previously stated, the Corey Chaykovsky reaction is not stereo selective, and produces a racemic mixture of enantiomers. As a result, enzymatic synthesis of cyclopropanes from olefins have been explored with the aim of synthesising enantiomer specific cyclopropanes[79] (**Scheme.5**), with **13**, **14** being *trans* enantiomers, and **15**, **16** *cis* enantiomers. Frances H. Arnold developed P450 enzymes to synthesise specific isomers of cyclopropanes.[79] Styrene (**11**) is

reacted with ethyl 2-diazoacetate (EDA) (**12**) to form cyclopropanes **13** – **16**. Hemin, iron based porphyrin, was used as reference catalysed for synthesising the cyclopropane, and resulted in predominantly *trans* enantiomers **13**, **14** with no selectivity between the two. $P450_{BM3}$ – T268A successfully synthesised 99% *trans* isomer, with 96% selectivity preference for **14**. Notably, this enzyme produced the highest yield of cyclopropane. Further to this, $P450_{BM3\text{-}cis}$ synthesised predominately *cis* isomers (71%) with a preference towards **15** of 94%. This enzyme underwent a mutation, T438S, which increased *cis* isomer formation to 92%, and slightly increased the selectivity towards **15** to 97%.

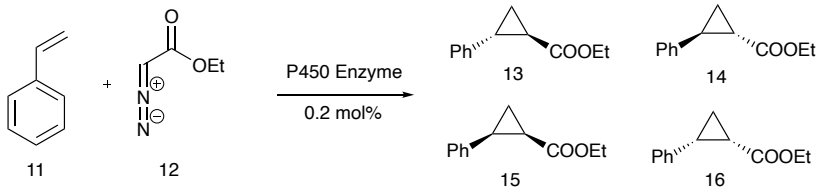

Scheme.5 Stereo specific synthesis of cyclopropanes from olefins using various P450 enzymes.

1.5 LSD1 Inhibition

1.5.1 Development of LSD1 inhibition from PCPA

The PCPA core molecule (FDA approved drug tranylcypromine) is not selective towards LSD1 having a K_i of 243 μM and MAOA and MAOB with values of 102 and 16 μM respectively. The development of PCPA derivatives with a high selectivity for LSD1 over the other MAO enzymes is necessary for reducing off-target effects of the PCPA core molecule.[71] The PCPA core has already been developed to become more selective towards the LSD1 enzyme. Inhibitors that expand on the PCPA core with substituents in the *meta* and *para* carbon position of the phenyl ring, **19** (NCL-1) and **20** (NCL-2) show increased selectivity from 400-11000 times greater than PCPA.[76] The compounds have been designed based upon the three dimensional coordinates from crystal data, mimicking the histone proteins affinity for the LSD1 active site. Inhibitors **19** and **20** were the first cell active LSD1 selective inhibitors. It is also reported that **(*1 S – 2 R*)-19** is approximately four time more potent than **(*1 R - 2 S*)-19**.

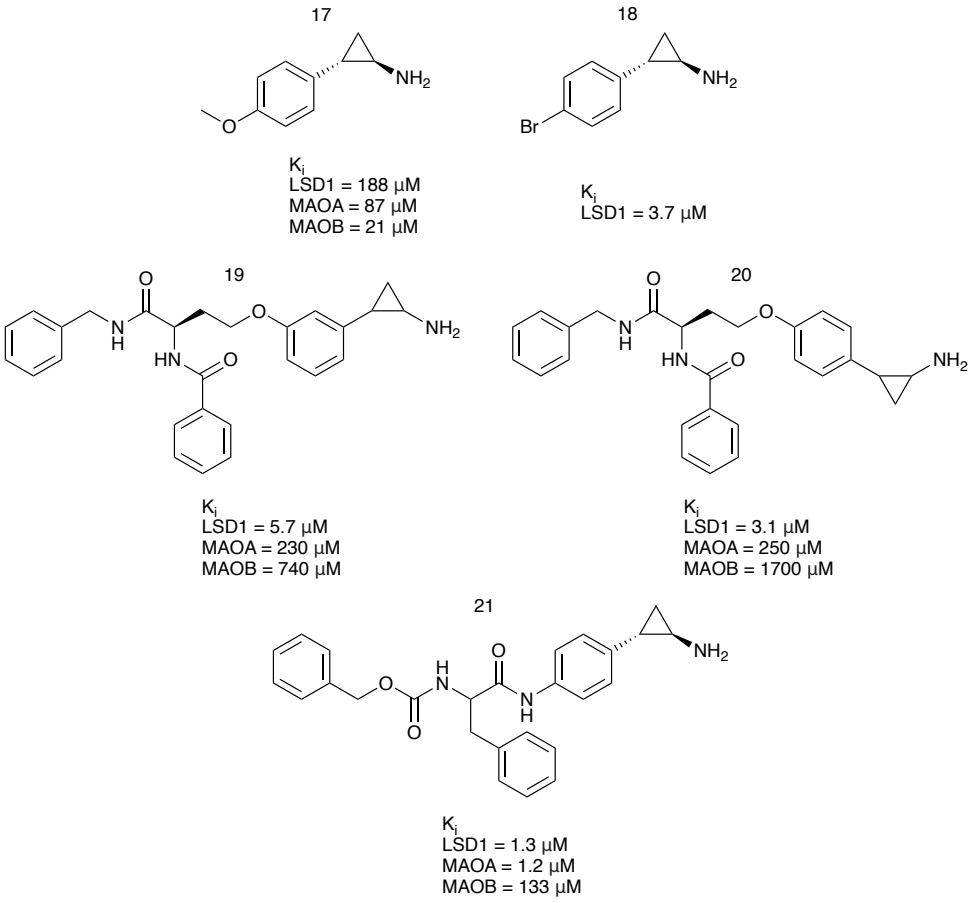

Figure.15 PCPA development by mimicking H3 bulk motif **17 – 21**

In the racemic mixture of these, they have been reported to inhibit cell growth at *6 – 67 μM* in human cancer cells lines, which distinctly changes in total accumulation of H3K4me2 which was detected by calculation of GI_{50} for each cell line.[11,80] Additionally, **19** and **20** showed positive response for anti-proliferation activities against, prostate cancer breast cancer, and glioma. Compound **21** (**Figure. 16**) shows increased selectivity for LSD1 and MAOA over MAOB and LSD2. This caused cell growth inhibition and acted synergistically with retinoic acid in a cellular model of acute promyelocytic leukemia.[81]

1.5.2 Hybrid LSD1 inhibitors

1.5.2.1 LSD1 – JMJD inhibitor

Substitution of the *para* position on the phenyl has produced inhibitors **22** and **23** (**Figure.16**). These target both LSD1 and JMJD class demethylase enzymes with IC_{50} values of 2.2 and 1.0 μM respectively, showing increased selectivity of 15 – 85 times that of PCPA. These appear less selective for LSD1 than **19** and **20**. However, they are able to inhibit both LSD1 and JMJD enzymes. Compounds **22** and **23** were tested in colon and prostate cancer cells *10 - 100 uM* and compared to PCPA, showing simultaneous increase in the methylated histone lysine by immunofluorescence-based assay.[75,82]

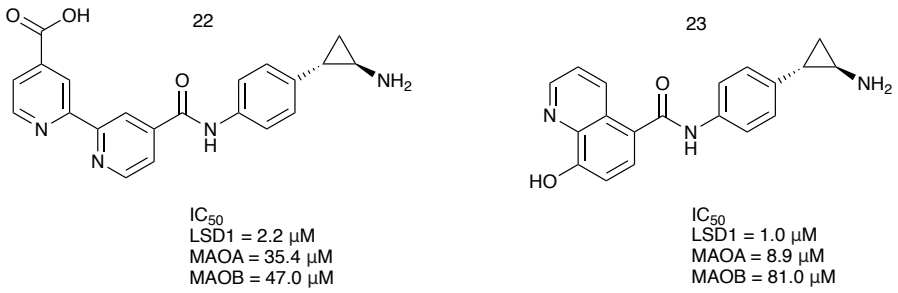

Figure.16 Hybrid LSD1 and JMJD inhibitors

1.5.2.2 LSD1-HDAC inhibitor

Substitution of Entinostat to the *para* position of the phenyl ring forms **24** (Corin), N-alkylation of PCPA with Vorinostat forms **25** (**Figure.17**). These both target LSD1 and HDAC, with **24** a potent inhibitor of HDAC1 (IC_{50} = 42.5 nM) and **25**, a potent inhibitor towards HDAC1 and HDAC2 with IC_{50} = 15 nM and 23 nM respectively. These are more selective towards inhibiting LSD1, **19** and **20,** by 1.5 to 5.5 times greater selectivity. Furthermore, **24** showed anti-proliferation

properties towards melanoma and cutaneous squamous cell carcinoma cell lines. Equally, **24** has shown that co-inhibition of LSD1 and HDAC decreases diffuse intrinsic pontine glioma (DIPA) by promoting cell death, differentiation which suppresses the cell cycle.[83,84]

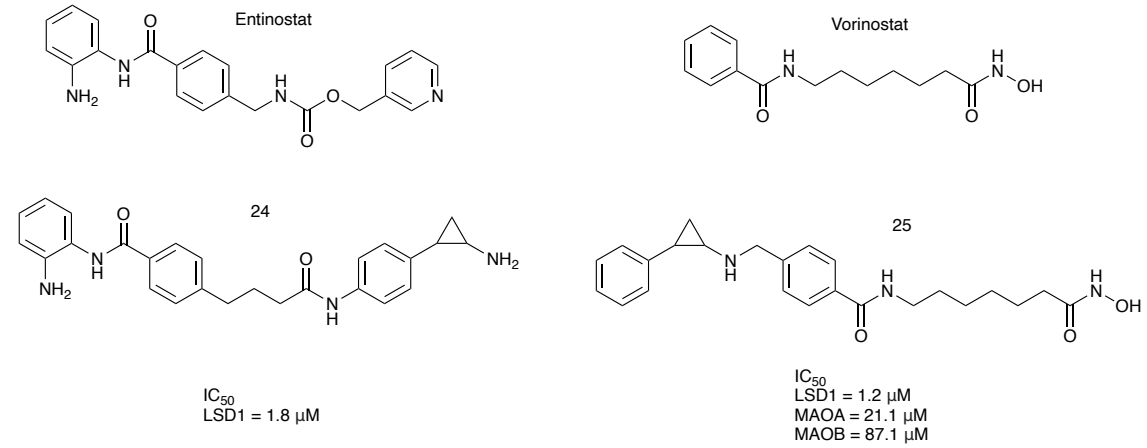

Figure.17 Hybrid LSD1 and HDAC inhibitor

1.5.3 N-Alkylation of PCPA for LSD1 inhibition

To further mimic the protein recognition of the histone substrate in LSD1, the desired selectivity can be obtained through N-alkylation (**Figure.18**) of the PCPA core. This increase in selectivity uses a volume of free space in the substrate binding pocket. **19** (**Figure.15**) is N-alkylated to form **26** to further increase the selectivity of **19** towards LSD1 by ~14 fold. However, unlike **19**, the increased polarity of the compound caused inactivity in SH-SY5Y cells due to poor membrane permeability.[10] The pharmaceutical industry, specifically Oryzon Genomics, GSK and Imago Bio-scientific have molecules in the pipeline that target LSD1 protected by patents. The lead molecule **GSK-LSD** has a reported 1000 fold selectivity towards LSD1 over MAOA/B.[85] This proceeded to the development of compound **GSK2879552**, which was submitted for phase I clinical trials against acute myeloid leukemia (AML)[86] (NCT02177812), and relapsed/refractory SCLC (NCT02034123), and phase I/II clinical trials against high risk Myelodysplastic syndromes (MDS) coupled with azacitidine (NCT02929498). Unfortunately, these trials were aborted because negative outcomes during the trials, most commonly thrombocytopenia, however more seriously, encephalopathy, which resulted in a number of deaths. Oryzon Genomics took a similar approach to GSK with N-alkylation to accommodate the free space, and synthesised **ORY-1001** (Iadaemstat) which shows inhibitory

activity over 1000 more selective towards LSD1 (IC_{50} = 18 nM) than MAOA and MAOB.[87,88] It is in phase I clinical trials for treatments for small cell lung cancer and phase IIa for treatment in leukemia. The pharmacokinetics (PK) for **ORY-1001** have been explored for acute leukemia (AL) and showed that the recommended dose was accepted and increased blast differentiation (EudraCT 2013-002447-29). Recently, **ORY-1001** has been combined with azacitidine to treat elderly AML patients.[89] In treated THP-1 cells, **ORY-1001** increased the overall accumulation of H3K4me2 in a dose and time dependent manner.[90] As a result, it induced THP-1 cells apoptosis and inhibited MV-4-11 cell proliferation and colony formation. Additionally, Oryzon Genomics have clinical trials for a brain penetrable, dual selective LSD1 and MAOB inhibitor (**ORY-2001**), with IC_{50} values of 101 nM and 73 nM respectively.[91] Its preliminary effect and safely have been assessed for treating moderate – mild Alzheimer's disease (AD) (NCT03867253). Coupled with this, a wider clinical trial was undertaken to assess its efficacy, tolerability and safety for the following; AD, Lewy body dementia (LBD), adult attention deficit hyperactivity disorder (ADHD) autism spectrum disorder (ASD) have been completed (EudraCT 2018-002140-88). Additionally, **ORY-2001** shows positive, long lasting therapeutic effect against multiple sclerosis (MS).

Unlike GSK and ORY's developments in N-alkylation to incorporate the free space with the additional motif, Imago Bio-scientific have N-alkylated PCPA to form **IMG-7289** which incorporates a peptide like structure, as a result, allowing PCPA scaffold to enter into the free space.

IMG-7289 has completed phase I clinical trial for treating AML and MS as an independent treatment or coupled with ATRA (NCT02842827). The results are yet to be published.

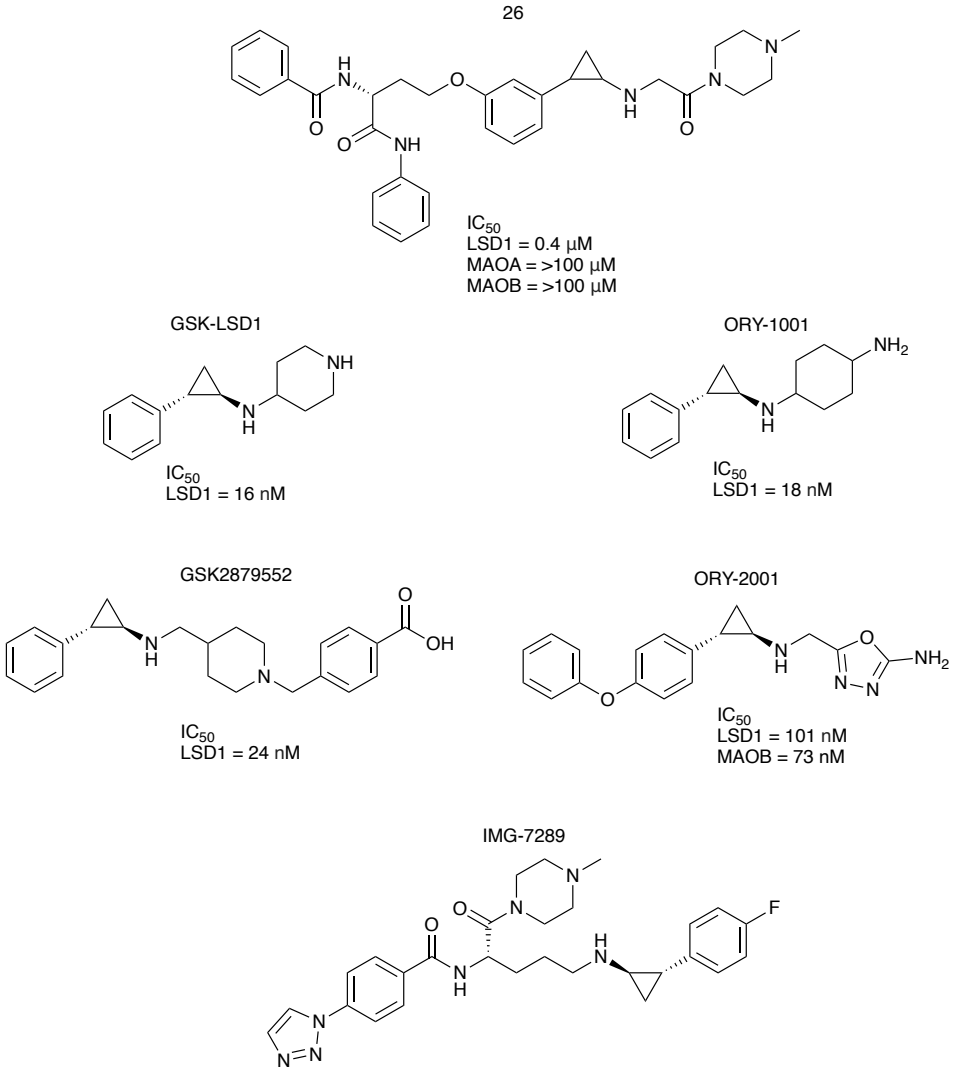

Figure.18 N-Alkylated PCPA analogues

1.5.4 Non-Covalent inhibitors

Inhibitors of LSD1 developed from **1** (**Figure.13**), which reversibly bind though hydrogen bonds to the FAD binding pocket have been synthesised and studied with recombinant enzymes and cell based models. The development compounds **27** and **28** (**Figure.19**) from **1**, use a hydroxylamine group that is a similar active group to hydrazine. In a comparative study compound **27** was found to have the highest inhibition of LSD1 after 24 hours, inhibiting 32% of the global LSD1. This led to the development of compound **28**, which shows slightly lower inhibition value of 30%, but the largest global increase of 3.7 fold of H3K4me2 after 48 hours rather than 0.62 fold increase. These were tested in Calu-6 cell lines, where **27** and **28**, show significant changes to promote the re-expression of aberrantly silenced tumor suppressor genes.[92,93] Complementary, **29** and **SP-2509**

(seclidemstat) were developed through high-throughput virtual screening with the identical hydrazine group to **1**. Both compounds have 430 times greater potency than phenelzine, and at least 46 times greater selectivity towards LSD1. From this, **SP-2509** was tested in a variety of cancer cell lines. These in cell studies demonstrated sensitivity towards **SP-2509** with observing EC_{50} values ranging from 300 nM to 3 μM providing an additional scaffold for further development for inhibition of LSD1 through covalent reversible interactions.[94]

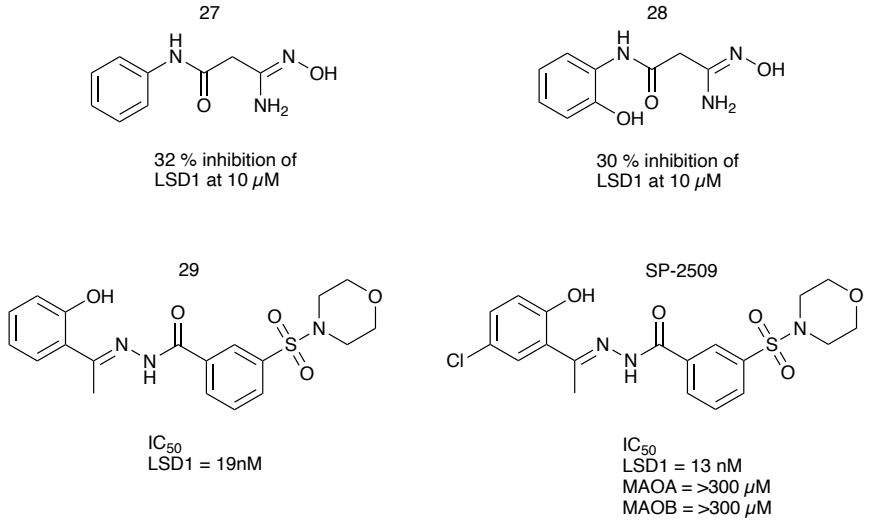

Figure.19 Covalent inhibition compounds for LSD1

1.5.5 Peptide mimicking LSD1 inhibitors

Currently, most of clinical trials for LSD1 inhibition use small molecule N-alkylated PCPA analogues. However, some inherent traits are lack of cell permeability.[168] To combat this, a series of H3-Lys mimicking inhibitors were developed and tested. Compounds **1, 2** and **3** (**Figure.13**) were coupled to Lys(4) H3-21 (**30**, **31** and **32**) (**Figure.20**) which exhibited high potency for LSD1 with IC_{50} values of 4.4 nM, 107 nM and 0.13 μM respectively. Theoretically, these were designed to serve as a carrier of their small molecule counterparts to deliver them to the active site of LSD1. However, **30** was discovered to be inactive in cancer cells, which is possible due to poor cell membrane permeability.[95] Nevertheless, this logic was employed to the NCD scaffold of molecules (**Figure.21**). **NCD18** shows potency towards LSD1 with IC_{50} 0.3 μM, with **NCD25**, **NCD38**, and **NCD41** showing higher inhibitions values (IC_{50} = 0.48, 0.59 and 0.58 μM respectively). **(*1 S – 2 R*)-NCD41** was found to have four fold more potency over its enantiomer (IC_{50} 0.31 and 1.4 μM respectively).[94]

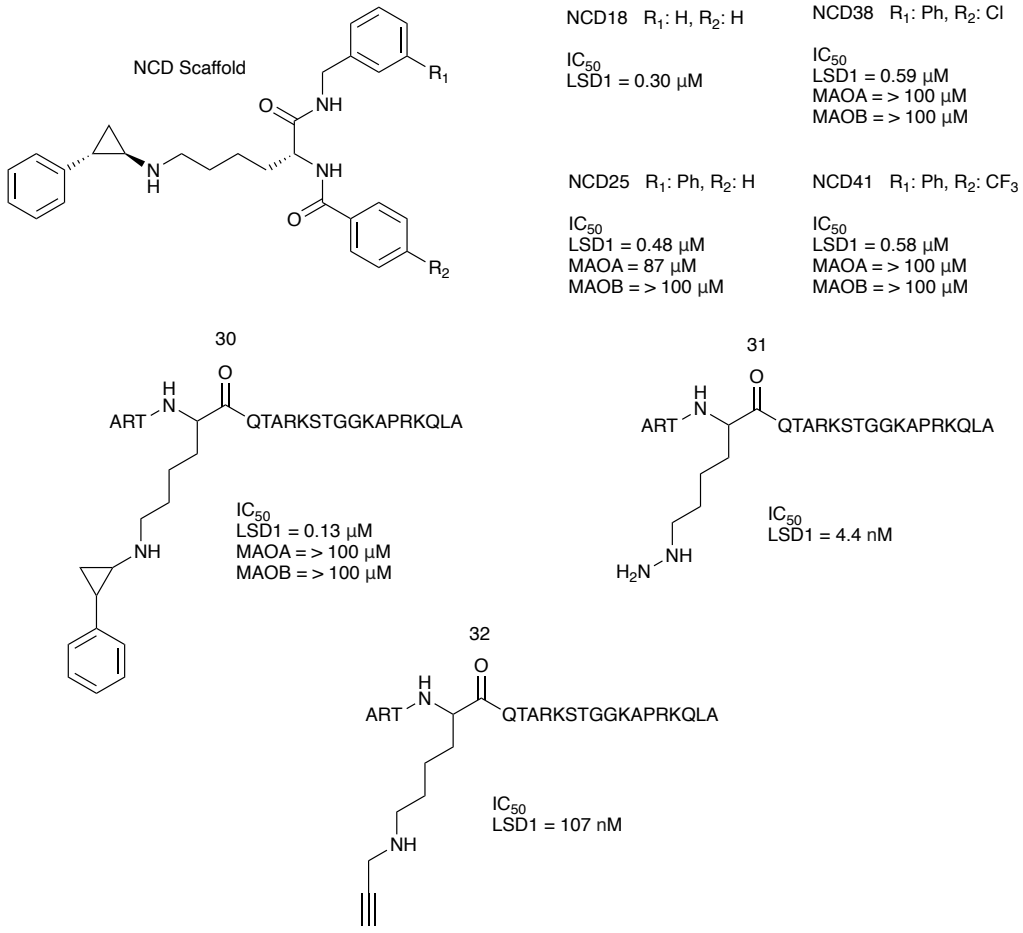

Figure.20 H3-Lys mimicking compounds for LSD1 inhibition

However, it was found that **(*1 R – 2 S*)-NCD18** and **(*1 R – 2 S*)-NCD25** have 11 and 4 fold more potency than their enantiomers **(*1 S – 2 R*)-NCD18** and **(*1 S – 2 R*)-NCD25** (IC_{50} = 0.13, 0.16, 1.4 and 0.62 μM respectively). Regardless, the **NCD scaffold** of molecules shows a potent anti-proliferative effect against HeLa (cervical cancer cell) and SH-SY5Y (Neuroblastoma cell line).[97] Additionally, **NCD38** and **19** are able to inhibit the growth of testicular and ovary tumors both *in vivo* and *in vitro*. Therefore, they could serve as therapeutic agents for testicular and ovary tumors.

1.6 Click Chemistry

Click chemistry has been developed for biorthogonal labelling,[114] which enables for visualisation of compounds in cells by reacting alkynes to azides to form a 1,2,3-triazole ring.[98] Development of PCPA can be completed with either alkyne or azide tag to allow for visualisation of LSD1, enabling PCPA to be used as a biological tool.

1.6.1 Development of Click Chemistry

Click Chemistry has been a useful development in biochemistry, allowing the ability to label enzymes. The click reaction originates from the Huisgen [2+3]-dipolar cycloaddition reaction (**Figure.21**).[98–100]

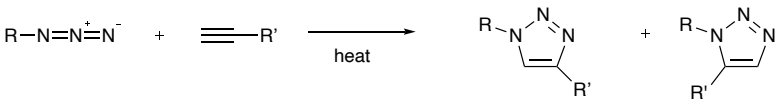

Figure.21 Huisgen [2+3]- dipolar cycloaddition producing racemic 1,2,3-triazoles

This reaction proceeds through the reflux of a terminal alkyne and azide, coupling to form a racemic mixture of 1,2,3-triazoles. The reaction is highly exothermic, to which this high activation barrier is responsible for the low rate of reaction. Furthermore, another hindrance is the formation of regioisomers caused by the HOMO – LUMO interactions of the substances are similar in terms of energy. Therefore, the thermal reaction generally gives a 1:1 racemic mixture and triazoles.[98]

From this, copper catalysed click chemistry was developed, which can be undertaken at room temperature and in aqueous conditions.[101] Further to this, copper click chemistry produces 1-4 disubstituted triazoles only (**Figure.22a**). By contrast, a ruthenium catalysed click chemistry has been developed which

specifically produces the 1-5 disubstituted only (**Figure.22b**). These developments make click chemistry suitable for labelling in complex biological environments,[102,103] as well as organic reactions.[104]

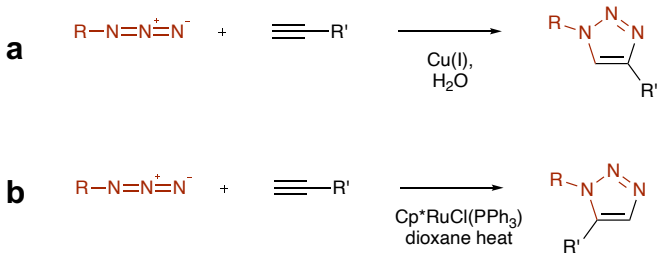

Figure 22a. Cu(I) Catalysed azide-alkyne cycloaddition (CuAAC) **b.** Ru Catalysed azide-alkyne cycloaddition

The CuAAC triazoles are produced through the mechanism shown in **Scheme.6.** The reaction proceeds through Cu interaction with the alkyne, allowing a second Cu to interchange with the terminal hydrogen of the alkyne, forming a di-copper intermediate. With the addition of the azide, the 1,3-dipolar cycloaddition reaction take place, where the alkyne attacks the terminal nitrogen of the azide, neutralising the positive nitrogen, with the negative charge attacking the Cu species on the alkyne. A Cu atom is then lost from this intermediate structure, forming the 1,2,3-triazole structure. Then within the slightly acid environment, the final Cu is substituted for the H^+ from the terminal alkyne, forming the final irreversible product.[105–107]

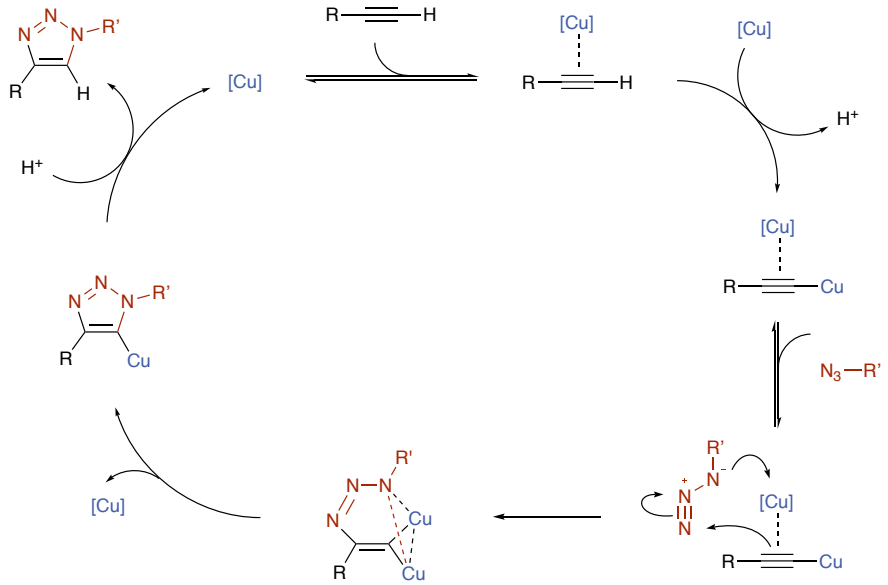

Scheme.6 Mechanism for 1,3-dipolar cycloaddition to form a 1,2,3-triazole structure

Although CuAACs are primarily effective *in vitro* studies, the reliance of copper hinders its application towards *in vivo* studies.[108] This is mainly due to the catalyst needed at the reaction site, and the concentrations of Cu needed for the click reaction to take place, are toxic to the cell. This is overcome by the development of copper free click reactions where the alkyne is incorporated in a strained cycloctyne system[109,110] which increases the alkynes reactivity, enabling the removal of Cu as a catalyst. This development enables the use of click chemistry *in vivo* studies, enabling the ability to label specific biological targets in complex systems (**Figure.23**).[111–113]

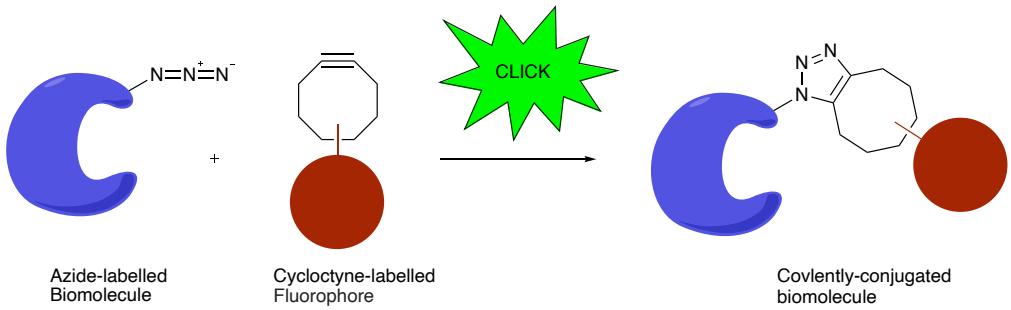

Figure.23 Biorthogonal azide-cycloctyne copper free coupling

1.6.2 Cell visualisation using Click Chemistry

1.6.2.1 DNA Proliferation visualisation

Click chemistry has been developed for visual detection of DNA synthesis in proliferating cells. Modifying **Thymidine** DNA nucleoside alkyl unit to terminal alkyne (5-ethylnyl-2'-deoyuridine (**EdU**)) (**Figure.24**) enables for a 'clickable' platform for organic azides.

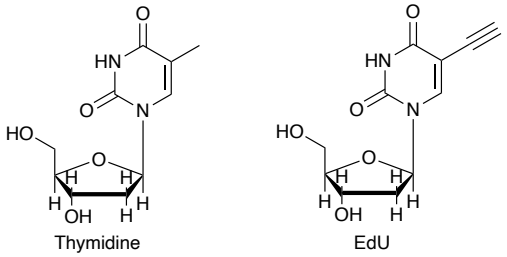

Figure.24 Modification of Thymidine to EdU

EdU serves as a replacement for **Thymidine** and is incorporated into the DNA, allowing for reactivity with organic azide's without steric hindrance (**Scheme.6**). Timothy J. Mitchson *et.al*. cultured NIT 3T3 and HeLa cells with **EdU**, fixed, and reacted with Cu(I) catalysed click reaction with fluorophor azide. This gave a

positive visualisation of **EdU** been incorporated within the cell cycle. This method was also demonstrated in intestine and brains of whole animals, to afford the same success.[114]

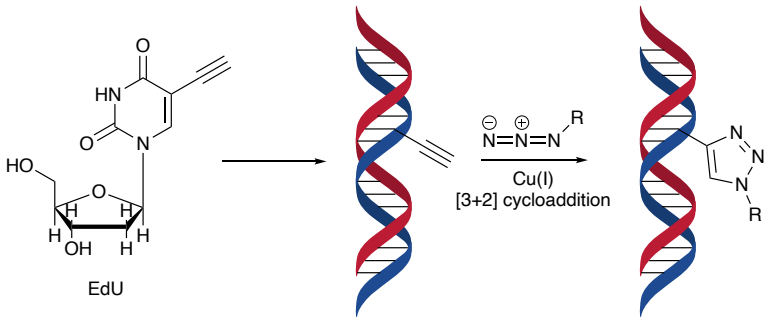

Scheme.7 Incorporation of EdU into DNA Helix, with availability for click chemistry with organic azide

1.6.2.2 Chondrocytes visualisation

Click chemistry has been also developed for labelling/visualising Chondrocytes. Chondrocytes for cartilage engineering can be labelled using modified azide sugars for *in vitro* and *in vivo* cell tracking studies. The use of metabolic glycoengineering provides the source of unnatural azide from sugar Ac_4ManNAz for the system. The azide of the metabolised sugar is coupled with DBCO-650 to biorthogonally label the chondrocyte (**Figure.25**). This biorthogonal labelling was highly effective, showing minimal toxicity, and low effect on cartilage formation, and yielded higher contrast *in vivo* and *in vitro* images compared to other methods; positron emission tomography, computed tomography, providing a greater understanding of the transplanted cells.[115]

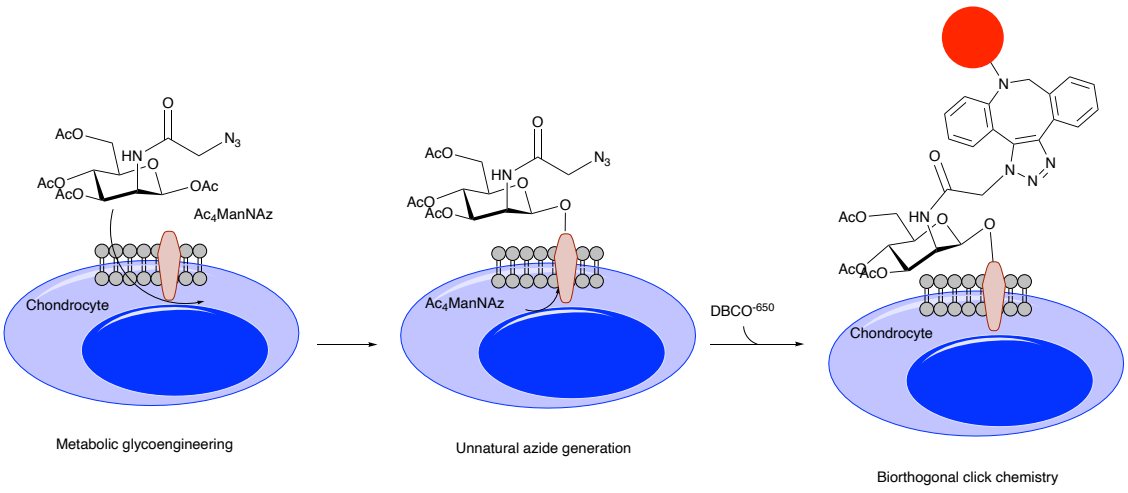

Figure.25 Schematic illustrations of metabolic glycoengineering and azide−alkyne Click chemistry for labelling chondrocytes

Aims of the project;

- Synthesise and develop molecular probes using the PCPA scaffold by addition of alkyne or azide tags. This will enable further visualisation of the LSD1 using click chemistry within cells
- Visualise the synthesised probes in cells and identify the antiproliferations effects. This will show if the synthesised probes inhibit the LSD1 in the cells, by causing an increase in the accumulation of H3K4me3
- Conjugate the synthesised probes to a peptide counterpart aiming for greater cellular permeability which can hinder some synthesised small molecules
- Identify the inhibitory values for the synthesised probes
- Isolate and characterise the individual diastereoisomers of the cyclopropane, to identify if there is any effect of the chirality on the inhibition of the MAO or LSD1 enzymes
- N-alkylate the synthesised probes to incorporate the free space in the LSD1, aiming to increasing the selectivity towards LSD1 over MAO

Chapter 2 Visualisation of Probes in LSD1

2.1 Introduction

The MAO inhibitor PCPA scaffold has been developed to selectively inhibit FAD cofactor of LSD1. In many diseases, LSD1 is over expressed,[2] causing changes in the expression of genes that control regulation of cellular functions, this aberration leads to the uncontrolled replication and repair of these cells. The MAO inhibitor, PCPA was one of the first identified drugs for the inhibition of LSD1, from this, NCL-1 was developed as the first cell active LSD1 inhibitor,[10,11] which has been shown to cause the accumulation of the H3K4me2 epigenetic mark and repress cancer cell growth.[12]

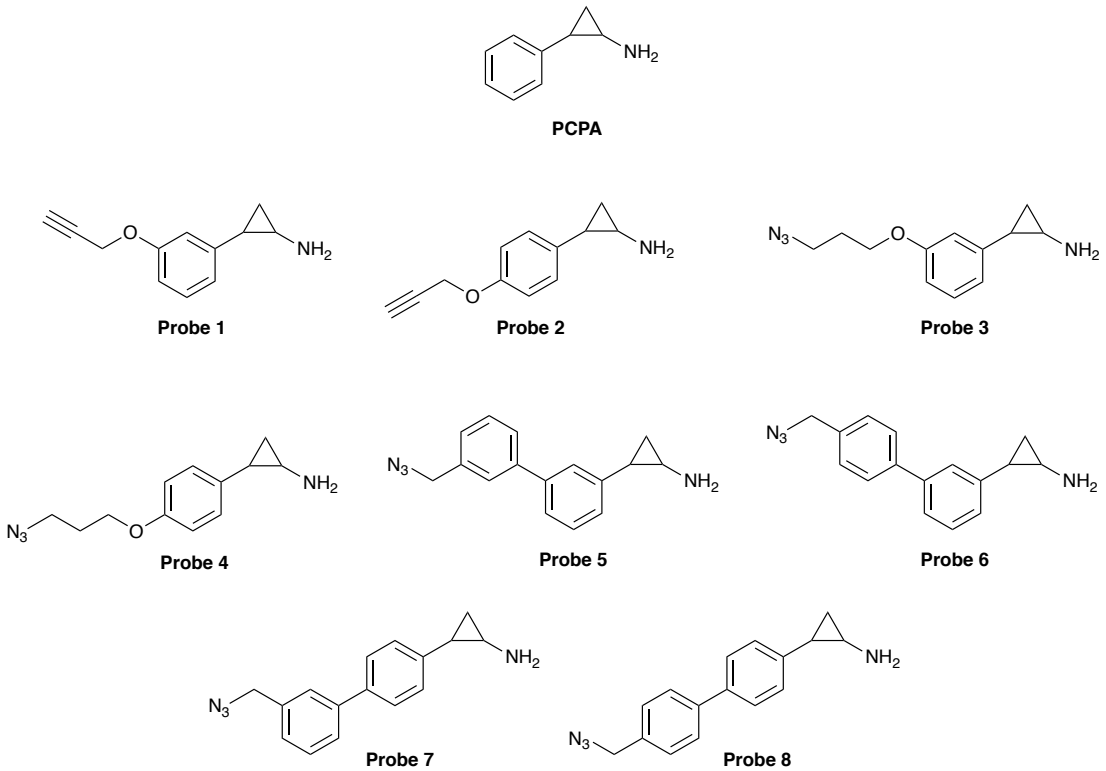

Figure.26 Synthesised target PCPA derivative probes for biorthogonal labelling and peptide conjugation

Initially, derivatives of PCPA were developed with alkyne tags **Probe 1 & 2** (**Figure.26**) and were synthesised through linear and divergent synthesise. This was to undertake biorthogonal labelling of LSD1 within cells using click chemistry. However, as the research progressed, a collaboration formed with the *Steve Brown group at University of Sheffield*. Therefore, development of new azide probes (**Probe 3 – 8, Figure.26**) was required to conjugate the PCPA scaffold to their synthesised peptide. To complete previous work, **Probe 1** would undertake further cellular and visualisation studies. For identification of the inhibitory values

for the synthesised probes, a coupled fluorescence assay will be used to measure the release of hydrogen peroxide from regenerated FAD from $FADH_2$ (**Figure.27**).[116]

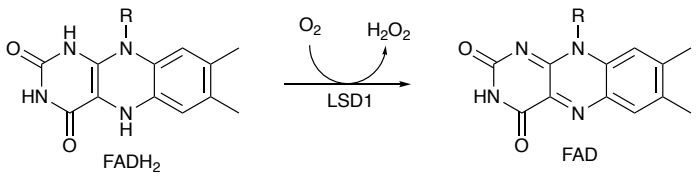

Figure.27 Regeneration of FAD cofactor in LSD1 and MAOs

Aims and objectives of this chapter;

- PCPA derived probes (**Figure.26**) have been developed to improve selectivity towards LSD1. To identify if these probes pass through cell membranes and inhibit LSD1 the PCPA scaffold will be modified with various alkyne and azide tags providing the opportunity to further functionalise the molecules with click chemistry in cells.
- The inhibitory value (IC_{50}) of these probes will be accessed by *in vitro* testing with recombinant MAOA, MAOB and LSD1 enzymes
- Selected probes will be used to treat NTERA2 cells to identify their bioavailability.

2.2 Probe Synthesis

The synthetic routes to **probes 1 - 8** are shown in **Schemes 8 - 11**. **Schemes 8 & 9** shows the linear progression synthesis for all probes. In **Scheme.8,** the protection of carboxylic acid **33** as a methyl ester **34** under acidic conditions (*meta* produced 5 % less yield and *para* produced 18 % less yield than in the literature).

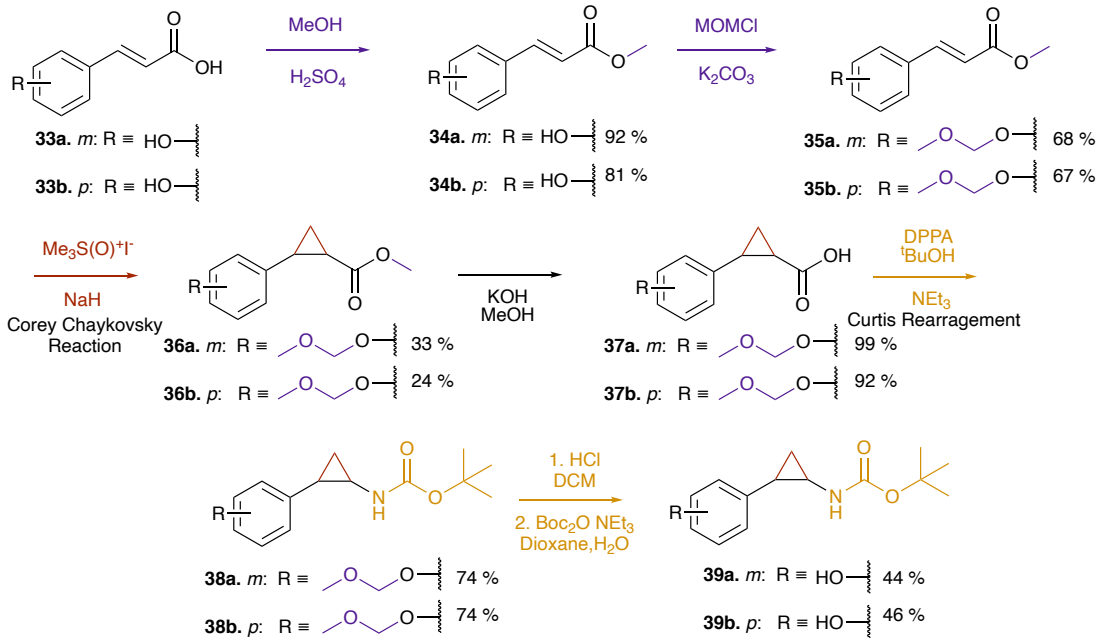

Scheme.8 Multistep linear synthesis for **probe 1 – 4**

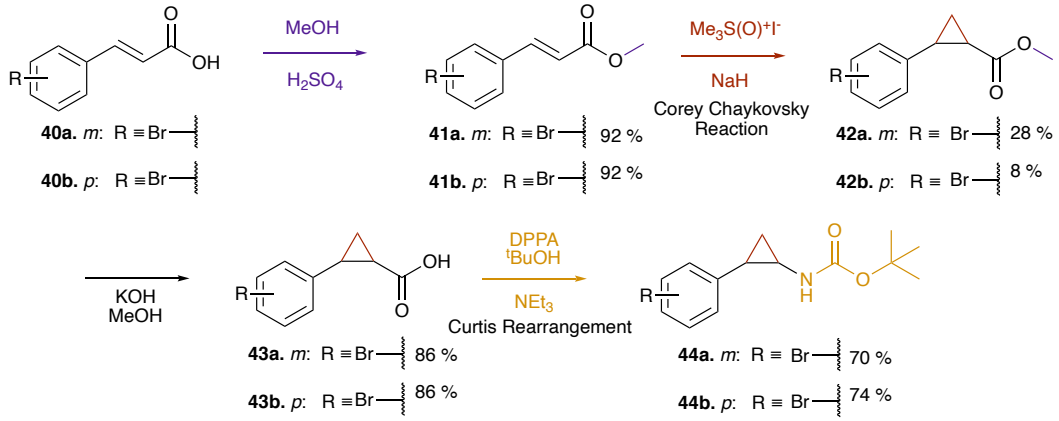

Scheme.9 Multistep linear syntheses for **probe 5 – 8**

MOMCl protection of the phenol **34** to affords ether **35,** (*meta* produced 16 % less yield and *para* produced 22 % less yield than in the literature). Formation of the cyclopropyl **36** from alkene **35** is achieved through the Corey-Chaykovsky reaction (*meta* produced 10 % more yield and *para* produced 10 % more yield than in the literature). The methyl ester **36** is hydrolysed in basic conditions to

give the carboxylic acid **37** (*meta* produced 4 % more yield and *para* produced 3 % less yield than in the literature).

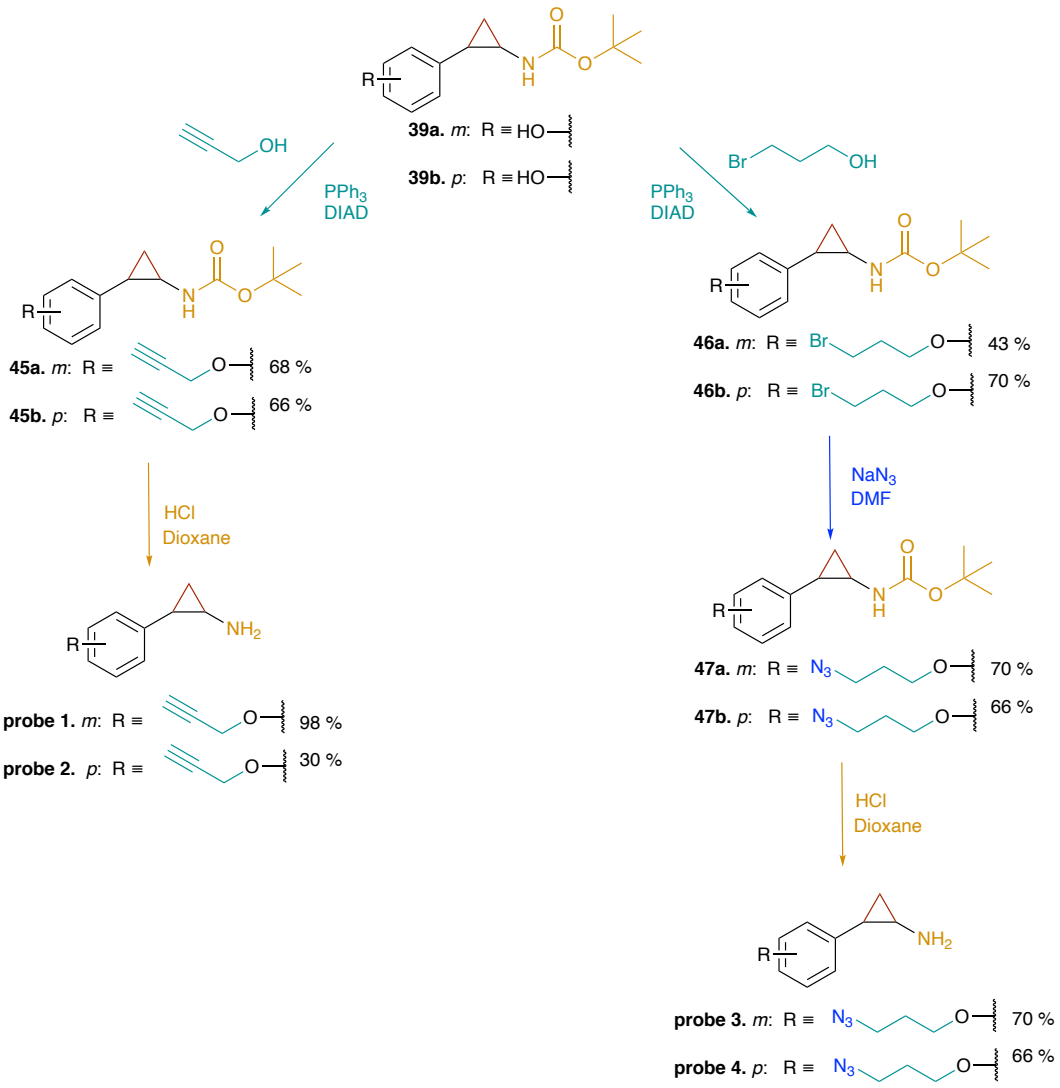

Scheme.10 Multistep divergent syntheses for **probe 1 - 4**

This is converted to the protected amine **38** through the Curtis rearrangement (*meta* produced 27 % more yield and *para* produced 20 % more yield than in the literature).[74] Double de-protection of Boc and MOM groups is achieved under acidic conditions, with subsequent Boc protection to afford **39** (*meta* produced 9 % more yield and *para* produced the same yield to the literature).[76] **Scheme.9** shows the protection of carboxylic acid **40** as a methyl ester **41** under acidic conditions. Formation of the cyclopropyl **42** from alkene **41** is achieved through the Corey-Chaykovsky reaction. The methyl ester **42** is hydrolysed in basic conditions to give the carboxylic acid **43**, this is converted to the protected amine **44** through the Curtis rearrangement.[76] **Scheme.10** shows divergent syntheses of **probes 1 - 4.** Phenols **39a, 39b,** are coupled to propargyl alcohol to afford **45a, 45b** through the Mitsunobu reaction.[172] The Mitsunobu reaction is used as it

produces reliable yields for the conversion of different alcohols to different ethers using phenols. This then allows for ease of probe development in future synthesis. The amine is de-protected under acidic conditions to afford **probe 1** and **probe 2.** Phenols **39a, 39b,** are coupled to 3-bromopropan-1-ol to produce **46a, 46b** through the Mitsunobu reaction.[172]

The bromine is substituted by azide to produce compound **47a, 47b**, of which the amine is de-protected under acidic conditions to afford **probe 3 - 4**. **Scheme.11** shows the divergent syntheses of **probe 5 – 8.** The bromine position in **44a, 44b** are coupled to 3-hydroxymethylbenzeneboronic acid or 4-hydroxymethylbenzeneboronic acid by the Suzuki coupling to afford **48a to 48d.**[117]

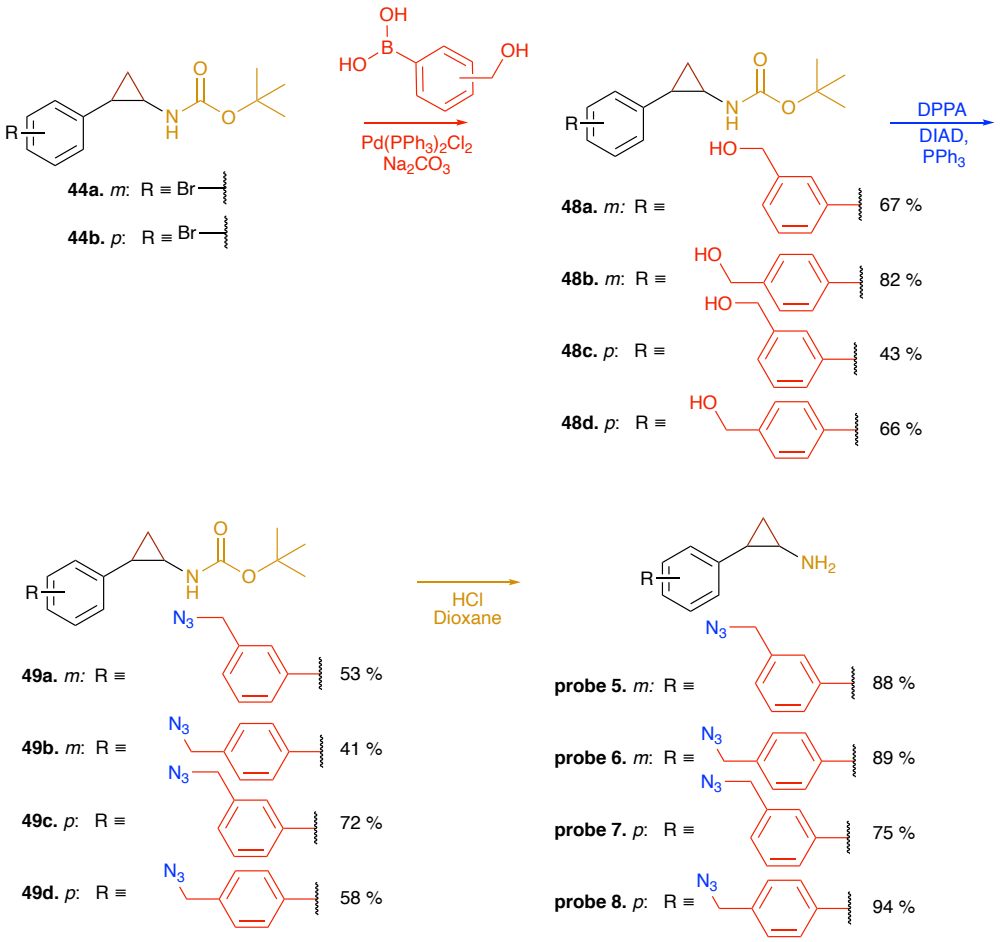

Scheme.11 Multistep divergent syntheses for **probe 5 – 8**

The benzyl alcohol in the *meta* and *para* positions of **48a to 48d,** were converted to azide **49a to 49d** through the Mitsunobu reaction with DPPA. The Boc-protected amine is de-protected under acidic conditions to afford for biphenyl PCPA derivatives **probes 5 – 8**. These synthetic routes will produce novel PCPA

derivatives probes, tagged with alkyne or azide functionalities for click chemistry applications.[118]

2.2.1 Alkene analysis

To confirm the stereo chemistry of the starting materials alkenes **33a, 33b**, **40a**, **40b**, proton environments H1a and H2a (**Figure.28**), were examined by ^{1}H NMR to assign *cis trans* isomerism, by measuring the ^{3}J coupling constants. Analysis of the H1a and H2a chemical shifts for all four starting materials, gave coupling constants ranging from 16.0 Hz - 16.1 Hz. This analysis of chemical shifts confirms the *trans* stereochemistry of the starting materials.

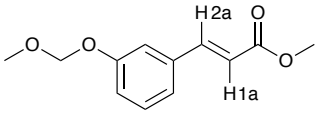

Figure.28 Stereo identification of the alkene in the starting materials for the probes

2.2.2 Cyclopropane Analysis

For analysis of the newly formed cyclopropane ring (**4** and **10**) from the alkene (**3** and **9**) (**Figure.29**), ^{1}H NMR was used to identify which hydrogen in the cyclopropane ring corresponds to which peak in the ^{1}H NMR spectrum (**Figure.30**). Reacting only the *trans* isomer in (**3** and **9**) will result in one pair of enantiomers (**Figure.29**), rather than two pairs of enantiomers when both *cis* and *trans* alkene isomers are reacted. Examination of the splitting pattern and expected coupling constants of each hydrogen in **Figure.29**. In addition to this, each hydrogen will be split into a doublet-doublet-doublet, according to the n+1 rule. Although the isomers are structurally different, the ^{1}H NMR experiment in this situation is not in a chiral environment, therefore, the different enantiomers cannot be distinguished. The coupling constants are identical for each hydrogen in each enantiomer, this will result in the same coupling constants for both isomers, which are summarised in **Table.1**.

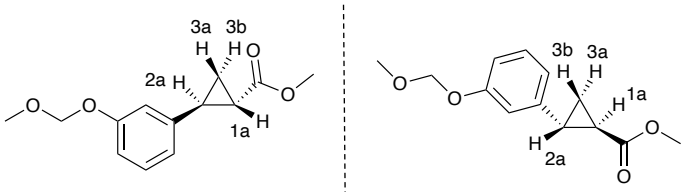

Figure.29 Two isomers produced when forming the cyclopropane though the Corey Chaykovsky reaction

The interpreted ^{1}H NMR data in **Table.9** from **Figure.41**, allows the peaks of the spectrum to be assigned to each hydrogen labelled in **Figure.29**. Firstly, **peak a**, it has a shifted to 2.49 ppm, and has j-coupling values of 9.2 Hz, 6.5 Hz, 4.2 Hz, which corresponds to three vicinal couplings (1 *cis*, and 2 *trans*). The analysis of the HMBC, shows correlation between **peak a** and an aromatic carbon, resulting in this peak belonging to H_{2a}. For **peak b**, it has shifted to 1.88 ppm, and has j-coupling values of 8.5 Hz, 4.2 Hz, 5.3 Hz, which corresponds to three vicinal couplings (1 *cis*, and 2 *trans*). Analysis of the HMBC, shows correlation to the carbonyl group resulting in the peak belonging to H_{1a}. The **peak c**, has a shift of 1.62 ppm, and has j-coupling values of 11.6 Hz, 5.3 Hz, 4.7 Hz, which corresponds two vicinal couplings (1 *cis*, and 1 *trans*). and one *geminal* couplet, this peak can be assigned as H_{3a}.

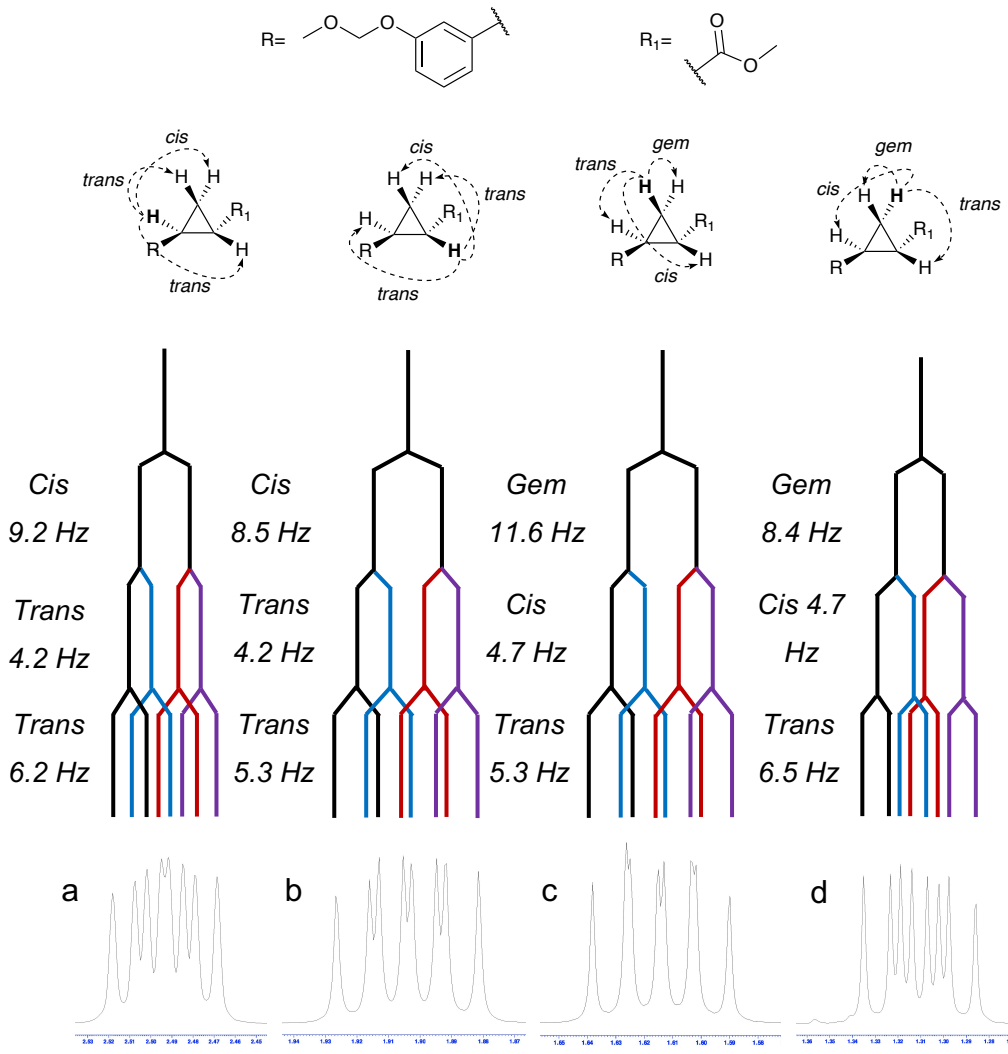

Figure.30 Identification of J-coupling of each hydrogen with a dashed line, with the corresponding splitting tree from the ^{1}H NMR spectrum peaks from the cyclopropane shown in **Figure.29**

Table.1 Cyclopropane coupling constants present in intermediates **4** and **10** that was synthesised.

	cis	***trans***	***gem***
H_{1a}	1	2	-
H_{2a}	1	2	-
H_{3a}	1	1	1
H_{3b}	1	1	1

The final **peak d**, has a shift of 1.29 ppm, and has j-coupling values of 8.4 Hz, 6.5 Hz, 4.7 Hz, which corresponds to two vicinal couplings (1 *cis*, and 1 *trans*). and one *geminal* couplet, allowing the assignment of this peak as H_{3b}.

Table.2 The analysis of the ^{1}H NMR spectrum in **Figure.30** showing the peak shift and J-coupling constant values.

Peak	**δ / ppm**	**J-Coupling / Hz**		
a	2.49	9.2	6.5	4.2
b	1.88	8.5	4.2	5.3
c	1.62	11.6	5.3	4.7
d	1.29	8.4	6.5	4.7

2.3 Enzyme Assays

Coupled fluorescence assays can be used to measure the release of peroxide by FAD cofactor in LSD1 and MAOs. This coupled with horseradish peroxidase (HRP) allows the oxidative reduction of Amplex Red® (10-acetyl-3,7-dihydroxyphenoxazine (ADPH))[116] (**Figure.31**) to the fluorescent resorufin.

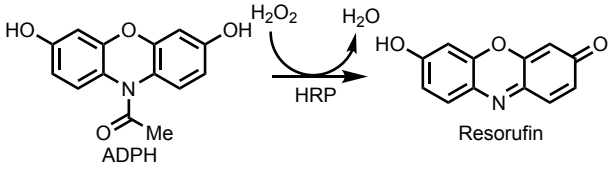

Figure.31 Formation of resorufin by oxidative reduction

The fluorescence signal of resorufin is directly proportional to the molar (M) concentration of H_2O_2 produced by the FAD catalytic cycle. This enables the measurement of substrate oxidation, which will be used to calculate Michaelis Menten constant (MM) for each enzyme. in addition to the IC_{50}, K_i values for each molecular probe. The Michaelis Menten constant is used to identify the optimum substrate concentration (Tyramine for MAOA/B and H3K4me2 for LSD1) to be used in the IC_{50} and K_i inhibition assays. The Michaelis Menten experiment also tells us the turnover of the enzyme (k_{cat}), describing the maximum amount of substrate that can be converted per active each minute.

2.3.1 H_2O_2 Standard Curve

A H_2O_2 standard curve (**Figure.32**) is used to convert Fluorescence unit (F.U.) to molar concentration, the results from Michaelis Menten, IC_{50} and K_i experiments.

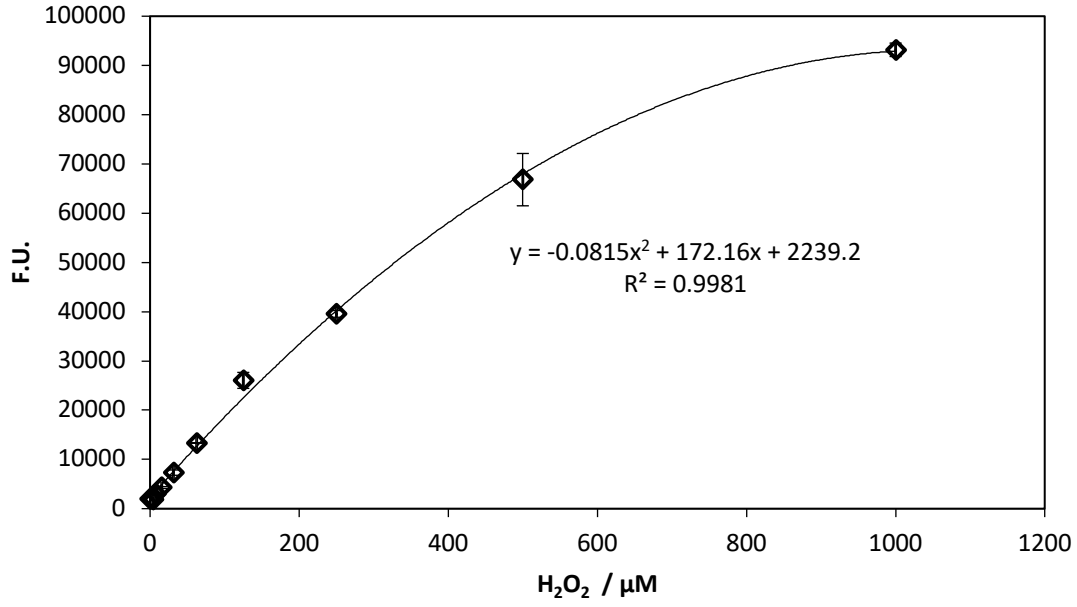

Figure.32 H_2O_2 standard curve plotted with Fluorescence unit (F.U.) against H_2O_2 concentration obtained to standardize IC_{50} and Michaelis Menten results (*n=3* for standard curve)

The standard curve is produced by plotting the fluorescence unit against H_2O_2 concentration, and fitted using quadratic **Equation.1**, giving values of -0.0815, 172.16 and 2239 for a, b, and c respectively.

$$y = ax^2 + bx + c \qquad \textbf{Equation.1}$$

2.3.2 Michaelis Menten (MM)

The Michaelis Menten (MM) experiment was undertaken to identify the Michaelis Menten constant (K_s), the maximum rate of the system (v_{max}) and catalytic turnover rate (k_{cat}) for each enzyme (**Table.3**). The fluorescence data acquired from the MM experiment was processed using **Equation.2** with a = -0.0815, b = 172.16, c = 2239.2 + reaction fluorescence value – negative control fluorescence value. The initial reaction velocity ($v_{0\ Exp}$) was calculated from plotting the molar concentration (M) against time (s). Using **Equation.3** with m = v_0 (Ms^{-1}), c = intercept, y = molar concentration (M), x = time (s) to extract the value of $v_{0\ Exp}$. The $v_{0\ Exp}$ is used in **Equation.5**, with $v_{0\ calc}$ = calculated initial reaction velocity (from **Equation.4**), $v_{0\ Exp}$ = initial reaction velocity, R^2 = experimental error squared. The sum of the R^2 values for each substrate concentration is used in conjunction with **Equation.5,** where [S] is concentration of the substrate. Solver software in Excel® is used to minimise the sum R^2 value, by changing K_s and v_{max} values, resulting in optimum values for K_s and v_{max} reported in **Table.3**. The graphs produced from the fitting are shown in **Figure.33**.[119]

$$x = \frac{-b \pm \sqrt{b^2 - 4ac}}{2a} \qquad \textbf{Equation.2}$$

$$y = mx + c \qquad \textbf{Equation.3}$$

$$R^2 = (V_{0\ Exp} - V_{0\ Calc})^2 \qquad \textbf{Equation.4}$$

$$v_{0\ Calc} = v_{max} + \left(\frac{[S]}{[S] + K_s}\right) \qquad \textbf{Equation.5}$$

$$Moles\ of\ Enzyme = \frac{[Enzyme]}{RMM} \qquad \textbf{Equation.6}$$

$$K_{cat} = \left(\frac{v_{max}}{Molar\ Enzyme}\right)\Big/_{60} \qquad \textbf{Equation.7}$$

From this plot, k_{cat} is calculated using **Equation.6**, where first the moles of enzyme is determined by the division of the enzyme concentration ([Enzyme]) (M) by the relative molecular mass (RMM) (g/mol). The moles of enzyme is used in **Equation.7**. To identify k_{cat}, v_{max} is divided by the moles of enzyme which is divided by 60 to report the k_{cat} value in min^{-1} shown in **Table.3.**[119]

Table.3 *In vitro* activities for enzyme – substrate activity

Enzyme	MAOA	MAOB	LSD1
K_s (μM)	265 ± 45	229 ± 40	53 ± 25
k_{cat} (min^{-1})	0.23 ± 0.03	0.04 ± 0.01	0.01 ± 0.002
v_{max} (μMs^{-1})	0.04 ± 0.01	0.01 ± 0.01	0.002 ± 0.001

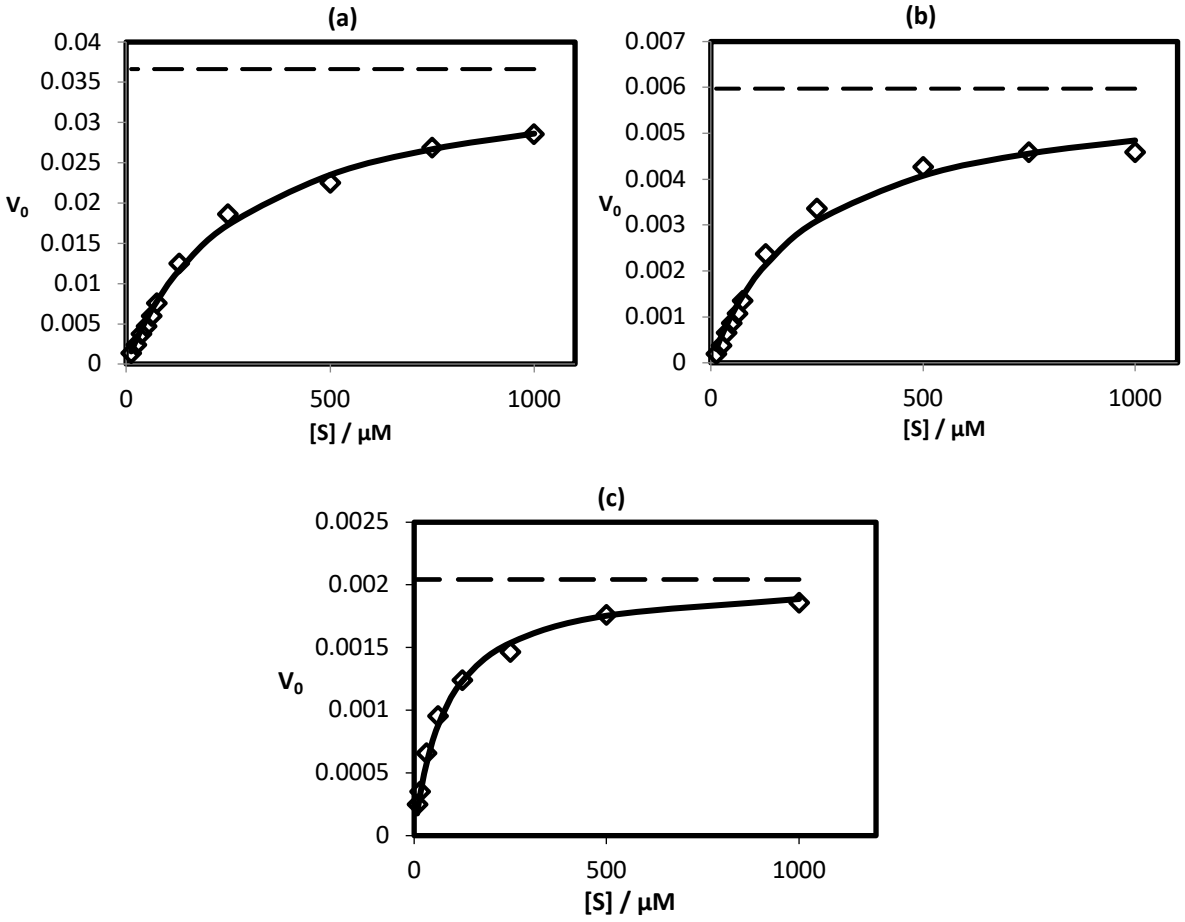

Figure.33 The Michaelis Menten curves produced for **(a)** MAOA, **(b)** MAOB and **(c)** LSD1. With; solid Line (v_0 Calc (M s^{-1})), hollow markers (v_0 Experimental (s^{-1})) and dashed line (v_{max} (μM s^{-1})) (*n=3* for all enzyme assays)

2.3.3 IC_{50} inhibition assay

The IC_{50} assay was undertaken to identify the concentration of the probe required to reduce the turnover of the substrate by the enzyme by half.[120] The fluorescence data acquired from the IC_{50} assay was converted using equation **(2)** with a = -0.0815, b = 172.16, c = 2239.2 + reaction fluorescence value – negative control fluorescence value. The initial reaction velocity ($v_{0\ Exp}$) was calculated by plotting the molar concentration (M) against time (s). Using **Equation.3**, the molar concentration was plotted as a function of time, to give a gradient equal to $v_{0\ Exp}$. The $v_{0\ Exp}$ is used in **Equation.5**, with $v_{0\ calc}$ = calculated initial reaction velocity (from **Equation.4**), R^2 = experimental error squared. The sum of the R^2 values for each inhibitor concentration is used in conjunction with **Equation.8**, where y = calculated response ($v_{0\ calc}$), x = molar concentration (M), IC_{50} = Inhibition required to result in half the response (M), Hill = Hill Coefficient. Solver software in Excel® is used to minimise the sum R^2 value, by changing the IC_{50}, Hill, min and max values, with constraints on the Hill to be: 4 > Hill > 0.1.[119]

$$y = \frac{\min + (\max - \min)}{1+\left(\frac{x}{IC_{50}}\right)^{Hill}} \qquad \textbf{Equation.8}$$

Table 4 *In vitro* MAOA, MAOB, LSD1 inhibitory activities (IC_{50}), for synthesised **probes 1 – 8** and **PCPA**.

Compound	MAOA / μM	MAOB / μM	LSD1 / μM
PCPA	100 ± 4	22 ± 5	12 ± 3
Probe 1	210 ± 67	40 ± 8	62 ± 2
Probe 2	12 ± 1	6.8 ± 0.3	64 ± 2
Probe 3	30 ± 2	41 ± 4	19 ± 4
Probe 4	4.4 ± 0.5	5.0 ± 0.8	46
Probe 5	18 ± 7	0.58 ± 0.11	14 ± 2
Probe 6	4.6 ± 0.2	2.0 ± 0.5	22 ± 14
Probe 7	5.3 ± 2.9	1.1 ± 0.2	8 ± 3
Probe 8	4.1 ± 2.4	0.05 ± 0.01	5 ± 1

a.

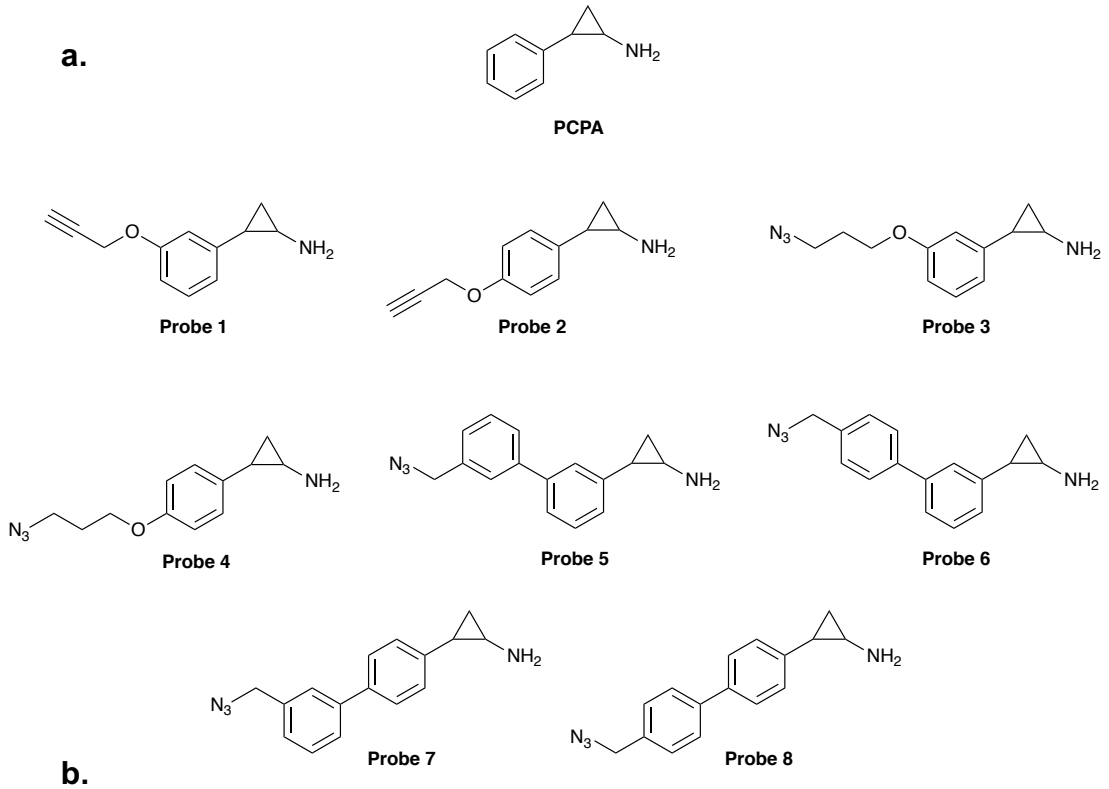

b.

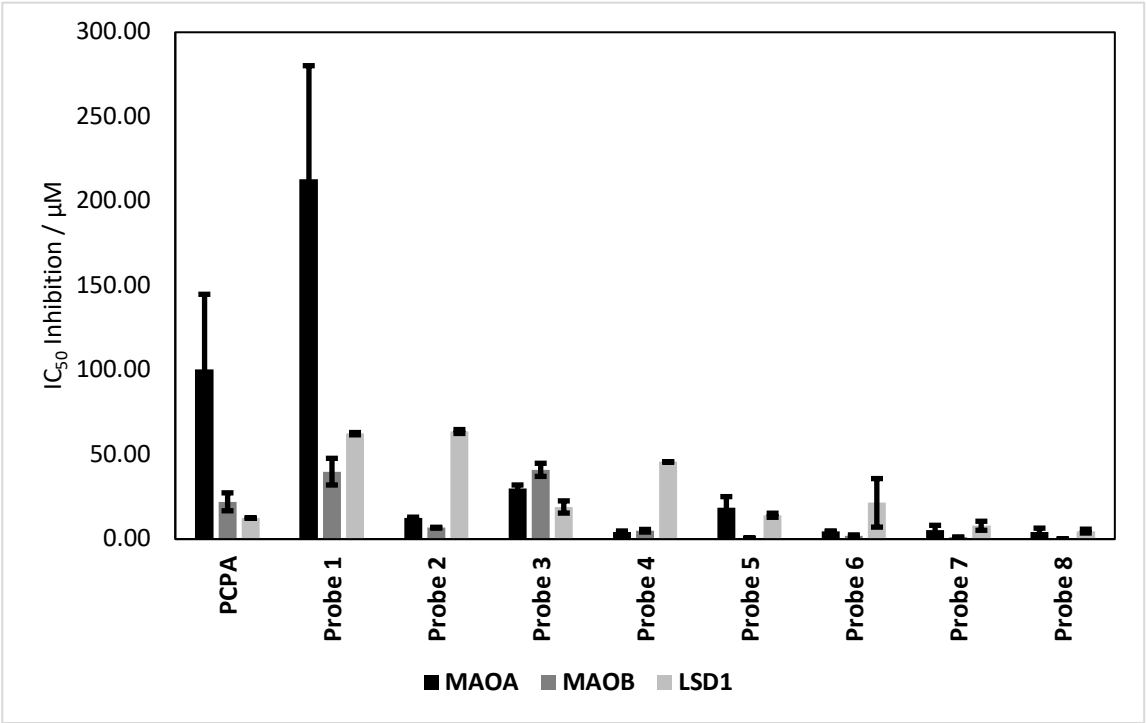

Figure.34a. Synthesised probes undertaken IC_{50} analysis **b.** Comparison of the inhibition of each probe for each enzyme, black showing MAOA inhibition, dark grey showing MAOB inhibition, light grey showing LSD1 Inhibition. (*n=3* for all enzyme assays except for **probe 4** LSD1, *n=1)*

The inhibition activity for the synthesised probes towards human LSD1, MAOA and MAOB were evaluated and results are reported in **Table.4**, with graphical representation in **Figure.34**. The inhibition assay data highlights that the addition

of the alkyl-alkyne, on the *meta* position, in **probe 1**, decreases the selectivity towards MAOA, MAOB and LSD1 (IC_{50} values: 210 μM, 40 μM and 62 μM respectively) by two fold for MAOA and MAOB, and five fold for LSD1 when compared to **PCPA**, (IC_{50} values: 100 μM, 22 μM and 12 μM respectively). When the alkyl-alkyne is moved to the *para* position, in **probe 2**, the selectivity towards MAOA and MAOB is increased by eight fold and three fold respectively when compared to **PCPA** (IC_{50} values: 12 μM and 6.8 μM). However, the selectivity towards LSD1 is similar to that of **probe 1**, where the selectivity has decreased five fold. It can be assumed that the difference in selectivity towards MAOA and MAOB is because of size of the active pocket of MAOA and MAOB, **probe 2** 'fits' better into the active site of MAOA and MAOB compared to **probe 1**. When compared to LSD1, the active pocket is much larger, which in this instance, makes the difference in inhibition of LSD1 between **probe 1** and **2** negligible.

The addition of alkyl-azide, **probe 3** results in an increase in activity for MAOA by three fold, decrease in selectivity for MAOB by two fold, and similar inhibition when compared to **PCPA** (IC_{50} values: 30 μM, 41 μM and 19 μM respectively). When the alkyl-azide is positioned in the *para* position in **probe 4**, the selectivity toward MAOA and MAOB is increased by 22 fold and eight fold respectively, but is decreased in selectivity towards LSD1 by four fold when compared to **PCPA** (IC_{50} values: 4.4 μM, 5 μM and 46 μM respectively). It can be assumed that **probe 1** and **2**, the **probe 4** 'fits' into the active site in MAOA and MAOB better than **probe 3**. Whereas for LSD1, **probe 3** is more selective than **probe 4**. This presumes that the azide moiety from **probe 3** is better positioned in the active site to undergo electrostatic interactions. When compared to **probe 4**, the **probe 3** azide moiety is positioned differently in the active site, due to the *para* substitution of the alkyl-azide chain. This change in substitution causes a decrease in selectivity towards LSD1. As **probe 1** and **2** lack the azide moiety, this causes a decrease in selectivity towards LSD1 when compared to **PCPA**, when the azide motif is introduced (**probe 3** and **4**), the selectivity increases compared to **probe 1** and **2**. The selectivity is further increased when the position of azide moiety is altered (**probe 3**).

The addition of benzyl azide fragment, **probes 5 - 8** resulted in the increased selectivity towards MAOA and MAOB. When comparing the **probes 5 – 8** to **PCPA** for selectivity towards MAOA they have increased selectivity by; 5.5 fold for **probe 5**, 22 fold for **probe 6**, 19 fold for **probe 7** and 24 fold for **probe 8** (IC_{50}

values: 18 μM, 4.6 μM, 5.3 μM and 4.1 μM respectively). When comparing the **probes 5 – 8** to **PCPA** for selectivity towards MAOB they have increased selectivity by; 38 fold for **probe 5**, 11 fold for **probe 6**, 20 fold for **probe 7** and 440 fold for **probe 8** (IC_{50} values: 0.58 μM, 2.0 μM, 1.1 μM and 0.05 μM respectively). **The probe 5** and **6**, with the benzyl azide substituent in the *meta* position, causes a decrease in selectivity of inhibition towards LSD1 when compared to PCPA, with a decrease of 1.2 fold for **probe 5** and 1.8 fold for **probe 6** (IC_{50} values: 14 μM and 22 μM respectively). Whereas the *para* substituted benzyl-azide, **probe 7** and **8**, show an increase in inhibition selectivity towards LSD1 when compared to PCPA, with an increase by 1.5 fold for **probe 7** and 2.4 fold for **probe 8** (IC_{50} values: 8 μM and 5 μM respectively).

The increase in selectivity of **probe 5 – 8** towards MAOA and MAOB is caused by the addition of the phenyl ring, able to π stack with Tyr-761 amino acid within the active pocket of MAO, as well as increased hydrophobic interactions within the active pocket, which causes the difference in inhibition. The change in structural isomers of the benzyl azide caused the difference in inhibition of by probes, altering the selectivity between them; with **probe 5** the least selective towards MAOA (IC_{50} value: 18 μM) and **probe 6** the least selective towards MAOB (IC50 value: 2 μM). The **probe 8** is the most selective towards both MAOA and MAOB, similarly, **probe 5** and **6** are the least selective towards LSD1 with both **probe 7** and **8** having increased in selectivity towards LSD1. This selectivity shows that the *para* substituted benzyl azide 'fits' better into the active site of LSD1 when compared to PCPA. This shows that the addition of the azide motif in **probe 3** increases the hydrogen bonding ability to residues in the active site. Furthermore, the addition of the phenyl ring allows for additional π bonding to Tyr-761 in the active site of LSD1, increasing the selectivity further, with **probe 8** having the largest selectivity towards LSD1.

2.4 Visualisation of molecular probes

The cellular uptake of **probe 1** was identified using NTERA2 testicular cancer cells. The cells were treated with 500 μM of **probe 1** for two and six hours, fixed and permeabilised, reacted with carboxamido-(6-Azidohexanyl), Triethylammonium Salt (Alexa Fluor® 594 azide) in a Cu(I) catalysed click reaction. The cells treated with **probe 1** showed an increase in fluorescence intensity in fluorescence imaging.

Initially, NTERA2 cells were treated with alkyne labelled nucleotide EdU, which is incorporated into the cell cycle.[114] This analysis provides a positive fluorescence signal to rule out any non-specific uptake of Alexa Fluor® 594 azide fluorophore during the click reaction, in fixed and permeabilised NTERA2 cells confirming the reliability of the experiment. Through qualitative analysis of **Figure.35**, where DMSO is used as a negative control, it is visually identifiable that there is no non-specific uptake of the Alexa Fluor® 594 azide. *The treatment of the NTERA2 cells with EdU was undertaken by the Andrews group. The treatment of the NTERA2 cells with DMSO and **probe 1** was undertaken by the Andrews group. Cell lysis, click chemistry and visualisation was undertaken by myself. (**Figure.35**).*

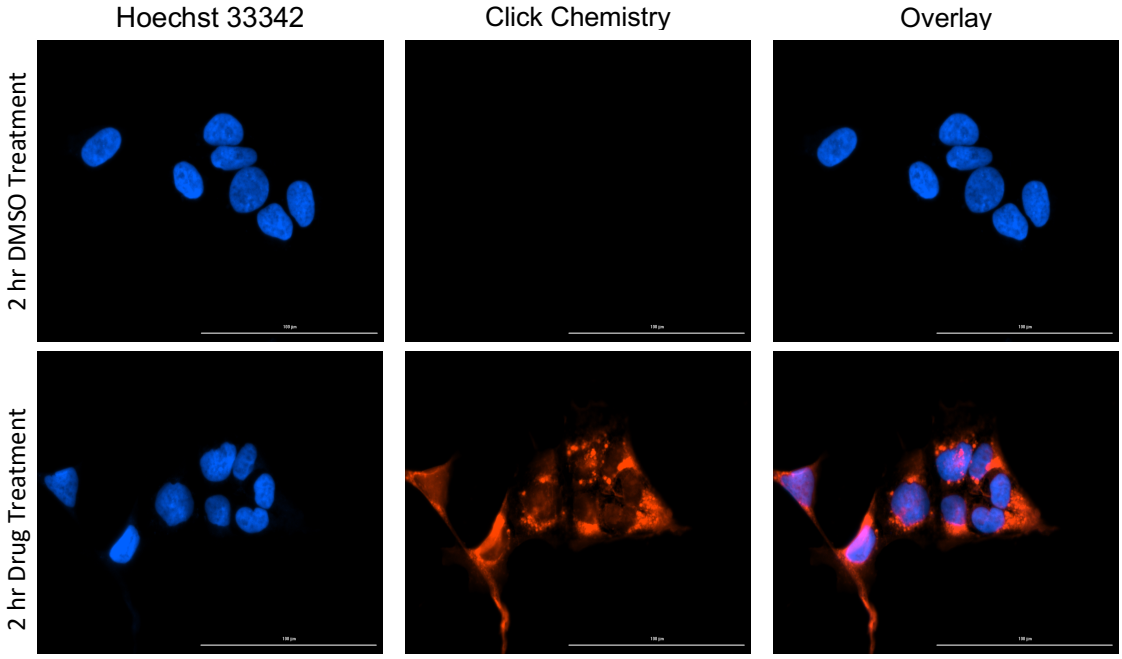

Figure.35 NTERA2 cells were treated for 2 hrs with DMSO and 500 μM of **probe 1** as a positive control. Visualised using Hoechst 33342 to stain the nucleus (Blue), Click Chemistry using AlexaFluor® 594 azide to fluoresce **probe 1** (Red).

For visualisation of the FAD cofactor of LSD1, **probe 1** must pass through the plasma membrane of the cell, and then through the nuclear membrane where the LSD1 forms complexes with DNA binding proteins. *The treatment of the NTERA2 cells with **probe 1** was undertaken by the Andrews group. Cell lysis, ICC, click chemistry and visualisation was undertaken by myself. (**Figure.36**)*

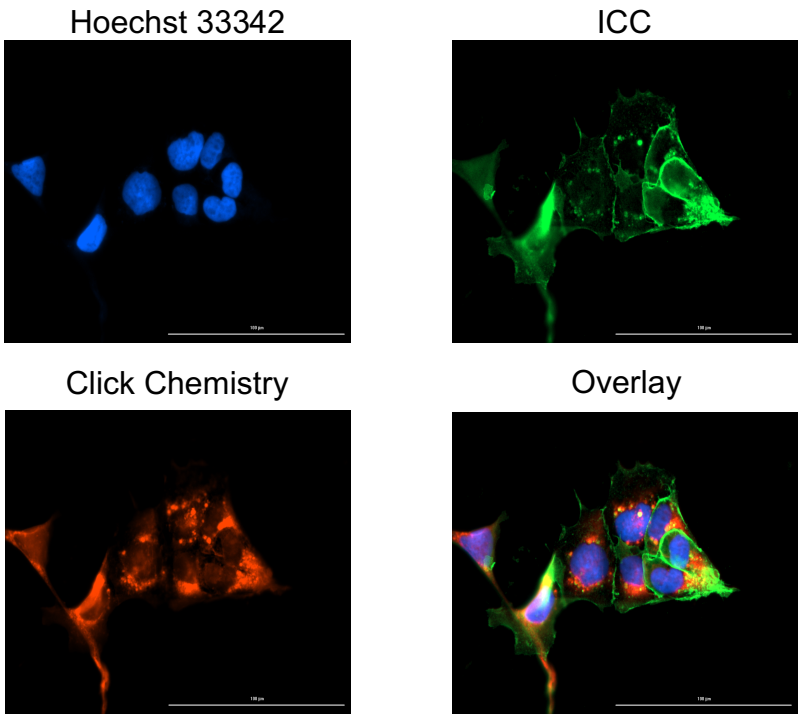

Figure.36 NTERA2 cells were treated for 2 hrs with 500 μM of **probe 1**. Visualised using Hoechst 33342 to stain the nucleus (Blue), ICC using TRA-1-85 to stain the membrane (Green), Click Chemistry using AlexaFluor® 594 azide to fluoresce **probe 1** (Red)

Treatment of NTERA2 cells with **probe 1** allows for visualisation of LSD1 through Cu(I) catalysed click reaction, with additional confirmation by immunocytochemistry (ICC) where a specific antibody is used to bind to the LSD1 enzyme only. This duel visualisation to ensure validation of the probes been able to be used for indication and location of the LSD1 enzyme in cells.[121,122] It is confirmed in **Figure.36** that the **probe 1** passes though the plasma membrane and the nuclear membrane by using TRA-1-85[123] to stain the membrane and visualised using FITC-488 (Green) channel. The probe underwent the click reaction with Alexa Fluor® 594 azide this was visualized with Texas Red-598 (Red) channel and is seen to be localised within the nucleus and peripheral areas of the NTERA2 cells, the nucleus is stained with Hoechst 33342 and visualized with the DAPI-405 (Blue) channel. Additionally, cross analysis between the

fluorescence **probe 1** and immunocytochemistry (ICC) of the LSD1 enzyme confirms that the probe is colocalizing with LSD1 in the nucleus. Similarly, using Texas Red-594 to identify fluorescent probe adduct and DAPI-405 (Blue) to identify the cell nucleus. ICC shows LSD1 enzyme in the NTERA2 cells, visualised by FITC-488 (Green) (**Figure.37**). *The treatment of the NTERA2 cells with **probe 1** was undertaken by the Andrews group. Cell lysis, ICC, click chemistry and visualisation was undertaken by myself. (**Figure.37, 38**)*

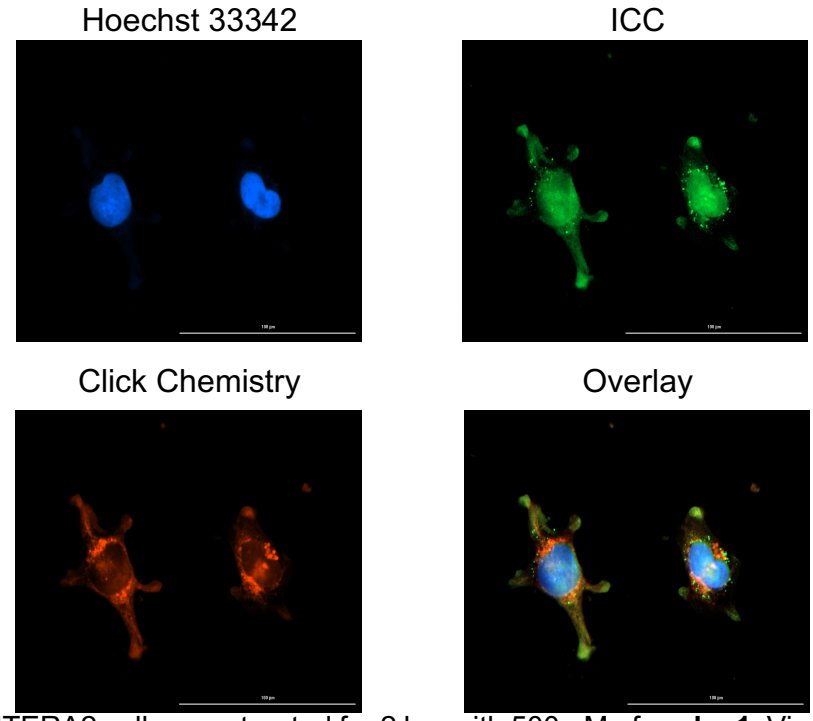

Figure.37 NTERA2 cells were treated for 2 hrs with 500 μM of **probe 1**. Visualised using Hoechst 33342 to stain the nucleus (Blue), ICC using TRA-1-85 to stain the membrane (Green), Click Chemistry using AlexaFluor® 594 azide to fluoresce **probe 1** (Red).

To investigate the effect of treatment time, the NTERA2 cells were treated with 500 μM of **probe 1** for two and six hours, to identity if an increase in time treatment time of **probe 1** leads to an increased visual inhibition of LSD1 enzyme. The NTERA2 cells were treated in the same manner as before, being treated with **probe 1**, fixed and permeabilised to allow for the click reaction to be undertaken. It can be seen in **Figure.38**, an increased treatment time of **probe 1**, from two – six hour, results in an increase of visual fluorescence of **probe 1**. Fluorescence of **probe 1** is achieved by the click reaction with Alexa Fluor® 594 azide, visualised with the Texas Red-598 channel.

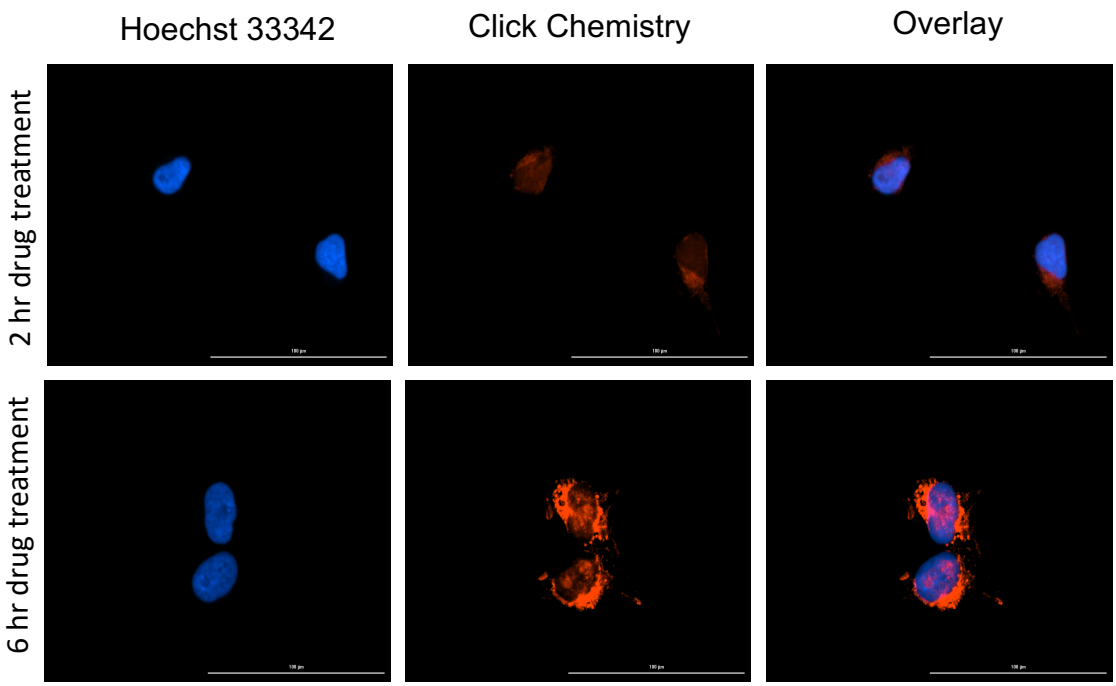

Figure.38 NTERA2 cells were treated for 2 and 6 hrs with 500 µM of **probe 1**. Visualised using Hoechst 33342 to stain the nucleus (Blue), Click Chemistry using AlexaFluor® 594 to fluoresce **probe 1** (Red).

The visualisation with the Texas Red-598 (red) channel shows an increase in non-nuclear fluorescence when treatment time is increased from two hour to six (**Figure.38**). It can be assumed that the accumulation of unreacted **probe 1** has accumulated in the cell vesicles which has reacted with the Alexa Fluor® 594 azide dye in the click reaction. In a model click reaction experiment using recombinant LSD1 enzyme, analysis of the adduct formed was achieved by MALDI-TOF MS. **Probe 1** was used to inhibit the FAD cofactor, which subsequently underwent a click reaction with Alexa Fluor® 594 azide to produce the FAD - **probe 1** - Alexa Fluor® 594 adduct.

A mass peak at 1818.5063 m/z was found which corresponded to the FAD - **probe 1** - Alexa Fluor® 594 adduct (calculated 1818.4879 m/z). This confirms the hypothesis that the adduct is successful produced during the visualisation of LSD1. Since **probe 1** is not highly selective towards LSD1, as previously discussed in section 2.2.3., identification of the expression rates of MAOs and LSD1 in the NTERA2 cells is required. To better understand the MAO isoforms in the NTERA2 cells at a mRNA or transcription level, qPCR was undertaken to

identify the mRNA of MAOs and LSD1. Of the MAO mRNA, 97% encoded LSD1, and 2% of the mRNA was other MAOs (**Figure.39**). *The qPCR work was undertaken by the Andrews group*. This implies that any effects of inhibition using **probe 1** can be attributed to the inhibition of LSD1.

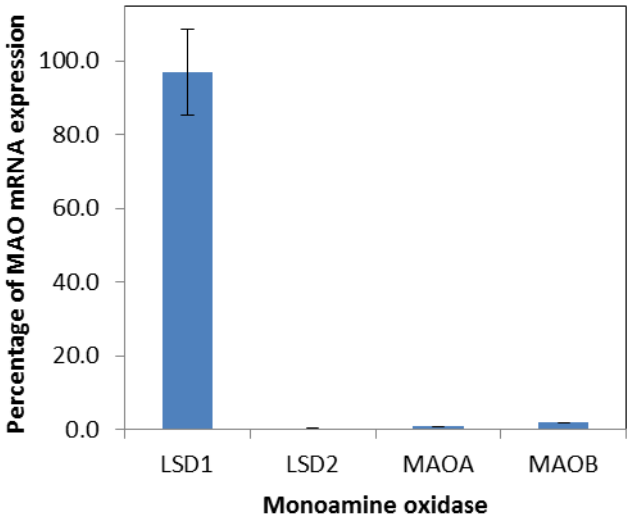

Figure.39 Percentage of MAO mRNA expression in NTERA2 cells, measured by qPCR

To confirm this at the translated protein level, the presence of the MAOA, MAOB and LSD1 was investigated using validated antibodies raised against these enzyme targets. NTERA2 cells were grown and each enzyme was probed individually by ICC, treated with the appropriate antigen and visualised using Texas Red-594 (Red) channel. The nucleus was stained with Hoechst 33342 and visualised with DAPI-405 (Blue) (**Figure.40**). From this, the ICC shows minimal fluorescence of MAOA and MAOB. The negative control also shows minimal fluorescence. This confirms that any fluorescence observed, is specific to the enzymes present in the NTERA2 cells. There was positive fluorescence for LSD1 and positive control H3, confirming along with the qPCR results that any visual inhibition of LSD1 by **probe 1** in the NTERA2 cells can be reasonably attributed to the presence of LSD1 in the NTERA2 cells.

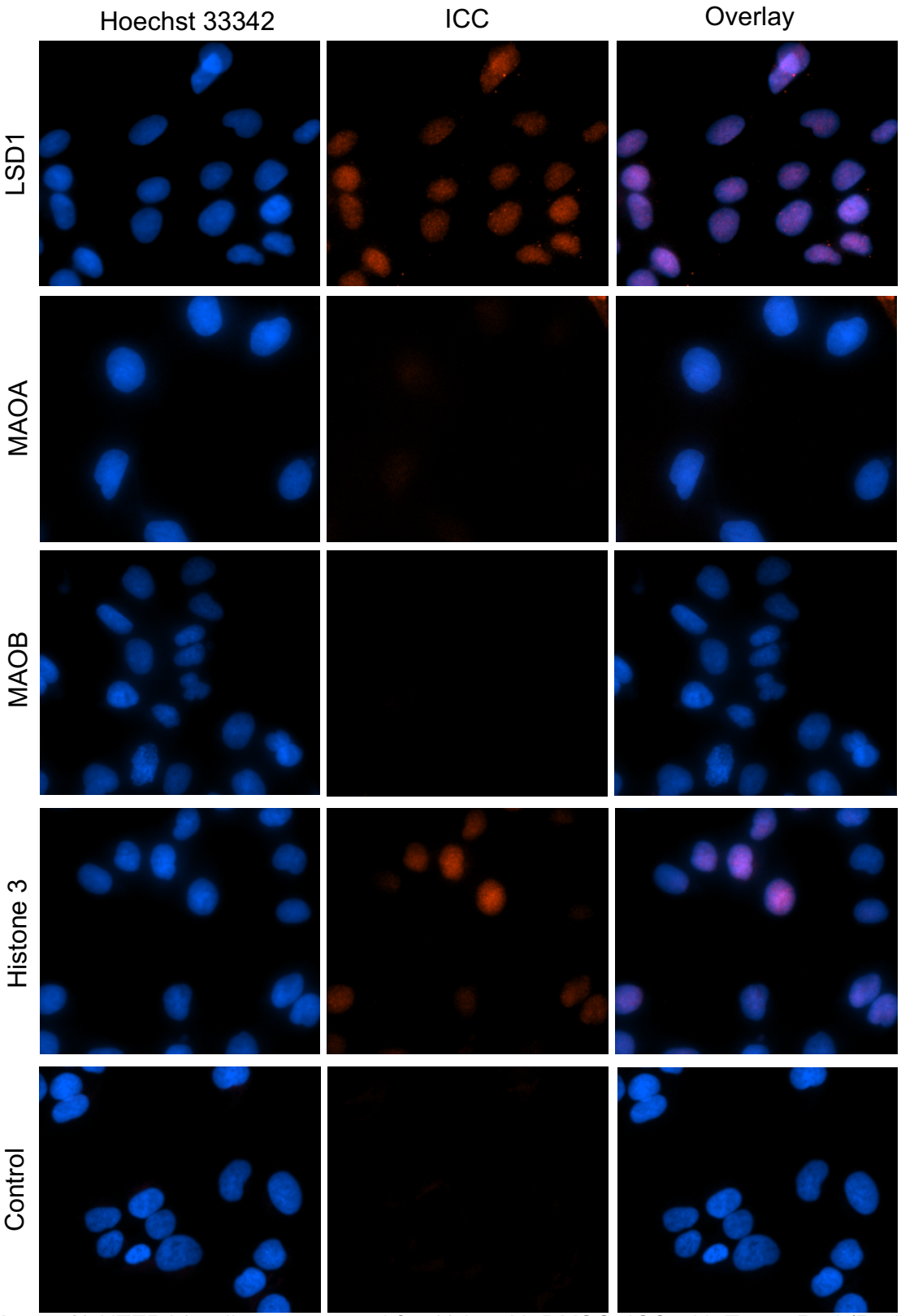

Figure.40 NTERA2 cells were treated for 18 hr with DMSO. ICC with Texas Red (Red) enables visualisation of enzymes **a.** LSD1, **b.** MAOA, **c.** MAOB, **d.** Histone 3, **e.** Control with Texas Red (Red). The nuclei were stained with Hoechst 33342 (Blue).

To confirm the visualisation of translated MAO enzymes by microscopy, cell lysates from the NTERA2 cells were analysed by western blot for MAOA, MAOB

and LSD1 enzymes (**Figure.41**). The western blots were investigated using validated antibodies raised against these enzyme targets where visual representation MAOA, MAOB and LSD1. The result from the NTERA2 cell lysates show a positive visualisation for LSD1 enzyme, and minimal fluoresce for MAO enzymes. Therefore, the Western blot confirmed the ICC results with minimal fluoresces for MAOA/B, and a positive fluorescence for LSD1.

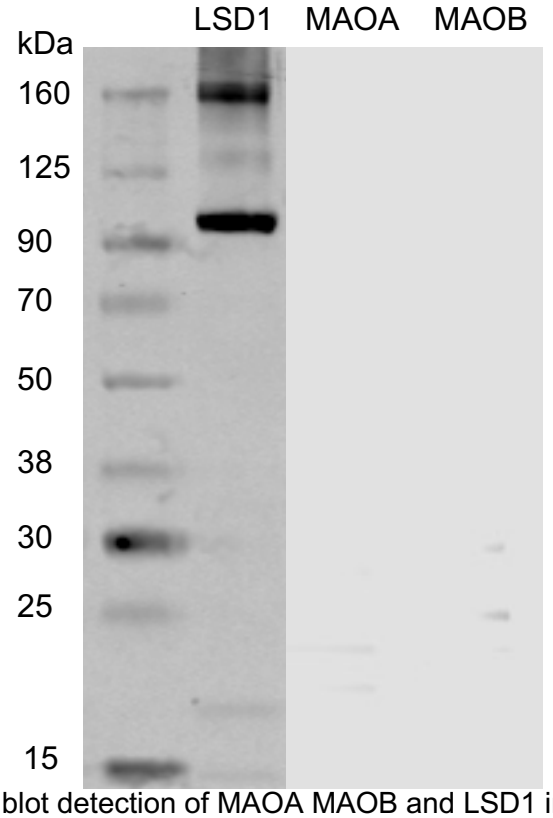

Figure.41 Western blot detection of MAOA MAOB and LSD1 in NTERA2 cells

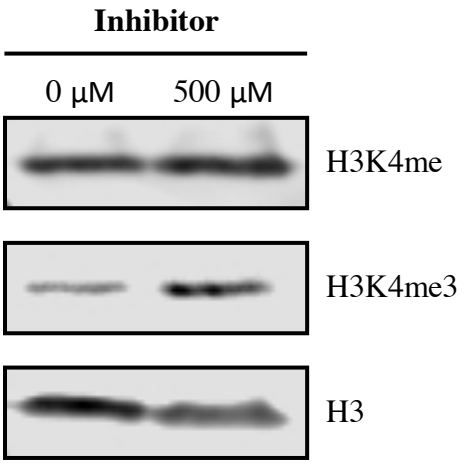

Figure.42 Western blot detection of H3K4me and H3K4me3 levels in NTERA2 cells after 18 hr incubation with **probe 1**.

For the inhibition of LSD1 by **probe 1** to influence gene regulation it must result in a change in epigenetic marks. It is expected that that the inhibition of LSD1 alters the methylation state of the H3K4, western blot analysis was used to identity the concentrations of H3K4me, H3K4me3, with H3 used as a loading control. NTERA2 cells were treated with no **probe 1** or 500 μM of **probe 1** and incubated for 18 hrs, the cells were lysed with RIPA buffer and analysed by western blot. As can be seen in **Figure.42**, there is little difference for H3K4me between untreated cells and treated cells. But upon comparison for the H3K4me3, there is a noticeable increase in fluoresces in the treated cells with **probe 1**. Additionally, the H3 loading control for the **probe 1** is less intense than the non-probe, making the difference in H3K4me3 fluorescence more intense. This concludes that **probe 1** inhibits the LSD1 enzyme, resulting in an increase in the tri-methylated state of the H3K4 protein in the cells. *The treatment of the NTERA2 cells with **probe 1** was undertaken by the Andrews group. Cell lysis, western blot and visualisation was undertaken by myself.*

2.5 Conclusion

A set of eight probes molecules were synthesised and characterised using appropriate analytical techniques. For all eight molecules their inhibitory effect against LSD1 and MAOs was investigated providing IC_{50} data. Alkyl-alkyne derived **probes 1** and **2** show decrease in selectivity towards LSD1 by five fold when compared to **PCPA**. But, **probe 1** showed decrease in selectivity towards MAOA and MAOB (two fold for each enzyme when compared to **PCPA**). Whereas **probe 2** showed the reverse, present an increase of eight fold towards MAOA and three fold towards MAOB. The same trend followed for alkyl-azide derived **probe 3** and **4**. Moreover, benzyl azide **probes 5 – 8** produced an overall increase in selectivity towards inhibiting all of the tested enzymes, with exceptions for **probe 6** inhibiting LSD1, which decreased the selectivity by almost two fold. **Probe 1**, one of the closest structural analogues to the PCPA scaffold, was developed as a lead in this work and the clinical candidate is currently undergoing clinical trials, and was chosen to undergo treatment of NTERA2 cells. The expression of MAO genes in the NTERA2 cell was investigated at mRNA and protein levels, highlighting that the only MAO enzyme present in detectable quantities is LSD1. The data collected shows that **probe 1** successfully passes through the cell membrane and inhibits LSD1. This was confirmed with

microscopy visualising outer cell membrane, nucleus and MAO enzymes with ICC. The *in-situ* visualisation of **probe 1** in cells using click chemistry allowed the detection of fluorescent signal in the cell nucleus and a small amount of non-nuclear fluoresce that increased with exposure time. In target based experiments the FAD - **probe 1** - Alexa Fluor® 594 adduct corresponding to the nuclear fluorescence and the **probe 1** - Alexa Fluor® 594 adduct corresponding to the non-nuclear fluorescence was identified by MALDI-TOF MS. Furthermore, the accumulation of H3K4me and H3K4me3 in NTERA2 was assessed by western blot analysis, where treatment with **probe 1** caused an increase in the accumulation of H3K4me3 in the cells. In summary, demonstrated for the first time is the development of PCPA with the alkyne or azide motif. This successfully inhibits the LSD1 enzyme and with click chemistry, enables a novel visualisation of LSD1 within NTERA2 cells.

2.6 Experimental

2.6.1 Materials and Methods

TLC: TLC Silica gel 60, F_{254}, Aluminium plate. **IR**: Bruker ALPHA, ATR stage (Diamond Crystal). **NMR**: Bruker AVANCE III 400 (^{1}HNMR; 400MHz, ^{13}CNMR; 100MHz) **MS**: Finnigan MAT, Electro Spray source, Flow Rate: 15 µL/min, Gas: Nitrogen. **HRMS:** Xevo G2-XS QTOF Mass Spectrometer. Electrospray (ES) ionisation source, Gas: Nitrogen, Temperature: Ramp heating Ambient – 300 °C over 7 mins. **UV/Vis:** CLARIOstar, BMG labtech, Excitation: λ 530-15, Emission: λ 580-20. **Melting Point:** Stuart SMP3. All chemicals used were bought from Sigma Aldrich, or Fisher Scientific. Dry DMSO (0.025% max H_2O) and THF (0.005% max H_2O) were purchased through Merck. Purification on silica were undertaken using Biotage Isolera One or Teledyne ISCO combiflash Rf systems. Human MAOA and Human MAOB were purchased though Sigma Aldrich with product codes of M7316 and M7441 respectively. Molecular grade DMSO was used in all enzyme assays.

2.6.2 Synthesis

methyl (*trans*)-3-(3-hydroxyphenyl)acrylate (34a)[76]

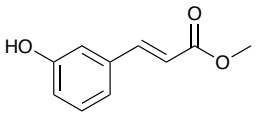

To (*trans*)-3-hydrocinnamic acid (50.0 g, 304 mmol) in methanol (162 mL) was added concentrated sulphuric acid (4 mL) and heated at reflux for 24 hr. The reaction mixture was condensed under reduced pressure and the white solid was dissolved in EtOAc (300 mL). The organic layer was washed with de-ionised water (4x100 mL), sat. $NaHCO_{3(aq)}$ (2x100 mL) and sat. $NaCl_{(aq)}$ (2x100 mL), dried with anhydrous $MgSO_4$ and condensed under reduced pressure to give 52.96 g (92%) of white amorphous solid.

IR (ν_{max}/cm^{-1}) 3015, 3007, 2955, 1685, 1530, 1160.

^{1}H NMR (400MHz, $CDCl_3$, 298 K) δ 7.66 (1 H, d, $^{3}J_{HH}$ = 16.0 Hz), 7.27 (1 H, dd, $^{3}J_{HH}$ = 7.7 Hz, $^{3}J_{HH}$ = 7.7 Hz), 7.10 (1 H, d, $^{3}J_{HH}$ = 7.7 Hz), 7.04 (1 H, m), 6.92 (1 H, d, $^{3}J_{HH}$ = 8.1 Hz), 6.42 (1 H, d, $^{3}J_{HH}$ = 16.0 Hz) 5.85 (1 H, s) 3.83 (3 H, s).

^{13}C {^{1}H} NMR (100MHz, $CDCl_3$, 298 K) δ 167.9, 156.2, 145.0, 135.8, 130.2, 120.8, 118.0, 117.7, 114.6, 52.0.

methyl (*trans*)-3-(4-hydroxyphenyl)acrylate (34b)[76]

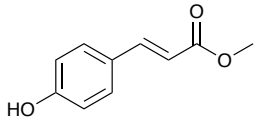

To (*trans*)-4-hydrocinnamic acid (50.00 g, 304 mmol) in methanol (162 mL) was added concentrated sulphuric acid (4 mL) and heated at reflux for 24 hr. The reaction mixture was condensed under reduced pressure and the white solid was dissolved in EtOAc (300 mL). The organic layer was washed with de-ionised water (4x100 mL), sat. $NaHCO_{3(aq)}$ (2x100 mL) and sat. $NaCl_{(aq)}$ (2x100 mL), dried with anhydrous $MgSO_4$ and condensed under reduced pressure to give 36.06 g (81 %) of brown amorphous solid.

IR (ν_{max}/cm^{-1}) 3030, 3005, 2952, 1683, 1432, 1167.

^{1}H NMR (400MHz, MeOD, 298 K) δ 7.63 (1 H, d, $^3J_{HH}$ = 16.1 Hz), 7.46 (2 H, d, $^3J_{HH}$ = 8.8 Hz), 6.82 (2 H, d, $^3J_{HH}$ = 8.8 Hz), 6.34 (1 H, d, $^3J_{HH}$ = 16.1 Hz), 3.77 (3 H, s).

^{13}C {^{1}H} NMR (100MHz, MeOD, 298 K) δ 169.8, 161.3, 146.6, 131.2, 127.2, 116.8, 114.9, 52.0.

methyl (*trans*)-3-(3-bromophenyl)acrylate (41a)[169]

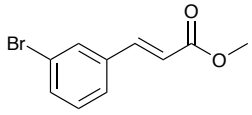

To (*trans*)-3-bromocinnamic acid (50.00 g, 304 mmol) in methanol (162 mL) was added concentrated sulphuric acid (4 mL) and heated at reflux for 24 hr. The reaction mixture was condensed under reduced pressure and the white solid was dissolved in EtOAc (300 mL). The organic layer was washed with de-ionised water (4x100 mL), sat. $NaHCO_{3(aq)}$ (2x100 mL) and sat. $NaCl_{(aq)}$ (2x100 mL), dried with anhydrous $MgSO_4$ and condensed under reduced pressure to give 49.10 g (92%) of white crystalline solid.

IR (ν_{max}/cm^{-1}) 3069, 3012, 2956, 1713, 1432, 1170.

^{1}H NMR (400MHz, $CDCl_3$, 298 K) δ 7.67 (1 H, s), 7.59 (1 H, d, $^3J_{HH}$ = 16.0 Hz), 7.51 (1 H, d, $^3J_{HH}$ = 7.9 Hz), 7.45 (1 H, d, $^3J_{HH}$ = 7.9 Hz), 7.26 (1 H, dd, $^3J_{HH}$ = 7.8 Hz, $^3J_{HH}$ = 7.8 Hz), 6.43 (1 H, d, $^3J_{HH}$ = 16.0 Hz), 3.82 (3 H, s).

^{13}C {^{1}H} NMR (100MHz, $CDCl_3$, 298 K) δ 167.0, 143.2, 136.5, 133.1, 130.8, 130.4, 126.7, 123.1, 119.4, 51.9.

methyl (*trans*)-3-(4-bromophenyl)acrylate (41b)[169]

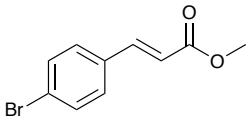

To (*trans*)-3-bromocinnamic acid (50.00 g, 304 mmol) in methanol (162 mL) was added concentrated sulphuric acid (4 mL) and heated at reflux for 24 hr. The reaction mixture was condensed under reduced pressure and the white solid was dissolved in EtOAc (300 mL). The organic layer was washed with de-ionised water (4x100 mL), sat. $NaHCO_{3(aq)}$ (2x100 mL) and sat. $NaCl_{(aq)}$ (2x100 mL), dried with anhydrous $MgSO_4$ and condensed under reduced pressure to give 49.18 g (92%) of white amorphous solid.

IR (ν_{max}/cm^{-1}) 3033, 2996, 2947, 2349, 1701, 1430, 1192.

^{1}H NMR (400MHz, $CDCl_3$, 298 K) δ 7.63 (1 H, d, $^3J_{HH}$ = 16.0 Hz), 7.53 (2 H, d, $^3J_{HH}$ = 8.4 Hz), 7.39 (2 H, d, $^3J_{HH}$ = 8.4 Hz), 6.44 (1 H, d, $^3J_{HH}$ = 16.0 Hz), 3.82 (3 H, s).

^{13}C {^{1}H} NMR (100MHz, $CDCl_3$, 298 K) δ 167.2, 143.5, 133.3, 132.2, 129.5, 124.6, 118.5, 51.9.

methyl (*trans*)-3-(3-(methoxymethoxy)phenyl)acrylate (35a)[76]

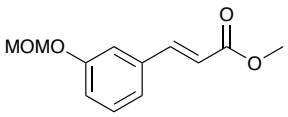

To methyl (*trans*)-3-(3-hydroxyphenyl)acrylate (55.3 g, 311 mmol) in acetone (500 mL) was added dry K_2CO_3 (107 g, 775 mmol), the solution was stirred at room temperature for 15 min. Then, MOMCl (25.0 g, 311 mmol) was added slowly. The reaction mixture was stirred at room temperature for 24 hr, filtered and condensed under reduced pressure. The white solid was dissolved in EtOAc (350 mL) was washed with sat. $NaHCO_{3(aq)}$ (2x100 mL), $NaOH_{(aq)}$ (2x100 mL, 2 M) and sat. $NaCl_{(aq)}$ (2x100 mL), dried with anhydrous $MgSO_4$ and condensed under reduced pressure to give 41.7 g (68%) of yellow oil.

IR (ν_{max}/cm^{-1}) 2951, 2904, 2827, 1712, 1487, 1148, 1006.

^{1}H NMR (400MHz, $CDCl_3$, 298 K) δ 7.67 (1 H, d, $^3J_{HH}$ = 17.0 Hz), 7.31 (1 H, dd, $^3J_{HH}$ = 8.5 Hz, $^3J_{HH}$ = 8.5 Hz), 7.22 – 7.17 (2 H, m), 7.08 (1 H, d, $^3J_{HH}$ = 8.2 Hz), 6.44 (1 H, d, $^3J_{HH}$ = 17.0 Hz), 5.20 (2 H, s), 3.81 (3 H, s), 3.49 (3 H, s).

^{13}C {^{1}H} NMR (100MHz, $CDCl_3$, 298 K) δ 167.4, 157.7, 144.6, 135.9, 130.0, 121.9, 118.3, 118.2, 115.5, 94.5, 56.1, 51.7.

methyl (*trans*)-3-(4-(methoxymethoxy)phenyl)acrylate (35b)[76]

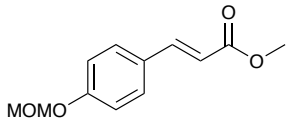

To methyl (*trans*)-3-(4-hydroxyphenyl)acrylate (49.0 g, 275 mmol) in acetone (500 mL) was added dry K_2CO_3 (95 g, 687 mmol), the solution was stirred at room temperature for 15 min. Then, MOMCl (25.0 g, 311 mmol) was added slowly. The reaction mixture was stirred at room temperature for 24 hr, filtered and condensed under reduced pressure. The white solid was dissolved in EtOAc (350 mL) was washed with sat. $NaHCO_{3(aq)}$ (2x100 mL), $NaOH_{(aq)}$ (2x100 mL, 2 M) and sat. $NaCl_{(aq)}$ (2x100 mL), dried with anhydrous $MgSO_4$ and condensed under reduced pressure to give 41.0 g (67%) of brown oil.

IR (ν_{max}/cm^{-1}) 2951, 2901, 2828, 1712, 1510, 1148.

^{1}H NMR (400MHz, $CDCl_3$, 298 K) δ 7.65 (1 H, d, $^3J_{HH}$ =16 Hz), 7.47 (2 H, d, $^3J_{HH}$ = 8.6 Hz), 7.04 (2 H, d, $^3J_{HH}$ = 8.7 Hz), 6.33 (1 H, d, $^3J_{HH}$ = 16 Hz), 5.20 (2 H, s), 3.79 (3 H, s), 3.47 (3 H, s).

^{13}C {^{1}H} NMR (100MHz, $CDCl_3$, 298 K) δ 167.7, 159.0, 144.5, 129.7, 128.2, 116.5, 115.8, 94.2, 56.2, 51.6.

methyl 2-(3-(methoxymethoxy)phenyl)cyclopropane-1-carboxylate (36a)[76]

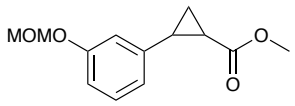

To a mixture of NaH (3.15 g, 79 mmol, 60 wt% in mineral oil) and trimethylsulfoxonium iodide (17.39 g, 79 mmol) was added dropwise dry DMSO (75 mL) with stirring at room temperature. The mixture was stirred at room temperature for 1 hr. A solution of methyl (*trans*)-3-(3-(methoxymethoxy)phenyl)acrylate (15.5 mL, 61 mmol) in dry DMSO (75 mL) was added. The mixture was stirred at room temperature for 3 hr, neutralised with citric $acid_{(aq)}$ (200 mL, 5%) and extracted with $CHCl_3$ (750 mL). The organic layer was washed with sat. $NaCl_{(aq)}$ (2x150 mL), dried with anhydrous $MgSO_4$ and condensed under reduced pressure and purified on silica (40 g), eluting with (EtOAc:hexane = 1:9) to give 4.80 g (33%) of clear oil.

IR (ν_{max}/cm^{-1}) 3010, 2964, 1723, 1428, 1170.

^{1}H NMR (400MHz, $CDCl_3$, 298 K) δ 7.20 (1 H, dd, $^3J_{HH}$ = 8.0 Hz, $^3J_{HH}$ = 8.0 Hz), 6.90 (1 H, d, $^3J_{HH}$ = 8.2 Hz), 6.79 (1 H, s), 6.75 (1 H, d, $^3J_{HH}$ = 7.7 Hz), 5.16 (2 H, s), 3.72 (3 H, s), 3.48 (3 H, s), 2.51 (1 H, ddd, $^3J_{HH}$ = 9.2 Hz, $^3J_{HH}$ = 6.5 Hz, $^3J_{HH}$ = 4.1 Hz), 1.92 (1 H, ddd, $^3J_{HH}$ = 8.4 Hz, $^3J_{HH}$ = 5.3 Hz, $^3J_{HH}$ = 4.2 Hz), 1.60 (1 H, ddd, $^3J_{HH}$ = 9.3 Hz, $^3J_{HH}$ = 5.2 Hz, $^2J_{HH}$ = 4.6 Hz), 1.33 (1 H, ddd, $^3J_{HH}$ = 8.4 Hz, $^3J_{HH}$ = 6.5 Hz, $^2J_{HH}$ = 4.6 Hz).

^{13}C {^{1}H} NMR (100MHz, $CDCl_3$, 298 K) δ 173.8, 157.5, 141.8, 129.6, 119.7, 114.4, 114.3, 94.4, 56.0, 51.9, 26.3, 24.0, 17.1.

methyl 2-(4-(methoxymethoxy)phenyl)cyclopropane-1-carboxylate (36b)[76]

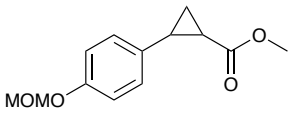

To a mixture of NaH (3.15 g, 79 mmol, 60 wt% in mineral oil) and trimethylsulfoxonium iodide (17.39 g, 79 mmol) was added dropwise dry DMSO (75 mL) with stirring at room temperature. The mixture was stirred at room temperature for 1 hr. A solution of methyl (*trans*)-3-(4-(methoxymethoxy)phenyl)acrylate (15.5 mL, 61 mmol) in dry DMSO (75 mL) was added. The mixture was stirred at room temperature for 3 hr, neutralised with citric $acid_{(aq)}$ (200 mL, 5%) and extracted with $CHCl_3$ (750 mL). The organic layer was washed with sat. $NaCl_{(aq)}$ (2x150 mL), dried with anhydrous $MgSO_4$ and condensed under reduced pressure and purified on silica (40 g), eluting with (EtOAc:hexane = 1:9) to give 3.45 g (24%) of clear oil.

IR (ν_{max}/cm^{-1}) 2994, 2942, 1712, 1436, 1165.

^{1}H NMR (400MHz, $CDCl_3$, 298 K) δ 7.04 (2 H, d, $^{3}J_{HH}$ = 8.7 Hz), 6.97 (2 H, d, $^{3}J_{HH}$ = 8.8 Hz), 5.15 (2 H, s), 3.72 (3 H, s), 3.47 (3 H, s), 2.50 (1 H, ddd, $^{3}J_{HH}$ = 9.2 Hz, $^{3}J_{HH}$ = 6.5 Hz, $^{3}J_{HH}$ = 4.1 Hz), 1.84 (1 H, ddd, $^{3}J_{HH}$ = 8.4 Hz, $^{3}J_{HH}$ = 5.2 Hz, $^{3}J_{HH}$ = 4.2 Hz), 1.57 (1 H, ddd, $^{3}J_{HH}$ = 9.3 Hz, $^{3}J_{HH}$ = 4.9 Hz, $^{2}J_{HH}$ = 4.7 Hz), 1.28 (1 H, ddd, $^{3}J_{HH}$ = 11.2 Hz, $^{3}J_{HH}$ = 7.5 Hz, $^{2}J_{HH}$ = 3.5 Hz).

^{13}C {^{1}H} NMR (100MHz, $CDCl_3$, 298 K) δ 174.0, 156.0, 133.3, 127.4, 116.4, 94.5, 56.0, 51.9, 25.8, 23.7, 16.8.

methyl 2-(3-bromophenyl)cyclopropane-1-carboxylate (42a)[117]

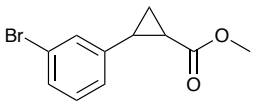

To a mixture of NaH (3.15 g, 79 mmol, 60 wt% in mineral oil) and trimethylsulfoxonium iodide (17.39 g, 79 mmol) was added dropwise dry DMSO (75 mL) with stirring at room temperature. The mixture was stirred at room temperature for 1 hr. A solution of methyl (*trans*)-3-(3-bromophenyl)acrylate (14.64 g, 61 mmol) in dry DMSO (75 mL) was added. The mixture was stirred at room temperature for 3 hr, neutralised with citric $acid_{(aq)}$ (200 mL, 5%) and extracted with $CHCl_3$ (750 mL). The organic layer was washed with sat. $NaCl_{(aq)}$ (2x150 mL), dried with anhydrous $MgSO_4$ and condensed under reduced pressure and purified on silica (40 g), eluting with (EtOAc:hexane = 1:9) to give 4.37 g (28%) of yellow oil.

IR (v_{max}/cm^{-1}) 3005, 2951, 1722, 1435, 1169.

^{1}H NMR (400MHz, $CDCl_3$, 298 K) δ 7.33 (1 H, d, $^3J_{HH}$ = 7.9 Hz), 7.24 (1 H, s), 7.14 (1 H, dd, $^3J_{HH}$ = 7.8 Hz, $^3J_{HH}$ = 7.8 Hz), 7.03 (1 H, d, $^3J_{HH}$ = 7.8 Hz), 3.73 (3 H, s), 2.49 (1 H, ddd, $^3J_{HH}$ = 9.2 Hz, $^3J_{HH}$ = 6.4 Hz, $^3J_{HH}$ = 4.1 Hz), 1.90 (1 H, ddd, $^3J_{HH}$ = 8.5 Hz, $^3J_{HH}$ = 5.4 Hz, $^3J_{HH}$ = 4.2 Hz), 1.61 (1 H, ddd, $^3J_{HH}$ = 9.2 Hz, $^3J_{HH}$ = 5.3 Hz, $^2J_{HH}$ = 4.8 Hz), 1.31 (1 H, ddd, $^3J_{HH}$ = 8.5 Hz, $^3J_{HH}$ = 6.5 Hz, $^2J_{HH}$ = 4.7 Hz).

^{13}C {^{1}H} NMR (100MHz, $CDCl_3$, 298 K) δ 173.5, 142.4, 130.0, 129.7, 129.4, 125.1, 122.6, 52.1, 25.7, 24.0, 17.0.

methyl 2-(4-bromophenyl)cyclopropane-1-carboxylate (42b)[117]

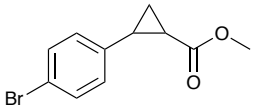

To a mixture of NaH (3.15 g, 79 mmol, 60 wt% in mineral oil) and trimethylsulfoxonium iodide (17.39 g, 79 mmol) was added dropwise dry DMSO (75 mL) with stirring at room temperature. The mixture was stirred at room temperature for 1 hr. A solution of methyl (*trans*)-3-(4-bromophenyl)acrylate (14.64 g, 61 mmol) in dry DMSO (75 mL) was added. The mixture was stirred at room temperature for 3 hr, neutralised with citric $acid_{(aq)}$ (200 mL, 5%) and extracted with $CHCl_3$ (750 mL). The organic layer was washed with sat. $NaCl_{(aq)}$ (2x150 mL), dried with anhydrous $MgSO_4$ and condensed under reduced pressure and purified on silica (40 g), eluting with (EtOAc:hexane = 1:9) to give 1.2 g (8%) of yellow oil.

IR (v_{max}/cm^{-1}) 3005, 2950, 1435, 1721, 1186.

^{1}H NMR (400MHz, $CDCl_3$, 298 K) δ 7.40 (2 H, d, $^3J_{HH}$ = 8.5 Hz), 6.97 (2 H, d, $^3J_{HH}$ = 8.4 Hz), 3.73 (3 H, s), 2.49 (1H, ddd, $^3J_{HH}$ = 9.2 Hz, $^3J_{HH}$ = 6.5 Hz, $^3J_{HH}$ = 4.2 Hz), 1.88 (1 H, ddd, $^3J_{HH}$ = 8.5 Hz, $^3J_{HH}$ = 4.2 Hz, $^3J_{HH}$ = 5.3 Hz), 1.62 (1 H, ddd, $^3J_{HH}$ = 11.6 Hz, $^3J_{HH}$ = 7.3 Hz, $^2J_{HH}$ = 4.7 Hz), 1.29 (1 H, ddd, $^3J_{HH}$ = 8.4 Hz, $^3J_{HH}$ = 6.5 Hz, $^2J_{HH}$ = 4.7 Hz).

^{13}C {^{1}H} NMR (100MHz, $CDCl_3$, 298 K) δ 173.6, 139.1, 131.6, 128.0, 120.2, 52.0, 25.7, 24.0, 17.0.

2-(3-(methoxymethoxy)phenyl)cyclopropane-1-carboxylic acid (37a)[76]

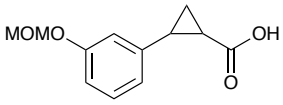

A solution of methyl 2-(3-(methoxymethoxy)-phenyl)cyclopropane-1-carboxylate (4.80 g, 20.33 mmol) in MeOH (60 mL) was added to KOH (14.83 g, 265 mmol) in MeOH (120 mL) at 0 °C. The reaction mixture was stirred for 72 hr at room temperature. The solvent

was removed under reduced pressure, re-dissolved in de-ionised water (130 mL) and washed with DCM (100 mL). The aqueous layer was adjusted to pH 4 with $HCl_{(aq)}$ (1.5 M) and extracted with DCM (3x100 mL). The combined DCM fractions were condensed under reduced pressure, giving 4.47 g (99%) of white amorphous solid.

IR (ν_{max}/cm^{-1}) 2870, 2957, 2901, 1679, 1461, 1219.

^{1}H NMR (400MHz, $CDCl_3$, 298 K) δ 10.05 (1 H, s), 7.21 (1 H, dd, $^3J_{HH}$ = 8.0 Hz, $^3J_{HH}$ = 8.0 Hz), 6.91 (1 H, m), 6.81 (1 H, s), 6.77 (1 H, d, $^3J_{HH}$ = 7.8 Hz), 5.18 (2 H, s), 3.49 (3 H, s), 2.59 (1 H, ddd, $^3J_{HH}$ = 9.2 Hz, $^3J_{HH}$ = 6.6 Hz, $^3J_{HH}$ = 4.0 Hz), 1.92 (1 H, ddd, $^3J_{HH}$ = 8.4 Hz, $^3J_{HH}$ = 5.2 Hz, $^3J_{HH}$ = 4.1 Hz), 1.67 (1 H, ddd, $^3J_{HH}$ = 11.5 Hz, $^3J_{HH}$ = 6.8 Hz, $^2J_{HH}$ = 6.8 Hz), 1.41 (1 H, ddd, $^3J_{HH}$ = 8.3 Hz, $^2J_{HH}$ = 6.6 Hz, $^3J_{HH}$ = 4.6 Hz).

^{13}C {^{1}H} NMR (100MHz, $CDCl_3$, 298 K) δ 179.7, 157.5, 141.3, 129.6, 119.8, 114.5, 114.4, 94.4, 56.0, 27.1, 24.1, 17.6.

2-(4-(methoxymethoxy)phenyl)cyclopropane-1-carboxylic acid (37b)[76]

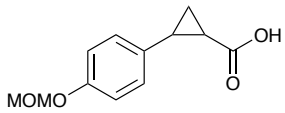

A solution of methyl 2-(4-(methoxymethoxy)-phenyl)cyclopropane-1-carboxylate (3.45 g, 14.61 mmol) in MeOH (60 mL) was added to KOH (10.64 g, 190 mmol) in MeOH (120 mL) at 0 °C. The reaction mixture was stirred for 72 hr at room temperature. The solvent was removed under reduced pressure, re-dissolved in de-ionised water (130 mL) and washed with DCM (100 mL). The aqueous layer was adjusted to pH 4 with $HCl_{(aq)}$ (1.5 M) and extracted with DCM (3x100 mL). The combined DCM fractions were condensed under reduced pressure, giving 2.99 g (92%) of white amorphous solid.

IR (ν_{max}/cm^{-1}) 2840, 2955, 2894, 1683, 1453, 1227.

^{1}H NMR (400MHz, $CDCl_3$, 298 K) δ 7.05 (2 H, d, $^3J_{HH}$ = 8.7 Hz), 6.97 (2 H, d, $^3J_{HH}$ = 8.8 Hz), 5.16 (2 H, s), 3.48 (3 H, s), 2.57 (1 H, ddd, $^3J_{HH}$ = 9.3 Hz, $^3J_{HH}$ = 6.6 Hz, $^3J_{HH}$ = 4.0 Hz), 1.84 (1 H, ddd, $^3J_{HH}$ = 8.3 Hz, $^3J_{HH}$ = 5.0 Hz, $^3J_{HH}$ = 4.1 Hz), 1.63 (1 H, ddd, $^3J_{HH}$ = 9.4 Hz, $^3J_{HH}$ = 4.7 Hz, $^2J_{HH}$ = 4.7 Hz), 1.36 (1 H, ddd, $^3J_{HH}$ = 8.3 Hz, $^3J_{HH}$ = 6.7 Hz, $^2J_{HH}$ = 4.6 Hz).

^{13}C {^{1}H} NMR (100MHz, $CDCl_3$, 298 K) δ 178.8, 156.1, 132.9, 127.5, 116.4, 94.5, 56.0, 26.6, 23.6, 17.3.

2-(3-bromophenyl)cyclopropane-1-carboxylic acid (43a)[117]

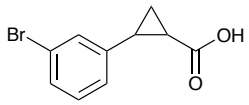

A solution of methyl 2-(3-bromophenyl)cyclopropane-1-carboxylate (4.37 g, 17.2 mmol) in MeOH (60 mL) was added to KOH (12.52 g, 224 mmol) in MeOH (120 mL) at 0 °C. The reaction mixture was stirred for 72 hr at room temperature. The solvent was removed under reduced pressure, re-dissolved in de-ionised water (130 mL) and washed with DCM (100 mL). The aqueous layer was adjusted to pH 2 with $HCl_{(aq)}$ (1.5 M) and extracted with DCM (3x100 mL). The combined DCM fractions were condensed under reduced pressure, giving 3.86 g (86%) of white crystalline solid.

IR (ν_{max}/cm^{-1}) 2862, 2956, 2911, 1503, 1674, 1222.

^{1}H NMR (400MHz, $CDCl_3$, 298 K) δ 7.36 (1 H, d, $^3J_{HH}$ = 7.9 Hz), 7.26 (1 H, s), 7.16 (1 H, dd, $^3J_{HH}$ = 7.8 Hz, $^3J_{HH}$ = 7.8 Hz), 7.05 (1 H, d, $^3J_{HH}$ = 7.8 Hz), 2.57 (1 H, ddd, $^3J_{HH}$ = 9.3 Hz, $^3J_{HH}$ = 6.5 Hz, $^3J_{HH}$ = 4.1 Hz), 1.91 (1 H, ddd, $^3J_{HH}$ = 8.5 Hz, $^3J_{HH}$ = 5.2 Hz, $^3J_{HH}$ = 4.1 Hz), 1.67 (1 H, ddd, $^3J_{HH}$ = 9.3 Hz, $^3J_{HH}$ = 5.0 Hz, $^2J_{HH}$ = 5.0 Hz), 1.40 (1 H, ddd, $^3J_{HH}$ = 8.4 Hz, $^3J_{HH}$ = 6.6 Hz, $^2J_{HH}$ = 4.8 Hz).

^{13}C {^{1}H} NMR (100MHz, $CDCl_3$, 298 K) δ 178.9, 141.9, 130.0, 129.9, 129.4, 125.1, 122.7, 26.5, 23.9, 17.4.

2-(4-bromophenyl)cyclopropane-1-carboxylic acid (43b)[117]

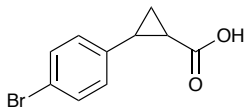

A solution of methyl 2-(4-bromophenyl)cyclopropane-1-carboxylate (1.20 g, 4.72 mmol) in MeOH (20 mL) was added to KOH (3.44 g, 61 mmol) in MeOH (40 mL) at 0 °C. The reaction mixture was stirred for 72 hr at room temperature. The solvent was removed under reduced pressure, re-dissolved in de-ionised water (130 mL) and washed with DCM (100 mL). The aqueous layer was adjusted to pH 2 with $HCl_{(aq)}$ (1.5 M) and extracted with DCM (3x100 mL). The combined DCM fractions were condensed under reduced pressure, giving 0.97 g (86%) of white crystalline solid.

IR (ν_{max}/cm^{-1}) 2760, 2902, 2831, 1675, 1456, 1236.

^{1}H NMR (400MHz, $CDCl_3$, 298 K) δ 7.42 (2 H, d, $^3J_{HH}$ = 8.4 Hz), 6.99 (2 H, d, $^3J_{HH}$ = 8.4 Hz), 2.56 (1 H, ddd, $^3J_{HH}$ = 9.6 Hz, $^3J_{HH}$ = 6.2 Hz, $^3J_{HH}$ = 3.7 Hz), 1.88 (1 H, ddd, $^3J_{HH}$ = 7.5 Hz, $^3J_{HH}$ = 5.5 Hz, $^3J_{HH}$ = 3.4 Hz), 1.67 (1 H, ddd, $^3J_{HH}$ = 9.4 Hz, $^3J_{HH}$ = 4.8 Hz, $^2J_{HH}$ = 4.8 Hz), 1.38 (1 H, ddd, $^3J_{HH}$ = 8.4 Hz, $^3J_{HH}$ = 6.6 Hz, $^2J_{HH}$ = 4.7 Hz).

^{13}C {^{1}H} NMR (100MHz, $CDCl_3$, 298 K) δ 179.0, 138.6, 131.6, 128.1, 120.5, 26.5, 23.9, 17.5.

***tert*-butyl (2-(3-(methoxymethoxy)phenyl)cyclopropyl)carbamate (38a)**[76]

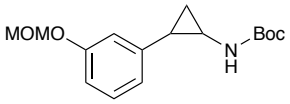

To a solution of 2-(3-(methoxymethoxy)phenyl)-cyclopropane-1-carboxylic acid (4.47 g, 20.13 mmol) in cyclohexane (220 mL) was added DPPA (4.76 mL, 22.14 mmol) and triethylamine (3.37 mL, 24.15 mmol) protected by a N_2 atmosphere. The reaction mixture was refluxed for 4 hr, dry *t*-BuOH (38.2 mL, 403 mmol) was added and refluxed for 14 hr. The reaction was cooled and the solvent removed under reduced pressure. The product was purified on silica (40 g), eluting with (EtOAc:hexane = 1:7) to give 4.35 g (74%) of white amorphous solid.

IR (ν_{max}/cm^{-1}) 3366, 2972, 2950, 1682, 1512, 1147, 1024.

^{1}H NMR (400MHz, $CDCl_3$, 298 K) δ 7.18 (1 H, dd, $^3J_{HH}$ = 8.2 Hz, $^3J_{HH}$ = 8.2 Hz), 6.85 (1 H, m), 6.81 – 6.77 (2 H, m), 5.16 (2 H, s), 4.85 (1 H, s), 3.48 (3 H, s), 2.75 (1 H, s), 2.01 (1 H, ddd, $^3J_{HH}$ = 9.3 Hz, $^3J_{HH}$ = 6.5 Hz, $^3J_{HH}$ = 3.0 Hz), 1.46 (9 H, s), 1.17 (2 H, m).

^{13}C {^{1}H} NMR (100MHz, $CDCl_3$, 298 K) δ 157.4, 142.9, 142.6, 129.4, 120.0, 114.4, 113.7, 94.4, 82.8 56.0, 32.6, 28.5, 24.8, 16.7.

MS (ESI+) $[M+H]^+$ (%) 294.2 (100)

HRMS (ESI+) calcd from $C_{16}H_{24}NO_4$ $[M+H]^+$: 294.1705; found 294.1692.

***tert*-butyl (2-(4-(methoxymethoxy)phenyl)cyclopropyl)carbamate (38b)**[76]

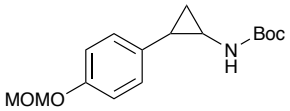

To a solution of 2-(4-(methoxymethoxy)phenyl)-cyclopropane-1-carboxylic acid (2.99 g, 13.46 mmol) in cyclohexane (140 mL) was added DPPA (3.18 mL, 14.81 mmol) and triethylamine (2.25 mL, 16.15 mmol) protected by a N_2 atmosphere. The reaction mixture was refluxed for 4 hr, dry *t*-BuOH (25.5 mL, 269 mmol) was added and refluxed for 14 hr. The reaction was cooled and the solvent removed under reduced pressure. The product was purified on silica (40 g), eluting with (EtOAc:hexane = 1:7) to give 2.90 g (74%) of white amorphous solid.

IR (ν_{max}/cm^{-1}) 3369, 2984, 2927, 1687, 1509, 1148, 1011.

^{1}H NMR (400MHz, $CDCl_3$, 298 K) δ 7.08 (2 H, d, $^3J_{HH}$ = 9.1 Hz), 6.95 (2 H, d, $^3J_{HH}$ = 8.4 Hz), 5.15 (2 H, s), 4.88 (1 H, s), 3.47 (3 H, s), 2.66 (1 H, s), 2.00 (1 H, ddd, $^3J_{HH}$ = 9.3 Hz, $^3J_{HH}$ = 6.5 Hz, $^3J_{HH}$ = 3.0 Hz), 1.46 (9 H, s) 1.11 (2 H, m).

^{13}C {^{1}H} NMR (100MHz, $CDCl_3$, 298 K) δ 156.4, 155.6, 134.1, 127.8, 116.3, 94.6, 79.6, 55.9, 32.2, 28.4, 24.4, 16.0.

MS (ESI+) $[M+H]^+$ (%) 294.2 (100)**.**

HRMS (ESI+) calcd from $C_{16}H_{24}NO_4$ $[M+H]^+$: 294.1705; found 294.1683.

***tert*-butyl (2-(3-bromophenyl)cyclopropyl)carbamate (44a)**[117]

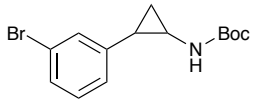

To a solution of 2-(3-bromophenyl)cyclopropane-1-carboxylic acid (1.35 g, 5.63 mmol) in cyclohexane (70 mL) was added DPPA (1.33 mL, 6.19 mmol) and triethylamine (0.94 mL, 6.76 mmol) protected by a N_2 atmosphere. The reaction mixture was refluxed for 4 hr, dry *t*-BuOH (10.7 mL, 113 mmol) was added and refluxed for 14 hr. The reaction was cooled and the solvent removed under reduced pressure. The product was purified on silica (40 g), eluting with (EtOAc:hexane = 1:7) to give 1.23 g (70%) of white amorphous solid.

IR (v_{max}/cm^{-1}) 3370, 2973, 2934, 1683, 1511, 1160, 1029.

^{1}H NMR (400MHz, $CDCl_3$, 298 K) δ 7.31 – 7.27 (2 H, m), 7.15 – 7.07 (2 H, m), 4.84 (1 H, s), 2.72 (1 H, s), 2.02 (1 H, m), 1.46 (9 H, s), 1.16 (2 H, m).

^{13}C {^{1}H} NMR (100MHz, $CDCl_3$, 298 K) δ 159.0, 143.2, 129.9, 129.6, 129.2, 125.3, 122.5, 80.0, 32.6, 28.4, 24.8, 16.3.

MS (ESI+) $[M+H]^+$ (%) 312.1 (100).

HRMS(ESI+) calcd from $C_{14}H_{19}BrNO_2$ $[M+H]^+$; 312.0599 found 312.0632.

***tert*-butyl (2-(4-bromophenyl)cyclopropyl)carbamate (44b)**[117]

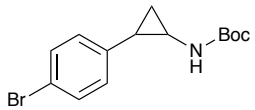

To a solution of 2-(4-bromophenyl)cyclopropane-1-carboxylic acid (0.97 g, 4.04 mmol) in cyclohexane (50 mL) was added DPPA (0.96 mL, 4.44 mmol) and triethylamine (0.68 mL, 4.85 mmol) protected by a N_2 atmosphere. The reaction mixture was refluxed for 4 hr, dry *t*-BuOH (7.7 mL, 81 mmol) was added and refluxed for 14 hr. The reaction was cooled and the solvent removed under reduced pressure. The product was purified on silica (40 g), eluting with (EtOAc:hexane = 1:7) to give 0.92 g (74%) of white amorphous solid.

IR (v_{max}/cm^{-1}) 3359, 2979, 2933, 1679, 1505, 1154, 1027.

^{1}H NMR (400MHz, $CDCl_3$, 298 K) δ 7.38 (2 H, d, $^3J_{HH}$ = 8.4 Hz), 7.02 (2 H, d, $^3J_{HH}$ = 8.1 Hz), 4.82 (1 H, s), 2.68 (1 H, s), 2.01 (1 H, m), 1.46 (9 H, s), 1.15 (2 H, m).

MS (ESI+) $[M+H]^+$ (%) 312.1 (100).

HRMS(ESI+) calcd from $C_{14}H_{19}BrNO_2$ $[M+H]^+$; 312.0599 found 312.0656.

***tert*-butyl (2-(3-hydroxyphenyl)cyclopropyl)carbamate (39a)**[76]

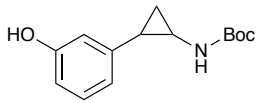

To solution of tert-butyl (2-(3-(methoxymethoxy)-phenyl)cyclopropyl)carbamate (4.35 g, 14.85 mmol) in DCM (87 mL) was added 4 M HCl in dioxane (87 mL, 23.88 mmol) and stirred for 2 hr at room temperature**.** The solvent was removed under reduced pressure, the residue was dissolved in de-ionised water (50 mL) and dioxane (50 mL). To the solution Et_3N (24.8 mL, 178 mmol) and Boc_2O (5.44 mL, 23.7 mmol) were added and the reaction was stirred for 17 hr. The reaction mixture was neutralised with citric $acid_{(aq)}$ (150 mL, 5%) and extracted with EtOAc (4x100 mL). The combined organic layer was washed with sat. $NaCl_{(aq)}$ (2x100 mL), dried with anhydrous $MgSO_4$ and condensed under reduced pressure. The crude oil was purified on silica (40 g), eluting with (EtOAc:hexane = 1:4) which gave 1.61 g (44%) of yellow oil.

IR (v_{max}/cm^{-1}) 3432, 2992, 2906, 1684, 1494, 1157.

^{1}H NMR (400MHz, $CDCl_3$, 298 K) δ 7.08 (1 H, dd, $^3J_{HH}$ = 8.2 Hz, $^3J_{HH}$ = 8.2 Hz), 6.68 – 6.63 (2H, m), 6.57 (1 H, s), 4.95 (1 H, s), 2.72 (1 H, s), 1.97 (1 H, s), 1.47 (9 H, s), 1.13 (2 H, m).

^{13}C {^{1}H} NMR (100MHz, $CDCl_3$, 298 K) δ 156.9, 142.6, 129.4, 120.5, 118.5, 115.5, 113.3, 113.1, 32.5, 28.5, 25.1, 16.7.

***tert*-butyl (2-(4-hydroxyphenyl)cyclopropyl)carbamate (39b)**[76]

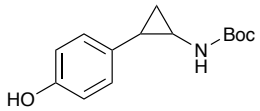

To solution of tert-butyl (2-(4-(methoxymethoxy)-phenyl)cyclopropyl)carbamate (2.00 g, 6.85 mmol) in DCM (44 mL) was added 4 M HCl in dioxane (44 mL, 11.5 mmol) and stirred for 2 hr at room temperature**.** The solvent was removed under reduced pressure, the residue was dissolved in de-ionised water (25 mL) and dioxane (25 mL). To the solution Et_3N (11.5 mL, 82 mmol) and Boc_2O (2.52 mL, 11 mmol) were added and the reaction was stirred for 17 hr. The reaction mixture was neutralised with citric $acid_{(aq)}$ (150 mL, 5%) and extracted with EtOAc (4x100 mL). The combined organic layer was washed with sat. $NaCl_{(aq)}$ (2x100 mL), dried with anhydrous $MgSO_4$ and condensed under reduced pressure. The crude oil was purified on silica (40 g), eluting with (EtOAc:hexane = 1:4) which gave 1.17 g (46%) of brown oil.

IR (v_{max}/cm^{-1}) 3437, 2980, 2912, 1650, 1503, 1143, 1012.

^{1}H NMR (400MHz, $CDCl_3$, 298 K) δ 6.95 (2H, d, $^3J_{HH}$ = 8.1 Hz), 6.71 (2 H, d, $^3J_{HH}$ = 8.1 Hz), 6.16 (1H, s), 4.89 (1 H, s), 2.66 (1 H, s), 1.98 (1 H, m), 1.47 (9 H, s), 1.08 (2 H, m).

^{13}C {^{1}H} NMR (100MHz, $CDCl_3$, 298 K) δ 154.5, 134.1, 131.0, 129.9, 127.7, 115.3, 32.2, 28.4, 24.5, 15.8.

***tert*-butyl (2-(3-(prop-2-yn-1-yloxy)phenyl)cyclopropyl)carbamate (45a)**

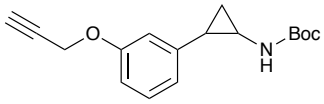

To *tert*-butyl (2-(3-hydroxyphenyl)cyclopropyl) carbamate (1500 mg, 6.02 mmol), $P(Ph)_3$ (2600 mg , 9.93 mmol) in dry THF (18.0 mL) was added propagyl alcohol (0.77 mL, 13.25 mmol) and protect by an N_2 atmosphere at 0 °C. DIAD (1.95 mL, 9.93 mmol) in dry THF (9.0 mL) was added dropwise and stirred for 4 hr at 0 ˚C and allowed to warm to room temperature and left overnight. The solvent was removed under reduced pressure and the residue was purified on silica (40 g), eluting with (EtOAc:n-Hexane 1:4) to give 1180 mg (68%) of white amorphous solid.

IR (v_{max}/cm^{-1}) 3372, 3272, 2981, 2934, 2134, 1680, 1510, 1152, 1040.

^{1}H NMR (400MHz, $CDCl_3$, 298 K) δ 7.18 (1 H, dd, $^3J_{HH}$ = 8.0 Hz, $^3J_{HH}$ = 8.0 Hz), 6.80 – 6.71 (3 H, m), 4.97 (1 H, s), 4.66 (2 H, d, $^4J_{HH}$ = 2.3 Hz), 2.73 (1 H, s), 2.52 (1 H, t, $^4J_{HH}$ = 2.5 Hz), 2.00 (1 H, m), 1.45 (9 H, s), 1.15 (2 H, m).

^{13}C {^{1}H} NMR (100MHz, $CDCl_3$, 298 K) δ 157.6, 156.3, 142.7, 129.3, 119.8, 113.2, 112.2, 79.6, 78.7, 75.5, 55.8, 32.6, 28.4, 24.9, 16.6.

MS (ESI+) $[M+H]^+$ (%) 288.2 (100).

HRMS(ESI+) calcd from $C_{17}H_{22}NO_3$ $[M+H]^+$: 288.1600; found 288.1579.

***tert*-butyl (2-(4-(prop-2-yn-1-yloxy)phenyl)cyclopropyl)carbamate (45b)**

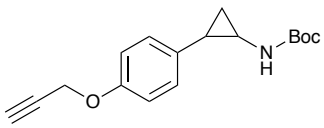

To *tert*-butyl (2-(4-hydroxyphenyl)cyclopropyl) carbamate (160 mg, 0.64 mmol), $P(Ph)_3$ (432 mg , 1.37 mmol) in dry THF (5.0 mL) was added propagyl alcohol (0.11 mL, 1.83 mmol) was added and protect by an N_2 atmosphere at 0 °C. DIAD (0.27 mL, 1.37 mmol) in dry THF (2.0 mL) was added dropwise and stirred for 4 hr at 0 °C and allowed to warm to room temperature and left overnight. The solvent was removed under reduced pressure and the residue was purified on silica (40 g), eluting with (EtOAc:n-Hexane 1:4) to give 121 mg (66%) of white amorphous solid.

IR (v_{max}/cm^{-1}) 3374, 3259, 3009, 2984, 2115, 1675, 1162, 1027.

^{1}H NMR (400MHz, $CDCl_3$, 298 K) δ 7.10 (2 H, d, $^3J_{HH}$ = 8.8 Hz), 6.89 (2 H, d, $^3J_{HH}$ = 8.9 Hz), 4.85 (1 H, s), 4.66 (2 H, d, $^4J_{HH}$ = 2.0 Hz), 2.66 (1 H, s), 2.51 (1 H, t, $^4J_{HH}$ = 2.4 Hz), 2.01 (1 H, m), 1.46 (9 H, s), 1.11 (2 H, m).

^{13}C {^{1}H} NMR (100MHz, $CDCl_3$, 298 K) δ 156.4, 156.0, 134.0, 127.8, 115.0, 79.6, 78.9, 75.5, 56.1, 32.1, 28.4, 24.4, 15.9.

MS (ESI+) $[M+H]^+$ (%) 288.2 (100).

HRMS (ESI+) calcd from $C_{17}H_{22}NO_3$ $[M+H]^+$: 288.1600; found 288.1576.

2-(3-(prop-2-yn-1-yloxy)phenyl)cyclopropan-1-amine (Probe 1)

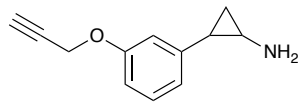

To *tert*-butyl (2-(3-(prop-2-yn-1-yloxy)phenyl)cyclopropyl)carbamate (210 mg, 0.731 mmol) in DCM (20 mL) was added HCl in dioxane (5.0 mL, 4 M) dropwise and protected by an N_2 atmosphere. The reaction mixture was stirred for 2 hr. The solvent was removed under reduced pressure, the oil was dissolved in DCM (4 mL) and precipitated by slow addition of hexane (6 mL). The precipitated was re-dissolved in DCM and condensed to give 160 mg (98%) of clear oil.

IR (v_{max}/cm^{-1}) 3399, 3275, 3011, 2965, 2129, 1580, 1199, 1052.

^{1}H NMR (400MHz, $CDCl_3$, 298 K) δ 8.63 (3 H, s), 7.13 (1 H, dd, $^3J_{HH}$ = 8.12 Hz, $^3J_{HH}$ = 8.12 Hz), 6.77 - 6.72 (3 H, m), 4.59 (2 H, d, $^4J_{HH}$ = 2.36 Hz), 2.84 (1 H, s), 2.64 (1 H, s), 2.49 (1 H, t, $^4J_{HH}$ = 2.36 Hz), 1.67 (1 H, s), 1.15 (1 H, m).

^{13}C {^{1}H} NMR (100MHz, $CDCl_3$, 298 K) δ 157.7, 140.0, 129.7, 120.0, 113.6, 113.0, 78.6, 75.8, 55.7, 31.0, 21.7, 13.4.

MS (ESI+) m/z (%) 188.1 (100).

HRMS(ESI+) calcd from $C_{12}H_{14}NO$ $[M+H]^+$: 188.1075; found 188.1062.

2-(4-(prop-2-yn-1-yloxy)phenyl)cyclopropan-1-amine (Probe 2)

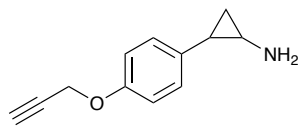

To *tert*-butyl (2-(4-(prop-2-yn-1-yloxy)phenyl)cyclopropyl)carbamate (170 mg, 0.731 mmol) in DCM (20 mL) was added HCl in dioxane (5.0 mL, 4 M) dropwise and protected by an N_2 atmosphere. The reaction mixture was stirred for 2 hr. The solvent was removed under reduced pressure. The oil was dissolved in DCM (4 mL) and precipitated by slow addition of hexane (6 mL). The precipitated was re-dissolved in DCM and condensed to give 40 mg (30%) of white crystalline solid.

IR (v_{max}/cm^{-1}) 3380, 3263, 3001, 2952, 2124, 1530, 1170, 1053.

^{1}H NMR (400MHz, MeOD, 298 K) δ 7.13 (2 H, d, $^3J_{HH}$ = 8.8 Hz), 6.94 (2 H, d, $^3J_{HH}$ = 8.8 Hz), 4.71 (2 H, d, $^4J_{HH}$ = 2.4 Hz), 2.94 (1 H, t, $^4J_{HH}$ = 2.4 Hz), 2.77 (1 H, m), 2.37 (1 H, m), 1.40 (1 H, m), 1.28 (1 H, m).

^{13}C {^{1}H} NMR (100MHz, MeOD, 298 K) δ 158.1, 132.7, 128.7, 116.2, 79.8, 76.8, 56.7, 32.0, 22.0, 13.7.

MS (ESI+) $[M+H]^+$ (%); 188.1 (100).

HRMS(ESI+) calcd from $C_{12}H_{14}NO$ $[M+H]^+$: 188.1075; found 188.1074

***tert*-butyl (2-(3-(3-bromopropoxy)phenyl)cyclopropyl)carbamate (46a)**

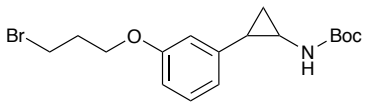

To *tert*-butyl (2-(3-hydroxyphenyl)cyclopropyl) carbamate (116 mg, 0.47 mmol), $P(Ph)_3$ (200 mg , 0.77 mmol) in dry THF (3 mL) was added 3-bromo-1-propanol (0.1 mL, 1.02 mmol) and protect by an N_2 atmosphere at 0 °C. DIAD (0.15 mL, 0.77 mmol) in dry THF (1 mL) was added dropwise and stirred for 4 hr at 0 °C and allowed to warm to room temperature and left overnight. The solvent was removed under reduced pressure and the residue was purified on silica (40 g), eluting with (EtOAc:n-Hexane 1:4) to give 76 mg (43%) of white amorphous solid.

IR (v_{max}/cm^{-1}) 3361, 3009, 2984, 2953, 2881, 1674, 1508, 1225, 1148.

^{1}H NMR (400MHz, $CDCl_3$, 298 K) δ 7.18 (1 H, dd, $^3J_{HH}$ = 7.9 Hz, $^3J_{HH}$ = 7.9 Hz), 6.75 – 6.71 (2 H, m), 6.67 (1 H, s) 4.86 (1 H, s), 4.09 (2 H, t, $^3J_{HH}$ = 5.8 Hz), 3.61 (2 H, t, $^3J_{HH}$ = 6.5 Hz) 2.74 (1 H, s), 2.31 (2 H, p, $^3J_{HH}$ = 6.5 Hz), 2.01 (1 H, m), 1.46 (9 H, s), 1.18 – 1.15 (2 H, m)

^{13}C {^{1}H} NMR (100MHz, $CDCl_3$, 298 K) δ 158.7, 156.2, 142.5, 129.3, 119.1, 112.8, 111.8, 79.7, 65.2, 32.6, 32.4, 30.1, 28.4, 25.1, 16.6.

MS (ESI+) $[M+H]^+$ (%) 370.1 (100).

HRMS(ESI+) calcd from $C_{17}H_{25}BrNO_3$ $[M+H]^+$: 370.1018; found 370.1008.

***tert*-butyl (2-(4-(3-bromopropoxy)phenyl)cyclopropyl)carbamate (46b)**

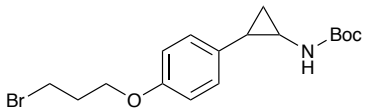

To *tert*-butyl (2-(4-hydroxyphenyl)cyclopropyl) carbamate (810 mg, 3.25 mmol), $P(Ph)_3$ (1404 mg, 5.36 mmol) in dry THF (12mL) was added 3-bromo-1-propanol (0.65 mL, 7.15 mmol) was added and protect by an N_2 atmosphere at 0 °C. DIAD (1.05 mL, 5.36 mmol) in dry THF (4 mL) was added dropwise and stirred for 4 hr at 0 °C and allowed to warm to room temperature and left overnight. The solvent was

removed under reduced pressure and the residue was purified on silica (40 g), eluting with (EtOAc:n-Hexane 1:4) to give 837 mg (70%) of white amorphous solid.

IR (v_{max}/cm^{-1}) 3366, 3004, 2977, 2929, 2877, 1684, 1504, 1239, 1155.

^{1}H NMR (400MHz, $CDCl_3$, 298 K) δ 7.08 (2 H, d, $^3J_{HH}$ = 8.6 Hz), 6.81 (2 H, d, $^3J_{HH}$ = 8.7 Hz), 4.84 (1 H, s), 4.02 (2 H, t, $^3J_{HH}$ = 5.9 Hz), 3.51 (2 H, t, $^3J_{HH}$ = 6.6 Hz), 2.66 (1 H, s), 2.04 (2 H, p, $^3J_{HH}$ = 6.3 Hz), 1.46 (9 H, s), 1.12 – 1.07 (2 H, m)

^{13}C {^{1}H} NMR (100MHz, $CDCl_3$, 298 K) δ 157.1, 133.1, 127.9, 114.4, 79.6, 77.1, 64.6, 48.3, 32.4, 28.4, 28.3, 24.3, 15.9.

MS (ESI+) $[M+H]^+$ (%) 370.1 (100).

HRMS(ESI+) calcd from $C_{17}H_{25}BrNO_3$ $[M+H]^+$: 370.1018; found 370.1004.

***tert*-butyl (2-(3-(3-azidopropoxy)phenyl)cyclopropyl)carbamate (47a)**

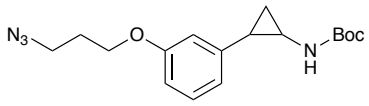

To *tert*-butyl (2-(3-(3-bromopropoxy)phenyl)cyclopropyl)carbamate (70 mg, 0.19 mmol) in dry DMF (5 mL) was added NaN_3 (190 mg, 2.85 mmol) protected by a N_2 atmosphere and stirred for 15 hr at 80 °C. The reaction mixture is diluted with EtOAc (5 mL), washed with sat. $NaCl_{(aq)}$ (2x10 mL), dried with anhydrous $MgSO_4$ and concentrated under reduced pressure. The resulting residue was purified on silica (12 g), eluting with (EtOAc:Hexane, 1:4) to give 44 mg (70%) of white amorphous solid.

IR (v_{max}/cm^{-1}) 3380, 2979, 2931, 2887, 2089, 1672, 1515, 1254, 1159.

^{1}H NMR (400MHz, $CDCl_3$, 298 K) δ 7.17 (1 H, dd, $^3J_{HH}$ = 7.9 Hz, $^3J_{HH}$ = 7.9 Hz), 6.74 – 6.66 (3 H, m), 4.89 (1 H, s), 4.03 (2 H, t, $^3J_{HH}$ = 5.8 Hz), 3.52 (2 H, t, $^3J_{HH}$ = 6.6 Hz) 2.74 (1 H, s), 2.04 (2 H, p, $^3J_{HH}$ = 6.3 Hz), 1.46 (9 H, s), 1.18 – 1.14 (2 H, m)

^{13}C {^{1}H} NMR (100MHz, $CDCl_3$, 298 K) δ 158.8, 156.3, 142.6, 129.4, 119.2, 112.8, 111.8, 79.7, 64.4, 48.3, 32.5, 28.8, 28.4, 25.1, 16.6.

MS (ESI+) $[M+H]^+$ (%) 333.2 (100).

HRMS(ESI+) calcd from $C_{17}H_{25}N_4O_3$ $[M]^+$: 333.1927; found 333.1932.

***tert*-butyl (2-(4-(3-azidopropoxy)phenyl)cyclopropyl)carbamate (47b)**

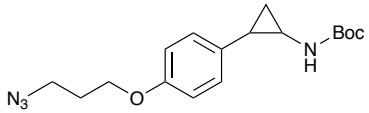

To *tert*-butyl (2-(4-(3-bromopropoxy)phenyl)cyclopropyl)carbamate (550 mg, 1.49 mmol) in dry DMF (40 mL) was added NaN_3 (1.4 g, 22.3 mmol) protected by a N_2 atmosphere and

stirred for 15 hr at 80 °C. The reaction mixture is diluted with EtOAc (40 mL), washed with sat. $NaCl_{(aq)}$ (2x30 mL), dried with anhydrous $MgSO_4$ and concentrated under reduced pressure. The resulting residue was purified on silica (12 g), eluting with (EtOAc:Hexane, 1:4) to give 325 mg (66%) of white amorphous power.

IR (v_{max}/cm^{-1}) 3364, 2980, 2935, 2881, 2087, 1685, 1503, 1239, 1162.

^{1}H NMR (400MHz,$CDCl_3$, 298 K) δ 7.14 (2 H, d, $^3J_{HH}$ = 8.5 Hz), 6.84 (2 H, d, $^3J_{HH}$ = 8.7 Hz), 4.87 (1 H, s), 4.05 (2 H, t, $^3J_{HH}$ = 6.0 Hz), 3.55 (2 H, t, $^3J_{HH}$ = 6.7 Hz), 2.69 (1 H, s), 2.10 – 2.01 (3 H, m), 1.50 (9 H, s), 1.15 – 1.11 (2 H, m).

^{13}C {^{1}H} NMR (100MHz, $CDCl_3$, 298 K) δ 157.1, 133.1, 127.9, 114.4, 79.7, 77.2, 64.6, 48.3, 32.1, 28.8, 28.4, 24.3, 15.9.

MS (ESI+) $[M+H]^+$ (%) 333.2 (100).

HRMS(ESI+) calcd from $C_{17}H_{25}N_4O_3$ $[M+H]^+$: 333.1927; found 333.1942.

2-(3-(3-azidopropoxy)phenyl)cyclopropan-1-amine (Probe 3)

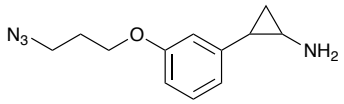

To *tert*-butyl (2-(3-(3-azidopropoxy)phenyl)cyclopropyl)carbamate (40 mg, 0.12 mmol) in DCM (2 mL) was added HCl in dioxane (2 mL, 4 M) dropwise and protected by an N_2 atmosphere. The reaction mixture was stirred for 2 hr. The solvent was removed under reduced pressure, the oil was dissolved in DCM (4 mL) and precipitated by slow addition of hexane (6 mL). The precipitated was re-dissolved in DCM and condensed to give 20 mg (74%) of white amorphous solid.

IR (v_{max}/cm^{-1}) 3334, 2928, 2870, 2754, 2114, 1613, 1502, 1252, 1032.

^{1}H NMR (400MHz, $CDCl_3$, 298 K) δ 8.70 (3 H, s), 7.16 (1 H, dd, $^3J_{HH}$ = 7.5 Hz, $^3J_{HH}$ = 7.5 Hz), 6.74 – 6.69 (3 H, m), 3.99 (2 H, t, $^3J_{HH}$ = 5.7 Hz), 3.48 (2 H, t, $^3J_{HH}$ = 6.6 Hz), 2.85 (1 H, s), 2.66 (1 H, s), 2.00 (2 H, m), 1.69 (1 H, s), 1.24 (1 H, s).

^{13}C {^{1}H} NMR (100MHz, $CDCl_3$, 298 K) δ 158.9, 139.8, 129.7, 119.2, 113.2, 112.8, 64.5, 48.2, 31.1, 28.8, 21.9, 13.6.

MS (ESI+) $[M+H]^+$ (%) 233.1 (100).

HRMS(ESI+) calcd from $C_{12}H_{17}N_4O$ $[M+H]^+$: 233.1402; found 233.1398

2-(4-(3-azidopropoxy)phenyl)cyclopropan-1-amine (Probe 4)

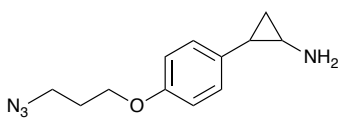

To *tert*-butyl (2-(4-(3-azidopropoxy)phenyl) cyclopropyl)carbamate (300 mg, 0.9 mmol) in DCM (5 mL) was added HCl in dioxane (5 mL, 4 M) dropwise and

protected by an N_2 atmosphere. The reaction mixture was stirred for 2 hr. The solvent was removed under reduced pressure. The oil was dissolved in DCM (8 mL) and precipitated by slow addition of hexane (16 mL). The precipitated was re-dissolved in DCM and condensed to give 198 mg (80%) of red amorphous solid.

IR (v_{max}/cm^{-1}) 3330, 2930, 2875, 2763, 2087, 1608, 1511, 1245, 1046.

^{1}H NMR (400MHz, MeOD, 298 K) δ 7.12 (2 H, d, $^3J_{HH}$ = 8.6 Hz), 6.89 (2 H, d, $^3J_{HH}$ = 8.8 Hz), 4.05 (2 H, t, $^3J_{HH}$ = 6.0 Hz), 3.51 (2 H, t, $^3J_{HH}$ = 6.6Hz), 2.78 (1 H, m), 2.35 (1 H, ddd, $^3J_{HH}$ = 10.1 Hz, $^3J_{HH}$ = 6.5 Hz, $^3J_{HH}$ = 3.6 Hz), 2.03 (2 H, p, $^3J_{HH}$ = 6.3 Hz), 1.38 (1 H, ddd, $^3J_{HH}$ = 10.4 Hz, $^3J_{HH}$ = 6.4 Hz, $^3J_{HH}$ = 4.2 Hz), 1.28 (1 H, m).

^{13}C {^{1}H} NMR (100MHz, MeOD, 298 K) δ 159.3, 131.8, 128.7, 115.8, 65.9, 49.4, 31.8, 29.9, 21.9, 13.42.

MS (ESI+) $[M+H]^+$ 233.1 (%) (100).

HRMS(ESI+) calcd from $C_{12}H_{17}N_4O$ $[M+H]^+$: 233.1402; found 233.1398

***tert*-butyl (2-(3'-(hydroxymethyl)-[1,1'-biphenyl]-3-yl)cyclopropyl)carbamate (48a)**

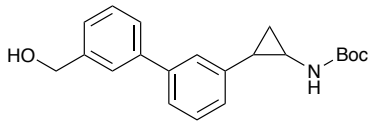

To a mixture of 3-(Hydroxymethyl)phenylboronic acid (216 mg, 1.41 mmol), $Pd(PPh_3)_2Cl_2$ (13 mg, 0.02 mmol) and Na_2CO_3 (190 mg, 1.6 mmol) protected by an N_2 atmosphere was added degassed dry THF (8 mL), toluene (8 mL) and de-ionised water (0.4 mL). This was stirred and *tert*-butyl (2-(3-bromophenyl)cyclopropyl)carbamate (400 mg, 1.28 mmol) was added, heated to 105 °C and stirred for 36 hr. The solution was allowed to cool, condensed under reduced pressure, and re-dissolved in DCM and washed with sat. $NaHCO_{3(aq)}$ (2x50 mL), sat. $NaCl_{(aq)}$ (2x50 mL), dried with anhydrous $MgSO_4$ and condensed under reduced pressure. The product was purified on silica (40 g), eluting with (EtOAc/hexane = 1:7) gave 290 mg (67%) of white amorphous solid.

IR (v_{max}/cm^{-1}) 3339, 2972, 2921, 1502, 1621, 1132, 1069

^{1}H NMR (400MHz, $CDCl_3$, 298 K) δ 7.57 (1 H, s), 7.48 (1 H, d, $^3J_{HH}$ = 7.6 Hz), 7.41 – 7.38 (2 H, m), 7.33 – 7.30 (3 H, m), 7.10 (1 H, d, $^3J_{HH}$ = 7.6 Hz), 5.05 (1 H, s), 4.72 (2 H, s), 2.79 – 2.71 (2 H, m), 2.08 (1 H, s), 1.47 (9 H, s), 1.23 – 1.17 (2 H, m).

^{13}C {^{1}H} NMR (100MHz, $CDCl_3$, 298 K) δ 156.5, 141.6, 141.5, 141.3, 141.1, 128.9, 128.8, 126.4, 125.9, 125.8, 125.5, 125.3, 125.0, 79.8, 65.2, 32.6, 28.5, 25.0, 16.6.

MS (ESI+) $[M+H]^+$ (%) 340.2 (100).

HRMS(ESI+) calcd from $C_{21}H_{25}NO_3$ $[M+H]^+$: 340.1913; found 340.1910.

***tert*-butyl (2-(4'-(hydroxymethyl)-[1,1'-biphenyl]-3-yl)cyclopropyl)carbamate (48b)**

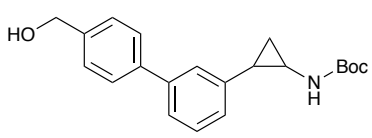

To a mixture of 4-(Hydroxymethyl)phenylboronic acid (216 mg, 1.41 mmol), $Pd(PPh_3)_2Cl_2$ (13 mg, 0.02 mmol) and Na_2CO_3 (190 mg, 1.6 mmol) protected by an N_2 atmosphere was added degassed dry THF (8 mL), toluene (8 mL) and de-ionised water (0.4 mL). This was stirred and *tert*-butyl (2-(3-bromophenyl)cyclopropyl)carbamate (400 mg, 1.28 mmol) was added, heated to 105 °C and stirred for 36 hr. The solution was allowed to cool, condensed under reduced pressure, and re-dissolved in DCM and washed with sat. $NaHCO_{3(aq)}$ (2x50 mL), sat. $NaCl_{(aq)}$ (2x50 mL), dried with anhydrous $MgSO_4$ and condensed under reduced pressure. The product was purified on silica (40 g) eluting with (EtOAc/hexane = 1:7) gave 354 mg (82%) of white amorphous solid.

IR (v_{max}/cm^{-1}) 3320, 2983, 2962, 1532, 1644, 1170, 1017

^{1}H NMR (400MHz, $CDCl_3$, 298 K) δ 7.54 (2 H, d, $^{3}J_{HH}$ = 8.2 Hz), 7.41 – 7.37 (3 H, m), 7.34 – 7.30 (2 H, m), 7.09 (1 H, d, $^{3}J_{HH}$ = 7.4 Hz), 5.21 (1 H, s), 4.69 (2 H, s), 3.32 (1 H, s), 2.79 (1 H, s), 2.07 (1 H, s), 1.49 (9 H, s), 1.19 (2 H, m).

^{13}C {^{1}H} NMR (100MHz, $CDCl_3$, 298 K) δ 156.6, 141.4, 141.0, 140.33, 140.26, 128.8, 127.4, 127.2, 125.3, 125.2, 124.9, 79.8, 64.7, 32.7, 28.5, 25.0, 16.6.

MS (ESI+) $[M+H]^+$ (%) 340.2 (100).

HRMS(ESI+) calcd from $C_{21}H_{25}NO_3$ $[M+H]^+$:340.1913; found 340.1904.

***tert*-butyl (2-(3'-(hydroxymethyl)-[1,1'-biphenyl]-4-yl)cyclopropyl)carbamate (48c)**

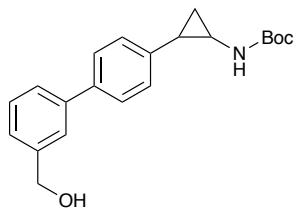

To a mixture of 3-(Hydroxymethyl)phenylboronic acid (161 mg, 1.06 mmol), $Pd(PPh_3)_2Cl_2$ (10 mg, 0.014 mmol) and Na_2CO_3 (127 mg, 1.20 mmol) protected by an N_2 atmosphere was added degassed dry THF (5 mL), toluene (5 mL) and de-ionised water (0.15 mL). This was

stirred and *tert*-butyl (2-(4-bromophenyl)cyclopropyl)carbamate (300 mg, 0.96 mmol) was added, heated to 105 °C and stirred for 36 hr. The solution was allowed to cool, condensed under reduced pressure, and re-dissolved in DCM and washed with sat. $NaHCO_{3(aq)}$ (2x50 mL), sat. $NaCl_{(aq)}$ (2x50 mL), dried with anhydrous $MgSO_4$ and condensed under reduced pressure. The product was purified on silica (40 g), eluting with (EtOAc/hexane = 1:7) gave 125 mg (43%) of white amorphous solid.

IR (v_{max}/cm^{-1}) 3334, 2978, 2931, 1516, 1685, 1168, 1031.

^{1}H NMR (400MHz, $CDCl_3$, 298 K) δ 7.58 (1 H, s), 7.52 – 7.50 (3 H, m), 7.43 (1 H, dd, $^3J_{HH}$ = 7.3 Hz, $^3J_{HH}$ = 7.3 Hz), 7.34 (1 H, d, $^3J_{HH}$ = 8.0 Hz), 7.22 (2 H, $^3J_{HH}$ = 8.0 Hz), 4.88 – 4.77 (3 H, m), 2.77 (1 H, s), 2.09 (1 H, m), 1.62 (1 H, s), 1.47 (9 H, s), 1.21 (2 H, m).

^{13}C {^{1}H} NMR (100MHz, $CDCl_3$, 298 K) δ 156.6, 141.4, 141.3, 140.1, 138.7, 129.0, 127.1, 126.9, 126.3, 125.7, 125.6, 82.3, 65.4, 32.7, 28.4, 24.8, 16.5.

MS (ESI+) $[M+H]^+$: (%) 361.9 (100).

HRMS(ESI+) calcd from $C_{21}H_{25}NO_3$ $[M+H]^+$: 340.1913 found 340.1900.

tert-butyl (2-(4'-(hydroxymethyl)-[1,1'-biphenyl]-4-yl)cyclopropyl)carbamate (48d)

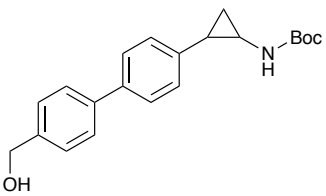

To a mixture of 4-(Hydroxymethyl)phenylboronic acid (216 mg, 1.41 mmol), $Pd(PPh_3)_2Cl_2$ (13 mg, 0.02 mmol) and Na_2CO_3 (190 mg, 1.6 mmol) protected by an N_2 atmosphere was added degassed dry THF (8 mL), Toluene (8 mL) and de-ionised water (0.4 mL). This was stirred and *tert*-butyl (2-(4-bromophenyl)cyclopropyl)carbamate (400 mg, 1.41 mmol) was added, heated to 105 °C and stirred for 36 hr. The solution was allowed to cool, condensed under reduced pressure, and re-dissolved in DCM and washed with sat. $NaHCO_{3(aq)}$ (2x50 mL), sat. $NaCl_{(aq)}$ (2x50 mL), dried with anhydrous $MgSO_4$ and condensed under reduced pressure. The product was purified on silica (40 g), eluting with (EtOAc/hexane = 1:7) gave 286 mg (66%) of white amorphous solid.

IR (v_{max}/cm^{-1}) 3379, 3004, 2988, 1484, 1683, 1121, 1073.

^{1}H NMR (400MHz, $CDCl_3$, 298 K) δ 7.56 (2 H, d, $^3J_{HH}$ = 8.2 Hz), 7.50 (2 H, d, $^3J_{HH}$ = 8.2 Hz), 7.43 (2 H, d, $^3J_{HH}$ = 8.2 Hz), 7.20 (2 H, d, $^3J_{HH}$ = 8.2 Hz), 4.90 (1 H, s), 4.74 (1 H, s), 2.76 (1 H, s), 2.08 (1 H, m), 1.65 (1 H, s), 1.47 (9 H, s), 1.23 – 1.19 (2 H, m).

^{13}C {^{1}H} NMR (100MHz, $CDCl_3$, 298 K) δ 156.4, 140.4, 140.0, 139.7, 138.6, 127.5, 127.1, 127.0, 126.9, 79.9, 65.1, 32.7, 28.4, 24.8, 16.5.

MS (ESI+) $[M+H]^+$ (%) 340.2 (100).

HRMS(ESI+) calcd from $C_{21}H_{25}NO_3$ $[M+H]^+$: 340.1913; found 340.1904

***tert*-butyl (2-(3'-(azidomethyl)-[1,1'-biphenyl]-3-yl)cyclopropyl)carbamate (49a)**

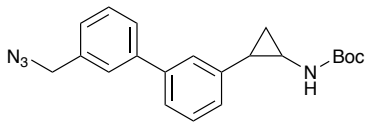

To *tert*-butyl (2-(3'-(hydroxymethyl)-[1,1'-biphenyl]-3-yl)cyclopropyl)carbamate (250 mg, 0.74 mmol), $P(Ph)_3$ (230 mg, 0.88 mmol) in THF (10 mL) was added DPPA (0.15 mL, 0.192 mmol) and protect by an N_2 atmosphere at 0 °C. DIAD (0.17 mL, 0.88 mmol) in dry THF (3.5 mL) was added dropwise and allowed to warm to room temperature and stirred for 48 hr. The solvent was removed under reduced pressure and the residue was purified on silica (40 g), eluting with DCM to give 142 mg (53%) of white amorphous solid.

IR (ν_{max}/cm^{-1}) 3338, 2976, 2931, 2095, 1703, 1248, 1163, 1090.

^{1}H NMR (400MHz, $CDCl_3$, 298 K) δ 7.56 – 7.27 (7 H, m), 7.15, (1 H, d, $^{3}J_{HH}$ = 6.6 Hz), 4.97 (1 H, s), 4.41 (2 H, s), 2.83 (1 H, s), 2.12 (1 H, s), 1.48 (9 H, s), 1.23 (2 H, s).

^{13}C {^{1}H} NMR (100MHz, $CDCl_3$, 298 K) δ 156.3, 142.0, 141.4, 140.8, 135.9, 129.9, 129.2, 128.9, 127.2, 127.0, 125.7, 125.3, 125.0, 79.7, 54.9, 32.6, 28.4, 25.1, 16.7.

MS (ESI+) $[M+H]^+$ (%) 365.2 (100).

HRMS(ESI+) calcd from $C_{21}H_{25}N_4O_2$ $[M+H]^+$: 365.1978; found 365.1991.

***tert*-butyl (2-(4'-(azidomethyl)-[1,1'-biphenyl]-3-yl)cyclopropyl)carbamate (49b)**

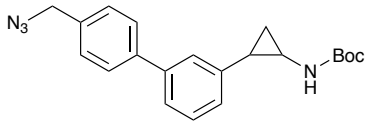

To *tert*-butyl (2-(4'-(hydroxymethyl)-[1,1'-biphenyl]-3-yl)cyclopropyl)carbamate (300 mg, 0.88 mmol), $P(Ph)_3$ (277 mg, 1.06 mmol) in THF (10 mL) was added DPPA (0.18 mL, 1.06 mmol) and protect by an N_2 atmosphere at 0 °C. DIAD (0.21 mL, 1.06 mmol) in dry THF (4 mL) was added dropwise and allowed to warm to room temperature and stirred for 48 hr. The solvent was removed under reduced pressure and the residue was purified on silica (40 g), eluting with DCM to give 133 mg (41%) of white amorphous solid.

IR (v_{max}/cm^{-1}). 3372, 2932, 2927, 2043, 1700, 1262, 1167, 1082.

^{1}H NMR (400MHz, $CDCl_3$, 298 K) δ 7.59 (2 H, d, $^3J_{HH}$ = 8.3 Hz), 7.41 – 7.33 (5 H, m), 7.14 (1 H, d, $^3J_{HH}$ = 7.5 Hz), 4.87 (1 H, s), 4.39 (2 H, s), 2.82 (1 H, s), 2.12 (1 H, m), 1.47 (9 H, s), 1.26 – 1.19 (2 H, m).

^{13}C {^{1}H} NMR (100MHz, $CDCl_3$, 298 K) δ 156.3, 141.4, 141.3, 140.6, 134.3, 128.8, 128.6, 127.6, 125.6, 125.3, 124.9, 79.7, 54.6, 32.6, 28.4, 25.1, 16.6.

MS (ESI+) $[M+H]^+$ (%) 365.2 (100).

HRMS(ESI+) calcd from $C_{21}H_{25}N_4O_2$ $[M+H]^+$: 365.1978; found 365.1980.

***tert*-butyl (2-(3'-(azidomethyl)-[1,1'-biphenyl]-4-yl)cyclopropyl)carbamate (49c)**

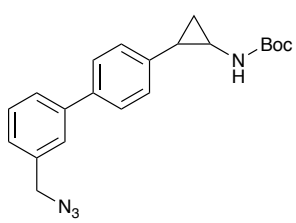

To *tert*-butyl (2-(3'-(hydroxymethyl)-[1,1'-biphenyl]-4-yl)cyclopropyl)carbamate (66 mg, 1.00 mmol), $P(Ph)_3$ (60 mg, 0.23 mmol) in THF (3.0 mL) was added DPPA (0.04 mL, 0.23 mmol) and protect by an N_2 atmosphere at 0 °C. DIAD (0.04 mL, 0.23 mmol) in dry THF (1.0 mL) was added dropwise and allowed to warm to room temperature and stirred for 48 hr. The solvent was removed under reduced pressure and the residue was purified on silica (40 g), eluting with DCM to give 50 mg (72%) of white amorphous solid.

IR (v_{max}/cm^{-1}) 3388, 2978, 2933, 2098, 1683, 1260, 1163, 1029.

^{1}H NMR (400MHz, $CDCl_3$, 298 K) δ 7.54 (1 H, d, $^3J_{HH}$ = 7.7 Hz), 7.52 - 7.49 (3 H, m), 7.45 (1 H, dd, $^3J_{HH}$ = 7.6 Hz, $^3J_{HH}$ = 7.6 Hz), 7.29 (1 H, d, $^3J_{HH}$ = 7.7 Hz), 7.22 (2 H, d, $^3J_{HH}$ = 8.0 Hz), 4.89 (1 H, s), 4.41 (2 H, s), 2.78 (1 H, s), 2.10 (1 H, m), 1.48 (9 H, s), 1.22 (2 H, m).

^{13}C {^{1}H} NMR (100MHz, $CDCl_3$, 298 K) δ 156.3, 142.3, 141.7, 140.3, 138.4, 135.9, 129.3, 127.1, 17.0, 126.8, 126.8, 79.7, 77.2, 60.4, 32.5, 28.4, 24.8, 14.2.

MS (ESI+) $[M+H]^+$: (%) 365.2 (100).

HRMS(ESI+) calcd from $C_{21}H_{25}N_4O_2$ $[M+H]^+$:365.1978; found 365.1982.

***tert*-butyl (2-(4'-(azidomethyl)-[1,1'-biphenyl]-4-yl)cyclopropyl)carbamate (49d)**

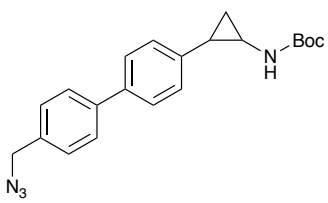

To *tert*-butyl (2-(4'-(hydroxymethyl)-[1,1'-biphenyl]-4-yl)cyclopropyl)carbamate (100 mg, 0.29 mmol), $P(Ph)_3$ (90 mg, 0.35 mmol) in THF (4.5 mL) was added DPPA (0.6 mL, 0.35 mmol) and protect by an N_2 atmosphere

at 0 °C. DIAD (0.07 mL, 0.35 mmol) in dry THF (1.5 mL) was added dropwise and allowed to warm to room temperature and stirred for 48 hr. The solvent was removed under reduced pressure and the residue was purified on silica (40 g), eluting with DCM to give 61 mg (58%) of white crystalline solid.

IR (ν_{max}/cm^{-1}) 3334, 2978, 2931, 2095, 1685, 1251, 1174, 1099.

^{1}H NMR (400MHz, $CDCl_3$, 298 K) δ 7.59 (2 H, d, $^3J_{HH}$ = 8.2 Hz), 7.50 (2 H, d, $^3J_{HH}$ = 8.3 Hz), 7.38 (2 H, d, $^3J_{HH}$ = 8.3 Hz), 7.22 (2 H, d, $^3J_{HH}$ = 8.2 Hz), 4.87 (1 H, s), 4.39 (2 H, s), 2.77 (1 H, s), 2.09 (1 H, m), 1.48 (9 H, s), 1.26 – 1.19 (2 H, m).

^{13}C {^{1}H} NMR (100MHz, $CDCl_3$, 298 K) δ 156.3, 141.0, 140.3, 138.3, 134.1, 128.7, 127.4, 127.0, 126.9, 79.7, 54.6, 32.7, 28.4, 24.9, 16.5.

MS (ESI+) $[M+H]^+$ (%) 365.2 (100).

HRMS(ESI+) calcd from $C_{21}H_{25}N_4O_2$ $[M+H]^+$: 365.1978; found 365.1974.

2-(3'-(azidomethyl)-[1,1'-biphenyl]-3-yl)cyclopropan-1-amine (Probe 5)

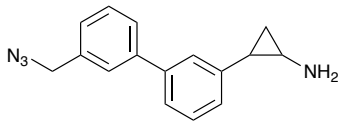

To *tert*-butyl (2-(3'-(azidomethyl)-[1,1'-biphenyl]-3-yl)cyclopropyl)carbamate (40 mg, 0.109 mmol) in DCM (4 mL) was added HCl in dioxane (3.5 mL, 4 M) dropwise and protected by a N_2 atmosphere. The reaction mixture was stirred for 3 hr. The solvent was removed under reduced pressure. The solvent was removed under reduced pressure, the oil was dissolved in DCM (4 mL) and precipitated by slow addition of hexane (6 mL). The precipitated was re-dissolved in DCM and condensed to give 28 mg (88%) of yellow crystalline solid.

IR (ν_{max}/cm^{-1}) 3325, 2974, 2938, 2089, 1705, 1245, 1171, 1111.

^{1}H NMR (400MHz, MeOD, 298 K) δ 7.63 – 7.61 (2 H, m), 7.54 – 7.37 (5 H, m), 7.19 (1 H, d, $^3J_{HH}$ = 7.7 Hz), 4.46 (2 H, s), 2.95 (1 H, m) 2.47 (1 H, ddd, $^3J_{HH}$ = 10.0 Hz, $^3J_{HH}$ = 6.7 Hz, $^3J_{HH}$ = 3.4 Hz), 1.50 – 1.41 (2 H, m).

^{13}C {^{1}H} NMR (100MHz, MeOD, 298 K) δ 142.7, 142.5, 140.5, 137.9, 130.4, 130.3, 128.6, 128.04, 127.97, 126.7, 126.5, 126.3, 55.5, 32.0, 22.7, 13.8.

MS (ESI+) $[M+H]^+$ (%) 265.1 (100).

HRMS(ESI+) calcd from $C_{16}H_{17}N_4$ $[M+H]^+$: 265.1453; found 265.1458.

2-(4'-(azidomethyl)-[1,1'-biphenyl]-3-yl)cyclopropan-1-amine (Probe 6)

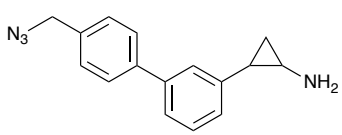

To *tert*-butyl (2-(4'-(azidomethyl)-[1,1'-biphenyl]-3-yl)cyclopropyl)carbamate (100 mg, 0.27 mmol) in DCM (6 mL) was added HCl dioxane (6 mL, 4 M) dropwise

and protected by a N_2 atmosphere. The reaction mixture was stirred for 3 hr. The solvent was removed under reduced pressure. The solvent was removed under reduced pressure, the oil was dissolved in DCM (4 mL) and precipitated by slow addition of hexane (6 mL). The precipitated was re-dissolved in DCM and condensed to give 73 mg (89%) of orange crystalline solid.

IR (ν_{max}/cm^{-1}) 3356, 2986, 2942, 2083, 1692, 1245, 1169, 1039.

^{1}H NMR (400MHz, MeOD, 298 K) δ 7.67 (2 H, d, $^3J_{HH}$ = 8.2 Hz), 7.53 (1 H, d, $^3J_{HH}$ = 7.8 Hz), 7.47 – 7.40 (4 H, m), 7.18, (1 H, d, $^3J_{HH}$ = 7.6 Hz), 4.42 (2 H, s), 2.96 – 2.92 (1 H, m), 2.50 – 2.45 (1 H, m), 1.50 – 1.41 (2 H, m).

^{13}C {^{1}H} NMR (100MHz, MeOD, 298 K) δ 142.4, 142.1, 140.5, 136.4, 130.3, 130.0, 128.4, 126.7, 126.5, 126.2, 55.2, 32.0, 22.7, 13.9.

MS (ESI+) $[M+H]^+$ (%) 265.1 (100).

HRMS(ESI+) calcd from $C_{16}H_{17}N_4$ $[M+H]^+$: 265.1453; found 265.1461.

2-(3'-(azidomethyl)-[1,1'-biphenyl]-4-yl)cyclopropan-1-amine (Probe 7)

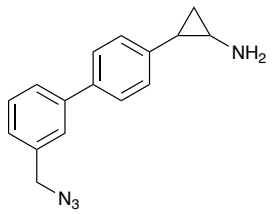

To *tert*-butyl (2-(3'-(azidomethyl)-[1,1'-biphenyl]-4-yl)cyclopropyl)carbamate (30 mg, 0.32 mmol) in DCM (2 mL) was added HCl in dioxane (2.5 mL, 4 M) dropwise and protected by a N_2 atmosphere. The reaction mixture was stirred for 3 hr. The solvent was removed under reduced pressure. The solvent was removed under reduced pressure, the oil was dissolved in DCM (4 mL) and precipitated by slow addition of hexane (6 mL). The precipitated was re-dissolved in DCM and condensed to give 18 mg (75%) of white crystalline solid.

IR (ν_{max}/cm^{-1}) 3300, 2976, 2935, 2099, 2078, 1507, 1019.

^{1}H NMR (400MHz, MeOD, 298 K) δ 7.63 – 7.59 (4 H, m), 7.49 (1 H, dd, $^3J_{HH}$ = 8.7 Hz, $^3J_{HH}$ = 8.7 Hz), 7.36 – 7.27 (3 H, m), 4.45 (2 H, s), 2.93 - 2.89 (1 H, m), 2.45 – 2.4 (1 H, m), 1.49 - 1.39 (2 H, m).

^{13}C {^{1}H} NMR (100MHz, MeOD, 298 K) δ 142.5, 140.5, 139.3, 137.8, 130.4, 128.4, 128.3, 128.0, 127.8, 127.7, 55.6, 32.1, 22.3, 14.0.

MS (ESI+) $[M+H]^+$ (%) 265.2 (100).

HRMS(ESI+) calcd from $C_{16}H_{17}N_4$ $[M+H]^+$: 265.1453 found; 265.1454.

2-(4'-(azidomethyl)-[1,1'-biphenyl]-4-yl)cyclopropan-1-amine (Probe 8)

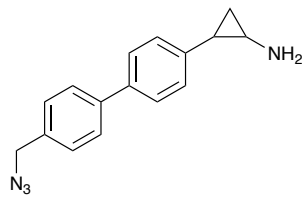

To *tert*-butyl (2-(4'-(azidomethyl)-[1,1'-biphenyl]-4-yl)cyclopropyl)carbamate (40 mg, 0.109 mmol) in DCM (4 mL) was added HCl in dioxane (4 mL, 4 M) dropwise and protected by a N_2 atmosphere. The reaction mixture was stirred for 3 hr. The solvent was removed under reduced pressure. The solvent was removed under reduced pressure, the oil was dissolved in DCM (4 mL) and precipitated by slow addition of hexane (6 mL). The precipitated was re-dissolved in DCM and condensed to give 30 mg (94%) of white crystalline solid.

IR (ν_{max}/cm^{-1}) 3300, 2975, 2925, 2100, 2075, 1500.

^{1}H NMR (400MHz, MeOD, 298 K) δ 7.66 – 7.61 (4 H, m), 7.45 (2 H, d, $^3J_{HH}$ = 8.2 Hz), 7.28 (2 H, d, $^3J_{HH}$ = 8.3 Hz), 4.42 (2 H, s), 2.93 – 2.89 (1 H, m), 2.45 – 2.40 (1 H, m), 1.49 – 1.38 (2 H, m).

^{13}C {^{1}H} NMR (100MHz, MeOD, 298 K) δ 141.8, 140.5, 139.1, 136.3, 130.0, 128.3, 128.2, 127.9, 55.3, 32.1, 22.3, 13.9.

MS (ESI+) $[M+H]^+$ (%) 265.1 (100).

HRMS(ESI+) calcd from $C_{16}H_{17}N_4$ $[M+H]^+$: 265.1453; found 265.1447.

2.6.3 Kinetics

2.6.3.1 H_2O_2 Standard Curve

To create a standard curve, 25 µL of serial dilution H_2O_2 (400 – 0.85 µM) were added to duplicate wells of a non-binding black flat bottomed chimney 384-well plate, this was diluted with the addition of 5 µL of phosphate buffer solution. 20 µL of freshly made chromogenic solution was added consisting of Amplex Red® (0.25 mM) and HRP (5 mM) was added to the wells containing H_2O_2 solution. 50 µL of phosphate buffer (50 mM, pH 7.47, ionic strength 154 mM, 2.5% v/v DMSO) was added to duplicate wells to serve as a blank. 30 µL of phosphate buffer (50 mM, pH 7.47, ionic strength 154 mM, 2.5% v/v DMSO) was added to duplicate wells, 20 µL of freshly made chromogenic solution added consisting of Amplex Red® (0.5 mM) and HRP (5 mM) was added to form another set of blanks. The fluorescence measurements were recorded on a mono-chromator based fluorescence microplate reader set to 37 °C in the dark, with excitation wavelength 560 ± 10 nm and emission wavelength 590 ± 10 nm. The gain was automatically set to H_2O_2 (0.4 mM) with a value of 1100. A single point experiment was conducted. The data was exported and processed using Microsoft® Excel.[119]

Table.5 Required volumes for preparing H_2O_2 standard curve at 50 µL total volume.

H_2O_2 concentration [mM]	Volume of chromogenic solution (µL)	Volume of phosphate buffer solution (µL)	Volume of Serial Dilution (µL)
0.40	20	5	25
0.20	20	5	25
0.10	20	5	25
0.05	20	5	25
0.025	20	5	25
0.013	20	5	25
0.0063	20	5	25
0.0031	20	5	25
0.0016	20	5	25
0.00078	20	5	25
0.00039	20	5	25
0.0	20	5	25

2.6.3.2 Michaelis Menten (MM)

2.6.3.2.1 MAOA- MAOB

The enzyme activities of MAOA and MAOB were identified though the metabolism of tyramine. The reactants present in a non-binding black flat bottomed chimney 384-well plate were as follows; 50 µL of phosphate buffer (50 mM, pH 7.47, ionic strength 154 mM, 2.5% v/v DMSO) was added to duplicate wells, , to serve as a negative control. 25 µL of phosphate buffer (50 mM, pH 7.47, ionic strength 154 mM, 2.5% v/v DMSO) was added to duplicate wells, 20 µL of freshly made chromogenic solution added consisting of Amplex Red® (0.5 mM) and HRP (5 mM) and 5 µL of MAOA / MAOB (3.8 enzyme units) were added to form a second set of negative controls. 5 µL of phosphate buffer (50 mM, pH 7.47, ionic strength 154 mM, 2.5% v/v DMSO) was added to duplicate wells, 20 µL of freshly made chromogenic solution added consisting of Amplex Red® (0.5 mM) and HRP (5 mM) and 25 µL of H_2O_2 (0.4 mM) were added to serve as a positive control. To identify the enzyme kinetics, 25 µL of serial dilution of tyramine (1000 – 0.13 µM) were added to duplicate wells. 20 µL of freshly made chromogenic solution added consisting of Amplex Red® (0.25 mM) and HRP (5 mM) was added to the wells contain tyramine solution. The reaction was initiated by the addition of 5 µL of MAOA / MAOB (3.8 active units / mL) to the tyramine solutions. The fluorescence measurements were recorded on a mono-chromator based fluorescence microplate reader set to 37 °C in the dark, with excitation wavelength 560 ± 10 nm and emission wavelength 590 ± 10 nm. The gain set was identical to that in the standard curve assay. A multiple point experiment was conducted, monitored every 25 secs for 1 hr. The kinetic parameters were determined using at least 9 different concentrations close to the estimated K_m value. Each experiment was reproduced three times using tyramine stock solutions prepared independently.[119]

Maximal slope was measured within the first 15 min (RFU min^{-1}) and converted to initial reaction velocities (µM min^{-1}), using the H_2O_2 standard curve. The reaction velocities were fitted to the MM equation using an excel program.

Table.6 Required volumes for preparing MAO's for Michaelis Menten experiment at 50 µL total volume.

Tyramine concentration [µM]	Volume of chromogenic solution (µL)	Volume of MAOA/MAOB (µL)	Volume of Serial Dilution (µL)
1000	20	5	25
750	20	5	25
500	20	5	25
250	20	5	25
130	20	5	25
75	20	5	25
62.5	20	5	25
50	20	5	25
37.5	20	5	25
25	20	5	25
12.5	20	5	25

2.6.3.2.2 LSD1

The enzyme activity of LSD1 was identified though the metabolism of H3K4me2 peptide. The reactants present in a non-binding black flat bottomed chimney 384-well plate, were as follows; 50 µL of phosphate buffer (50 mM, pH 7.47, ionic strength 154 mM, 2.5% v/v DMSO) was added to duplicate wells, to serve as a negative control. 25 µL of phosphate buffer (50 mM, pH 7.47, ionic strength 154 mM, 2.5% v/v DMSO) was added to duplicate wells, 20 µL of freshly made chromogenic solution added consisting of Amplex Red® (0.5 mM) and HRP (5 mM) and 5 µL of LSD1 (0.75 mg/mL) was added to form a second set of negative controls. 5 µL of phosphate buffer (50 mM, pH 7.47, ionic strength 154 mM, 2.5% v/v DMSO) was added to duplicate wells, 20 µL of freshly made chromogenic solution added consisting of Amplex Red® (0.5 mM) and HRP (5 mM) and 25 µL of H_2O_2 (0.4 mM) was added to serve as a positive control. To identify the enzyme kinetics, 25 µL of serial dilution of H3K4me2 peptide (1000 – 3.43 µM) was added to duplicate wells. 20 µL of freshly made chromogenic solution added consisting of Amplex Red® (0.25 mM) and HRP (5 mM) was added to the wells contain H3K4me2 solution. The reaction was initiated by the addition of 5 µL of LSD1 (0.75 mg/mL) to the H3K4me2 peptide solutions. The fluorescence

measurements were recorded on a mono-chromator based fluorescence microplate reader set to 37 °C in the dark, with excitation wavelength 560 ± 10 nm and emission wavelength 590 ± 10 nm. The gain set was identical to that in the standard curve assay. A multiple point experiment was conducted, monitored every 20 secs for 3 hr. The kinetic parameters were determined using at least 8 different concentrations close to the estimated K_m value. Each experiment was reproduced three times using H3K4me2 peptide stock solutions prepared independently.[119]

Maximal slope was measured within the first 45 min (RFU min^{-1}) and converted to initial reaction velocities (μM min^{-1}), using the H_2O_2 standard curve. The reaction velocities were fitted to the MM equation using an excel program.

Table.7 Required volumes for preparing LSD1 for Michaelis Menten experiment at 50 μL total volume.

H3K4me2 concentration [μM]	Volume of chromogenic solution (μL)	Volume of LSD1 (μL)	Volume of Serial Dilution (μL)
2000	20	5	25
1000	20	5	25
500	20	5	25
250	20	5	25
125	20	5	25
62.5	20	5	25
31.25	20	5	25
15.6	20	5	25
7.8	20	5	25

2.6.3.3 IC_{50} Inhibition assay

2.6.3.3.1 MAOA & MAOB

The drug affinity to inhibit the enzyme were identified through the change in oxidation of tyramine through varying concentrations of drug. The reactants present in a non-binding black flat bottomed chimney 384-well plate were as follows; 50 μL of phosphate buffer (50 mM, pH 7.47, ionic strength 154 mM, 2.5% v/v DMSO) was added to duplicate wells, to serve as a negative control. 25 μL of phosphate buffer (50 mM, pH 7.47, ionic strength 154 mM, 2.5% v/v DMSO) was

added to duplicate wells, 20 µL of freshly made chromogenic solution added consisting of Amplex Red® (0.5 mM) and HRP (5 mM) and 5 µL of MAOA / MAOB (3.8 enzyme units) were added to form a second set of negative controls. 5 µL of phosphate buffer (50 mM, pH 7.47, ionic strength 154 mM, 2.5% v/v DMSO) was added to duplicate wells, 20 µL of freshly made chromogenic solution added consisting of Amplex Red® (0.5 mM) and HRP (5 mM) and 25 µL of H_2O_2 (0.4 mM) were added to serve as a positive control. To identify the drug affinity to the enzyme, 25 µL of serial dilution of probe (500 – 0.00052 µM) were added to duplicate wells. The reaction was initiated by the addition of 5 µL of MAOA / MAOB (3.8 active units / mL) to the probe solutions and were incubated for 10 mins at 37 °C. 20 µL of freshly made chromogenic solution added consisting of Amplex Red® (0.25 mM), HRP (5 mM) and tyramine (500 mM) was added to the wells contain probe and enzyme solution. The fluorescence measurements were recorded on a mono-chromator based fluorescence microplate reader set to 37 °C in the dark, with excitation wavelength 560 ± 10 nm and emission wavelength 590 ± 10 nm. The gain set was identical to that in the standard curve assay. A multiple point experiment was conducted, monitored every 20 secs for 30 mins. The kinetic parameters were determined using at least 9 different concentrations close to the estimated IC_{50} value. Maximal slope was measured within the first 15 min (RFU min^{-1}) and converted to initial reaction velocities (µM min^{-1}), using the H_2O_2 standard curve. The reaction velocities were fitted to the IC_{50} equation using an excel program.[119]

Table.8 Required volumes for preparing synthesised probes for IC_{50} inhibition experiment for MAOs at 50 µL total volume.

Tyramine concentration [µM]	Volume of chromogenic solution (µL)	Volume of MAOA/MAOB (µL)	Probe Concentration [µM]	Volume of Serial Dilution (µL)
500	20	5	500	25
500	20	5	143	25
500	20	5	40.8	25
500	20	5	11.7	25
500	20	5	3.33	25
500	20	5	0.952	25
500	20	5	0.272	25
500	20	5	0.0777	25
500	20	5	0.0222	25
500	20	5	0.0065	25
500	20	5	0.0018	25
500	20	5	0.0005	25

2.6.3.4 K_i (inhibitory constant) assay

2.6.3.4.1 MAOA - MAOB

The drug affinity to inhibit the enzyme were identified through the change in oxidation of tyramine through varying concentrations of drug. The reactants present in a non-binding black flat bottomed chimney 384-well plate, were as follows; 50 µL of phosphate buffer (50 mM, pH 7.47, ionic strength 154 mM, 2.5% v/v DMSO) was added to duplicate wells, to serve as a negative control. 25 µL of phosphate buffer (50 mM, pH 7.47, ionic strength 154 mM, 2.5% v/v DMSO) was added to duplicate wells, 20 µL of freshly made chromogenic solution added consisting of Amplex Red® (0.5 mM) and HRP (5 mM) and 5 µL of MAOA / MAOB (3.8 enzyme units) were added to form a second set of negative controls. 5 µL of phosphate buffer (50 mM, pH 7.47, ionic strength 154 mM, 2.5% v/v DMSO) was added to duplicate wells, 20 µL of freshly made chromogenic solution added consisting of Amplex Red® (0.5 mM) and HRP (5 mM) and 25 µL of H_2O_2 (0.4 mM) were added to serve as a positive control. To identify the drug affinity to the enzyme, 25 µL of serial dilution of probe (1250 – 0.00052 µM) were added to

duplicate wells. The reaction was initiated by the addition of 5 µL of MAOA / MAOB (3.8 active units / mL) and 20 µL of freshly made chromogenic solution added consisting of Amplex Red® (0.25 mM), HRP (5 mM) and tyramine (500 mM) were added to the wells contain probe solution. The fluorescence measurements were recorded on a mono-chromator based fluorescence microplate reader set to 37 °C in the dark, with excitation wavelength 560 ± 10 nm and emission wavelength 590 ± 10 nm. The gain set was identical to that in the standard curve assay. A multiple point experiment was conducted, monitored every 50 secs for 120 mins. The kinetic parameters were determined using at least 9 different concentrations close to the estimated K_i value.[124]

Table.9 Required volumes for preparing synthesised probes for K_i inhibition experiment for MAOs at 50 µL total volume.

Tyramine concentration [µM]	Volume of chromogenic solution (µL)	Volume of MAOA/MAOB (µL)	Probe Concentration [µM]	Volume of Serial Dilution (µL)
500	20	5	1250	25
500	20	5	625	25
500	20	5	312.5	25
500	20	5	156.25	25
500	20	5	78.125	25
500	20	5	39.063	25
500	20	5	19.531	25
500	20	5	9.766	25
500	20	5	4.883	25
500	20	5	2.442	25
500	20	5	1.221	25
500	20	5	0.610	25

2.6.3.4.2 LSD1 Inhibition Assay

The drug affinity to inhibit the enzyme were identified through the change in metabolism of H3K4me2 peptide through varying concentrations of drug. The reactants present in a non-binding black flat bottomed chimney 384-well plate were as follows; 50 µL of phosphate buffer (50 mM, pH 7.47, ionic strength 154 mM, 2.5% v/v DMSO) was added to duplicate wells, , to serve as a negative control. 25 µL of phosphate buffer (50 mM, pH 7.47, ionic strength 154 mM, 2.5% v/v DMSO) was added to duplicate wells, 20 µL of freshly made chromogenic solution added consisting of Amplex Red® (0.5 mM) and HRP (5 mM) and 5 µL of LSD1 (0.75 mg/mL) was added to form a second set of negative controls. 5 µL of phosphate buffer (50 mM, pH 7.47, ionic strength 154 mM, 2.5% v/v DMSO) was added to duplicate wells, 20 µL of freshly made chromogenic solution added consisting of Amplex Red® (0.5 mM) and HRP (5 mM) and 25 µL of H_2O_2 (0.4 mM) was added to serve as a positive control. To identify the drug affinity to the enzyme, 25 µL of serial dilution of probe (1250 – 0.00052 µM) were added to duplicate wells. To this, 20 µL of freshly made chromogenic solution added consisting of Amplex Red® (0.25 mM), HRP (5 mM) and H3K4me2 peptide (200 mM) were added to the wells contain probe solution. The reaction was initiated by the addition of 5 µL of LSD1 (0.75 mg/mL). The fluorescence measurements were recorded on a mono-chromator based fluorescence microplate reader set to 37 °C in the dark, with excitation wavelength 560 ± 10 nm and emission wavelength 590 ± 10 nm. The gain set was identical to that in the standard curve assay. A multiple point experiment was conducted, monitored every 50 secs for 120 mins. The kinetic parameters were determined using at least 8 different concentrations close to the estimated K_i value.[124]

Table.10 Required volumes for preparing synthesised probes for K_i inhibition experiment for LSD1 at 50 µL total volume

H3K4me2 peptide concentration [µM]	Volume of chromogenic solution (µL)	Volume of LSD1 (µL)	Probe Concentration [µM]	Volume of Serial Dilution (µL)
50	20	5	1250	25
50	20	5	625	25
50	20	5	312.5	25
50	20	5	156.25	25
50	20	5	78.125	25
50	20	5	39.063	25
50	20	5	19.531	25
50	20	5	9.766	25
50	20	5	4.883	25
50	20	5	2.442	25
50	20	5	1.221	25
50	20	5	0.610	25

2.6.3.5 Solutions

Phosphate buffer solutions

Phosphate buffer solution (50 mM, pH 7.47, 154 mM KCl, 0.0% v/v DMSO) was prepared by dissolving $NaH_2PO_4.2H_2O$ (7.8 g, 156 g/mol) and KCl (1.54 g, 74.6 g/mol) in 900 mL of de-ionised water. The pH was altered using NaOH (1 M) and HCl (1 M) to 7.51 at 20 °C. The volume was made up to 1000 mL with de-ionised water.

Phosphate buffer solution (50 mM, pH 7.47, 154 mM KCl, 2.5% v/v DMSO) was prepared by dissolving $NaH_2PO_4.2H_2O$ (7.8 g, 156 g/mol), KCl (1.54 g, 74.6 g/mol) and Molecular Biology grade DMSO (25 mL) in 875 mL of de-ionised water. The pH was altered using NaOH (1 M) and HCl (1 M) to 7.51 at 20 °C. The volume was made up to 1000 mL with de-ionised water.

Phosphate buffer solution (50 mM, pH 7.47, 154 mM KCl, 3.33% v/v DMSO) was prepared by dissolving $NaH_2PO_4.2H_2O$ (7.8 g, 156 g/mol), KCl (1.54 g, 74.6

g/mol) and Molecular Biology grade DMSO (33 mL) in 867 mL of de-ionised water. The pH was altered using NaOH (1 M) and HCl (1 M) to 7.51 at 20 °C. The volume was made up to 1000 mL with de-ionised water.

Phosphate buffer solution (50 mM, pH 7.47, 154 mM KCl, 4.0% v/v DMSO) was prepared by dissolving $NaH_2PO_4.2H_2O$ (7.8 g, 156 g/mol), KCl (1.54 g, 74.6 g/mol) and Molecular Biology grade DMSO (40 mL) in 860 mL of de-ionised water. The pH was altered using NaOH (1 M) and HCl (1 M) to 7.51 at 20 °C. The volume was made up to 1000 mL with de-ionised water.

Phosphate buffer solution (55 mM, pH 7.47, 154 mM KCl, 0.0% v/v DMSO) was prepared by dissolving $NaH_2PO_4.2H_2O$ (8.69 g, 156 g/mol) and KCl (0.544 g, 74.6 g/mol) in 900 mL of de-ionised water. The pH was altered using NaOH (1 M) and HCl (1 M) to 7.51 at 20 °C. The volume was made up to 1000 mL with de-ionised water.

Stock Solutions of MAOA and MAOB (3.8 active units/mL)

MAOA and MAOB enzymes (0.5 mL, 5 mg/mL), containing a variety of enzyme activity units, in a solution of potassium phosphate (100 mM, pH 7.4, 0.25 mM sucrose, 0.1 mM EDTA, 5% glycerol). The enzymes were defrosted on ice upon arrival and partitioned into aliquots to produce the working solution (3.8 active units, 200 µL). and quickly frozen to −80 °C. Before use, the enzyme was defrosted on ice and diluted before use with phosphate buffer (50 mM, pH 7.47, ionic strength 154 mM).

Stock solutions of LSD1

The LSD1 enzyme were expressed in E. coli (BL21 DE3) cells which is described in section 3.5.4. The resulting solution were partitioned into aliquots of 1.5 mg/mL, which were stored at −80 °C.

Amplex Red® (1 mM)

The working solution of Amplex Red® was prepared by dissolving Amplex red® (5 mg, 257.25 g/mol) in molecular grade DMSO (1 mL). This was subsequently diluted with phosphate buffer (18 mL, 55 mM, pH 7.47, ionic strength 154 mM) to

acquire the 1 mM solution. There were partitioned into aliquots and stored away from light at -20 °C.

Horseradish Peroxidase (HRP) (20 mM)

The working solution of HRP was prepared by dissolving HRP (8 mg) into phosphate buffer (100 mL, 50 mM, pH = 7.47, ionic strength 154 mM, 0.0% v/v DMSO). This was partitioned into aliquots and stored at -20 °C.

Tyramine Solution (2 mM)

The working solution of tyramine was prepared by dissolving tyramine (0.0138 g, 137.18 g/mol) in phosphate buffer (50 mL, 50 mM, pH = 7.47, ionic strength 154 mM, 4.0% v/v DMSO). This was partitioned into aliquots and stored at -20 °C.

H3 21mer (K4me2) peptide solution (100 µM)

The H3 21mer (K4me2) peptide (1 mg, 2282 g/mol) was dissolved in sterilised de-ionised water (438 uL) to make the final concentration of 100 µM. This was partitioned into aliquots and stored at -20 °C.

H_2O_2 Solution (40 mM)

The stock solution of H_2O_2 was prepared by diluting H_2O_2 (2 mL, 30% v/v) with de-ionised water (998 mL). The obtained solution is less stable. This was titrated before use, using the following proceedure to identify the accurate concentration through a 1:2 stoichiometry.

$$H_2O_{2\,(aq)} + H_2SO_{4\,(aq)} + 2KI_{\,(aq)} \rightarrow I_{2\,(aq)} + 2H_2O_{\,(l)} + K_2SO_{4\,(aq)}$$

$$Na_2S_2O_{3\,(aq)} + I_{2\,(aq)} \rightarrow 2NaI_{\,(aq)} + Na_2S_4O_{6\,(aq)}$$

Potassium iodide (10 mL, 2.5 M) and H_2O_2 (20 mL) was added to sulphuric acid (50 mL, 1 M) and cooled on ice. The mixture was titrated with sodium thiosulfate (0.1 M) until the brown colour almost disappeared. Starch solution (1 mL) was added and produced a dark grey solution. Additional sodium thiosulfate was added until the solution turned clear.

Potassium Iodide Solution (2.5 M)

The stock solution of potassium iodide was prepared by adding potassium iodide (415 g, 166 g/mol) to de-ionised water (1000 mL). The solution was stored at room temperature.

Solution of probe inhibitors

A solution of probe inhibitors was prepared by adding molecular biology grade DMSO to the individual vials to make a concentration of 0.1 M. This was partitioned into aliquots and stored away from light at -20 °C.

2.6.4 Expression of Recombinant LSD1 Enzyme

2.6.4.1 Expression

For production of LSD1 recombinant protein in bacteria, a truncated portion of human LSD1 cDNA [2559 base pairs (bp); GenBank accession number NM_015013) was amplified by polymerase chain reaction (PCR) from human cDNA and sequentially cloned into the N-terminal 6 x Histidine (HIS)-tag bacterial expression vector pET302/NT-His.

pET302/NT-His plasmid was defrosted on ice for 45 mins. To E. coli (BL21 DE3 pLysS) cells, was added 2 µL of the DNA plasmid (75 ng) and incubated for 30 mins at 0 °C. The E. coli were heat shocked at 42 °C for 45 secs, and cooled on ice for 2 mins. Super Optimal Broth (S.O.B.) Medium (500 µL) was added to the transformed cells and aliquoted onto agar plates and were incubated overnight at 37°C.

To 100 mL of Lysogeny Broth (LB) media (100 mL) (Ampicillin 0.1 mg/ mL) was inoculated with a single colony from a freshly transformed plate as the starting culture, cultured at 37 °C overnight. 20 mL of the starting culture was expanded in 2 L of LB media (Ampicillin 0.1 mg/mL) and incubated at the same temperature. When the culture reached an OD_{600} of 0.5, the expression of the recombinant proteins was induced by addition of IPTG (isopropyl B-D-1-thiogalactopyranoside) (3000 µL, 1 M) with final concentration of 1.5 mM and incubated at 37 °C for 9 hrs. The cell suspension was collected and spun down for 15 mins at 7000 g at 4 °C. The cell pellets were frozen at -80 °C. The cell pellets were re-suspended in a cold lysis buffer (50 mM NaH_2PO_4, 300 mM NaCl, 10 mM imidazole, pH 8), supplemented with PMSF (1.5% v/v, 1 M) protease inhibitor. The cells suspension was lysed using a high pressure homogenizer (French press) for two to three rounds and centrifuged twice for 30 mins at 35000 g, 4 °C, and once for 90 mins at 50000 g, 4 °C.

The supernatant was applied to a column Amintra® Ni-NTA Affinity resin (expedeon) previously equilibrated with the lysis buffer. The column was washed intensively with lysis buffer until the absorbance at 280 nm read less than 0.001.

Following this, the column was washed with buffer (50 mM NaH_2PO_4, 300 mM NaCl, 50 mM imidazole, pH 8), until the absorbance at 280 nm read less than 0.001. The HIS-Tagged LSD1 was eluted from the resin over several fractions using buffer (50 mM NaH_2PO_4, 300 mM NaCl, 250 mM imidazole, pH 8). The fractions were run on SDS-Page gel and the fractions containing LSD1 was identified by Instant Blue staining. The fraction was combined, condensed and buffer solution changed to phosphate buffer solution (50 mM NaH_2PO_4, 154 mM KCl, pH 7.47) using Merck™ Amicon™ Ultra Centrifugal Filter 30000 MWCO. The recombinant LSD1 protein was aliquoted and stored at -80 °C. The concentration of LSD1 was estimated using BCA protein assay, with bovine serum albumin (BSA) as standard. This method routinely produces recombinant LSD1 protein with a purity of greater than 90%, with an average yield of 1 – 1.75 mg per litre of culture.[125]

2.6.4.2 Solutions

LB Agar

Miller's LB Agar was prepared by dissolving LB Agar (2.5 g) into 100 mL of de-ionised water. The solution was sterilised, cooled to 50 °C and Ampicillin (0.1 mL, 0.1 g/mL) was added. The solution was partitioned into aliquots in agar plates and cooled to room temperature. The plates were stored at +4 °C.

LB Broth (Miller's) Solutions

Miller's LB Broth was prepared by dissolving LB broth (25 g) into 1 L of de-ionised water. The solution was sterilised before use.

Miller's LB Broth was prepared by dissolving LB broth (2.5 g) into 100 mL of de-ionised water. The solution was sterilised before use.

Ampicillin (0.1 g/mL)

The stock solution for Ampicillin was prepared by dissolving Ampicillin sodium salt (0.186 g, 371.39 g/mol) in de-ionised water (5 mL) to make a 0.1 g/mL solution. The solution was filter sterilised, partitioned into aliquots and stored at – 80 °C.

IPTG (1 M)

The stock solution for IPTG (isopropyl B-D-1-thiogalactopyranoside) was prepared by dissolving IPTG (4.766 g, 238.3 g/mol) in 20 mL of de-ionised water to make a 1 M solution, which was filter sterilised and stored at -20 °C.

PMSF Protease Inhibitor (1 M)

The stock solution for PMSF was prepared by dissolving PMSF (phenylmethylsulfonyl fluoride) (0.87 g, 174.2 g/mol) in propan-2-ol (5 mL) to make a 1 M solution. This solution was partitioned into aliquots and stored at – 20 °C.

Phosphate buffer solutions

Lysis Buffer: Phosphate buffer solution (50 mM, pH 8.0, 300 mM NaCl, 10 mM Imidazole) was prepared by dissolving $NaH_2PO_4.2H_2O$ (7.8 g, 156 g/mol), NaCl (9.15 g, 74.6 g/mol) and imidazole (0.68 g, 68.077 g/mol) in 900 mL of de-ionised water. The pH was altered using NaOH (1 M) and HCl (1 M) to 7.95 at 20 °C. The volume was made up to 1000 mL with de-ionised water.

Wash Buffer: Phosphate buffer solution (50 mM, pH 8.0, 300 mM NaCl, 50 mM Imidazole) was prepared by dissolving $NaH_2PO_4.2H_2O$ (7.8 g, 156 g/mol), NaCl (9.15 g, 74.6 g/mol) and imidazole (3.40 g, 68.077 g/mol) in 900 mL of de-ionised water. The pH was altered using NaOH (1 M) and HCl (1 M) to 7.95 at 20 °C. The volume was made up to 1000 mL with de-ionised water.

Elution Buffer: Phosphate buffer solution (50 mM, pH 8.0, 300 mM NaCl, 250 mM Imidazole) was prepared by dissolving $NaH_2PO_4.2H_2O$ (7.8 g, 156 g/mol), NaCl (9.15 g, 74.6 g/mol) and imidazole (17.06 g, 68.077 g/mol) in 900 mL of de-ionised water. The pH was altered using NaOH (1 M) and HCl (1 M) to 7.95 at 20 °C. The volume was made up to 1000 mL with de-ionised water.

Phosphate buffer solution (50 mM, pH 7.47, 154 mM KCl, 0.0% v/v DMSO) was prepared by dissolving $NaH_2PO_4.2H_2O$ (7.8 g, 156 g/mol) and KCl (1.54 g, 74.6 g/mol) in 900 mL of de-ionised water. The pH was altered using NaOH (1 M) and HCl (1 M) to 7.51 at 20 °C. The volume was made up to 1000 mL with de-ionised water.

2.6.5 Visualisation in cells

2.6.5.1 Cell culture

NTERA2 cells were maintained in DMEM medium supplemented with 10% fetal calf serum (FCS), at 37 °C in a humidified atmosphere of 10% CO_2 in air. Dulbecco's phosphate buffered saline without Ca^{2+} and Mg^{2+} (PBS) or PBS with 3% fetal calf serum (FCS) was used as a wash buffer in the NTERA2 work.

2.6.5.2 Fluorescent Imaging and Analysis.

NTERA2 cells were harvested with 0.25% trypsin / 1 mM EDTA in PBS, and reseeded, at 2000 cell per well in a 96-well plate. After culturing for 24 hr the medium was replaced with DMEM, 10% FCS supplemented with either 0.1% DMSO or **probe 1** (0.1 - 1 mM). These cells were grown on for a further 2 hr, washed with PBS, washed with 3 % FCS in PBS. The cells were fixed with 4% paraformaldehyde for 10 min, washed with PBS, then 3% FCS in PBS. The cells were permeabilised with 0.25% Triton X100 in PBS for 20 min, washed with PBS, and 3% FCS in PBS. The click reagents were added and incubated at room temperature with gentle agitation, in Tris (100 mM, pH 8.5), $Cu(II)SO_4.5H_2O$ (0.5 mM), Alexa Fluor® 594 azide (5 μM), ascorbic acid (100 mM) for 30 min, washed with PBS, then 3% FCS in PBS. The cells were stained with either; an antibody to a pan-human marker: TRA-1-85, primary polyclonal LSD1 antibody (Dilution 1:100 in blocking buffer), primary monoclonal MAOA antibody (Abcam, ab126751) (Dilution 1:100 in blocking buffer), primary polyclonal MAOB antibody (Sigma, SAB1406105) (Dilution 1:100 in blocking buffer), primary polyclonal Histone 3 antibody (Abcam, ab1791) (1:100 in blocking buffer) and Hoechst 33342 for 1 hour, washed with PBS, and then 3% FCS in PBS. The relevant secondary antibody Alexa Fluor® 488 (Dilution 1:200) was incubated with the cells for 1 hr washed with PBS, then 3% FCS in PBS. The plate was washed with PBS a further two times then stored with PBS in the wells at 4 °C. Cells were visualized with an in Cell Analyzer microscopy system (GE healthcare, Cytation 5). TRA-1-85 staining was used to generate a cellular outline (Cyto mask),[123] the enzyme antibodies (MAOA, MAOB, LSD1) were used to identify the presence of the enzymes, and co-localisation with the inhibited LSD1 enzyme, Histone 3 was used as a positive control and Hoechst 33342 to visualize the nucleus.[126] Therefore, the cell position in each microscope field (Nuclear mask) is visualised in the appropriate software (Investigator Toolbox, GE Healthcare, Cytation 5).[127]

2.6.5.3 Solutions

DMEM + 10% FCS

The working solution of 10% FCS was prepared by dilution of FCS (25 mL) in DMEM solution. The solution was stored at 4 °C.

0.25% Trypsin / 1mM EDTA in PBS

The working solution of 0.25% Trypsin / 1mM EDTA was prepared by dissolving EDTA (0.15 g, 292.4 g/mol) in PBS (498.75 mL) and adding Trypsin (1.25 mL, 0.25%). The solution was stored at 4 °C.

10% FCS in PBS

The working solution of 10% FCS was prepared by dilution of FCS (25 mL) in PBS solution. The solution was stored at 4 °C.

3% FCS in PBS

The working solution of 3% FCS was prepared by dilution of FCS (7.5 mL) in PBS solution. The solution was stored at 4 °C.

4% Paraformaldehyde

The working solution of paraformaldehyde was prepared by diluting paraformaldehyde (108 mL, 37%) in 891 mL of de-ionised water. This was partitioned into aliquots and stored at – 20 °C.

0.25% TritonX-100 in PBS

The working solution of TritonX-100 was prepared by diluting TritonX-100 (0.25 mL) into 100 mL of PBS solution.

Click Chemistry Reagents

Tris (1 M, pH 8.0)

The stock solution of Tris was prepared by dissolving Tris base (12.2 g, 121.1 g/mol) into 100 mL of de-ionised water. The pH was altered using NaOH (1 M) and HCl (1 M) to 7.51 at 20 °C. This was partitioned into aliquots and stored at – 20 °C.

Copper Sulfate (0.1 M)

The stock solution of Copper Sulfate was prepared by dissolving $Cu(II)SO_4.5H_2O$ (0.25 g, 249.7 g/mol) into 10 mL of de-ionised water. This was partitioned into aliquots and stored at 4 °C.

Ascorbic Acid (0.1 M)

The stock solution of ascorbic acid was prepared by dissolving sodium ascorbate (0.20 g, 198.1 g/mol) into 10 mL of de-ionised water. This was partitioned into aliquots and stored at – 20 °C.

Alexa Fluor™ 594 azide (0.008 M)

The stock solution of Alexa Fluor™ 594 azide was prepared by dissolving Alexa Fluor™ 594 azide triethylammonium salt (0.5 mg, 948.16 g/mol) into 66 µL of molecular biology grade DMSO. This was partitioned into aliquots and stored as – 20 °C.

Hoechst 33342 (5 mg/mL)

The stock solution of Hoechst 33342 was prepared by dilution of the Hoechst 33342 (10 mL, 10 mg/mL) in 10 mL of ultrapure water. This was partitioned into aliquots and stored at – 20 °C.

Hoechst 33342 (5 µg/mL)

The working solution of Hoechst 33342 was prepared by dilution of the stock solution 1:1000 with ultrapure water.

PBST (PBS + 0.1% Tween 20)

The working solution of PBST was prepared by adding Tween 20 (0.2 mL, 0.1%) to PBS (200 mL). The solution was stored at 4 °C.

Blocking Buffer (1% BSA, 300 mM Glycine)

The working solution of the blocking buffer was prepared by dissolving Glycine (2.2 g, 75.1 g/mol) and BSA (1mL, 1%) into PBST (99 mL). The solution was stored at +4 °C.

2.6.6 Western Blot Analysis.

2.6.6.1 Visualisation

NTERA2 cells (2 x 10^6) were treated for 2 - 18 hr with inhibitor at the indicated concentrations in DMEM medium, then collected and extracted with RIPA Buffer. Protein concentrations of the lysates were determined using a bicinchoninic acid (BCA) assay; equivalent amounts of proteins from each lysate were resolved in 4 – 25% SDS-polyacrylamide gel and then transferred onto 22 nitrocellulose membranes (Bio-Rad Laboratories). After having been blocked for 1 hr with Tris-buffered saline – TWEEN 20 (TBS-T) containing 3% skim milk, the transblotted membrane was incubated overnight at 4 °C with H3K4me antibody (Cell Signalling, D1A9) (1:1000 dilution), H3K4me3 antibody (Cell Signalling, C42D8) (1:1000 dilution), H3 antibody (Abcam, ab1791) (1:1000 dilution), primary polyclonal LSD1 antibody (Dilution 1:1000), primary monoclonal MAOA antibody (Abcam, ab126751) (Dilution 1:1000), primary polyclonal MAOB antibody (Sigma, SAB1406105) (Dilution 1:1000) in TBS-T containing 5% skim milk. The membrane was probed with the primary antibody for 16 h, then washed twice with TBS-T, incubated with goat anti-rabbit IgG- horseradish peroxidase conjugate (Li-cor, 926-32211) (diluted 1:5000) or donkey anti-mouse IgG- horseradish peroxidase conjugate (Li-cor, 926-32212) (diluted 1:5000), in TBS-T containing 3% skim milk, for 1 h at room temperature, and again washed twice with TBS-T. The immunoblots were visualized by enhanced chemiluminescence.

2.6.6.2 Solutions

RIPA Buffer (50 mM Tris, 150 mM Sodium Chloride, 1% Triton X-100, 0.5% Sodium Deoxycholate, 0.1% SDS)

The working solution of RIPA buffer was prepared by dissolving Tris base (6.06 g, 121.1 g/mol), NaCl (4.58 g, 58.4 g/mol), TritonX-100 (10 mL), Sodium Deoxycholate (1 g) and SDS (1 g) into 1 L of de-ionised water. The solution was partitioned into aliquots and stored at - 20 °C.

10x Transfer Buffer (Tris 250 mM, Glycine 1900 mM, SDS 1%)

The stock solution of 10x transfer buffer was prepared by dissolving Tris base (30.28 g, 121.1 g/mol), glycine (142.6 g, 75.07 g/mol) and SDS (10 g) into 1 L of de-ionised water. The solution was stored at 4 °C.

1x Transfer Buffer (Tris 25 mM, Glycine 190 mM, SDS 0.1%, Methanol 10%)

The working solution of 1x transfer buffer was prepared by dilution 10x transfer buffer (100 mL) into methanol (100 mL) and de-ionised water (800 mL). The solution was cooled to 4 °C before use.

10x TBS (Tris 100 mM, NaCl 1500 mM, pH 8.0)

The stock solution of 10x TBS buffer was prepared by dissolving Tris base (12.11 g, 121.1 g/mol) and NaCl (87.7 g, 58.4 g/mol) in 900 mL of de-ionised water. The pH was altered using NaOH (1 M) and HCl (1 M) to 7.95 at 20 °C. The volume was made up to 1000 mL with de-ionised water. The solution was stored at 4 °C.

1x TBS-T (Tris 10 mM, NaCl 150 mM, pH 8.0, Tween20 10%)

The working solution of 1x TBS-T buffer was prepared by dilution 10x TBS (100 mL) in Tween20 (10 mL) and de-ionised water (890 mL). The solution was cooled to 4 °C before use.

5% Blocking Buffer

The working solution of 5% blocking buffer was prepared by dissolving non-fat dried milk (2.5 g) in 1x TBS-T (50 mL). The solution was cooled to 4 °C before use.

2.6.7 MALDI-TOF/MS analysis.

LSD1 (0.75 mg/mL, 100 µL) was incubated with **probe 1** (2 mM) for 2 hr at room temperature in phosphate buffer (50 mM, ionic strength 154 mM, pH 7.4). The click reagents were added and incubated at room temperature with gentle agitation, in Tris (100 mM, pH 8.5), $Cu(II)SO_4.5H_2O$ (0.5 mM), Alexa Fluor® 594 azide (5 µM), ascorbic acid (100 mM) for 30 min. The reaction mixture were denatured with SDS (0.1%) plus Trifluoroacetic acid 0.1% (TFA), applied to a C_{18} Zip-Tip (Sigma-Aldrich) column, and eluted with 50:50 CH_3CN/H_2O containing 0.1% TFA. The eluent was mixed 50:50 with α-Cyano-4-hydroxycinnamic acid (CHCA) (5 mg/mL) and analysed using matrix assisted laser desorption ionization time-of-flight (MALDI-TOF) instrument (Bruker, Synapt) in reflectron positive mode with 25 kV acceleration.

Chapter 3 Peptide-probe conjugates

3.1 Introduction

As previously stated in Chapter 1.5.5, some small molecules lack cell permeability.[128] The creation of histone peptide conjugated inhibitors and peptide like inhibitors has be used as a strategy to overcome these potential traits.[95] The synthesis of the peptide probes will be achieved through conjugation of the azide tagged probes to a C-terminal, L-C-propargylglycine residue on the peptide using click chemistry, selected due it its readily availability, ease of purification and reliability. Reagents for the reaction are shown in **Table.11** where $Cu(II)SO_4$ as the source of copper, ascorbic acid is used as a reducing agent to convert Cu(II) to Cu(I), and tris is used as a chelating ligand to support the generated Cu(I) ion. Due to the toxicity of Cu(I) ions,[129] tris buffer is used to reduce side redox of reactive oxygen species (ROS) which can lead the degradation of amino acids, principally arginine, peptides, and dehydroascorbate. Therefore, a copper to tris ligand ratio of 1:250 will be used.[130]

Table.11 Reagents used for Click Chemistry reaction.

Reagents	Role
Tris Buffer	Ligand
Ascorbic acid	Reducing agent
$Cu(II)SO_4$	Catalyst
Water	Solvent

Increasing cell permeability of molecules by addition of peptides though click chemistry has been achieved before. I. M. Eggleston *et.al* successfully achieved cell permeability of porphyrins by the addition of a cell penetrating peptides. This was completed by the modification of an asymmetric porphyrin to received either alkyne, azide or cycloctyne motifs to enable clickable linkage to the cell penetrating peptides. This offered an ideal way to repurpose simple porphyrins derivatives for photochemical internalisation which was directly resulted from attaching the cell penetrating peptides.[170]

An initial peptide sequence based upon the repeating LLKK subunit, LLKKLLKKLLKKLLG(Propargyl) was provided by Dr Steve Brown of the RNAi Screening Facility, Department of Biomedical Sciences, the University of Sheffield. This peptide sequence was selected from high-content screening

experiments due to its cell permeability and anti-proliferation effects as seen in colorectal cancer cell lines*. Dr Steve Brown provided 250 mg of LLKKLLKKLLKKLLG(Propargyl), for use in small molecule conjugation experiments details of the peptides screens, antiproliferative effects in colorectal cancer cell lines and the resulting pharmacology will be published in the PhD thesis of Roja Hadianamrei.*

Aims and objectives of this chapter;

- The probes developed in Chapter 2 will be combined with peptide (**Scheme.12**) to afford novel peptide probe conjugates (**PP**) with the aim of using the peptide to guide the probe into the cell nucleus and increasing selectivity of inhibition towards LSD1 over the other MAO enzymes.
- The inhibitory activities (IC_{50}) of these conjugates will be assessed by *in vitro* testing with recombinant MAOA, MAOB and LSD1 enzymes.
- To analyse the cell permeability of the peptide, click chemistry will be used to attach a fluorophor to the peptide, this will allow for visualisation of the peptide in HCT 116 colorectal cancer cells.

3.2 Synthesis of Peptide Probe Conjugates

The synthetic route for novel **PP 1 - 5** is shown in **Scheme.12**. The synthesis of the peptide probes proceeds through a Cu(I) catalysed click reaction, with Cu(II)SO_4 as the source of copper. Ascorbic acid as a reducing agent to convert Cu(II) to Cu(I), and Tris used as a chelating ligand to support the generated Cu(I) ion.[170-171]

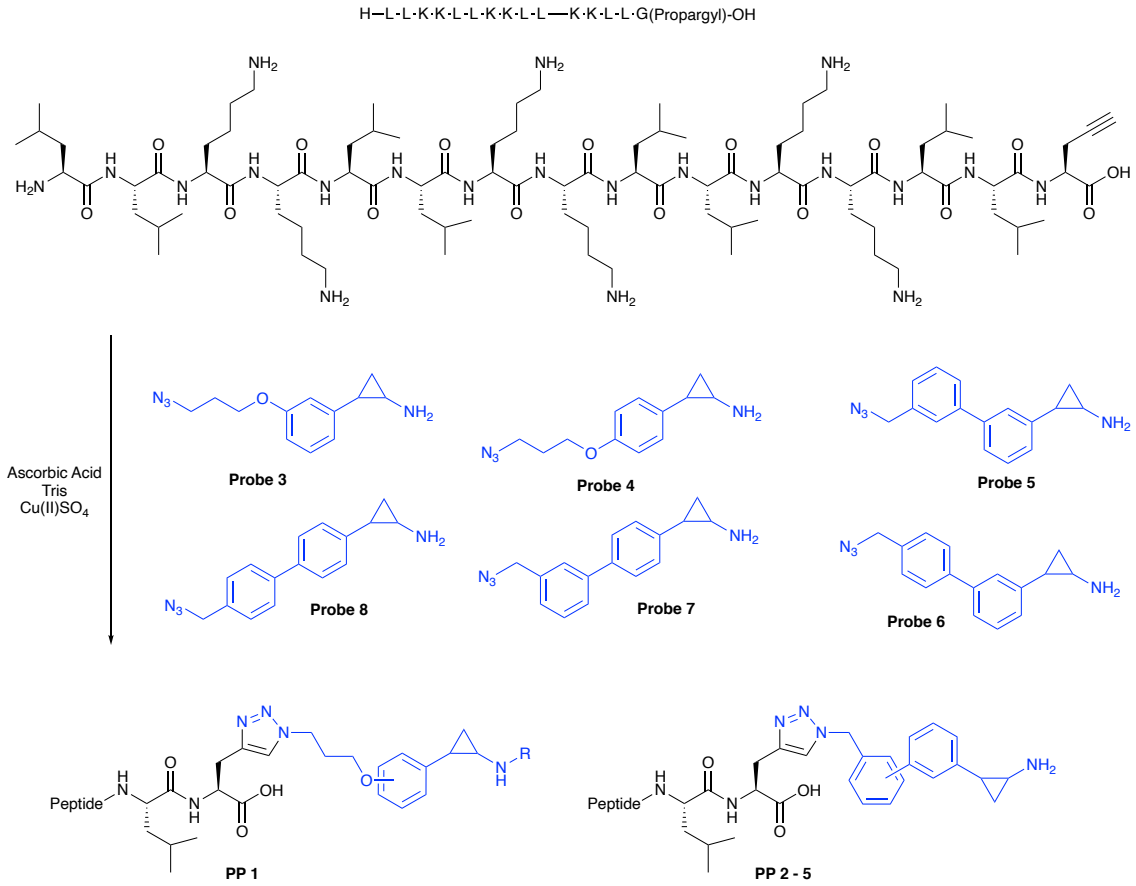

Scheme.12 Cu(I) catalysed click synthesis for **PP 1 - 5**

3.3 Enzyme Assays

The coupled fluorescence assay measures the stoichiometric release of peroxide from the oxidation of FAD cofactor. The reported inhibition data collected is standardised using the H_2O_2 standard curve (2.3.1), the Michaelis Menten experiment (2.3.2) to identify the optimum substrate concentration for the inhibition assay.

3.3.1 Inhibition Assays

The inhibition activity for the synthesised probes towards recombinant human LSD1, MAOA and MAOB were evaluated by IC_{50} assays. This data was collected using methods described in Chapter 2.3.3, the inhibition data was standardised and characterised in identical fashion. The inhibition activities, IC_{50} for the peptide conjugates **PP 1 – 5** with MAOA, MAOB and LSD1 are reported in **Table.12**.

Table.12 *In vitro* MAOA, MAOB, LSD1 inhibitory activities (IC_{50}) of synthesised **PP 1 - 5** and **PCPA**. (*n=3* for all enzyme assays except for **PP 1** for LSD1, *n=1*)

Compound	MAOA / μM	MAOB / μM	LSD1 / μM
PCPA	100 ± 44	22 ± 5	12 ± 3
PP 1	69 ± 9	16 ± 3	117
PP 2	126 ± 1	27 ± 4	72 ± 16
PP 3	15 ± 8	7.6 ± 4.9	81 ± 27
PP 4	28 ± 4	13 ± 2	145 ± 44
PP 5	57 ± 7	28 ± 5	113 ± 36

The inhibition data allowed a study of the effects the addition of the peptide has to the synthesised small molecules **probes 4 - 8** for the inhibition of MAOs and LSD1 enzymes when compared to **PCPA** (IC_{50} values: MAOA: 100 μM, MAOB: 22 μM and LSD1: 12 μM). For **PP 1**, with the hydroxy-alkyl-clicked peptide in the *para* position an increase in selectivity towards MAOA and MAOB by 1.4 fold for MAOA and MAOB (IC_{50} values: 69 μM and 16 μM respectively) but an eight fold decrease in selectivity towards LSD1 (IC_{50} value: 117 μM) is seen. **PP 2 – 5** all contain the benzyl-clicked peptide but with differing *meta* or *para* substitution positions around the phenyl ring, for each peptide conjugate molecule. **PP 2** shows a decrease in selectivity of 1.3 fold for MAOA, 1.2 fold for MAOB and 5.1

fold for LSD1 (IC_{50} values: 126 μM, 27 μM and 72 μM respectively). **PP 3** shows an increase in selectivity of 6.7 fold for MAOA and 2.9 fold for MAOB (IC_{50} values: 15 μM and 7.6 μM respectively) but a decrease in selectivity of 5.8 fold for LSD1 (IC_{50} values: 81 μM). **PP 4** shows an increase in selectivity of 3.5 fold for MAOA and 1.7 fold for MAOB (IC_{50} values: 28 μM and 13 μM respectively) but a decrease in selectivity of ten fold for LSD1 (IC_{50} values: 145 μM). **PP 5** shows an increase in selectivity of 1.8 fold for MAOA (IC_{50} values: 57 μM) but a decrease in selectivity of 1.3 fold for MAOB and eight fold for LSD1 (IC_{50} values: 28 μM and 145 μM respectively).

To expand upon this, the peptide molecules are compared to the small molecular origin in **Figure.43**. The addition of the peptide to each of the probes causes an overall decrease in selectivity towards each enzyme. When comparing **PP 1** to **probe 4,** this causes a decrease in selectivity towards the tested enzymes with 15 fold towards MAOA, 3.2 fold towards MAOB and 2.5 fold for LSD1 (IC_{50} values: 69 μM, 16 μM and 117 μM respectively). When comparing **PP 2** to **probe 5**, this causes a decrease in selectivity towards the tested enzymes with 6.6 fold towards MAOA, 46 fold towards MAOB and five fold for LSD1 (IC_{50} values: 125 μM, 27 μM and 72 μM respectively). When comparing **PP 3** to **probe 6**, this causes a decrease in selectivity towards the tested enzymes with 3.3 fold towards MAOA, 3.8 fold towards MAOB and 3.6 fold for LSD1 (IC_{50} values: 15 μM, 7.6 μM and 81 μM respectively). When comparing **PP 4** to **probe 7**, this causes a decrease in selectivity towards the tested enzymes with 5.6 fold towards MAOA, 13 fold towards MAOB and 18 fold for LSD1 (IC_{50} values: 28 μM, 13 μM and 144 μM respectively). When comparing **PP 5** to **probe 8**, this causes a decrease in selectivity towards the tested enzymes with 14 fold towards MAOA, 540 fold towards MAOB and 22 fold for LSD1 (IC_{50} values: 56 μM, 27 μM and 113 μM respectively). The peptide was clicked to the probes to increase the selectivity towards LSD1.

As expected, the addition of the peptide to each probes causes a successful decrease in selectivity towards the MAO enzymes. This decrease in selectivity is due to addition of the bulky peptide to the probe molecules restricting the access of the probe to the small active site, resulting in the decrease of selectivity towards both MAOA and MAOB.

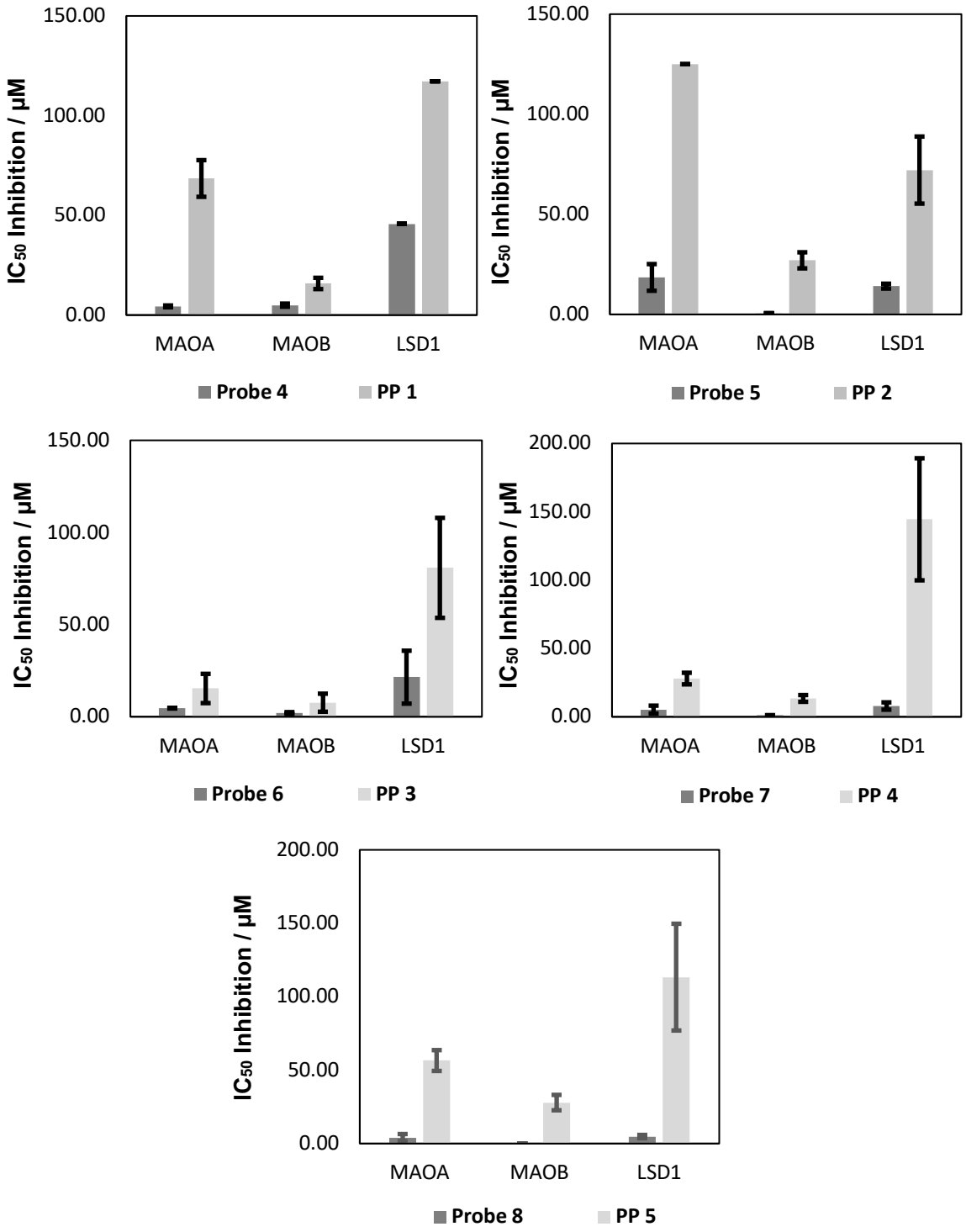

Figure.43 *In vitro* Inhibition comparison (IC_{50}) of individual probes against the peptide probe derivatives for MAOA, MAOB and LSD1 enzymes.

The inhibition data showed that the addition of the peptide had an adverse effect, decreasing each probes selectivity towards LSD1. The addition of the peptide causes two main changes to the probe; 1. addition of the bulky peptide group, 2. removal of the azide moiety on the probes. The addition of the bulky peptide group mimics the bulk of H3K4 from the chromatin, but not the molecular recognition profile, the differences between the two could be a detriment to

increasing the selectivity towards LSD1. Furthermore, the addition of the peptide to the probes causes the phenyl rings of the probes to be situated differently in the active site. As a result, causing weaker π - π interactions in the between the probe and the active site. Due to the nature of the reaction of the peptide conjugates, the azide is reacted and formed a triazole moiety. The change in moiety will alter the electrostatic interactions within the active site. Further adding to the increase in inhibition in LSD1.

3.4 Visualisation tracking of peptide in cells.

The cellular uptake of the peptide was identified using HCT 116 colorectal cancer cells. The peptide was reacted with Alexa-Fluor 594 in a Cu(I) catalysed click reaction. The cells were treated with 50 μM of peptide and 50 μM of peptide-Alexa-Fluor for 24 hours, fixed, permeabilised and visualised.

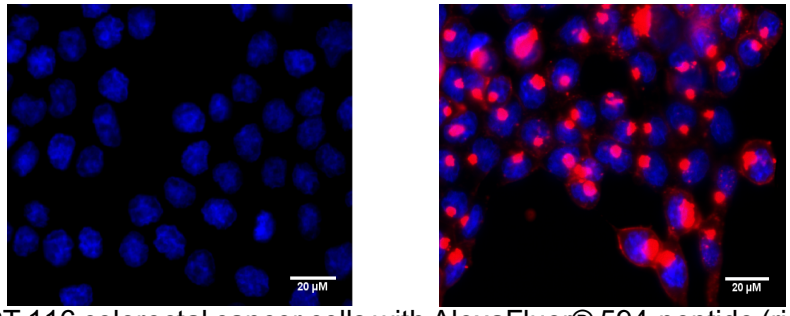

Figure.44 HCT 116 colorectal cancer cells with AlexaFluor® 594-peptide (right) and non-fluorescent peptide (left), stained with Hoechst 33342.

Through qualitative analysis of **Figure.44**, it is shown that the peptide passes through the membrane and undertakes nuclear localisation in the HCT 116 colorectal cancer cells. *The treatment and visualisation of the HCT 116 cells was undertaken by the Steven Brown group at the RNAi Screening Facility, Department of Biomedical Sciences, University of Sheffield. The click chemistry reaction was undertaken by myself.*

3.5 Conclusion

A set of five peptide probe conjugates were synthesised and characterised using appropriate analytical techniques. For all five conjugates their inhibitory effect against LSD1 and MAOs was investigated providing IC_{50} data. To our surprise, the addition of the peptide to the probes increases all the potency towards LSD1. However, the bulky peptide group decreases the potency for MAOA and MAOB. The visualisation of the pre-conjugated peptide shows that it is successfully

passed through the HCT 116 cell membrane, the probe-peptide conjugates **PP 1-5** are being investigated for antiproliferative effects in colorectal cancer cell lines[167] in the laboratory of Dr Steve Brown of the RNAi Screening Facility, Department of Biomedical Sciences, the University of Sheffield Additionally, further development of the peptide probes will be needed to increase the inhibition potency towards LSD1. This can be achieved substituting the LLKK subunit variant for a H3 mimicking peptide, to increase the molecular recognition profile. Alternatively, increasing the potency towards LSD1 can also be achieved through imitation of GSK and Oryzon's approach by N-alkylation of the PCPA scaffold.

3.6 Experimental

3.6.1 Materials and Methods

Peptide purification.

Dr Steve Brown provided 250 mg of the peptide LLKKLLKKLLKKLLG(Propargyl). Peptide purification was performed using HPLC (Perkin Elmer Series 200) with a C_{18} column (250 mm × 4.6 mm, 5 µm) with a mixture of 0.1% formic acid in ultrapure water (A) and 0.1% formic acid in acetonitrile (B) as the mobile phase. The gradient elution was performed as follows: 0 - 60 min, 2 - 60% B; 60 - 80 min, 60% B; and 80 - 95 min, 2% B. The injection volume was 600 µL and the column temperature was at room temperature. The mobile phase flow rate was 5 mL min^{-1} and the detection wavelength was 254 nm. Fractions of the eluate were collected, and those containing the same component were combined. The resulting residues were freeze-dried for further use.

MS: Finnigan MAT, Electro Spray source, Flow Rate: 15 µL/min, Gas: Nitrogen.

HRMS: Xevo G2-XS QTOF Mass Spectrometer. Electro Spray (ES) ionisation source, Gas: Nitrogen, Flow rate: 5 µL/min.

LCMS: LCMS purification analysis was performed using a Triple Quad LC/MS (Aglient Technologies 6420) with a C_{18} column (150 mm × 1 mm, 5 µm) with a mixture of 0.1% formic acid in ultrapure water (A) and 0.1% formic acid in acetonitrile (B) as the mobile phase. The gradient elution was performed as follows: 0–60 min, 5–60% B; 60–65 min, 60% B; 65-70 min, 60-5%B; 70–82 min, 5% B. The injection volume was 1 µL and the column temperature was at room temperature. The mobile phase flow rate was 0.12 mL min^{-1} and the detection wavelength 254 nm. The eluent is then ionised with electro spray source, Flow Rate: 15 µL/min, Gas: Nitrogen. The analyses mass range was 300 – 2000 m/z. The variation in baseline of the chromatographs is directly due to the gradient change in mobile phase.

3.6.2 Synthesis

Peptide Probe 1 (PP 1)

To synthetic peptide (0.006 M, 300 µL) in de-ionised water (12 µL) was added Tris Buffer (1 M, 60 µL), Ascorbic acid (0.4 M, 150 µL), $Cu(II)SO_4$ (0.01 M, 10 µL) and **probe 4** (0.1 M, 50 µL) and stirred for 2 hr at room temperature. The reaction mixture was purified using reverse phase chromatography to give 1.5 mg (42%) of white amorphous solid.

LCMS: t_R (Peptide Purification): 31.1 min**.**

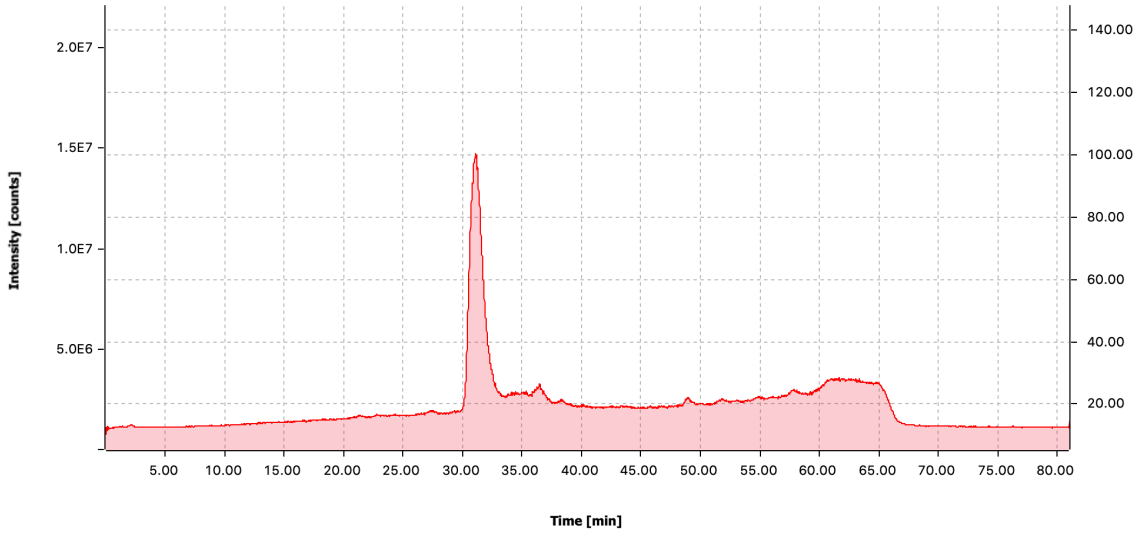

HRMS(ESI+) calcd from $C_{101}H_{184}N_{25}O_{17}$ $[M+H]^+$; 2019.4302 found 2019.4371.

Peptide Probe 2 (PP 2)

To synthetic peptide (0.006 M, 300 µL) in de-ionised water (12 µL) was added Tris Buffer (1 M, 60 µL), Ascorbic acid (0.4 M, 150 µL), $Cu(II)SO_4$ (0.01 M, 10 µL) and **probe 5** (0.1 M, 50 µL) and stirred for 2 hr at room temperature. The reaction mixture was purified using reverse phase chromatography to give 1.9 mg (51%) of white amorphous solid.

LCMS: t_R (LCMS Method): 30.4 min**.**

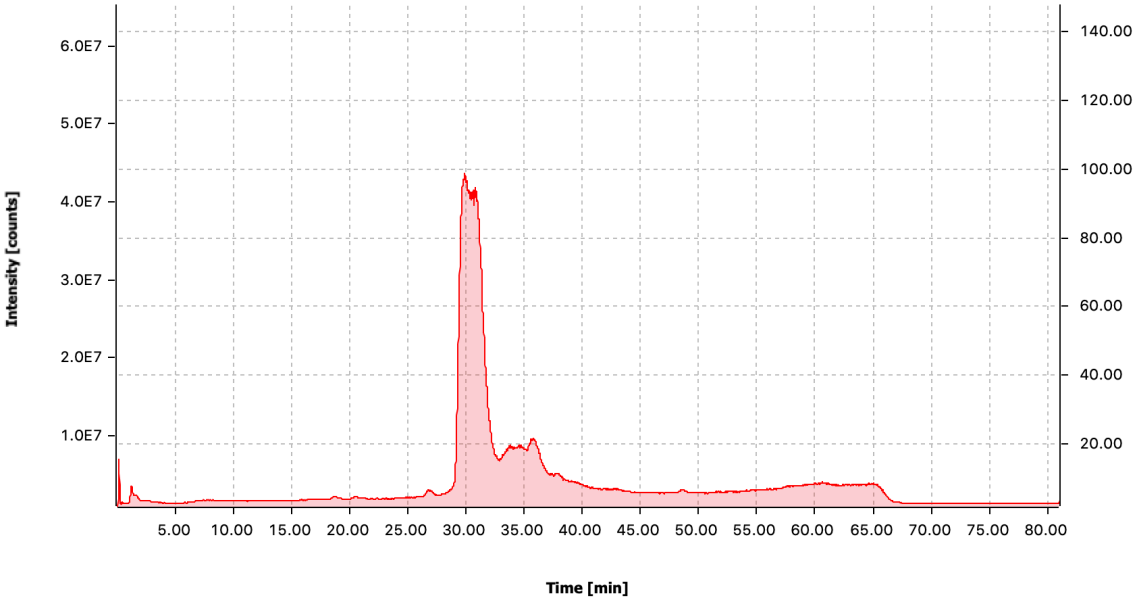

HRMS(ESI+) calcd from $C_{105}H_{184}N_{25}O_{16}$ $[M+H]^+$; 2051.4353 found 2051.4470.

Peptide Probe 3 (PP 3)

To synthetic peptide (0.006 M, 300 µL) in de-ionised water (12 µL) was added Tris Buffer (1 M, 60 µL), Ascorbic acid (0.4 M, 150 µL), Cu(II)SO_4 (0.01 M, 10 µL) and **probe 6** (0.1 M, 50 µL) and stirred for 2 hr at room temperature. The reaction mixture was purified using reverse phase chromatography to give 1.7 mg (46%) of white amorphous solid.

LCMS: t_R (LCMS Method): 34.8 min**.**

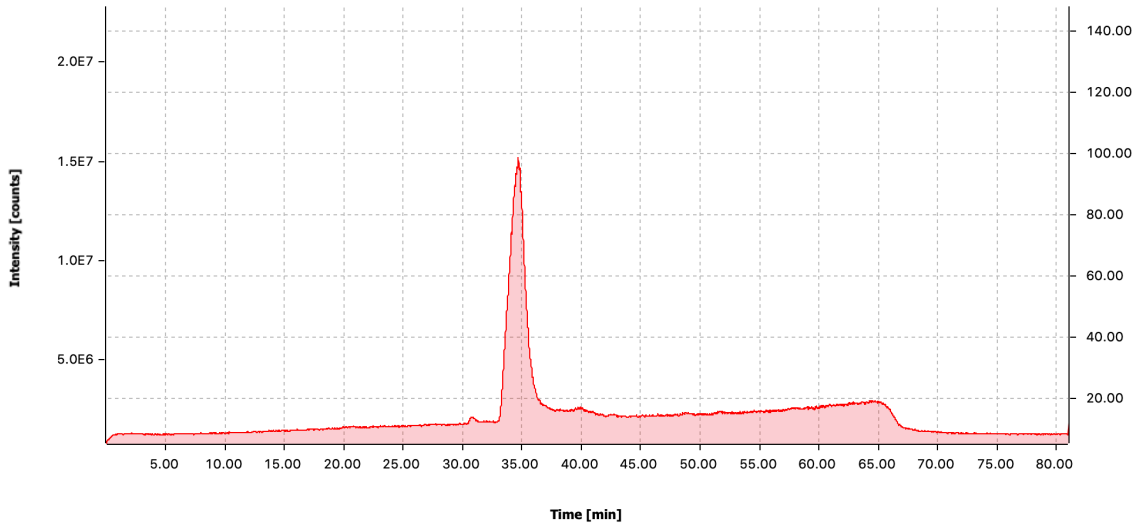

HRMS(ESI+) calcd from $C_{105}H_{184}N_{25}O_{16}$ $[M+H]^+$; 2051.4353 found 2051.4475.

Peptide Probe 4 (PP 4)

To synthetic peptide (0.006 M, 300 µL) in de-ionised water (12 µL) was added Tris Buffer (1 M, 60 µL), Ascorbic acid (0.4 M, 150 µL), Cu(II)SO_4 (0.01 M, 10 µL) and **probe 7** (0.1 M, 50 µL) and stirred for 2 hr at room temperature. The reaction mixture was purified using reverse phase chromatography to give 2.2 mg (59%) of white amorphous solid.

LCMS: t_R (LCMS Method): 34.6 min**.**

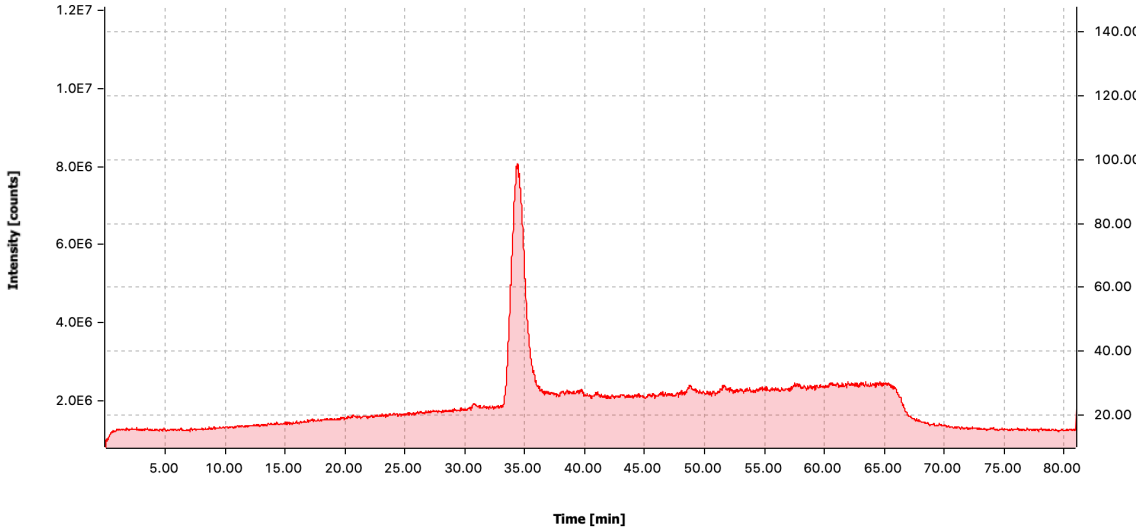

HRMS(ESI+) calcd from $C_{105}H_{184}N_{25}O_{16}$ $[M+H]^+$; 2051.4353 found 2051.4482.

Peptide Probe 5 (PP 5)

To synthetic peptide (0.006 M, 300 µL) in de-ionised water (12 µL) was added Tris Buffer (1 M, 60 µL), Ascorbic acid (0.4 M, 150 µL), Cu(II)SO_4 (0.01 M, 10 µL) and **probe 8** (0.1 M, 50 µL) and stirred for 2 hr at room temperature. The reaction mixture was purified using reverse phase chromatography to give 2.1 mg (57%) of white amorphous solid.

LCMS: t_R (LCMS Method): 34.5 min**.**

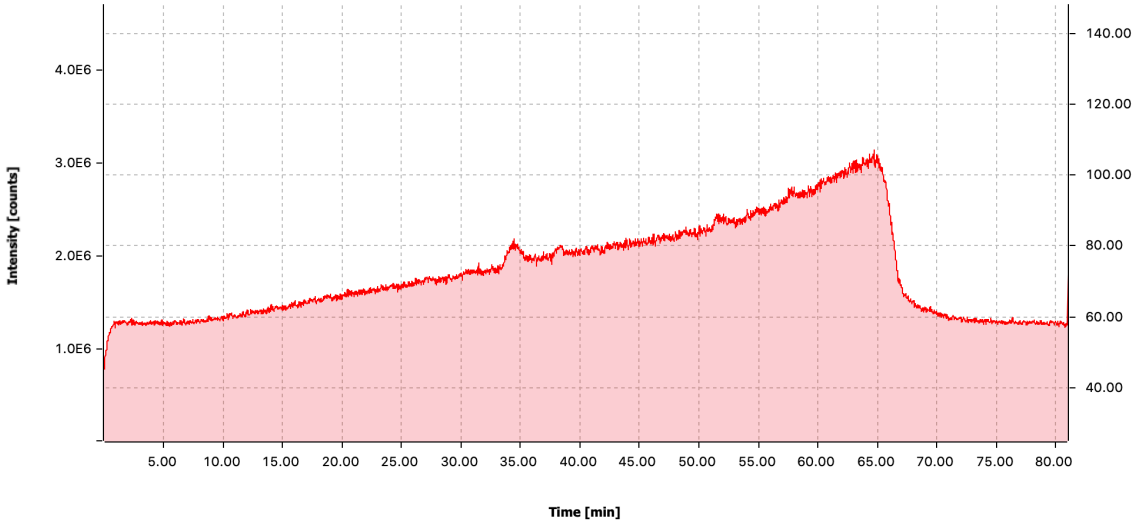

HRMS(ESI+) calcd from $C_{105}H_{184}N_{25}O_{16}$ $[M+H]^+$; 2051.4353 found 2051.4458.

3.6.3 Solution

Synthetic Peptide (0.006 M)

The stock solution of the synthetic peptide was prepared by dissolving peptide (0.01 g, 1787.45 g/mol) into de-ionised water (932 µL). This was evenly portioned into aliquots and stored at -20 °C.

Tris Buffer (1 M, pH 8)

The stock solution Tris Buffer was prepared by dissolving Tris base (60.57 g, 121.14 g/mol) into de-ionised water (450 mL). The pH was altered using NaOH (1 M) and HCl (1 M) to 8.0 at 20 °C. The volume was made up to 500 mL with de-ionised water.

Ascorbic Acid (0.4 M)

The stock solution of Ascorbic Acid was prepared by dissolving sodium ascorbate (0.79 g, 198.1 g/mol) into de-ionised water (10 mL). This was evenly portioned into aliquots and store at -20 °C.

$Cu(II)SO_4$ (0.01 M)

The stock solution of $Cu(II)SO_4$ was prepared by dissolving $Cu(II)SO_4.5H_2O$ (0.025 g, 249.69 g/mol) into de-ionised water (10 mL). This was evenly portioned into aliquots and stored at -20 °C.

Chapter 4 Chiral Separation & N-Alkylation

4.1 Introduction

Many of the LSD1 inhibitors currently in clinical trials are N-alkylated PCPA analogues, that increases the potency of the inhibitors by incorporating the free space in LSD1, which is absent in MAOA and MAOB[10] (See Chapter 1). Equally, all PCPA derived inhibitors, in clinical trials are single enantiomer drugs with controlled stereochemistry around cyclopropane ring. Confirmation of the stereochemistry has been confirmed in the literature by the use of a chiral shift reagent in ^{1}H NMR. This confirms the presence of the enantiomer present by identification of different ppm shifts between the (*1 S - 2 R*) and (*1 R - 2 S*) isomers.[11] Identification of the bio-isosteres of the clinical trial drugs (**Figure.45a**) will guide the development of our probes. Modifications of our probes will be achieved though chiral separation of the cyclopropane ring to afford single enantiomer probes, together with N-alkylation to increase the potency of the probes towards LSD1.

Aims and objectives of this chapter;

- The synthesis of the enantiomeric pair for the '*trans*' isomer of **probe 7** will be completed using reported synthesis by Naoki Miyata *et.al.,* where a chiral auxiliary is used to separate the diastereoisomers by column chromatography (**Figure.45**).[11]

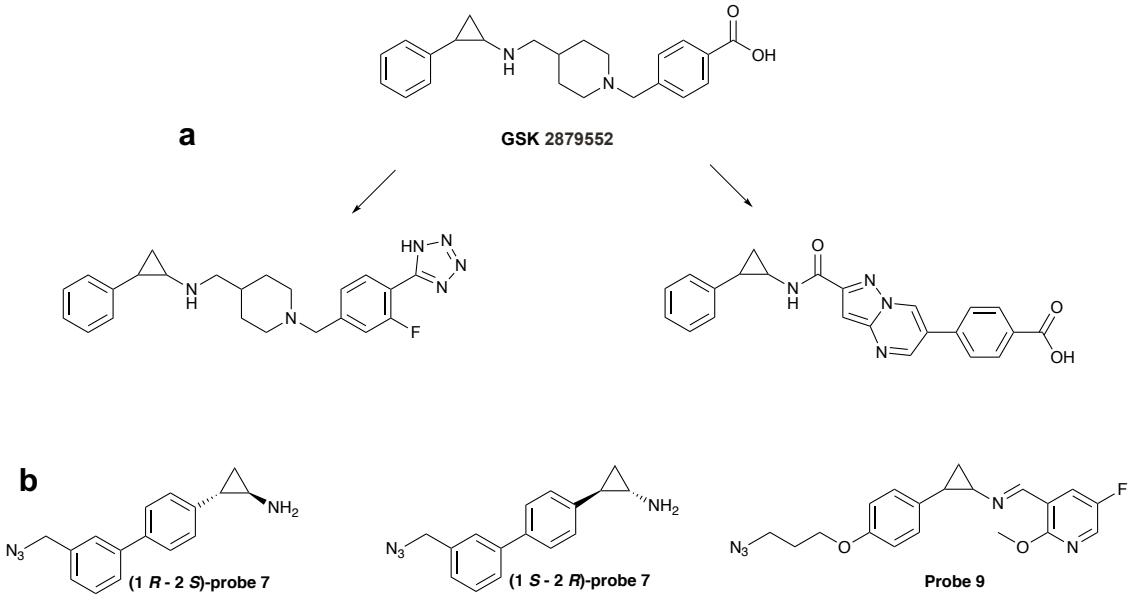

Figure.45a. Development of current N-alkylated PCPA molecules to discover new derivatives **b.** Synthesised of enantiomer probes and N-alkylated probe

- ^{1}H NMR nOe studies will be used to identify the difference in nOe responses between the separated enantiomers. An expected difference in the highlighted hydrogens (**Figure.46**) will occur due to them residing in different environments.[131]

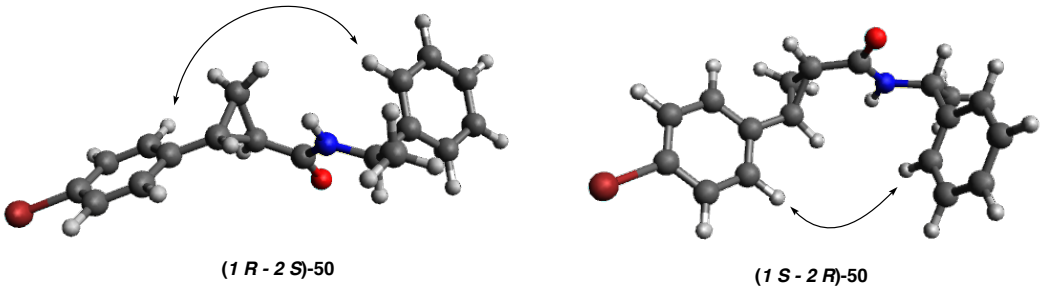

(*1 R - 2 S*)-50 (*1 S - 2 R*)-50

Figure.46 Predicated difference in nOe for enantiomers **(1 *R* - 2 *S*)-50** and **(1 *S* - 2 *R*)-50**

- Single Crystal X-Ray Diffraction analysis will be undertaken on **(1 *R* - 2 *S*)-50** and **(1 *S* - 2 *R*)-50** to confirm the result from the ^{1}H NMR nOe studies.
- The synthesis of the N-alkylated **probe 4** will be completed using GSK's method for reductive amination use for synthesis of inhibitor **GSK2879552**.[164]
- The inhibitory activities (IC_{50}) of the synthesised probes will be assessed by *in vitro* testing with recombinant MAOA, MAOB and LSD1 enzymes.

4.2 Synthesis of diastereoisomers and N-Alkylation

The synthetic route for enantiomer separation of **(1 *R* - 2 *S*)-probe 7**, **(1 *S* - 2 *R*)-probe 7** is shown in **Scheme.13** and the synthetic route for **probe 9** is shown in **Scheme.14**. **Scheme.13** shows the reaction of carboxylic acid **43b** with chiral auxiliary (*S*)-1-phenylethan-1-amine to afford **50**. The diastereoisomers formed from **50** are separated by column chromatography to afford the enantiomeric pair **(1 *R* - 2 *S*)-50** and **(1 *S* - 2 *R*)-50**, with differences in yield due to overlapping peaks.

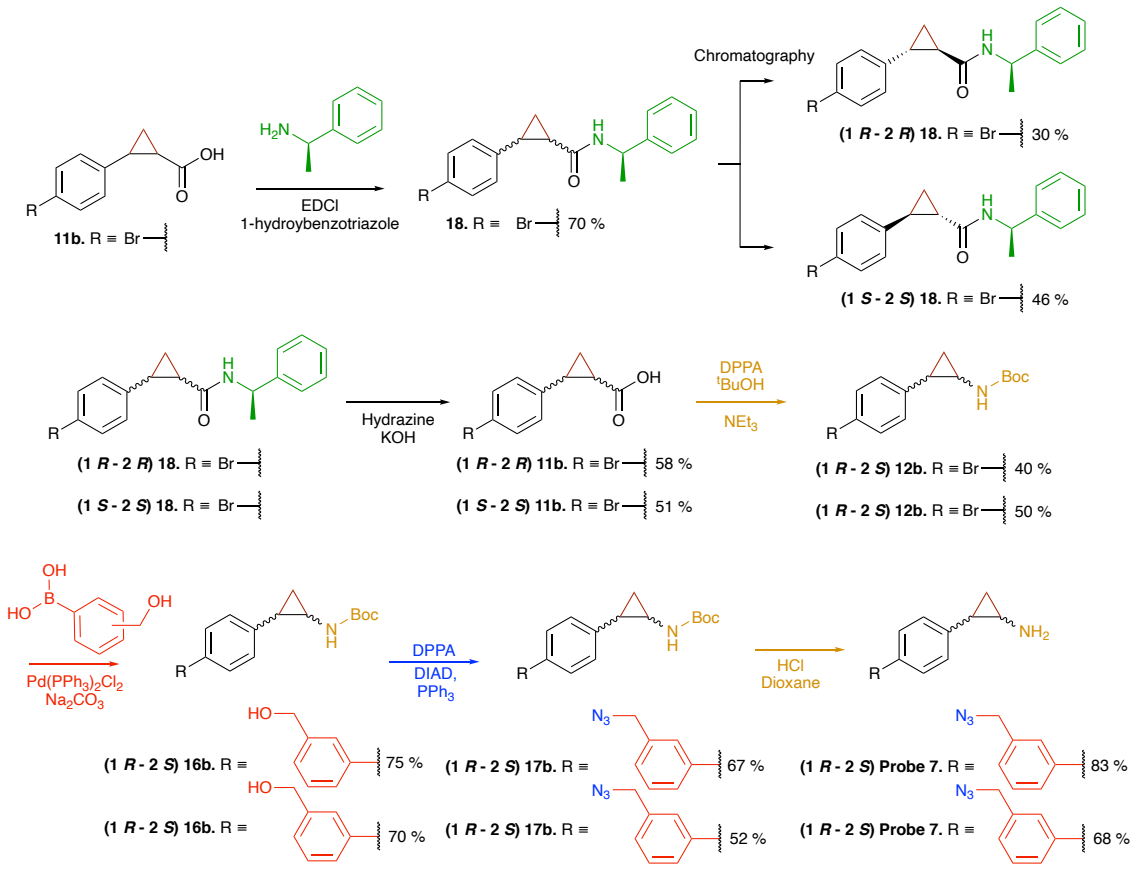

Scheme.13 Multistep syntheses for probe **(1 *R* - 2 *S*)-probe 7** and **(1 *S* - 2 *R*)-probe 7**

Removal of the chiral auxiliary was achieved using hydrazine in basic conditions to give the carboxylic acid's **(1 *R* - 2 *S*)-43b**, **(1 *S* - 2 *R*)-43b**. These are converted to a Boc protected amine **(1 *R* - 2 *S*)-44b**, **(1 *S* - 2 *R*)-44b** through the Curtis rearrangement.[11] The bromine is substituted with 3-hydroxymethylbenzene-boronic acid by the Suzuki coupling to afford **(1 *R* - 2 *S*)-48b**, **(1 *S* - 2 *R*)-48b**.[117] The alcohol was converted to azide **(1 *R* - 2 *S*)-49b**, **(1 *S* - 2 *R*)-49b** through the Mitsunobu reaction.[171] The amine is deprotected under acidic conditions to afford **(1 *R* - 2 *S*)-probe 7** and **(1 *S* - 2 *R*)-probe 7**.[118]

Scheme.14 shows the N-alkylation of **probe 4** through amination with 5-fluoro-2-methoxynicotinaldehyde to afford Schiff base, imine, **probe 9**.[164,165] Due to time restraints, alternative aldehyde substitutes were not attempted to synthesis more N-alkylated probes. Additionally, due to time restraints, other N-alkylation methods were not undertaken to achieve the desired secondary amine.

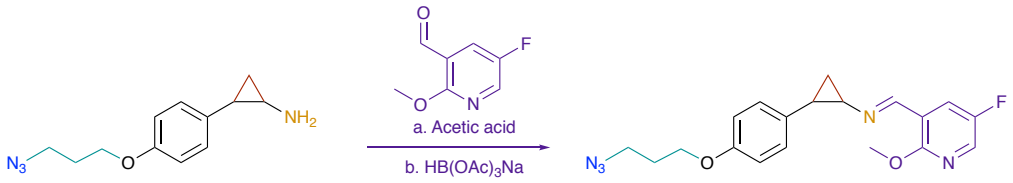

Probe 4 **Probe 9** 38 %

Scheme.14 N-Alkylation of **probe 4** to syntheses **probe 9**

4.3 Chiral crystal structure.

Assigning the absolute stereochemistry to each isomer was identified by two methods, Crystallography and ^{1}H NMR nOe experiments. For Single Crystal X-Ray Diffraction analysis, single crystals were prepared in a variety of conditions (**Table.13**). The single crystals were taken and analysed using Bruker APEX-II CCD Diffractometer to give the structures in **Figure.47**. The crystals analysed gave a low Flack parameter (0.090(17)),[132] and a low ESD value (1.075). The Flack parameter is close to zero which confirms the crystal structure shown is the absolute structure. Therefore, the chiral separation is a success. *The treatment and visualisation of the Crystals was undertaken by the Craig Robertson at Department of Biomedical Sciences, University of Sheffield, the crystals were grown by myself.*

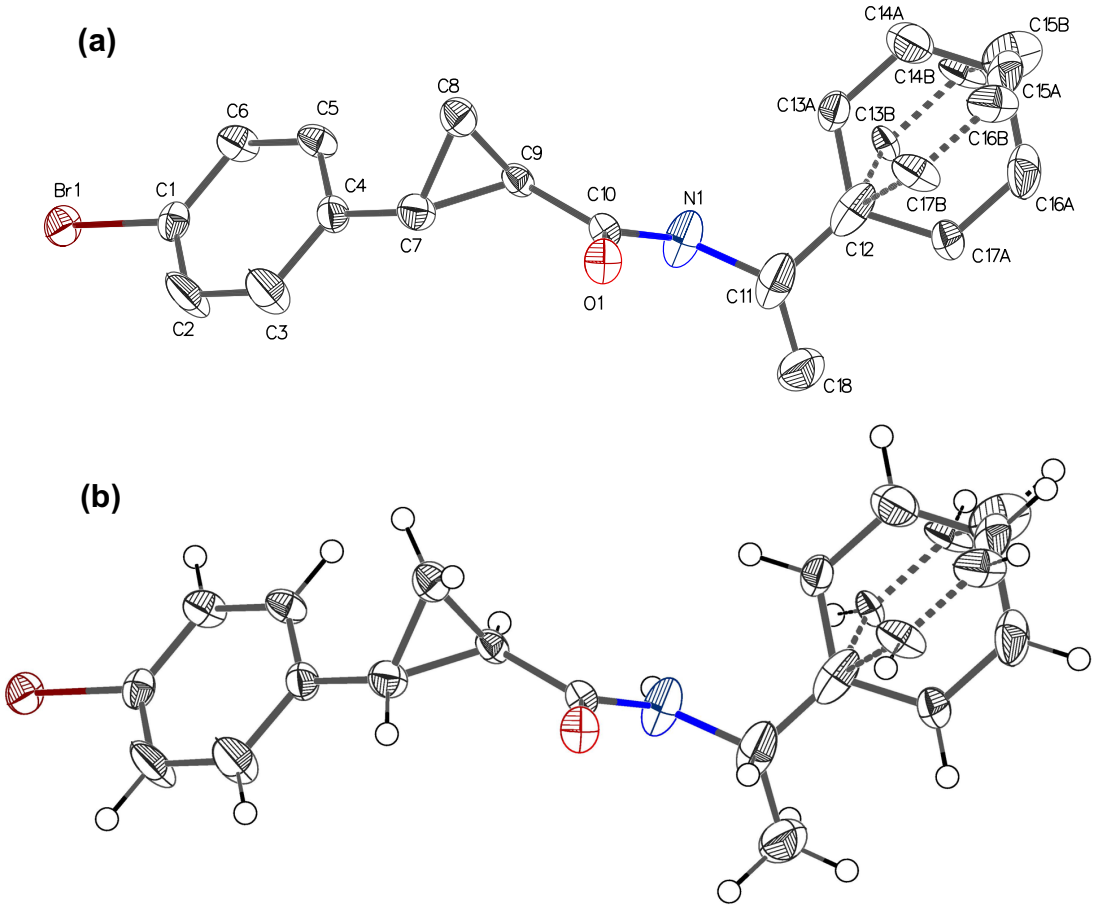

Figure.47(a) Crystal structure for **(1 *R* - 2 *S*)-50** with labelled atoms. **(b)** Crystal structure for **(1 *R* - 2 *S*)-50** showing the position of the calculated hydrogens. Formula: $C_{18}H_{18}BrNO$ (M_r =344.24 g/mol): monoclinic, space group $P2_1$ (no. 4), a = 8.4473(4) Å, b = 4.9222(3) Å, c = 19.0314(10) Å, β = 96.191(3)°, V = 786.70(7) Å^3, Z = 2, T = 100.0 K, μ(CuKα) = 3.536 mm^{-1}, D_{calc} = 1.453 g/cm^3, 30685 reflections measured (4.67° ≤ 2Θ ≤ 133.132°), 2779 unique (R_{int} = 0.0834, R_{sigma} = 0.0372) which were used in all calculations. The final R_1 was 0.0474 (I > 2σ(I)) and wR_2 was 0.1135 (all data).

Table.13 Different conditions used to grow crystals of **50**, to be used to analysed the enantiomer present in the solution. The row in bold are the crystals used to obtain the structures shown in **Figure.47**

50 Enantiomer	Concentration / mM	Dissolved Solvent	Diffusing solvent
(1 *R* - 2 *S*)	1	Ethyl Acetate	Hexane
(1 *R* - 2 *S*)	1	DCM	Hexane
(1 *R* - 2 *S*)	**5**	**Ethyl Acetate**	**Hexane**
(1 *R* - 2 *S*)	5	DCM	Hexane
(1 *S* - 2 *R*)	1	Ethyl Acetate	Hexane
(1 *S* - 2 *R*)	1	DCM	Hexane
(1 *S* - 2 *R*)	5	Ethyl Acetate	Hexane
(1 *S* - 2 *R*)	5	DCM	Hexane

Additionally, the stereochemistry was confirmed by ^{1}H NMR with nOe spectra acquired for **(1 *S* - 2 *R*)-50** (**Figure.48a**) and **(1 *R* - 2 *S*)-50** (**Figure.49a**). **H9**, **H6** and **H3** hydrogens (**Figure 48 & 49**) were irradiated to give 1D nOe spectra for each of these hydrogens on both enantiomers.[131,133] The irradiation of **H9** on **(1 *S* - 2 *R*)-50** shows a response from **NH**, **H2**, **H7** and **H8** (**Figure.48b**). Likewise, irradiation of **H6** shows a response from **H1** and **H8** or **H4/5** (**Figure.48c**), and irradiation of **H3** shows a response from **NH**, **H1** and **H4/5** (**Figure.48d**). Similarly, for **(1 *R* - 2 *S*)-50,** the irradiation of **H9** shows a response from **NH**, **H2**, **H7** and **H8** (**Figure.49b**). Likewise, irradiation of **H6** shows a response from **H1** and **H8** or **H4/5** (**Figure.49c**), and irradiation of **H3** shows a response from **NH**, **H1** and **H4/5** (**Figure.49d**). When comparing the response factors for **H2** when irradiating **H9**, **(1 *S* - 2 *R*)-18** has a large nOe response whereas **(1 *R* - 2 *S*)-50** has a much lower nOe response. Additionally, when comparing the response from **H1** when irradiating **H9**, **(1 *S* - 2 *R*)-50**, It has an opposite nOe response when comparing to **(1 *R* - 2 *S*)-50**. Therefore, confirming with the crystallography data that the chiral separation was successful.[131]

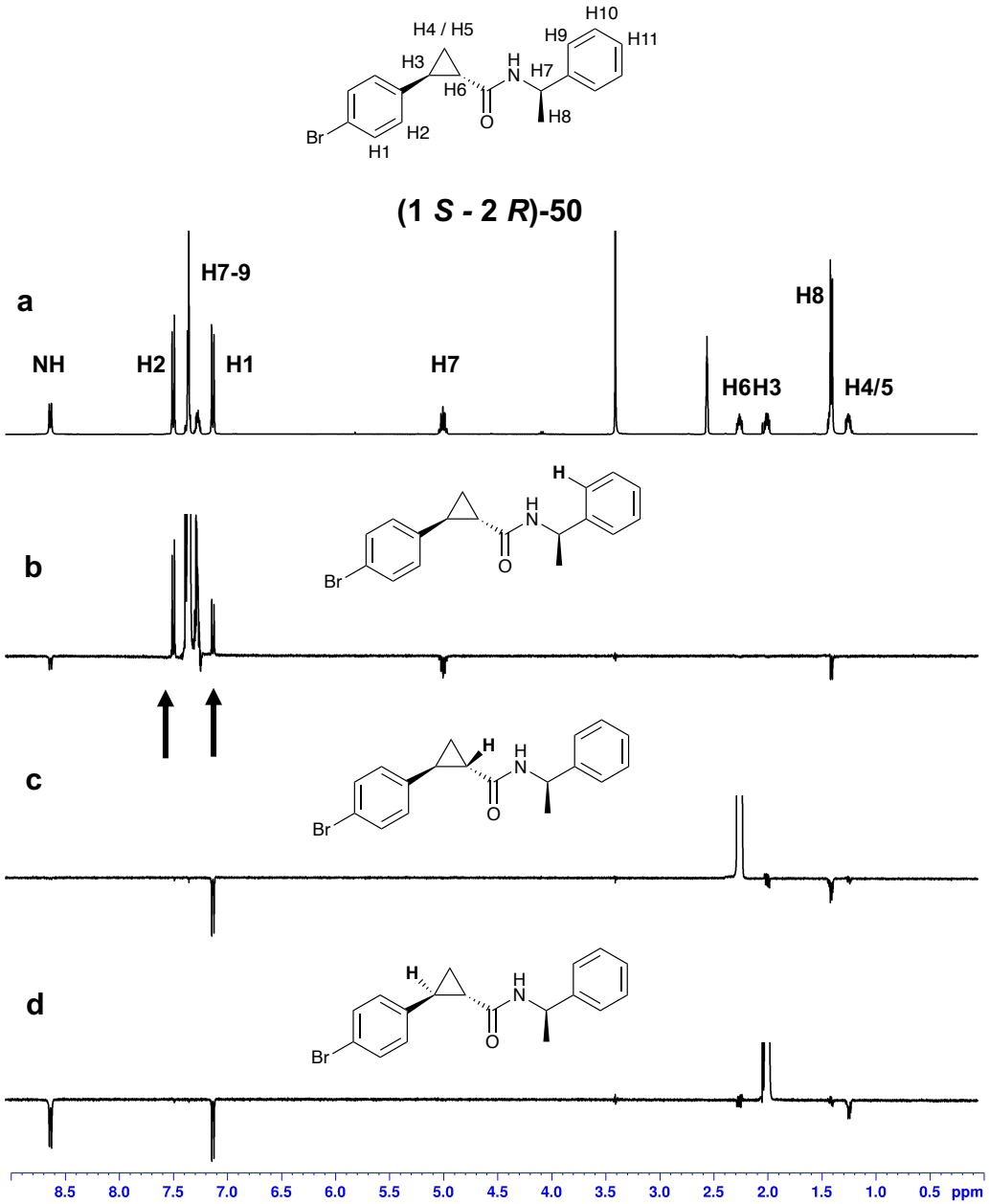

Figure.48 ^{1}H NMR and nOe spectra for **(1 *S* - 2 *R*)-50** with **a.** Showing ^{1}H NMR spectra, **b.** nOe spectra for the irradiation of **H9**, with black arrows highlighting peaks of interest. **c.** nOe spectra for the irradiation of **H6**, **d.** nOe spectra for the irradiation of **H3**.

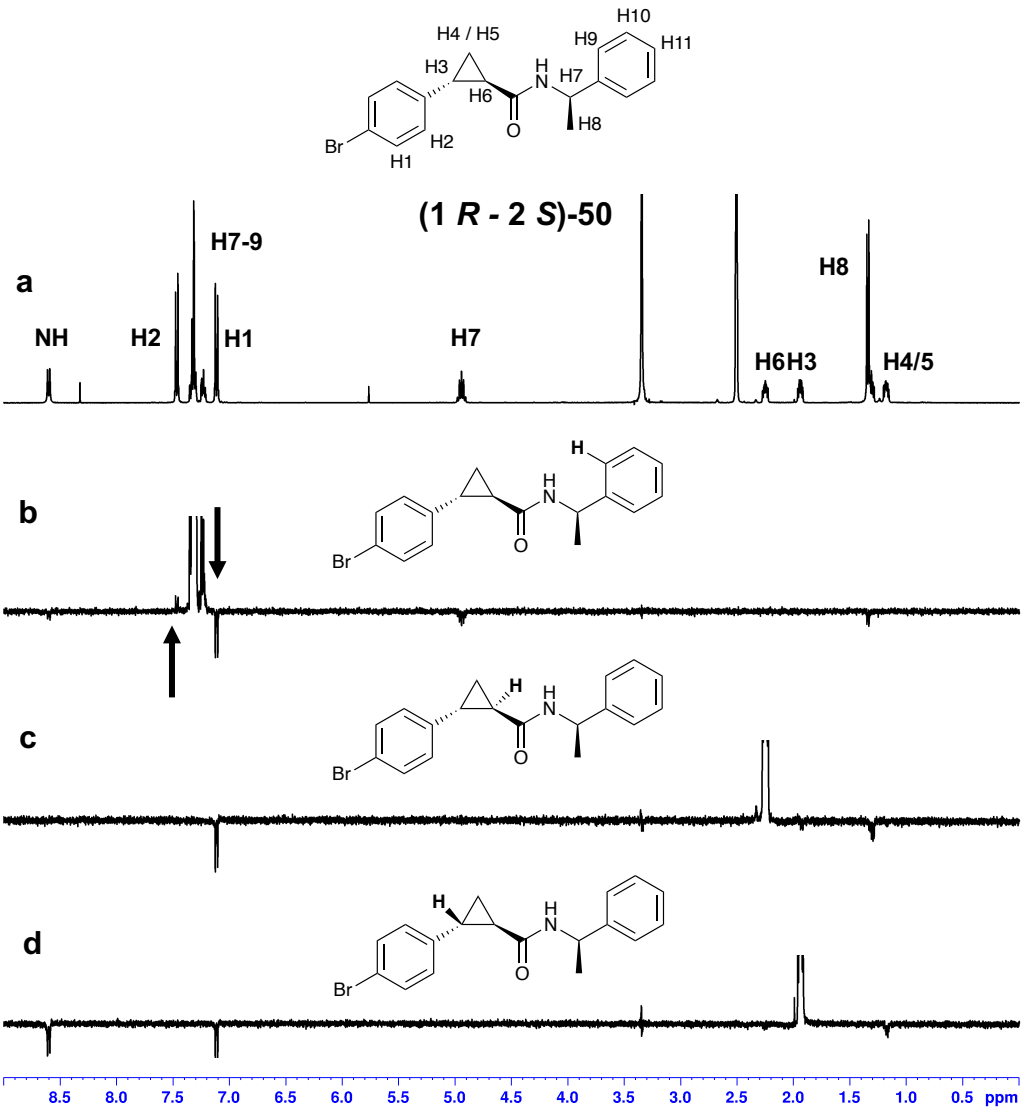

Figure.49 ^{1}H NMR and nOe spectra for **(1 *R* - 2 *S*)-50** with **a.** Showing ^{1}H NMR spectra, **b.** nOe spectra for the irradiation of **H9**, with black arrows highlighting peaks of interest. **c.** nOe spectra for the irradiation of **H6**, **d.** nOe spectra for the irradiation of **H3**.

4.4 Enzyme Assays

The coupled fluorescence assay measures the stoichiometric release of peroxide from the oxidation of FAD cofactor. The reported inhibition data is standardised using the H_2O_2 standard curve (2.3.1), the Michaelis Menten experiment (2.3.2) was used to identify the optimum substrate concentration for the inhibition assay.

4.4.1 Inhibition Assays

The inhibition activity for the synthesised probes towards human recombinant LSD1, MAOA and MAOB were evaluated by IC_{50} assays. As previously discussed in chapter 2.3.3, the inhibition data was standardised and characterised in identical fashion. The inhibition activity for the synthesised probes are reported in **Table.14.**

Table.14 *In vitro* MAOA, MAOB, LSD1 inhibitory activities (IC_{50}), for diastereoisomers **probe 7**, N-alkylated **probe 9**, **Probe 7** and **PCPA**. (*n=3* for all enzyme assays expect **probe 4** for LSD1, *n=1*)

Compound	MAOA / μM	MAOB / μM	LSD1 / μM
PCPA	100 ± 44	22 ± 5	12 ± 3
Probe 7	5.3 ± 2.9	1.1 ± 0.2	8 ± 3
(1 *R* - 2 *S*) Probe 7	6.7 ± 0.5	2.8 ± 0.1	2.0 ± 0.1
(1 *S* - 2 *R*) Probe 7	12.9 ± 4.8	5.0 ± 1.2	5.2 ± 1.1
Probe 4	4.4 ± 0.5	5.0 ± 0.8	46
Probe 9	16.1 ± 0.4	4.9 ± 0.3	7.7 ± 0.1

The inhibition data demonstrates that the two enantiomerically pure isomers, of **probe 7** have differing selectivity's for LSD1 and MAO enzymes**.** The **(1 *R* - 2 *S*)** enantiomer causes an increase in selectivity by four fold towards LSD1 when comparing to **probe 7**, and an increase of six fold when comparing to **PCPA** (IC_{50} values: 2.0 μM, 8.0 μM and 12 μM respectively). The inhibition is similar, within two standard deviations, for MAOA when comparing to **probe 7**, but has an increase in selectivity of 15 fold when comparing to **PCPA** (IC_{50} values: 6.7 μM, 5.3 μM and 100 μM respectively). The selectivity towards MAOB is decreased by 2.5 fold when comparing to **probe 7**, but has increased by eight fold when comparing to **PCPA** (IC_{50} values: 2.8 μM, 1.1 μM and 22 μM respectively). However, **(1 *S* - 2 *R*)** enantiomer has a similar inhibition, within two standard

deviations, for LSD1 when comparing to **probe 7**, and an increase in selective by when comparing to **PCPA** (IC_{50} values: 5.2 μM, 8.0 μM and 12 μM respectively). Likewise, the inhibition is similar, within two standard deviations, for MAOA when comparing to **probe 7**. Equally, there is an increase in selectivity of 7.7 fold when comparing to **PCPA** (IC_{50} values: 12.9 μM, 5.3 μM and 100 μM respectively). The selectivity towards MAOB is decreased by five fold when comparing to **probe 7**, but has increased by 7.8 fold when comparing to **PCPA** (IC_{50} values: 2.8 μM, 1.1 μM and 22 μM respectively). From this, it is shown that the separation of the enantiomers does cause a difference in the inhibition towards LSD1, with **(1 *R* - 2 *S*)** isomer 'fitting' better into the active site of LSD1. However, the separation of the enantiomers does not affect the inhibition towards MAOs. Showing that any significant change in selectivity is due to the addition of the bulky phenyl group.

To further increase selectivity of the synthesised probes, inspiration is taken from clinical trial drug such as **GSK2879552**, **ORY-1001**,[164,165] to increase selectivity towards LSD1 by N-alkylation the probes. The reductive amination of the **probe 4** is undertaken to increase the selectivity towards LSD1. From the reaction was isolated the Schiff base/imine which was unexpected. Nevertheless, the imine was expected to increase the potency of **probe 4** towards LSD1.

The N-alkylation of **probe 4** (**probe 9**) resulted in an increase in selectivity of six fold towards LSD1 when comparing to **probe 4**, and an increase of 1.5 fold when comparing to **PCPA** (IC_{50} values: 7.7 μM, 46 μM and 12 μM respectively). The selectivity towards MAOA is decreased by 3.6 fold when comparing to **probe 4**, and an increase in selectivity of 6.3 fold when comparing to **PCPA** (IC_{50} values: 16.1 μM, 4.4 μM and 100 μM respectively). The selectivity towards MAOB is similar when comparing to **probe 4**, when accounting for two standard deviations, but has increased by 4.5 fold when comparing to **PCPA** (IC_{50} values: 4.9 μM, 5.0 μM and 22 μM respectively). The difference in selectivity of **probe 9** when compared to **PCPA** is because of the alkyl-azide chain, as discussed in chapter 2. Furthermore, the addition of the N-alkyl group to **probe 4** (**probe 9**) increases the selectivity towards LSD1 as this 'fits' into the active site of LSD1 and incorporates the 'free space' that is located within the pocket. As expected, this decreases the selectivity towards MAOA because the active site lacks the free space needed to fit the bulky n-alkyl group. However, the bulky group does not affect the MAOB inhibition. This can be assumed that the active site is larger than MAOA.[134–136]

4.5 Conclusion

Synthesis of the enantiomeric pair of the '*trans*' isomer of **probe 7** and N-alkylated probe have been completed with investigation into their inhibitory effect against LSD1 and MAOs. Successful separation of diastereoisomers was confirmed by both nOe studies and Single Crystal X-Ray Diffraction. The results from nOe confirmed the differences in ^{1}H NMR that was hypothesised from the consideration of the three dimensional structure. The crystallography concurred with the nOe studies, showing absolute stereo chemistry with a Flack parameter of 0.09. Unfortunately, the separation of enantiomers for **probe 7** made only a small difference for the inhibition activities towards MAOs. The separation caused **(1 *R* - 2 *S*)-probe 7** to 'fit' better into the active site of LSD1, with just over 2.5 fold selectivity over **(1 *S* - 2 *R*)-probe 7**. Furthermore, **probe 9** showed significant increase in selectivity towards LSD1 by six fold when compared to its parent **probe 4**. As discussed, there was a slight decrease in selectivity towards MAOA (3.6 fold), but identical inhibitory values towards MAOB when comparing to **probe 4**, which can be presumed to better accommodate a larger molecule.

4.6 Experimental

4.6.1 Materials and Methods

TLC: TLC Silica gel 60, F_{254}, Aluminium plate. **IR**: Bruker ALPHA, ATR stage (Diamond Crystal). **NMR**: Bruker AVANCE III 400 (^{1}HNMR; 400MHz, ^{13}CNMR; 100MHz) **MS**: Finnigan MAT, Electro Spray source, Flow Rate: 15 µL/min, Gas: Nitrogen. **HRMS:** Xevo G2-XS QTOF Mass Spectrometer. Electrospray (ES) ionisation source, Gas: Nitrogen, Temperature: Ramp heating Ambient – 300 °C over 7 mins. **UV/Vis:** CLARIOstar, BMG labtech, Excitation: λ 530-15, Emission: λ 580-20. **Melting Point:** Stuart SMP3. All chemicals used were bought from Sigma Aldrich, or Fisher Scientific. Dry DMSO (0.025% max H_2O) and THF (0.005% max H_2O) were purchased through Merck. Purification on silica were undertaken using Biotage Isolera One or Teledyne ISCO combiflash R_f systems. Human MAOA and Human MAOB were purchased though Sigma Aldrich with product codes of M7316 and M7441 respectively. Molecular grade DMSO was used in all enzyme assays.

4.6.2 Synthesis

(1 *R* - 2 *S*)-2-(4-bromophenyl)-N-((*S*)-1-phenylethyl)cyclopropane-1-carboxamide, ((1 *R*, 2 *S*)-50) &

(1 *S* - 2 *R*)-2-(4-bromophenyl)-N-((*S*)-1-phenylethyl)cyclo-propane-1-carboxamide, ((1 *S*, 2 *R*)-50

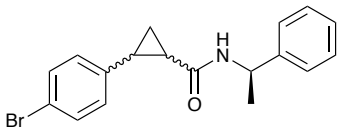

To a solution of 2-(4-(methoxymethoxy)phenyl)-cyclopropane-1-carboxylic acid (1.07 g, 4.44 mmol) in DMF (60 mL) was added, EDCI (1.17 mL, 6.66 mmol), 1-hydroxybenzotriazole hydrate (0.9 g, 6.66 mmol) and (*S)*-1-phenylethan-1-amine (0.85 mL, 6.66 mmol) and stirred for 7 days at room temperature. The mixture was diluted with de-ionised water (100 mL), and extracted with chloroform (3 x 50 mL), washed with sat. $NaCl_{(aq)}$ (2 x 50 mL), dried with anhydrous $MgSO_4$ and condensed under reduced pressure. The product was purified on silica (20 g) eluting with (EtOAc/n-hexane = 1:9) to give a total yield of 1.18 g (76%). ((1 *R* - 2 *S*) isomer 0.47 g (30%) of white amorphous solid, ((1 *S* - 2 *R*) isomer 0.71 g (46%) of white amorphous solid).

(1 *R* - 2 *S*)

IR (ν_{max}/cm^{-1}) 3380, 3000, 2950, 2925, 1650, 1225.

^{1}H NMR (400MHz, DMSO-d6, 298 K) δ 8.60 (1 H, d, $^{3}J_{HH}$ = 8.0 Hz), 7.47 (2 H, d, $^{3}J_{HH}$ = 8.4 Hz), 7.35 – 7.30 (4 H, m), 7.25 – 7.21 (1H, m), 7.11 (2 H, d, $^{3}J_{HH}$ = 8.4

Hz), 4.94 (1 H, p, $^3J_{HH}$ = 7.0 Hz) 2.28 – 2.23 (1 H, m), 1.96 – 1.92 (1 H, m), 1.35 – 1.29 (4 H, m), 1.20 – 1.16 (1 H, m).

^{13}C {^{1}H} NMR (100MHz, DMSO-d6, 298 K) δ 170.2, 145.2, 141.3, 131.6, 128.7, 128.5, 127.1, 126.4, 119.2, 48.5, 26.3, 23.7, 23.1, 15.9.

MS (ESI+) $[M+H]^+$ (%) 344.1 (100).

HRMS(ESI+) calcd from $C_{18}H_{19}BrNO$ $[M+H]^+$; 344.0650 found 344.0649.

(1 *S* - 2 *R*)

IR (ν_{max}/cm^{-1}): 3400, 3100, 2970, 2920, 1650, 1225.

^{1}H NMR (400MHz, DMSO-d6, 298 K) δ 8.58 (1 H, d, $^3J_{HH}$ = 8.1 Hz), 7.45 (2 H, d, $^3J_{HH}$ = 8.4 Hz), 7.34 – 7.30 (4 H, m), 7.24 – 7.19 (1H, m), 7.08 (2 H, d, $^3J_{HH}$ = 8.4 Hz), 4.95 (1 H, p, $^3J_{HH}$ = 7.0 Hz) 2.23 – 2.18 (1 H, m), 1.97 – 1.93 (1 H, m), 1.39 – 1.35 (4 H, m), 1.22 – 1.8 (1 H, m).

^{13}C {^{1}H} NMR (100MHz, DMSO-d6, 298 K) δ 170.2, 145.0, 141.3, 131.6, 128.8, 128.5, 127.1, 126.5, 119.2, 48.5, 26.2, 23.6, 23.1, 15.9.

MS (ESI+) $[M+H]^+$ (%) 344.1 (100).

HRMS(ESI+) calcd from $C_{18}H_{19}BrNO$ $[M+H]^+$; 344.0650 found 344.0668.

(1 *R* - 2 *S*)-2-(4-bromophenyl)cyclopropane-1-carboxylic acid ((1 *R* - 2 *S*)-43b)

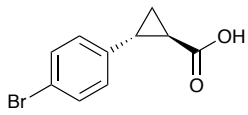

To a suspension of (1 *R* - 2 *S*)-2-(4-bromophenyl)-N-((*R*)-1-phenylethyl)-cyclopropane-1-carbox-amide (0.2 g, 0.58 mmol) in ethylene glycol, (3 mL) was added hydrazine monohydrate (0.12 mL, 2.3 mmol) and KOH (0.2 g, 3.5 mmol). The reaction mixture was stirred for 7 days at 120 °C. The reaction mixture was diluted with HCl (50 mL, 2 M) and extracted with chloroform (3 x 50 mL), washed with sat. $NaCl_{(aq)}$ (2 x 50 mL), dried with $MgSO_4$ and condensed under reduced pressure to give 80 mg (58%) of white amorphous solid.

IR (ν_{max}/cm^{-1}) 3026, 2639, 1687, 1454, 1229.

^{1}H NMR (400MHz, $CDCl_3$, 298 K) δ 7.42 (2 H, d, $^3J_{HH}$ = 8.4 Hz), 6.98 (2 H, d, $^3J_{HH}$ = 8.4 Hz), 2.58 – 2.54 (1 H, m), 1.90 – 1.86 (1 H, m), 1.70 – 1.65 (1 H, m), 1.40 – 1.35 (1 H, m).

^{13}C {^{1}H} NMR (100MHz, $CDCl_3$, 298 K) δ 179.4, 138.6, 131.6, 128.0, 120.5, 26.5, 24.0, 17.5.

(1 *S* - 2 *R*)-2-(4-bromophenyl)cyclopropane-1-carboxylic acid ((1 *S* - 2 *R*)-43b)

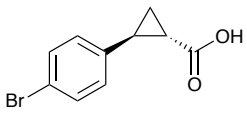

To a suspension of (1 *S* - 2 *R*)-2-(4-bromophenyl)-N-((*R*)-1-phenylethyl)-cyclopropane-1-carbox-amide (0.6 g, 1.7 mmol) in ethylene glycol, (9 mL) was added hydrazine monohydrate (0.0.34 mL, 6.8 mmol) and KOH (0.59 g, 10.5 mmol). The reaction mixture was stirred for 14 days at 120 °C. The reaction mixture was diluted with HCl (75 mL, 2 M) and extracted with chloroform (3 x 50 mL), washed with sat. $NaCl_{(aq)}$ (2 x 50 mL), dried with $MgSO_4$ and condensed under reduced pressure to give 210 mg (51%) of white amorphous solid.

IR (ν_{max}/cm^{-1}) 3311, 3029, 2970, 1635, 1541, 1237.

^{1}H NMR (400MHz, $CDCl_3$, 298 K) δ 7.41 (2 H, d, $^3J_{HH}$ = 8.5 Hz), 6.98 (2 H, d, $^3J_{HH}$ = 8.4 Hz), 2.59 – 2.54 (1 H, m), 1.90 – 1.86 (1 H, m), 1.70 – 1.65 (1 H, m), 1.40 – 1.35 (1 H, m).

^{13}C {^{1}H} NMR (100MHz, $CDCl_3$, 298 K) δ 179.3, 138.6, 131.6, 128.0, 120.4, 26.5, 24.0, 17.4.

***tert*-butyl ((1 *R* - 2 *S*)-2-(4-bromophenyl)cyclopropyl)carbamate ((1 *R* - 2 *S*)-44b)**

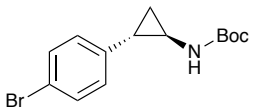

To a solution of (1 *R* - 2 *R*)-2-(4-bromophenyl)cyclopropane-1-carboxylic acid (80 mg, 0.33 mmol) in cyclohexane (5 mL) was added DPPA (0.06 mL, 0.37 mmol) and triethylamine (0.06 mL, 0.4 mmol) protected by a N_2 atmosphere. The reaction mixture was refluxed for 4 hr, dry *t*-BuOH (0.63 mL, 6.6 mmol) was added and refluxed for 14 hr. The reaction was cooled and the solvent removed under reduced pressure. The product was purified on silica (10 g), eluting with (EtOAc:hexane = 1:7) to give 40 mg (40%) of white amorphous solid.

IR (ν_{max}/cm^{-1}) 3365, 3011, 2979, 2934, 1681, 1250.

^{1}H NMR (400MHz, $CDCl_3$, 298 K) δ 7.38 (2 H, d, $^3J_{HH}$ = 8.4 Hz), 7.02 (2 H, d, $^3J_{HH}$ = 7.9 Hz), 4.86 (1H, s) 2.68 (1 H, s), 2.00 (1 H, s), 1.46 (9 H, s), 1.16 – 1.13 (2 H, m).

^{13}C {^{1}H} NMR (100MHz, $CDCl_3$, 298 K) δ 156.3, 139.8, 131.3, 128.4, 119.7, 79.7, 32.5, 28.4, 24.7, 16.1.

MS (ESI+) $[M+H]^+$ (%) 312.1 (100).

HRMS(ESI+) calcd from $C_{14}H_{19}BrNO_2$ $[M+H]^+$; 312.0599 found 312.0608.

***tert*-butyl ((1 *S* - 2 *R*)-2-(4-bromophenyl)cyclopropyl)carbamate ((1 *S* - 2 *R*)-44b)**

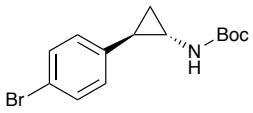

To a solution of (1 *S* - 2 *R*)-2-(4-bromophenyl)cyclopropane-1-carboxylic acid (200 mg, 0.83 mmol) in cyclohexane (15 mL) was added DPPA (0.15 mL, 0.93 mmol) and triethylamine (0.15 mL, 1.0 mmol) protected by a N_2 atmosphere. The reaction mixture was refluxed for 4 hr, dry *t*-BuOH (1.58 mL, 16.5 mmol) was added and refluxed for 14 hr. The reaction was cooled and the solvent removed under reduced pressure. The product was purified on silica (20 g), eluting with (EtOAc:hexane = 1:7) to give 129 mg (50%) of white amorphous solid.

IR (ν_{max}/cm^{-1}) 3365, 3011, 2979, 2934, 1681, 1250.

^{1}H NMR (400MHz, $CDCl_3$, 298 K) δ 7.39 (2 H, d, $^3J_{HH}$ = 8.5 Hz), 7.04 (2 H, d, $^3J_{HH}$ = 8.2 Hz), 4.87 (1H, s) 2.69 (1 H, s), 2.04 – 2.00 (1 H, m), 1.47 (9 H, s), 1.18 – 1.14 (2 H, m).

^{13}C {^{1}H} NMR (100MHz, $CDCl_3$, 298 K) δ 156.2, 139.8, 131.3, 128.4, 119.7, 79.7, 32.4, 28.4, 24.7, 16.1.

MS (ESI+) $[M+H]^+$ (%) 312.1 (100).

HRMS(ESI+) calcd from $C_{14}H_{19}BrNO_2$ $[M+H]^+$; 312.0599 found 312.0610.

***tert*-butyl ((1 *R* - 2 *S*)-2-(3'-(hydroxymethyl)-[1,1'-biphenyl]-4-yl)cyclopropyl)-carbamate ((1 *R* - 2 *S*)-48b)**

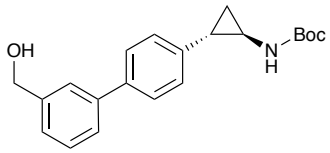

To a mixture of 3-(Hydroxymethyl)phenylboronic acid (22 mg, 0.14 mmol), $Pd(PPh_3)_2Cl_2$ (1 mg, 0.002 mmol) and Na_2CO_3 (19 mg, 0.16 mmol) protected by an N_2 atmosphere was added degassed dry THF (0.8 mL), Toluene (0.8 mL) and de-ionised water (0.04 mL). This was stirred and *tert*-butyl ((1 *R* - 2 *S*)-2-(4-bromophenyl)cyclopropyl)carbamate (40 mg, 0.13 mmol) was added, heated to 105 °C and stirred for 36 hr. The solution was allowed to cool, condensed under reduced pressure, and re-dissolved in DCM and washed with sat. $NaHCO_{3(aq)}$ (2x50 mL), sat. $NaCl_{(aq)}$ (2x50 mL), dried with anhydrous $MgSO_4$ and condensed under reduced pressure. The product was purified on silica (10 g), eluting with (EtOAc/hexane = 1:7) gave 30 mg (75%) of white amorphous solid.

IR (ν_{max}/cm^{-1}) 3326, 2977, 2931, 1685, 1278.

^{1}H NMR (400MHz, $CDCl_3$, 298 K) δ 7.57 (1 H, s), 7.52 – 7.49 (3 H, m), 7.43 (1 H, t, $^3J_{HH}$ = 7.5 Hz), 7.34 (1 H, d, $^3J_{HH}$ = 7.6 Hz), 7.20 (2 H, d, $^3J_{HH}$ = 8.2 Hz), 4.89

(1 H, s), 4.77 (2 H, s), 2.77 (1 H, s), 2.11 – 2.06 (1 H, m), 1.47 (9 H, s), 1.25 – 1.18 (2 H, s).

^{13}C {^{1}H} NMR (100MHz, MeOD, 298 K) δ 156.4, 141.4, 141.3, 140.0, 138.7, 129.0, 127.1, 126.9, 126.3, 125.7, 125.6, 79.6, 65.4, 32.6, 28.4, 16.5.

MS (ESI+) $[M+H]^+$ (%) 340.2 (100).

HRMS(ESI+) calcd from $C_{21}H_{25}NO_3$ $[M+H]^+$: 340.1913 found 340.1902.

tert-butyl ((1 *S* - 2 *R*)-2-(3'-(hydroxymethyl)-[1,1'-biphenyl]-4-yl)cyclopropyl)-carbamate ((1 *S* - 2 *R*)-48b)

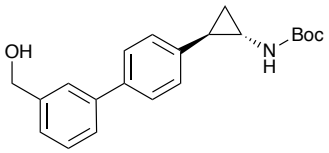

To a mixture of 3-(Hydroxymethyl)phenylboronic acid (70.4 mg, 0.45 mmol), $Pd(PPh_3)_2Cl_2$ (3 mg, 0.006 mmol) and Na_2CO_3 (61 mg, 0.51 mmol) protected by an N_2 atmosphere was added degassed dry THF (2.6 mL), Toluene (2.6 mL) and de-ionised water (0.13 mL). This was stirred and *tert*-butyl ((1 *S* - 2 *R*)-2-(4-bromophenyl)cyclopropyl)carbamate (128 mg, 0.42 mmol) was added, heated to 105 °C and stirred for 36 hr. The solution was allowed to cool, condensed under reduced pressure, and re-dissolved in DCM and washed with sat. $NaHCO_{3(aq)}$ (2x50 mL), sat. $NaCl_{(aq)}$ (2x50 mL), dried with anhydrous $MgSO_4$ and condensed under reduced pressure. The product was purified on silica (10 g), eluting with (EtOAc/hexane = 1:7) gave 99 mg (70%) of white amorphous solid.

IR (ν_{max}/cm^{-1}) 3300, 2980, 2930, 1670, 1275.

^{1}H NMR (400MHz, $CDCl_3$, 298 K) δ 7.57 (1 H, s), 7.51 – 7.48 (3 H, m), 7.41 (1 H, t, $^{3}J_{HH}$ = 7.5 Hz), 7.33 (1 H, d, $^{3}J_{HH}$ = 7.5 Hz), 7.18 (2 H, d, $^{3}J_{HH}$ = 8.1 Hz), 4.95 (1 H, s), 4.74 (2 H, s), 2.76 (1 H, s), 2.07 (1 H, s), 1.47 (9 H, s), 1.21 – 1.18 (2 H, s).

^{13}C {^{1}H} NMR (100MHz, $CDCl_3$, 298 K) δ 156.4, 141.5, 141.3, 140.1, 138.7, 129.0, 127.1, 126.9, 126.2, 125.7, 125.6, 79.8, 65.3, 32.7, 28.4, 24.8, 16.5.

MS (ESI+) $[M+H]^+$ (%) 340.2 (100).

HRMS(ESI+) calcd from $C_{21}H_{25}NO_3$ $[M+H]^+$: 340.1913 found 340.1904.

tert-butyl ((1 *R* - 2 *S*)-2-(3'-(azidomethyl)-[1,1'-biphenyl]-4-yl)cyclopropyl)-carbamate ((1 *R* - 2 *S*)-49b)

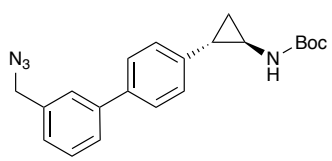

To tert-butyl ((1 *R* - 2 *S*)-2-(3'-(hydroxymethyl)-[1,1'-biphenyl]-4-yl)cyclopropyl)-carbamate (30 mg, 0.088 mmol), $P(Ph)_3$ (30 mg, 0.106 mmol) in THF (1.5 mL)

was added DPPA (0.02 mL, 0.106 mmol) and protect by an N_2 atmosphere at 0 °C. DIAD (0.02 mL, 0.106 mmol) in dry THF (0.5 mL) was added dropwise and allowed to warm to room temperature and stirred for 48 hr. The solvent was removed under reduced pressure and the residue was purified on silica (10 g), eluting with DCM to give 25 mg (67%) of white amorphous solid.

IR (v_{max}/cm^{-1}) 3367, 3013, 2978, 2935, 2169, 1682, 1252.

^{1}H NMR (400MHz, $CDCl_3$, 298 K) δ 7.57 (1 H, s), 7.51 – 7.49 (3 H, m), 7.42 (1 H, t, $^3J_{HH}$ = 7.5 Hz), 7.33 (1 H, d, $^3J_{HH}$ = 7.6 Hz), 7.19 (2 H, d, $^3J_{HH}$ = 8.2 Hz), 4.91 (1 H, s), 4.76 (2 H, s), 2.77 (1 H, s), 2.08 (1 H, s), 1.47 (9 H, s), 1.22 – 1.19 (2 H, s).

^{13}C {^{1}H} NMR (100MHz, $CDCl_3$, 298 K) δ 156.4, 141.4, 141.3, 140.0, 138.7, 129.0, 127.1, 126.9, 126.3, 125.7, 125.6, 79.7, 65.4, 32.7, 28.4, 24.9, 16.5.

MS (ESI+) $[M+H]^+$: (%) 365.2 (100).

HRMS(ESI+) calcd from $C_{21}H_{25}N_4O_2$ $[M+H]^+$: 365.1978; found 365.1996.

***tert*-butyl ((1 *S* - 2 *R*)-2-(3'-(azidomethyl)-[1,1'-biphenyl]-4-yl)cyclopropyl)-carbamate ((1 *S*,2 *R*)-49b)**

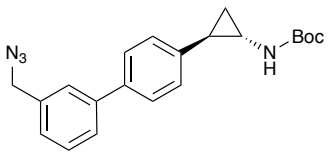

To tert-butyl ((1 *S* - 2 *R*)-2-(3'-(hydroxymethyl)-[1,1'-biphenyl]-4-yl)cyclopropyl)-carbamate (90 mg, 0.264 mmol), $P(Ph)_3$ (90 mg, 0.318 mmol) in THF (3.0 mL) was added DPPA (0.06 mL, 0.318 mmol) and protect by an N_2 atmosphere at 0 °C. DIAD (0.06 mL, 0.318 mmol) in dry THF (1.0 mL) was added dropwise and allowed to warm to room temperature and stirred for 48 hr. The solvent was removed under reduced pressure and the residue was purified on silica (10 g), eluting with DCM to give 50 mg (52%) of white amorphous solid.

IR (v_{max}/cm^{-1}) 3375, 3000, 2975, 2925, 2150, 1675, 1250.

^{1}H NMR (400MHz, $CDCl_3$, 298 K) δ 7.55 – 7.43 (5 H, m), 7.30 – 7.21 (3 H, m), 4.88 (1 H, s), 4.41 (2 H, s), 2.77 (1 H, s), 2.09 (1 H, m), 1.47 (9 H, s), 1.47 – 1.25 (2 H, m).

^{13}C {^{1}H} NMR (100MHz, $CDCl_3$, 298 K) δ 156.3, 142.3, 141.7, 140.3, 138.4, 135.9, 129.3, 127.1, 127.0, 126.8, 126.8, 79.7, 60.4, 32.5, 28.4, 24.8, 14.2.

MS (ESI+) $[M+H]^+$: (%) 365.2 (100).

HRMS(ESI+) calcd from $C_{21}H_{25}N_4O_2$ $[M+H]^+$: 365.1978; found 365.1993.

(1 *R* - 2 *S*)-2-(3'-(azidomethyl)-[1,1'-biphenyl]-4-yl)cyclopropan-1-amine ((1 *R* - 2 *S*)–probe 7)

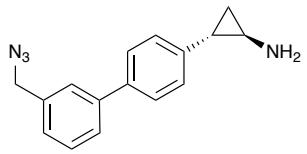

To tert-butyl ((1 *R* - 2 *S*)-2-(3'-(azidomethyl)-[1,1'-biphenyl]-4-yl)cyclopropyl)-carbamate (25 mg, 0.068 mmol) in DCM (1 mL) was added HCl in dioxane (1.5 mL, 4 M) dropwise and protected by a N_2 atmosphere. The reaction mixture was stirred for 3 hr. The solvent was removed under reduced pressure. The solid was washed with DCM (2 mL) and hexane (3 mL) to give 15 mg (83%) of white crystalline solid.

IR (v_{max}/cm^{-1}) 3300, 2975, 2930, 2100, 2075, 1500.

^{1}H NMR (400MHz, MeOD, 298 K) δ 7.61 – 7.58 (4 H, m) 7.47 (1 H, dd, $^3J_{HH}$ = 7.8 Hz, $^3J_{HH}$ = 7.8 Hz), 7.35 – 7.27 (3 H, m), 4.44 (2 H, s), 2.93 – 2.89 (1 H, m), 2.49 – 2.44 (1 H, m), 1.52 - 1.46 (1 H, m) 1.42 – 1.37 (1 H, m).

^{13}C {^{1}H} NMR (100MHz, $CDCl_3$, 298 K) δ 142.5, 140.5, 139.3, 137.8, 130.4, 128.37, 128.3, 128.0, 127.8, 127.7, 55.6, 32.1, 22.3, 14.0.

MS (ESI+) $[M+H]^+$ (%) 265.2 (100).

HRMS(ESI+) calcd from $C_{16}H_{17}N_4$ $[M+H]^+$: 265.1453 found; 265.1464.

(1 *S* - 2 *R*)-2-(3'-(azidomethyl)-[1,1'-biphenyl]-4-yl)cyclopropan-1-amine ((1 *S*,2 *R*)-probe 7)

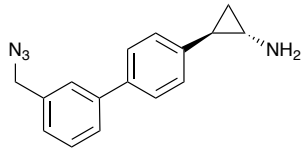

To tert-butyl ((1 *S* - 2 *R*)-2-(3'-(azidomethyl)-[1,1'-biphenyl]-4-yl)cyclopropyl)-carbamate (50 mg, 0.136 mmol) in DCM (1 mL) was added HCl in dioxane (1.5 mL, 4 M) dropwise and protected by a N_2 atmosphere. The reaction mixture was stirred for 3 hr. The solvent was removed under reduced pressure. The solid was washed with DCM (2 mL) and hexane (3 mL) to give 24 mg (68%) of white crystalline solid.

IR (v_{max}/cm^{-1}) 3300, 2975, 2930, 2100, 2075, 1500.

^{1}H NMR (400MHz, DMSO-d6, 298 K) δ 7.61 – 7.26 (8 H, m), 4.69 (2 H, s), 2.91 – 2.90 (1H m), 2.46 – 2.41 (1 H, m), 1.47 – 1.39 (2 H, m).

^{13}C {^{1}H} NMR (100MHz, $CDCl_3$, 298 K) δ 142.5, 140.6, 139.2, 137.9, 130.4, 128.4, 128.3, 127.9, 127.7, 55.5, 32.1, 22.3, 14.0.

MS (ESI+) $[M+H]^+$ (%) 265.2 (100).

HRMS(ESI+) calcd from $C_{16}H_{17}N_4$ $[M+H]^+$: 265.1453 found; 265.1461.

(*trans*)-N-(2-(4-(3-azidopropoxy)phenyl)cyclopropyl)-1-(5-fluoro-2-methoxypyridin-3-yl)methanimine (probe 9)

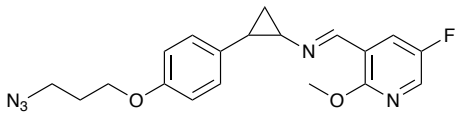

To 5-fluoro-2-methyoxynicotinaldehyde (11 mg, 0.073 mmol) and acetic acid (4 µL, 0.073 mmol) in DCE (1 mL) was added 2-(4-(3-azidopropoxy)phenyl)cyclopropan-1-amine (39 mg, 0.146 mmol). The reaction mixture was stirred for 2 hours at room temperature then sodium triacetoxyborohydride (62 mg, 0.292 mmol) was added and the reaction mixture was stirred for 3 hours at room temperature. The reaction mixture was quenched with sat. $NH_4Cl_{(aq)}$ (10 mL) and extracted with DCM (3x20 mL). The DCM layers were combined and washed with sat. $NaCl_{(aq)}$ (2x20 mL), dried with anhydrous $MgSO_4$ and condensed under reduced pressure to give 10 mg (38%) of yellow crystalline solid.

IR (ν_{max}/cm^{-1}) 3050, 3010, 2250, 1250, 1100.

^{1}H NMR (400MHz, $CDCl_3$, 298 K) δ 8.56 (1 H, d, $^4J_{HH}$ = 2.4 Hz), 7.95 (1 H, d, $^4J_{HH}$ = 3.1 Hz), 7.88 – 7.86 (1 H, m), 6.97 (2 H, d, $^3J_{HH}$ = 8.6 Hz), 6.77 (2 H, d, $^3J_{HH}$ = 8.7 Hz), 3.96 (2 H, t, $^3J_{HH}$ = 5.9 Hz), 3.89 (3 H, s), 3.45 (2 H, t, $^3J_{HH}$ = 6.6 Hz), 3.11 – 3.08 (1 H, m), 2.42 – 2.37 (1 H, m), 1.97 (2 H, p, $^3J_{HH}$ = 6.4 Hz), 1.55 – 1.52 (1 H, m), 1.38 – 1.34 (1 H, m).

^{13}C {^{1}H} NMR (100MHz, $CDCl_3$, 298 K) δ 158.1, 157.1, 152.7, 135.1, 134.8, 133.2, 127.2, 122.7, 122.5, 114.5, 64.6, 53.9, 53.1, 48.3, 28.8, 26.6, 18.4**.**

MS (ESI+) $[M+H]^+$ (%) 370.2 (100).

HRMS(ESI+) calcd from $C_{19}H_{21}FN_5O_2$ $[M+H]^+$: 370.1674, found; 370.1679.

4.6.3 Small molecule X-ray structural analysis

(1 *R* - 2 *S*)-50. Clear needle crystals were obtained for crystallization in Hexane/Ethyl acetate. Cell parameters: $C_{18}H_{18}BrNO$, Molecular Weight, 344.24, monoclinic, space group $P2_1$(no. 4), a=8.4473(4), b=4.9222(3), c=19.0314(10). Å, α=90°, β=96.191(3)°, γ=90°, V=786.70(7) Å^3, Z=2, D_{calc}=1.407 g/cm^3, µ =3.761 mm^{-1}, Crystal size, 0.49 × 0.06 × 0.016 mm^3, Radiation CuKα (λ = 1.54178). F(000)=352.0 reflections were collected with a 0.49° < 2Θ < 133.132° range with a completeness to theta 90.5%; 30685 Reflections collected, 2779 were independent [R_{int} = 0.0834, R_{sigma} = 0.0372]. The parameters were 229 and the final R index(R_1) was 0.0474 for reflections having [I>=2σ (I)], and 0.1135 for all data(wR_2). The asymmetric unit contains two independent molecules, Flack parameter indicates the correct configuration (0.090(17)).

Analysis was carried out with a Bruker APEX-II CCD Diffractometer at 100 K. A Graphite-monochromated CuKα (λ = 1.54178) (40 kV, 30 mA) and a APEX-II CCD detector have been used for cell parameter determination and data collection. The integrated intensities, measured using f and ω scan mode's, were corrected for Lorentz and polarization effects. The substantial redundancy in data allows empirical absorption corrections (SADABS) to be applied using multiple measurements of symmetry-equivalent reflections. These structures were solved by direct methods of SAINT V8.38A and refined using the full-matrix least squares on F2 provided by SHELXL. The non-hydrogen atoms were refined anisotropically whereas hydrogen atoms were refined as isotropic. In both cases hydrogens were assigned in calculated positions.

Table.15 Fractional Atomic Coordinates ($\times 10^4$) and Equivalent Isotropic Displacement Parameters ($Å^2 \times 10^3$) for **(1 *R* - 2 S)-50**. U_{eq} is defined as 1/3 of the trace of the orthogonalised U_{IJ} tensor.

Atom	*x*	*y*	*z*	U(eq)
Br1	13507.6(8)	1666.3(17)	9511.6(4)	31.9(3)
O1	4809(7)	8523(12)	6969(3)	27.6(14)
N1	4204(11)	4109(16)	6765(4)	39(2)
C1	11597(9)	3214(16)	9056(4)	23.6(16)
C2	11691(10)	5200(20)	8569(6)	53(3)
C3	10292(10)	6400(40)	8240(5)	69(4)
C4	8829(9)	5526(16)	8408(4)	25.3(17)
C5	8774(9)	3507(17)	8902(4)	25.5(17)
C6	10148(9)	2305(15)	9231(4)	27(2)
C7	7381(8)	6850(30)	8059(3)	27.9(17)
C8	5911(8)	7080(20)	8425(4)	30(2)
C9	5905(8)	5226(16)	7811(4)	21.6(16)
C10	4933(8)	6068(13)	7146(4)	15.8(16)
C11	3147(13)	4550(20)	6124(5)	47(3)
C12	1545(8)	3739(16)	6205(4)	41(2)
C17A	406(10)	3850(20)	5621(3)	32(4)
C16A	-1163(9)	3140(30)	5689(5)	44(5)

C15A	-1592(9)	2320(30)	6341(7)	47(15)
C14A	-453(13)	2200(30)	6925(5)	41(5)
C13A	1115(11)	2910(20)	6857(3)	27(4)
C18	3793(14)	3050(20)	5507(5)	56(3)
C13B	951(16)	1080(30)	6452(8)	28(5)
C14B	-626(17)	240(30)	6531(9)	29(4)
C15B	-1820(30)	2110(50)	6408(16)	54(12)
C16B	-1557(19)	4700(50)	6212(9)	40(5)
C17B	14(16)	5510(30)	6140(9)	32(4)

Chapter 5 Theoretical analysis for LSD1 inhibition by PCPA

5.1 Introduction

The LSD1 enzyme catalyses the oxidative demethylation of mono and dimethylated H3K4 residues (H3K4me, H3K4me2) through FAD within a MAO domain, found in the MAO family. The proposed inhibition mechanism for LSD1 occurs by a single electron transfer with FAD, and could form a potencial three adducts (**Figure.14**) all of which covalently interact with the FAD cofactor.[74] However, there are three proposed reaction mechanisms for oxidative deamination of primary and secondary amines by MAOs[137] (**Scheme.3**). Johannes Kästner *et.al*, proposed a mechanism using Quantum Mechanics/Molecular Mechanics (QM/MM) calculation (**Scheme.15**), which proceeds though a non-textbook polar nucleophilic mechanism, with some hydride transfer characteristics.[73] This interaction proceeds to oxidative reduce the amine.[138] The protein crystallography of **GSK2879552** inhibiting FAD cofactor shows that, during the inhibition of FAD, the N-alkyl portion is removed, demonstrating that oxidative deamination does occur (**Figure.50**).[139]

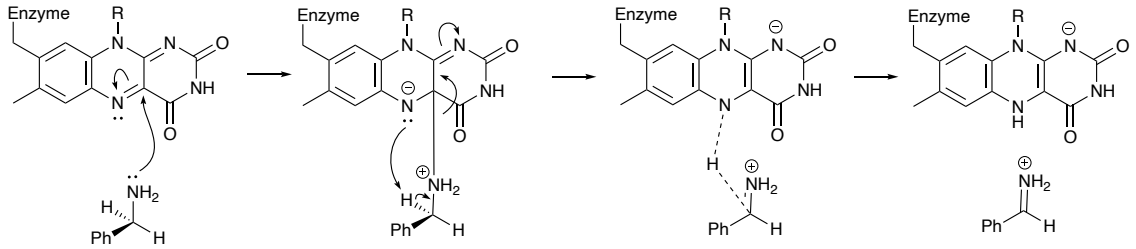

Scheme.15 Proposed mechanism by Johannes Kästner *et.al*. for oxidative deamination of primary and secondary amines

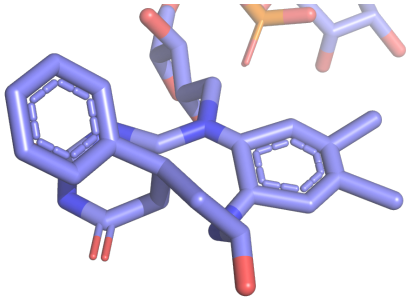

Figure.50 Crystallography of inhibited FAD Cofactor by **GSK2879552** (PDB code 6NQU). The inhibited FAD cofactor is shown as purple sticks with blue (nitrogen), red (oxygen) and orange (phosphorus).

As demonstrated by Johannes Kästner *et.al*, elucidation of enzymatic mechanistic pathways is often determined using a QM/MM where the advantages of QM (accurate) and MM (fast) are combined to reduce computational cost.[140] The QM region, most commonly at the Density Functional Theory (DFT) level of theory is undertaken on active site of the enzyme, with MM on the remaining structure. These values are combined to give the energy value for the system. However, limitations of QM/MM occur at the arbitrary sections which link the QM and MM calculations,[141] because some covalent interactions between the truncated QM region, and the MM region may differ, a common approach of truncation is; truncation by hydrogen atoms.[142,143] As an alternative method, QM can be used on an extracted active site of the enzyme to create a cluster model. Nino Russo *et.al.* compared the QM/MM (consisting of 2154 atoms with 118 in QM region) and QM (consisting of 126 atoms, with net neutral charge) cluster model's for LigW (5-carboxyvanillate decarboxylase) catalyses the decarboxylation of 5-carboxyvanillate which produces vanillate.[144] They found that both structures and energies obtained for the intermediates and transitions states were consistent between the QM/MM and QM cluster models. The QM cluster model is extracted from the active site, containing amino acid residue from around the active site. The amino acid cluster is 'fixed' in space using the fixed Cartesian redundant coordinates. Furthermore, abbreviation of sidechain compounds is to methyl units, which is to achieve a more simplified system.[145,146] In this Chapter, initial investigations into the proposed pathway by N. Miyata reaction pathway is shown in **Figure.51**,[76] where there is an SET between FAD and PCPA, followed by covalent bond formation between PCPA and FAD, concluded with oxidative reductive amination with cyclisation. Based on the work by D. Warner *et.al.,* the covalent interactions between PCPA and LSD1 with be explored using DFT. Inspiration will be taken from Nino Russo to analyse a cluster model incorporating the active site and FAD cofactor of LSD1.[140,145] Different cluster models will be used to identify the inhibition pathway. A smaller cluster model will be used to identify how PCPA interacts with LSD1. The proposed inhibition of single electron transfer exchange will be investigated, as well as the other proposed MAO oxidative reductive amination methods. The energetically favourable structure from the smaller cluster (comprised of 135 atoms with net neutral charge) will be inserted into a larger Cluster model (comprised of 218 atoms with net neutral charge), to better represent the active site of LSD1.

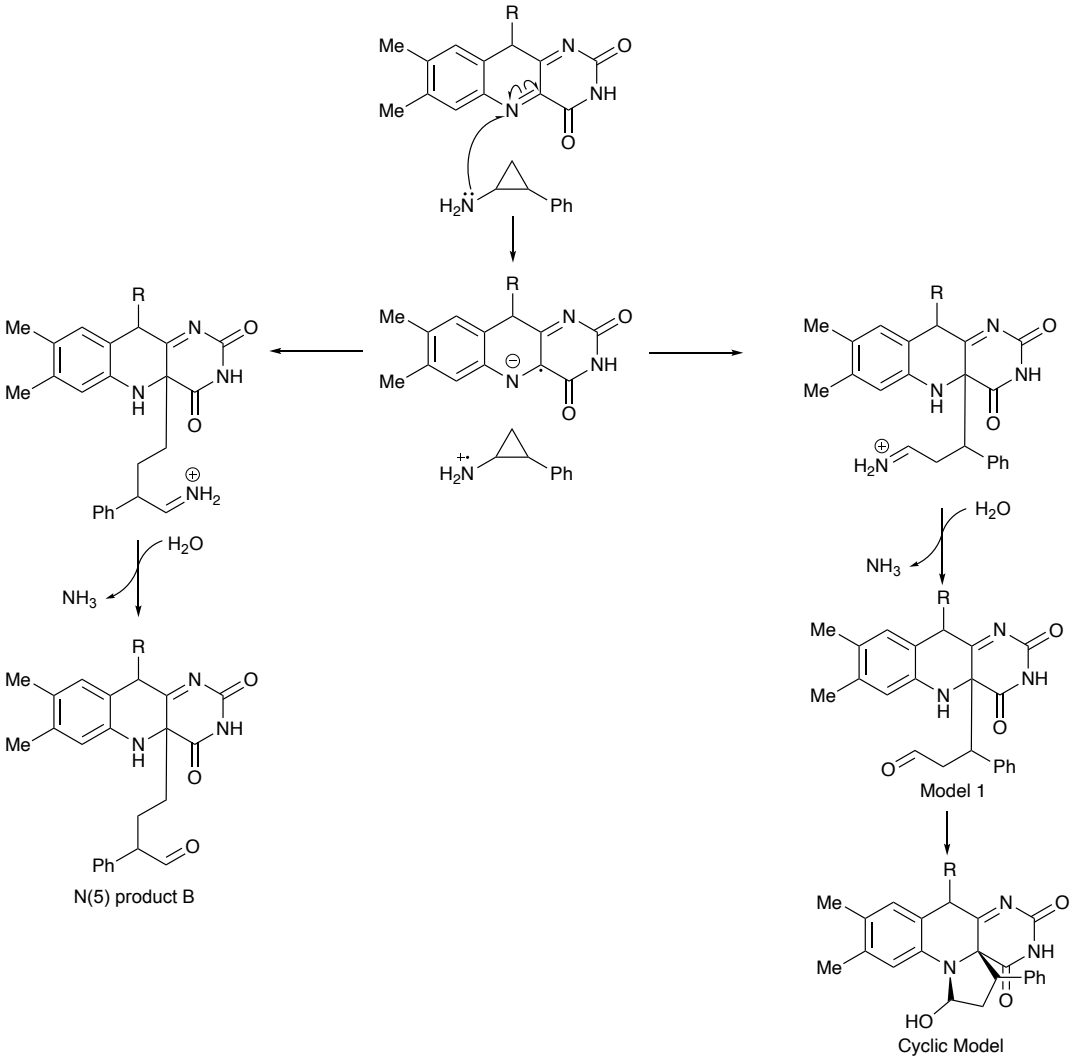

Figure.51 Initial proposed pathway for PCPA inhibition of LSD1

Initially, a local GGA method, BP86, will be used with def2-/SV(P) basis set to optimise the reaction coordinates and transition states. This level of theory has been shown in the literature to give a good cost to accuracy balance for the geometries of large structures.[147,148] However, the local nature of the BP86 functional, especially when pair with the small def2-SV(P) basis set, may not be sufficient to accurately describe the long range interactions within the protein structure, and therefore may not yield accurate energetics.[149] Inclusion of empirical dispersion correction term, D3BJ, goes someway to mitigate these errors.[150] However for comparison, the select geometries system will be re-optimised with a larger def2-TZVP basis set,[151] and the whole mechanism will be evaluated with solvated single point energy calculations at the M062X/def2-TZVP level of theory. This hybrid functional contains 54% *Hatree-Fock (HF)* exchange in its wavefunction,[152] which results in a better approximation of long range

interactions over BP86.[153] The resultant rate determining free energy will be compared to experimental activation energy.

5.2 The difference between the orientations of the PCPA (Initial Structures) (Docking the PCPA into the Active site)

PCPA was docked into the active site of LSD1 wand constrained, solvated calculations were optimised using BP86 functional, def2-SV(P) and def2-TZVP basis sets. These were used to identify the lowest energy confirmation for the possible orientations of the PCPA in LSD1. With **(a)**, positioning the CH_2 towards the FAD cofactor. **(b)**, a '180 ° flip', resulting in the NH_2 positioned towards the FAD cofactor (**Figure.52**). The optimised ground state structures from BP86(D3BJ)/def2-SV(P) were used to identify the energetic value at M062X/def2-TZVP. The optimised ground state structures (**Figure.53**) were compared to evaluate the differences in relative energies, which are reported in **Table.16, Figure.52**, and relative free energy (ΔG) (**Figure 52, 53**).

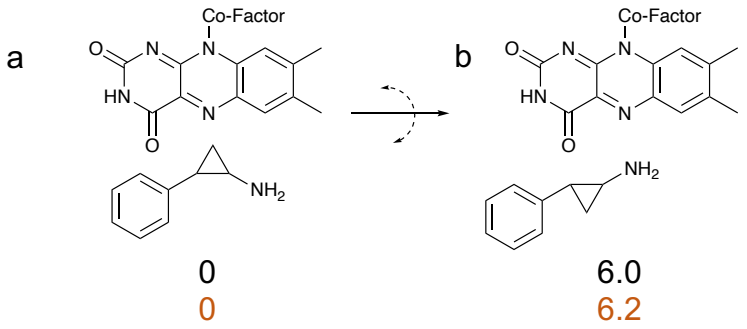

Figure.52 Differing orientations of PCPA in the active site of LSD1. **Black** showing: ΔG kcal: M062X/def2-TZVP/COSMO(water) and **Orange** showing: relative energy kcal mol^{-1}: M062X/def2-TZVP/COSMO(water)

Table.16 Comparison of relative energy / kcal mol^{-1} for different orientations of PCPA docked into the active site of LSD1 **(Figure.53).**

Level of Theory	a	b
BP86(D3BJ)-def2-SV(P)	0	3.4
BP86(D3BJ)-def2-TZVP	0	3.7

The ΔG at M062X/def2-TZVP shows that it is more thermodynamically favourable in position **a** by 6.0 kcal mol^{-1}. Equally, position **a** is also preferred when comparing the difference relative energy of the two orientations. The difference at BP86 def2-SV(P) is 3.4 kcal mol^{-1}. With the larger basis set, def2-TZVP, the enthalpy increases by 0.3 kcal mol^{-1} to 3.7 kcal mol^{-1}. Furthermore, when the functional is changed: M062X, the enthalpy difference increases to 6.2 kcal mol^{-}

[1]. This is assumed to be caused by M062X incorporating more long ranged interactions of the system.

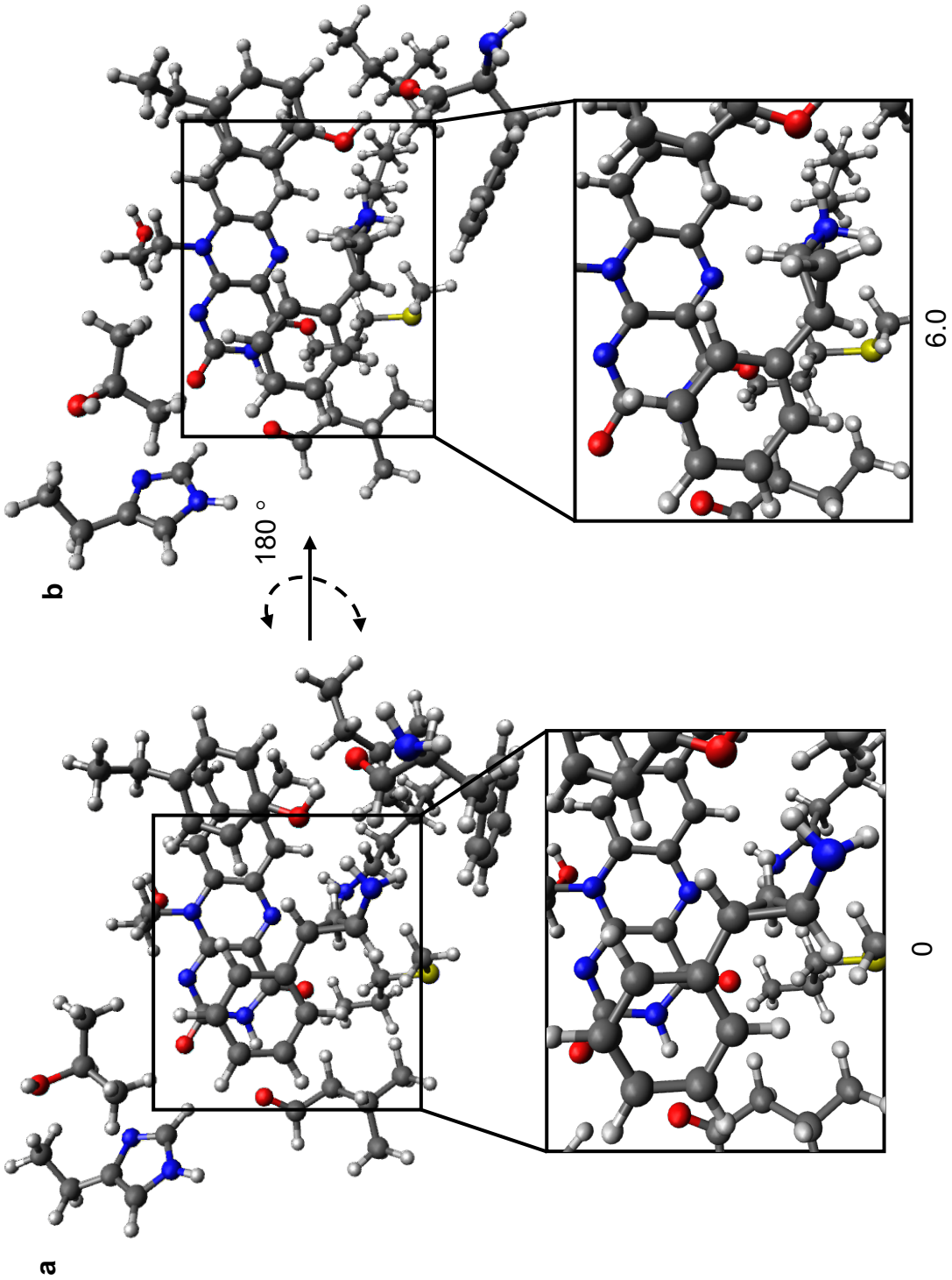

Figure.53 Calculated ground states of diffing orientations of PCPA in the active site of LSD1. ΔG kcal: M062X/def2-TZVP/COSMO(water)

5.3 Small Model for initial inhibition (Hydride, SET and PCET)

The overall view of free energy for the initial inhibition is shown in **Figure.54**, where Hydride Transfer (**RC 1 – RC 2**), Single Electron Transfer (SET) (**RC 1 - RC 3**) and Proton Coupled Electron Transfer (PCET) (**RC 1** – **RC 5**) mechanisms are investigated. To reduce computational cost, PCPA is docked into a smaller amino acid system when calculating the PCET step. PCPA (**RC 1**) reacts with FAD to form (**RC 3**).

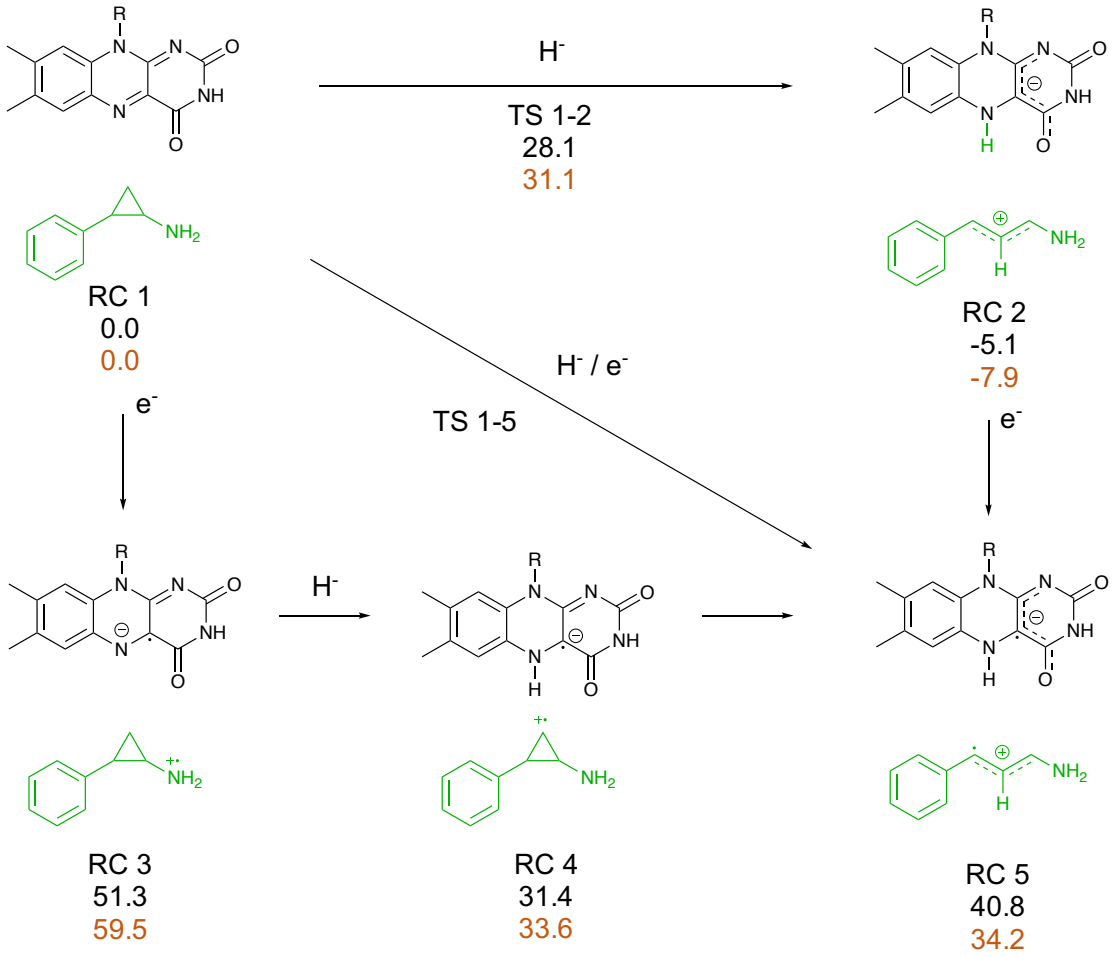

Figure.54 Reaction co-ordinates and transition state for Model 1 & Cyclic Model. **Black** showing: ΔG kcal mol^{-1}: M062X/def2-TZVP/COSMO(water) and **Orange** showing: relative energy / kcal mol^{-1}: M062X/def2-TZVP/COSMO(water)

Table.17 Comparison relative energy / kcal mol^{-1} for the interactions of PCPA with FAD cofactor **(Figure.30)**

Level of Theory	Reaction Coordinates, relative energy / kcal mol $^{-1}$						
	1	**1-2**	**1-5**	**2**	**3**	**4**	**5**
BP86(D3BJ)/def2-SV(P)	0	26.8	22.5	-14.5	37.9	48.0	-2.2
BP86(D3BJ)/def2-TZVP	0	-	-	-15.5	39.5	47.5	-3.3

RC 1 **RC 2**

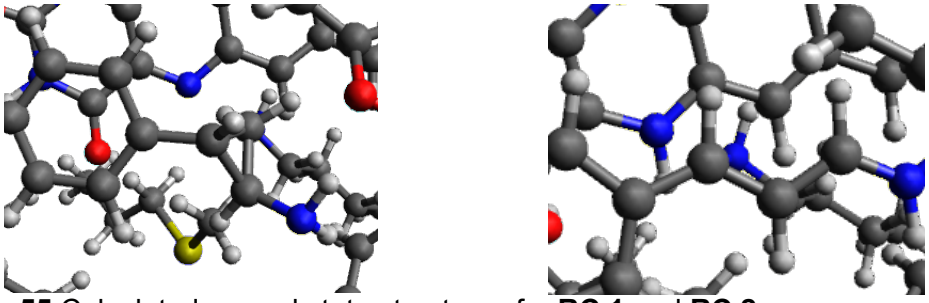

Figure.55 Calculated ground state structures for **RC 1** and **RC 2**

For the hydride transfer mechanism, PCPA reacts with FAD in **RC 1** losing a Hydride from CH_2 to FAD with a free energy barrier of 31.1 kcal mol^{-1} at M062X/def2-TZVP/Cosmo(water), and a relative energy barrier of 26.8 kcal mol^{-1} (**TS 1-2**) (**Figure.55**). As a result, collapsing the cyclopropane ring and forming a delocalised positive charge on PCPA and a delocalised negative charge on FAD with a resulting ground state ΔG = -5.1 kcal mol^{-1} (**RC 2**). Equally, PCPA could also undergo SET with FAD to form **RC 3** with relative energy = 59.5 kcal mol^{-1}. This undergoes hydride transfer to form **RC 4**, which decreases the relative energy by 25.9 kcal mol^{-1} to 33.6 kcal mol^{-1}. The cyclopropane ring then collapses to form **RC 5** which releases the ring strain, this increase the relative energy by 9.4 kcal mol^{-1}. Additionally, PCPA could undergo PCET, combining both hydride and SET mechanisms, **RC 1** would exchange a hydride from the CH_2 and an electron to the FAD from a relative energy barrier height of 22.5 kcal mol^{-1} (**TS 1 – 5**) (BP86(D3BJ)/def2-SV(P)Cosmo(water)). This was achieved by optimising the scanned singlet and triplet surface to find the minimum energy crossing point (MECP).[154] Resulting in collapsing the cyclopropane ring, releasing the ring strain resulting in **RC 5** with ground state relative energy = 34.2 kcal mol^{-1} and a ΔG = 40.8 kcal mol^{-1} higher than **RC 1**.

Re-optimisation of the structure's with a larger basis set, def2-TZVP (**Table.17**), remains fairly consistent relative energy values when compared to def2-SV(P)

(**Table.17**), with a maximum relative energy difference of 1.6 kcal mol^{-1}. Although, changing the functional from BP86 to M062X (**Figure.54**), does affect the relative energy.

For the Hydride transfer mechanism, relative energy ground state for **RC 2** is -7.9 kcal mol^{-1}, an increase of 7.6 kcal mol^{-1} over BP86. This larger difference in relative energy can be accounted by the overstabilisation with the BP86 functional,[147] and a more accurate representation of the long range attractive and repulsive forces with M062X.[155,156], The SET mechanism intermediates are different, an increase of relative energy of 20.0 kcal mol^{-1} for **RC 3** and **RC 5** differs significantly, with a relative energy difference of 37.5 kcal mol^{-1}. Therefore, further analysis of this intermediate is required to confirm this energetic difference.

The initial calculations from the small cluster investigating into the initial interactions between PCPA and FAD show that the triplet energetic surface is very high, suggesting that the initial proposed mechanism in the literature[76] is not correct.

5.4 Larger inhibition model

The overall free energy and relative energy view of the continued reaction between PCPA and FAD is showed in **Figure.56**. Where the product from Section 2.3 is docked in a larger amino acid system. The PCPA product (**RC 2**) reacts with water to form a tetrahedral intermediate (**RC 6**). FAD forms a covalent bond to the PCPA resulting in the loss of ammonia (**RC 7**). Finally, intramolecular bonds to form a carbinolamine ring (**RC 8**). Although docking the product from the small amino acid system into the larger amino acid system cause an increase in free energy from -5.1 kcal mol^{-1} to -1.8 kcal mol^{-1}. This increase comes from the extra amino acids causing an increase in entropic contribution and to the free energy value.

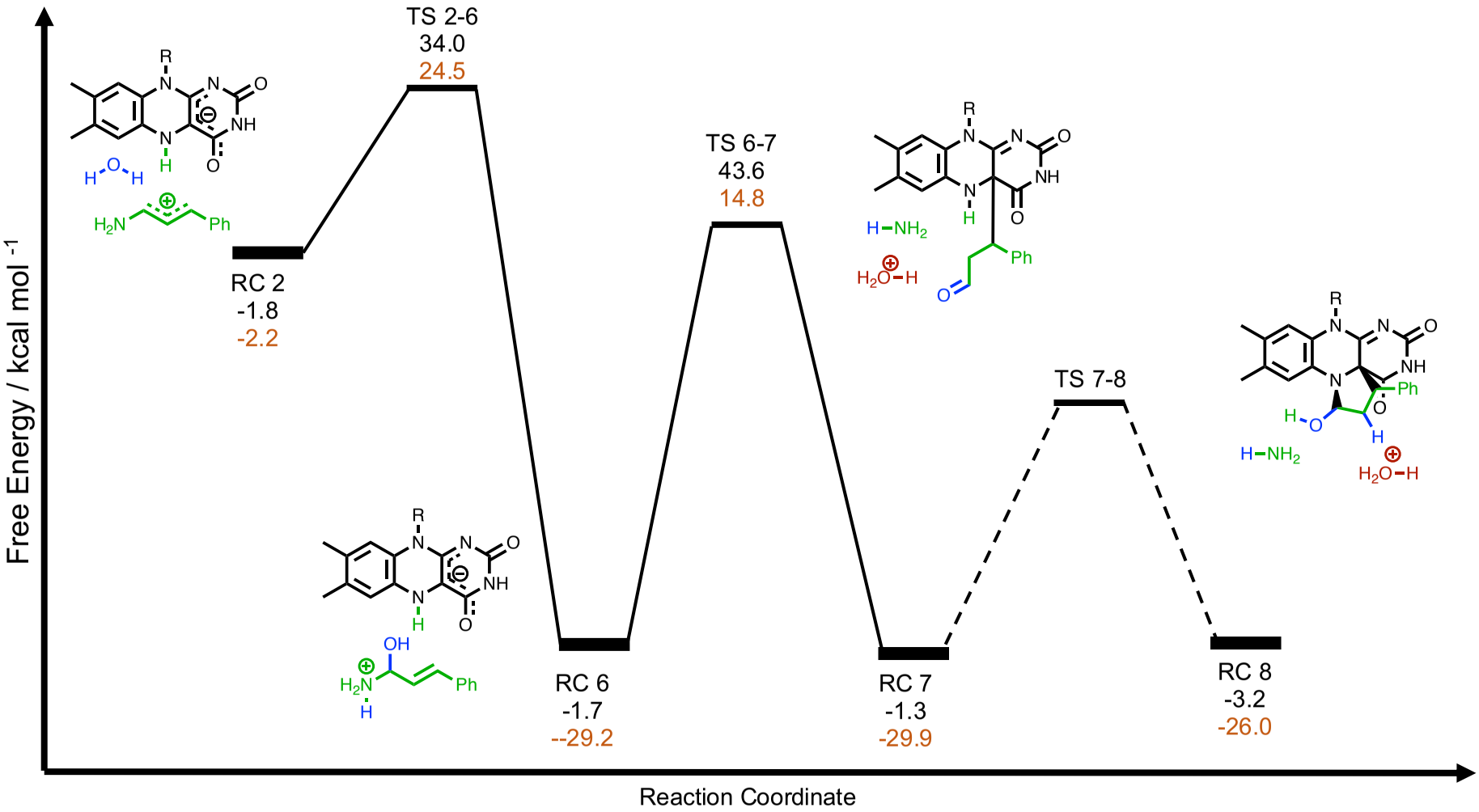

Figure.56 Reaction co-ordinates and transition states for Model 1 & Cyclic Model. **Black** showing: ΔG kcal mol^{-1}: M062X/def2-TZVP//COSMO(water) and **Orange** showing: relative energy kcal mol^{-1}: M062X/def2-TZVP//COSMO(water)

Table.18 Comparison of relative energy / kcal mol^{-1} for a inhibition pathway for PCPA with FAD cofactor **(Figure.56)**

Level of Theory	Reaction Coordinates, relative energy / kcal mol $^{-1}$						
	2	**2-6**	**6**	**6-7**	**7**	**7-8**	**8**
BP86(D3BJ)/def2-SV(P)	-3.3	17.6	-44	-12.2	-45.7	-	-61.3
BP86(D3BJ)/def2-TZVP	-14.4	29.0	-22.0	13.3	-21.9	-	-35.0

The ring opened PCPA product, from Section 5.3 (**RC 2**), reacts with water, forming a cyclic transition state (**TS 2-6**) with a free energy barrier height of 30.4 kcal mol^{-1}. The reaction specifically involves the O-H from the water, and the C-N from the PCPA (**Figure.57**).

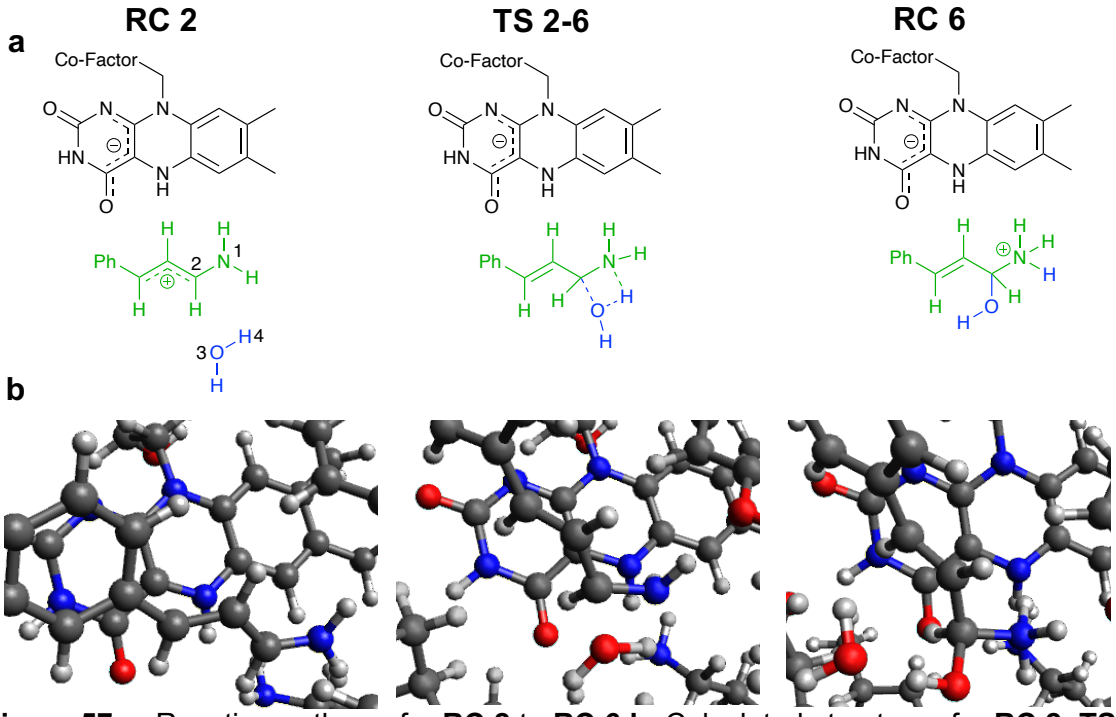

Figure.57 a. Reaction pathway for **RC 2** to **RC 6 b.** Calculated structures for **RC 2, TS 2-6** and **RC 6**.

The bond lengths for this step are shown in **Table.19**. With the introduction of water, this causes the C (2) and N (1) bond to increase from 1.342 to 1.446, and the angle of the imine hydrogens and CH to change, resulting in a free energy transition state barrier of ΔG = 30.4 kcal mol^{-1}. As the reaction proceeds, the O (3) and H (4) bonds break, with the H (4) forming a positive amine, and O (3) forming a covalent bond with C (2) forming the tetrahedral intermediate. This results in intermediate **RC 6** with a relative free energy of -1.7 kcal mol^{-1}.

Table.19 Selected bond lengths (Å) for **RC 2, TS 2-6, RC 6**

Bond	RC 2	TS 2-6	RC 6
N (1) – C (2)	1.342	1.446	1.502
N (1) – H (4)		1.488	1.038
C (2) – O (3)		1.624	1.408
O (3) – H (4)	0.984	1.155	2.459

From **RC 6**, the carbanion (9) from the FAD reacts with the carbon (8) in an electrophilic addition reaction via **TS 6-7** (**Figure.58**). giving a free energy barrier height of 45.3 kcal mol^{-1} for **TS 6-7**.

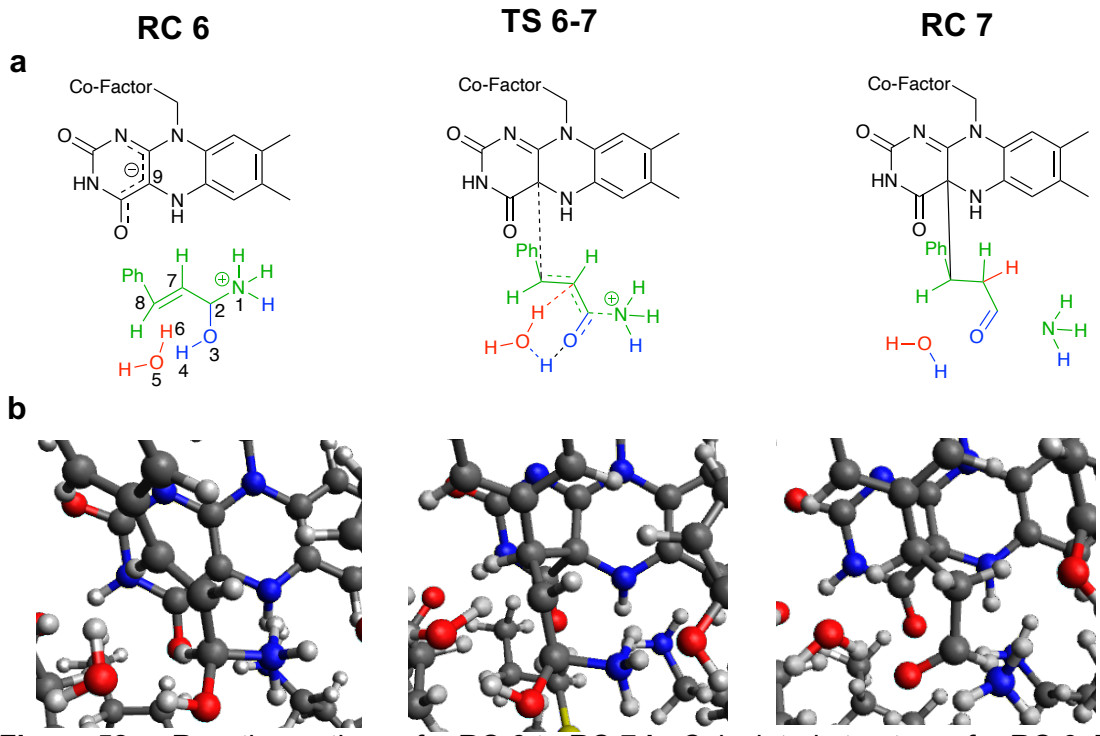

Figure.58 a. Reaction pathway for **RC 6** to **RC 7 b.** Calculated structures for **RC 6**, **TS 6-7** and **RC 7**.

The reaction proceeds by nucleophilic attack from C(9) to C (8) resulting in the double bond transferring to C (7) – C (2) and forming an enol. As a result, causing N (1) – C (2) to break, resulting in oxidative reduction of the amine. Simultaneously to this, the enol rearranges to the keto tautomer with the aid of a water molecule; which facilitates proton transfer (H 4) from the enol (O 3), to C (2). This results in intermediate **RC 7** (N(5)product A) with a relative free energy of -1.3 kcal mol^{-1}. The bond lengths for this step are shown in **Table.20**.

Table.20 Selected bond lengths (Å) for **RS 6, TS 6-7, RC 7.**

Bond	RC 6	TS 6-7	RC 7
N (1) – C (2)	1.502	1.527	2.066
C (2) – O (3)	1.408	1.407	1.254
H (4) – O (5)	1.651	1.595	1.014
O (5) – H (6)	0.984	1.140	2.746
H (6) – C (7)	2.682	1.558	1.110
C (8) – C (9)	3.617	1.778	1.635

This **RC 7** then self-cyclises to form a pyrrolidine ring (**RC 8**) (**Figure.59**) which is a higher in free energy than **RC 7** by 1.9 kcal mol^{-1}. Attempts to optimise the transition state between **RC 7** and **RC 8** proved unsuccessful, however, a reaction coordinate scan suggested a transition state in the region of 30 kcal mol^{-1}.

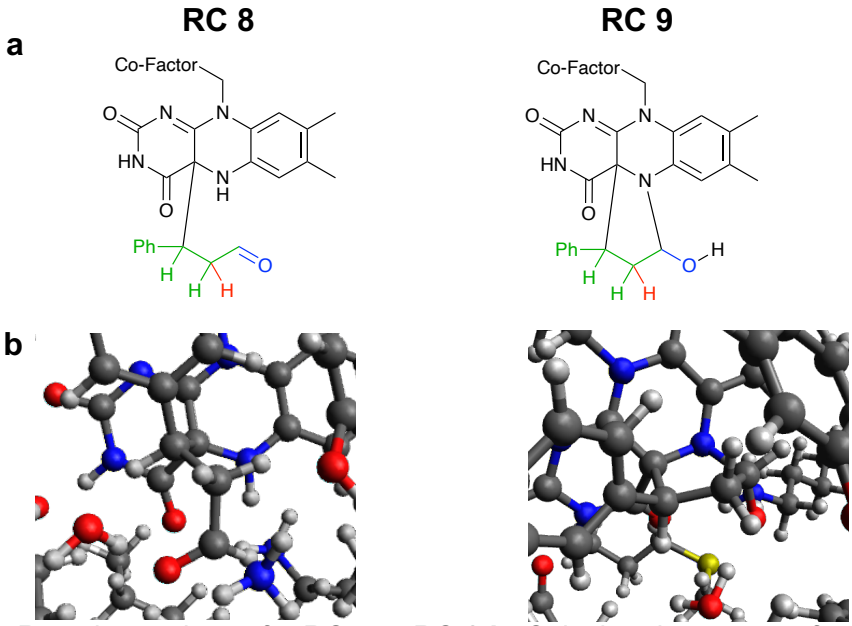

Figure.59 a. Reaction pathway for **RC 7** to **RC 8 b.** Calculated structures for **RC 7** and **RC 8.**

Unlike before, when the basis set is changed from def2-SV(P) to def2-TZVP (**Table.17**), the relative energy remained fairly consistent between the different basis sets. However for this system (**Table.18**), the relative energy vary more. For **RC 2**, def2-TZVP decreases the relative energy by 11.1 kcal mol^{-1}. The reaction proceeds though a barrier height (**RC 2 – 6**) for def2-TZVP is 43.4 kcal mol^{-1}, whereas for def2-SV(P) the barrier height is 20.9 kcal mol^{-1}. The resulting def2-TZVP for **RC 6** increases the relative energy by 22.0 kcal mol^{-1}. The def2-

TZVP relative energy barrier height (**RC 6-7**) is 35.3 kcal mol^{-1}, which is 20.9 kcal mol^{-1} lower in energy than def2-SV(P) (relative energy = 56.2 kcal mol^{-1}). Similar to **RC 6**, def2-TZVP increase the relative energy for **RC 7** by 23.8 kcal mol^{-1}. However, a slightly larger increase of 26.3 kcal mol^{-1} of relative energy for **RC 8**. Furthermore, these large differences between the basis sets relative energies are not expected, and further investigative work would be required.

Further to this, change in the functional from BP86(D3BJ)/def2-TZVP (**Table.18**), to M062X/def2-TZVP (**Figure.56**) also effects the relative energy. As can be seen, the initial intermediate (**RC 2**) starts with a higher enthalpy of -2.2 kcal mol^{-1}, which is 12.2 kcal mol^{-1} higher than the BP86. This proceeds through a barrier height (**TS 2 - 6**) of 26.7 kcal mol^{-1}, which is 16.7 kcal mol^{-1} less than BP86. This produces the tetrahedral intermediate **RC 6** with a ground state relative energy of -29.2 kcal mol^{-1}, which is 7.2 kcal mol^{-1} lower than BP86. This reacts with FAD (**TS 6 - 7**) through a barrier height of 44 kcal mol^{-1}. This is 8.7 kcal mol^{-1} greater when compared to BP86. Oxidative reduction amination occurs resulting in **RC 7** (N(5) product B with relative energy of -29.9 kcal mol^{-1}, which is 8.0 kcal mol^{-1} lower than BP86. This difference relative energy increases to 9.0 kcal mol^{-1} for **RC 8**. Although there is still some differences in relative energy between the functional's, the relative energy are more consistent.

In our cluster models, there is significant reason to confirm that PCPA interacts with FAD through either a hydride transfer mechanism or PCET, and not the SET mechanism that is proposed in the literature.[76] The relative energy for PCET (**TS 1 – 5**) is lower than the Hydride mechanism (**TS 1 – 2**) by 4.3 kcal mol^{-1} at BP86(D3BJ)/def2-SV(P) level of theory. However, the product from PCET mechanism (**RC 5**) has a larger free energy than the product for the hydride mechanism (**RC 2**) by 45.9 kcal mol^{-1} at M062X/def2-TZVP level of theory. The rate determining step from these cluster models is **TS 6 - 7** with a free energy barrier height of 45.3 kcal mol^{-1} at M062X/def2-TZVPcosmo(water). Due to the inconsistencies with the relative energy between theoretical methods, continued analysis and more in depth calculations on this system are required to confirm the proposed mechanism.

5.5 Experimental, Free energy of the reaction (ΔG)

The coupled fluorescence assays preformed measure the stoichiometric release of peroxide from the oxidation of FAD cofactors. The reported inhibition data is standardised using the H_2O_2 standard curve (2.3.1), the Michaelis Menten experiment (2.3.2) to identify the optimum substrate concentration for the inhibition assay.

5.5.1 k_i/K_i inhibition assay

The k_i/K_i inhibition assay was undertaken to identify the concentration of PCPA required to produce half maximum inhibition.[124] The fluorescence data acquired from the K_i assay was processed using quadratic **Equation.2** with a = -0.0815, b = 172.16, c = 2239.2 – reaction fluorescence value + blank fluorescence value. The resulting standardised curves where fit directly to **Equation.9** describing time-dependent inactivation to obtain values of k_{obs}

$$product = \left(\frac{v_i}{k_{obs}}\right)(1 - exp^{-k_{obs}t}) \qquad \textbf{Equation.9}$$

Where V_i, is the initial rate prior to inactivation, t = time (s), k_{obs} = the observed rate of inactivation and product = standardised experimental data. Excel solver was used to optimise the maximum value for k_{obs} for each concentration individually. The resulting values of k_{obs} were plotted as a function of inhibitor concentration to obtain values of K_i and k_i using **Equation.10**.

$$k_{obs(calc)} = {(k_i[I])}\Big/{(K_i + [I])} \qquad \textbf{Equation.10}$$

where [I] = concentration of inhibitor, K_i = Inhibition constant (μM), k_i = rate of inactivity(s^{-1}) and $k_{obs(calc)}$ the calculated rate of inactivation. To calculate K_i and k_i, **Equation.10** is used with **Equation.11**,

$$R^2 = (k_{obs(calc)} - k_{obs})^2 \qquad \textbf{Equation.11}$$

where, the sum of the R^2 values for each inhibitor concentration is used in conjunction with **Equation.10.** Solver alters constants of K_i and k_i used **Equation.10** to minimise the sum of R^2 is **Equation.11**, to find values of K_i and k_i.

5.5.2 Eyring plot and calculation of Free energy of the reaction (ΔG)

The rate of inhibition is used to identify the activation energy of PCPA inhibiting FAD cofactor of LSD1. The rate of the reaction acquired from the k_i/K_i inhibition assay is used in the Eyring plot where ln(k_i/Temperature) is plotted against 1/Temperature shown in **Figure.60**. This gives a gradient and intercept values of -5874.6 and 7.2774 respectively. The gradient can be used with **Equation.12** to identify the enthalpy of activation ($\Delta H^{\ddagger}$) of the inhibition, where R = the universal gas constant (8.314 J $mol^{-1}K^{-1}$), to give a value of 48.84 kJ mol^{-1} (11.67 kcal mol^{-1}).

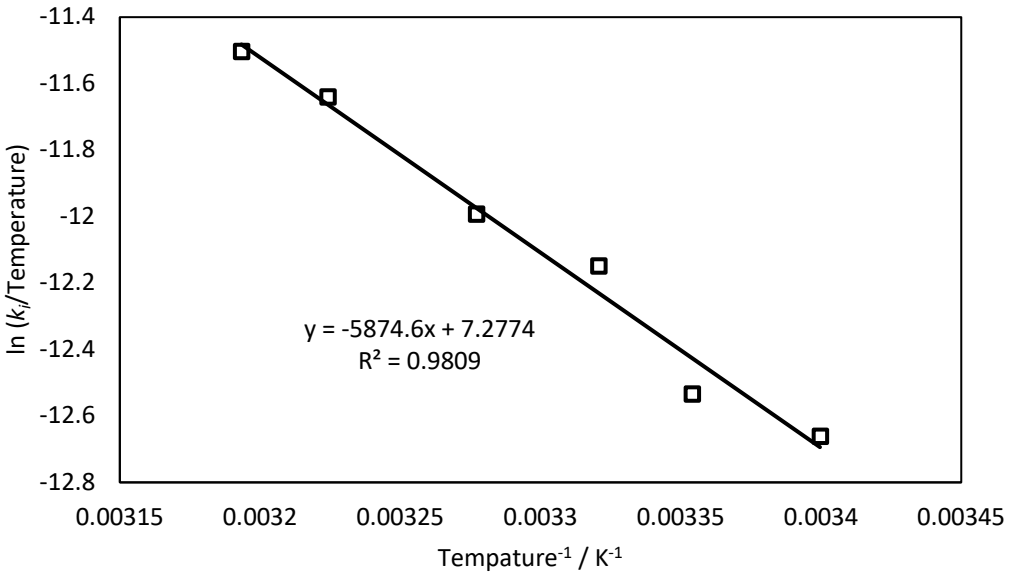

Figure.60 Eyring Plot, giving a gradient value: -5874.6 and intercept value: 7.2774. With solid line (Line of best Fit), Squares (Individual plots). Raw data shown in **Table.22.**

$$Gradient = -\frac{\Delta H}{R} \qquad \textbf{Equation.12}$$

$$Intercept = \ln\left(\frac{k_B}{h}\right) + \left(\frac{\Delta S}{R}\right) \qquad \textbf{Equation.13}$$

$$\Delta G = \Delta H - T\Delta S \qquad \textbf{Equation.14}$$

The intercept can be used with **Equation.13** to identify the entropy of activation (ΔS) of the inhibition. Where, k_B = Boltzmann constant (1.38x10^{-23} m^2 kg s^{-2} k^{-1}), h = plancks constant (6.63x10^{-34} m^2 kg s^{-1}), to give a value of -0.137 kJ mol^{-1} K^{-1}, implying an association reaction at the rate determining step. The entropy and enthalpy values are used in **Equation.14** to identify the Gibbs free activation

energy of the reaction. Where T = Temperature (310.15 K), to give a value of -- 91.3 kJ mol^{-1} (21.8 kcal mol^{-1}). This is a difference of ΔG = 23.5 kcal mol^{-1} when compared to the theoretical free energy of the rate determining step (**TS 6 – 7**).

5.6 Conclusion

Initial investigations have been completed for the inhibition pathway for PCPA inhibiting FAD. The findings show that due to the high triplet energetic surface, the initial reaction pathway proceeds through either a hydride transfer from the CH_2 on the cyclopropane, to the FAD, or a PCET transfer. These finding contradicts current proposed literature mechanisms of SET mechanism of inhibition.[76] Furthermore, the theorical rate determining step is found at **TS 6 – 7**, with a ΔG = 45.3 kcal mol^{-1}, which is 23.5 kcal mol^{-1}greater than the experimental activation energy. Unexpectedly, the larger model shows the more favourable pathway for the inhibition is by the hydride product reacting with water to form a tetrahedral intermediate, followed by a covalent bond forming between FAD and PCPA, coupled with oxidative amination. Attempts to elucidate the mechanism for the initial proposed inhibition were investigates. However, the isolation of the transition states proved elusive. Resulting in changes to our working hypothesis, altering the order of the inhibition steps to what is presented herein. As noted, there are some discrepancies between the theoretical and experimental results, and work is ongoing to understand these in more detail, along with investigative work into the reaction pathway for N(5) product A and N(5) product B.

5.7 Experimental

5.7.1 Materials and Methods

5.7.2 Computational

Coordinates of LSD1 complex were taken from the RCSB Protein data bank (PDB code: 2HKO) and hydrogen atoms were added at appropriate positions using PyMOL (2.0.3). The LSD1 complex was trimmed and the structure of PCPA was docked into the pocket.[144,145] All DFT calculations where undertaken using Orca 3.03 computational software.[157] Optimisations were performed at the RI-BP86-D3BJ/def2-SV(P) level of theory[147,158–161] with solvation correction implemented with COSMO model for water.[162] Single point energies were calculated using RI-BP86(D3BJ)/def2-TZVP and RIJCOSX-M062X/def2-TZVP.[163] Analytical Frequency calculations at BP86 def2-SV(P) level of theory were used to approximate the ZPE correction and entropic contributions to the free energy term. Additionally, confirming that no imaginary modes are present in the intermediates, and transition states had the correct frequency of decomposition. Graphical visualisation of all structures was obtained by Gabedit (2.4.8) and Avogadro (1.2.0) programs.

5.7.3 Kinetics

The rate of drug affinity to inhibit the enzyme were identified through the change in metabolism of H3K4me2 peptide through varying concentrations of drug and temperatures. The reactants present in a non-binding black flat bottomed chimney 384-well plate, are as follows; 50 µL of phosphate buffer (50 mM, pH 7.47, ionic strength 154 mM, 2.5% v/v DMSO) was added to duplicate wells, to serve as a negative control. 25 µL of phosphate buffer (50 mM, pH 7.47, ionic strength 154 mM, 2.5% v/v DMSO) was added to duplicate wells, 20 µL of freshly made chromogenic solution add consisting of Amplex Red® (0.5 mM) and HRP (5 mM) and 5 µL of LSD1 (0.75 mg/mL) was added to form a second set of negative controls. 5 µL of phosphate buffer (50 mM, pH 7.47, ionic strength 154 mM, 2.5% v/v DMSO) was added to duplicate wells, 20 µL of freshly made chromogenic solution add consisting of Amplex Red® (0.5 mM) and HRP (5 mM) and 25 µL of H_2O_2 (0.4 mM) was added to serve as a positive control. To identify the drug affinity to the enzyme, 25 µL of serial dilution of probe (1500 – 11.72 µM) were added to duplicate wells. To this, 20 µL of freshly made chromogenic solution add consisting of Amplex Red® (0.25 mM), HRP (5 mM) and H3K4me2

peptide (250 mM) were added to the wells contain probe solution. The reaction was initiated by the addition of 5 µL of LSD1 (0.75 mg/mL) (**Table.21**). The fluorescence measurements were recorded on a mono-chromator based fluorescence microplate reader set to varying temperatures (**Table.22**), in the dark, with excitation wavelength 560 ± 10 nm and emission wavelength 590 ± 10 nm. The gain set was identical to that in the standard curve assay. A multiple point experiment was conducted, monitored every 15 secs for 120 mins. The kinetic parameters were determined using at least 6 different concentrations close to the estimated K_i and k values.

Table.21 Required volumes for preparing synthesised probes for K_i inhibition experiment for LSD1 at 50 µL total volume

H3K4me2 peptide concentration [µM]	Volume of chromogenic solution (µL)	Volume of LSD1 (µL)	PCPA Concentration [µM]	Volume of Serial Dilution (µL)
50	20	5	1500	25
50	20	5	750	25
50	20	5	375	25
50	20	5	187.5	25
50	20	5	93.75	25
50	20	5	46.88	25
50	20	5	23.44	25
50	20	5	11.72	25

Table.22 Kinetic inactivation of LSD1 by PCPA at different temperatures.

Temperature / K	k / s^{-1}	Temperature^{-1} / K^{-1}	ln(k/Temperature)
294.15	0.000934	0.003399	-12.660
298.15	0.001076	0.003354	-12.532
301.15	0.001598	0.003321	-12.146
305.15	0.001893	0.003277	-11.991
310.15	0.002734	0.003224	-11.639
313.15	0.003167	0.003193	-11.502

Chapter 6 Conclusion

In this thesis, development of alkyne and azide PCPA probes for visualisation of LSD1 in cells has been achieved and their inhibitory values have been assessed. The addition of hydroxy-alkyne motif (**probes 1** and **2**) results in a negative response of increasing selectivity towards LSD1 by five fold. However, **probe 1** shows a positive response in the decrease in selectivity towards MAOs by two fold, although **probe 2** has the opposite response, and increases selectivity towards MAOs. Changing the motif for **probe 3** and **4** to hydroxy-alkyl-azide resulting in the same effect as **probe 1** and **2**. Indicating that the decrease in selectivity towards MAOs for **probe 1** and **3** is due to the *meta* position of the motif on the phenyl ring. Moreover, the change in motif to phenyl-alkyl-azide for **probes 5 – 8** results positive response for increase selectivity towards LSD1, with the exception of **probe 6**. However, they produce a negative response in decreasing the selectivity towards MAOs. One of the closest structural analogues to PCPA is **probe 1**, which resulted in this probe undergoing cellular treatment with NTERA2 cells. The NTERA2 cells confirm at mRNA and translated protein levels to which deduced that the majority of MAO present in the cells was LSD1 enzyme, giving confidence in the results from the cellular studies undertaken, as **probe 1** lacks potency towards LSD1. The novel visualisation of LSD1 was achieved though click chemistry, catalytically reacting with the alkyne tag of the probe. The click chemistry method for visualisation was validated identification of no non-specific uptake of the Alexa Fluor® 594 azide. The resulting cellular studies showed that **probe 1** successfully passes through the cell membrane. The inhibition of LSD1 with **probe 1** was demonstrated by co-localisation of the enzyme by click chemistry to visualise the probe, and ICC to visualise LSD1. This conjugation of the adduct was confirmed by MADLI-TOF mass spectrometry, yielding a peak of 1818.4879 m/z. this results in the reliability in using the probes as a tool to reveal biological functions of enzymes. Additionally, change in epigenetic marks was evaluated to confirm the involvement of LSD1 in the gene regulation system of NTERA2 cells. The effect of LSD1 inhibition upon the change in epigenetic marks was accessed by the accumulation of H3K4me3 in NTERA2 cells. The western blot analysis confirmed that the inhibition of LSD1 causes an increase in the global accumulation of H3K4me3 in the cells, confirming that the inhibition of LSD1 could be used as a therapeutic agent.

Further synthesis of the probes was undertaken to increase their cellular permeability. This was achieved by using the additional motif of the probe and coupling a peptide with LLKK repeating sub unit, which was chosen from a high content screening due to its cell permeability and proliferation effects. Five peptide probes were successfully synthesised through click chemistry, and their inhibitory activity were evaluated. To our surprise, the addition of the peptide resulting in a negative response for increasing the selectivity towards LSD1. Although the peptide mimics the bulk of the H3 motif, it lacks the molecular recognition, which causes the increase in selectivity. However, the bulk of the peptide resulted in a positive response for increase the selectivity towards MAOs. The cellular studies with Steven Brown group showed that the peptide passes through the cellular membrane of the HCT 116 cells. However, to access if LSD1 can be used as a therapeutic agent in HCT 116 cells, further cellular experiments are required to identify and confirm the expression rates of MAOs and LSD1 enzymes within the cells at translated protein and mRNA levels. Subsequently, experiments should be attempted to confirm the effect LSD1 has on cellular growth and proliferation effects using the epigenetic marks as an indicator. This will provide LSD1s readability to be used as a therapeutic agent in HCT 116 cells. Currently, clinical trial PCPA derived drugs are enantiomer specific, and most are N-alkylated derivatives. Therefore, synthesis of enantiomer specific and N-alkylated probes and their corresponding inhibitory values were explored. Single Crystal X-Ray Diffraction and ^{1}H NMR nOe studies were employed to evaluate the separation of the enantiomers using a chiral auxiliary. These methods confirmed with a Crystal X-Ray Diffraction Flack parameter of 0.09, and the nOe showed the differences that were hypothesised, concluding the successful separation of the enantiomers. The resulting separation for **probe 7** made little difference for the inhibition activities towards MAOs. However, the separation resulting in positive response for **(1 *R* - 2 *S*)-probe 7** to 'fit' better into the active site of LSD1, with just over 2.5 fold selectivity over **(1 *S* - 2 *R*)-probe 7**. Furthermore, N-alkylation of **probe 4** using GSK's reductive amination method resulted in **probe 9**, which unexpectedly resulted in the Schiff base/imine. Nevertheless, the addition to the amine of PCPA resulting in a positive response to increase inhibition towards LSD1, by six fold (when comparing to **probe 4**). However, this addition has no effect on the MAOB inhibition, but results in a positive response for increasing selectivity towards MAOA. This highted that the

difference in size of the MAO active sites allows MAOB to better accommodate larger molecules.

Elucidation of mechanistic pathway of PCPA inhibiting FAD cofactor of LSD1 has begun by undertaking density functional theory analysis on the mechanistic pathway using two cluster models (comprised of 135 atoms and 218 atoms with net neutral charge's). Identification of the initial interactions of PCPA with FAD was undertaken using a smaller cluster model, where hydride transfer, single electron transfer and proton coupled electron transfer where investigated. The initial findings show that the reaction pathway progress's through either a hydride transfer from the CH_2 on the cyclopropane, to the FAD, or a PCET transfer, from the same CH_2 on the cyclopropane, contradicting the literatures current proposed mechanism of single electron transfer. Due to isolation of the transition states proved elusive for our original hypothesis. It was unexpectedly found that the larger model shows a more favourable pathway for the inhibition is by the hydride product reacting with water to form a tetrahedral intermediate, followed by a covalent bond forming between FAD and PCPA, coupled with oxidative amination. This contradicts our hypothesis that PCPA reacts with FAD, and then undergo oxidative amination. However, there are questionable discrepancies between the theoretical and experimental results, and current work is ongoing to understand these in greater detail, along with investigative work into the reaction pathway for N(5) product A and N(5) product B. Furthermore, form the data presented, the theorical rate determining step is found at **TS 6 – 7**, with a ΔG = 45.3 kcal mol^{-1}, which is 23.5 kcal mol^{-1}greater than the experimental activation energy.

Chapter 7 Future Direction

Future direction of this work would initiate by development of different peptide probes to increase the selectivity towards LSD1. For this, initial synthesis of the probes would be altered from the Corey Chaykovsky cyclopropane synthesis to the enzymatic synthesis demonstrated by Frances H. Arnold,[77] resulting in sterically synthesising the desired cyclopropane, resulting in a more efficient synthesis of the molecular probes.

The insufficient selectivity of the LLKK peptide subunit would call for additional screening of the peptides. This would incorporate molecular recognition of the H3 motif, in addition to the previous specificities of cell permeability and proliferation effects. Inspirations can be taken from the peptide mimicking molecules such as, **NCL-1**, **IMG-7289** and **30**, incorporating the cellular permeability and selectivity towards LSD1.

Alongside this, a larger range of N-alkylated probes would be investigated to improve the selectivity towards LSD1 further, with exploration into innovative development of N-alkylated PCPA molecules from bioisostere analysis on current clinical trial drugs. The resulting molecules would be synthesised and likewise undergo the identical inhibitory activity analysis, molecular biology and cellular testing to **probe 1** to validate their inhibition and cellular proliferation.

Successful candidates from the peptide screen and N-alkylated probe library would be combined, incorporating the selectivity portion from the N-alkylation probe, and the cellular permeability from the screened peptide. These conjugates would be tested for their cellular functionalities. This could result in a successful clinical trial candidate for inhibition LSD1.

Continued elucidation of the mechanistic pathway for PCPA inhibiting FAD should be completed, with exploration into the other possible product, N(5) product A and N(5) product B, from the inhibition pathway. Further to this, the energetics for a N-alkylated PCPA molecule should be evaluated to identify if the addition of the N-alkylated motif is energetically beneficial for PCPA inhibiting the FAD cofactor.

Chapter 8 Appendix A

methyl (*E*)-3-(3-hydroxyphenyl)acrylate **(34a)**

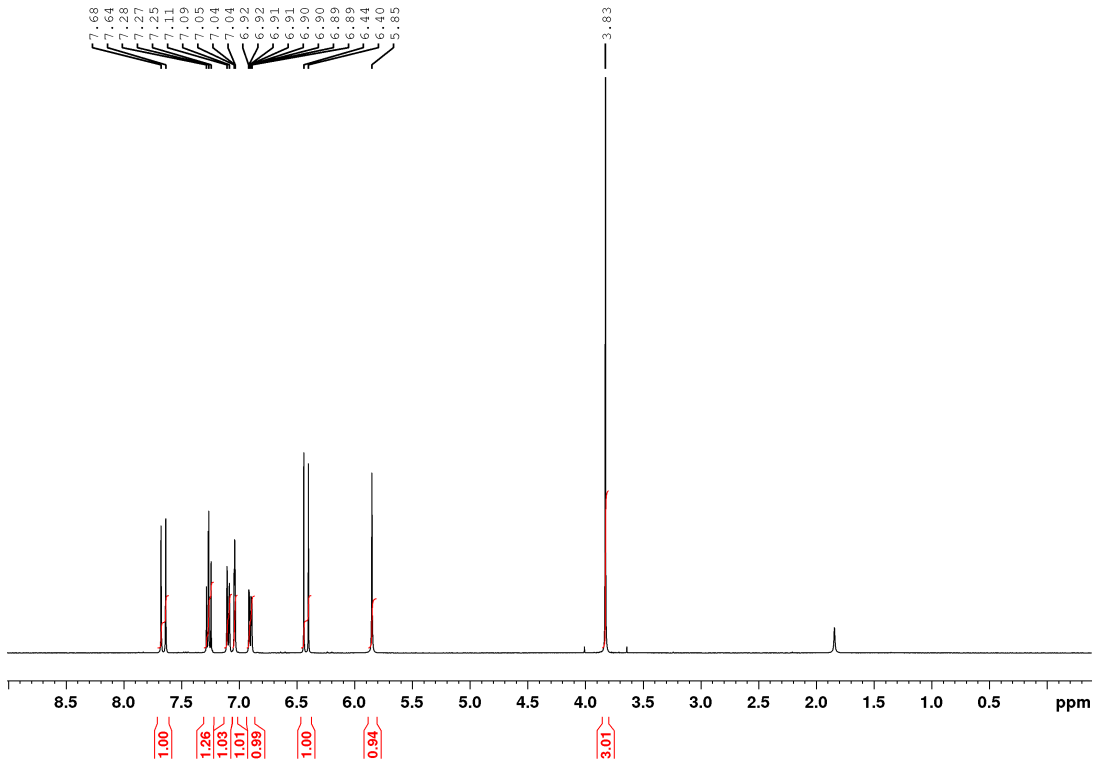

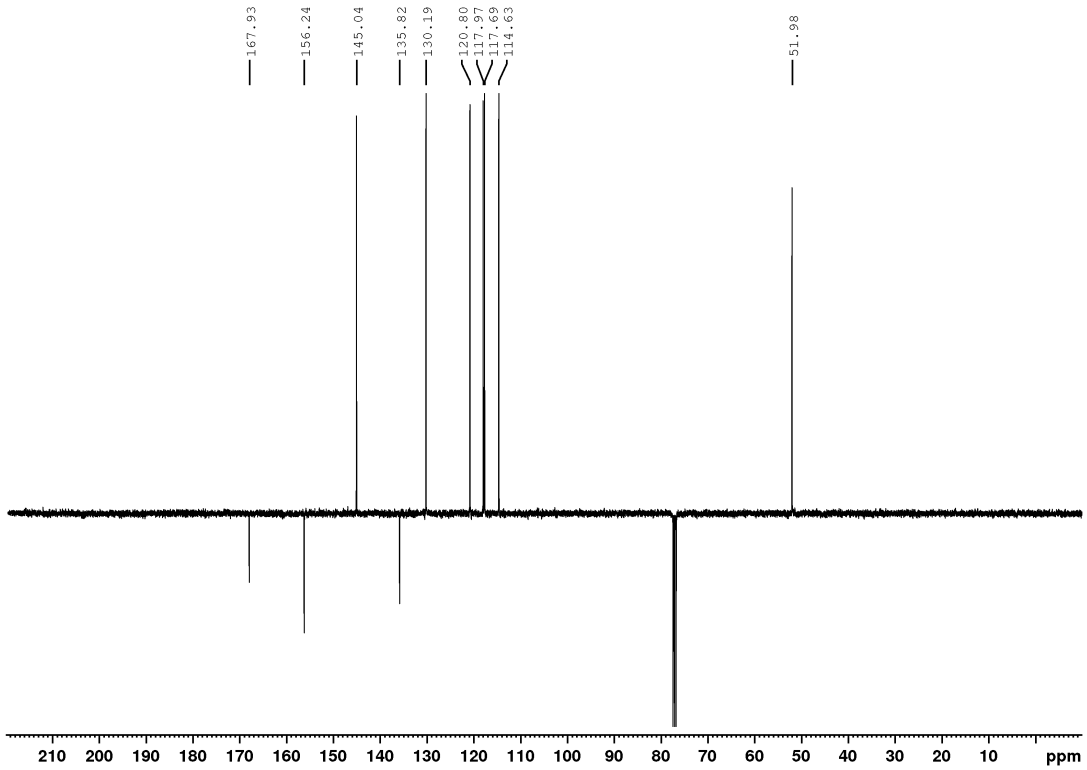

methyl (*E*)-3-(4-hydroxyphenyl)acrylate **(34b)**

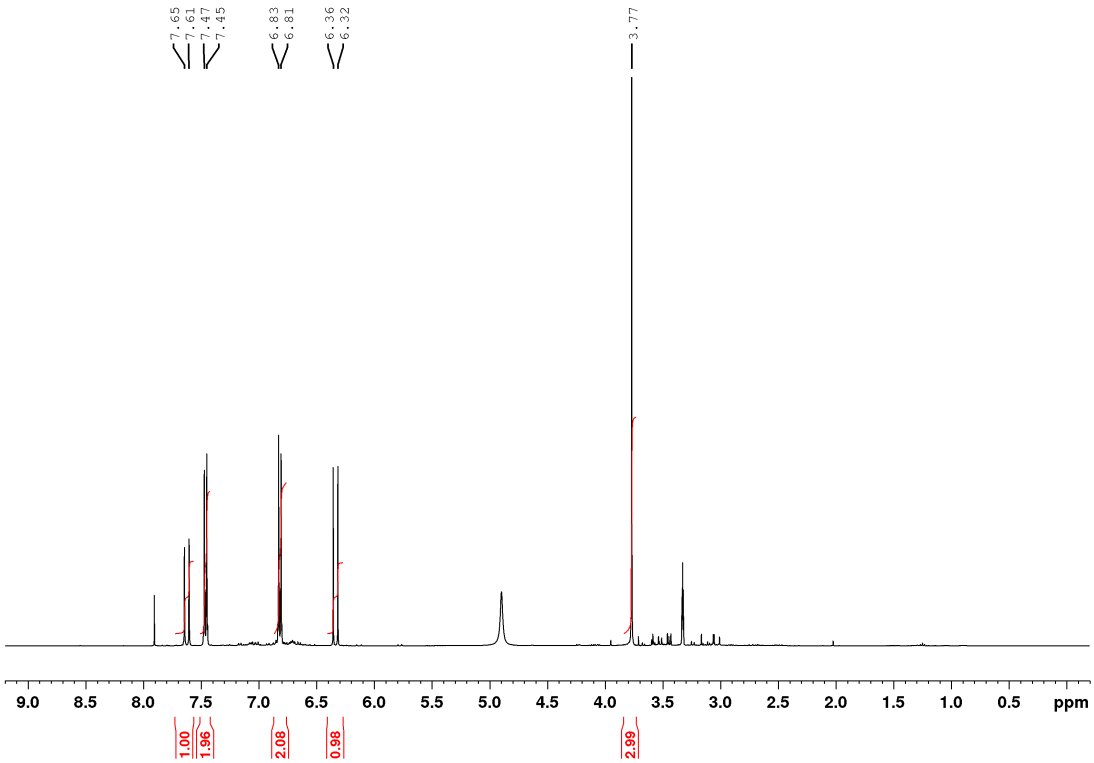

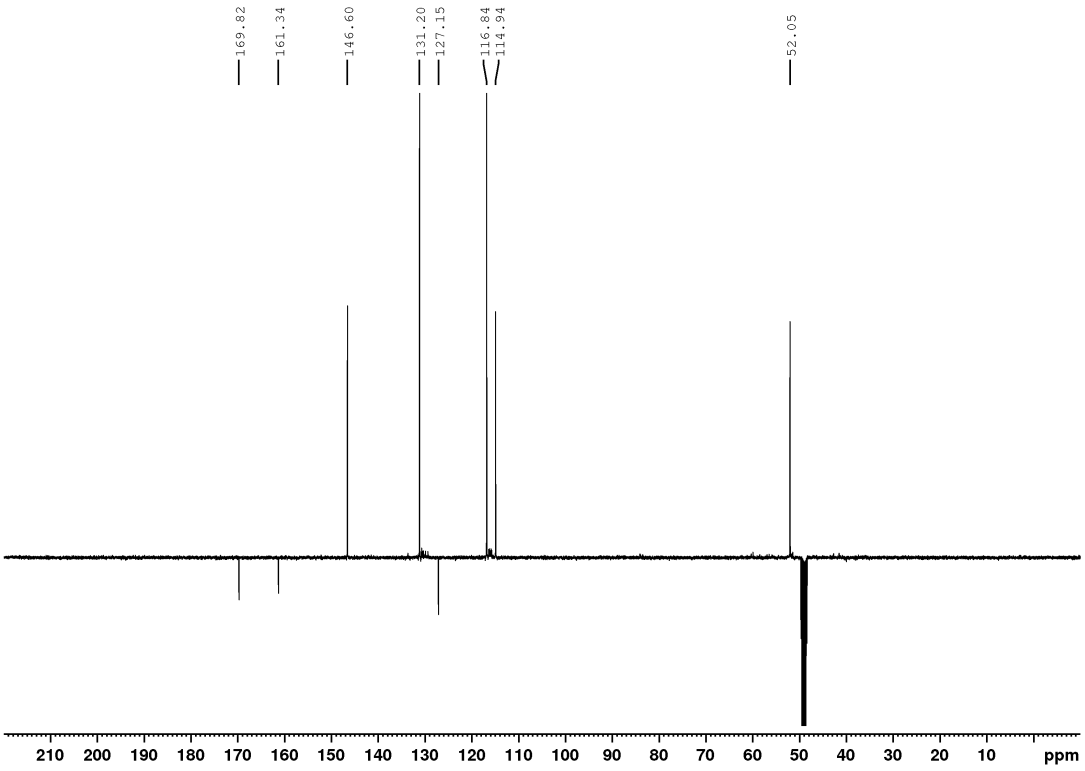

methyl (*E*)-3-(3-bromophenyl)acrylate **(41a)**

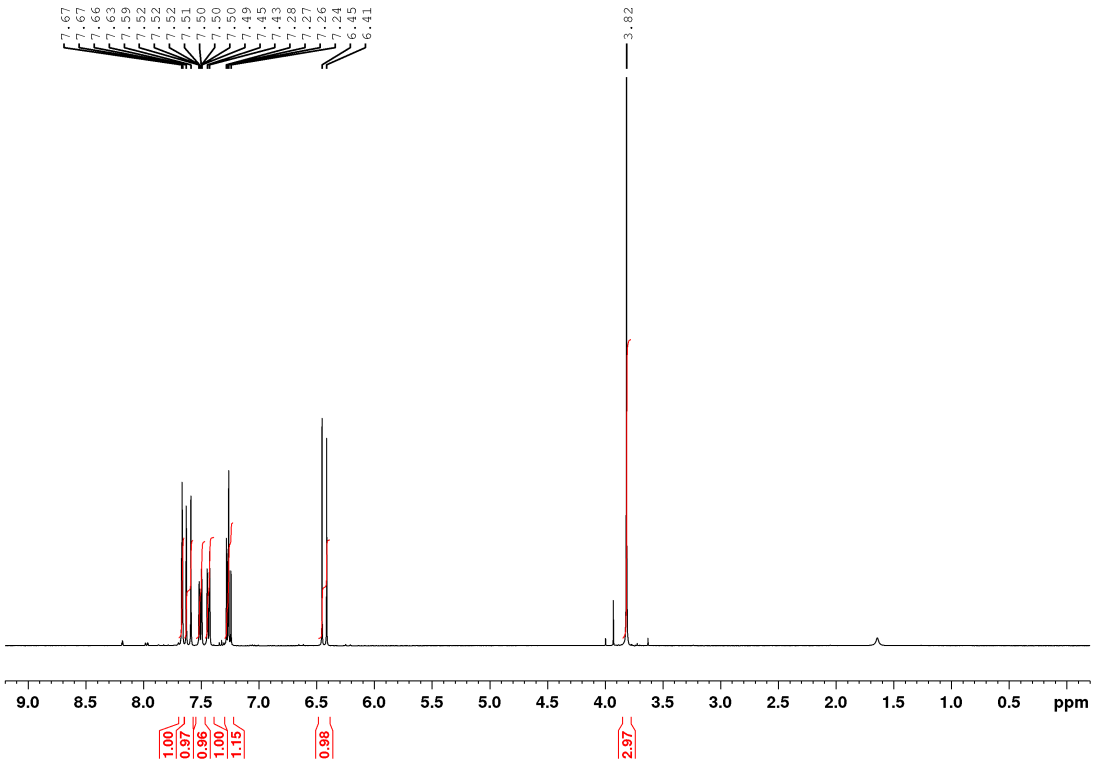

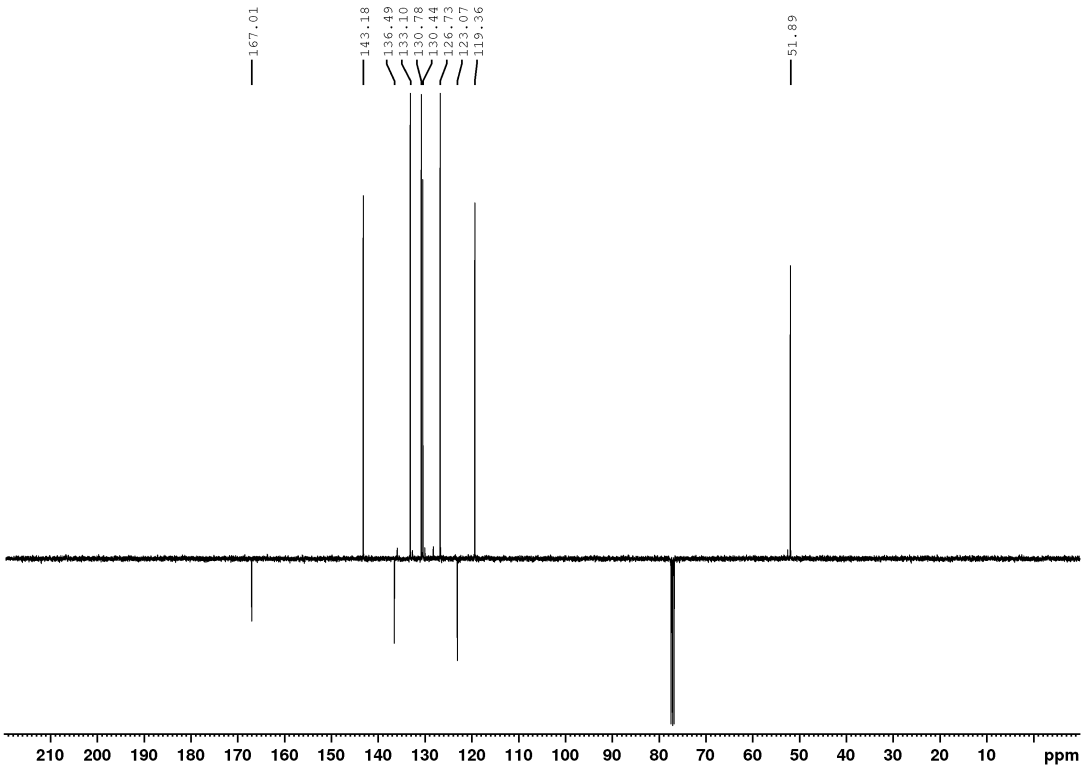

methyl (*E*)-3-(4-bromophenyl)acrylate **(41b)**

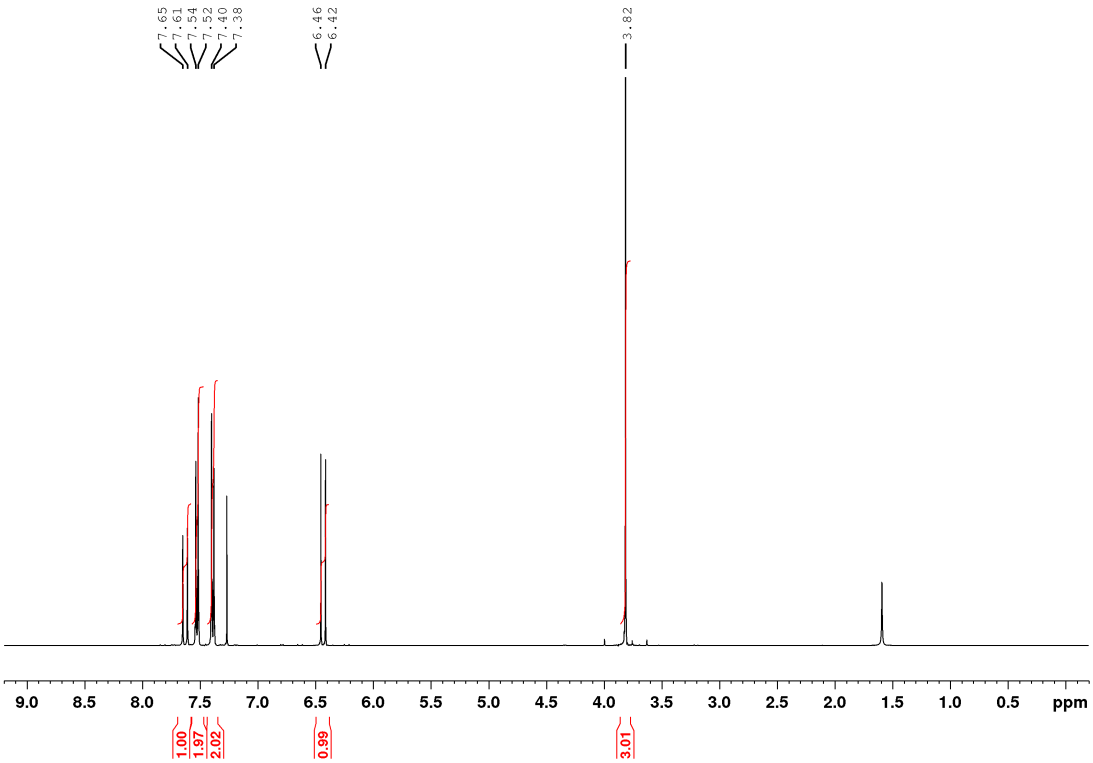

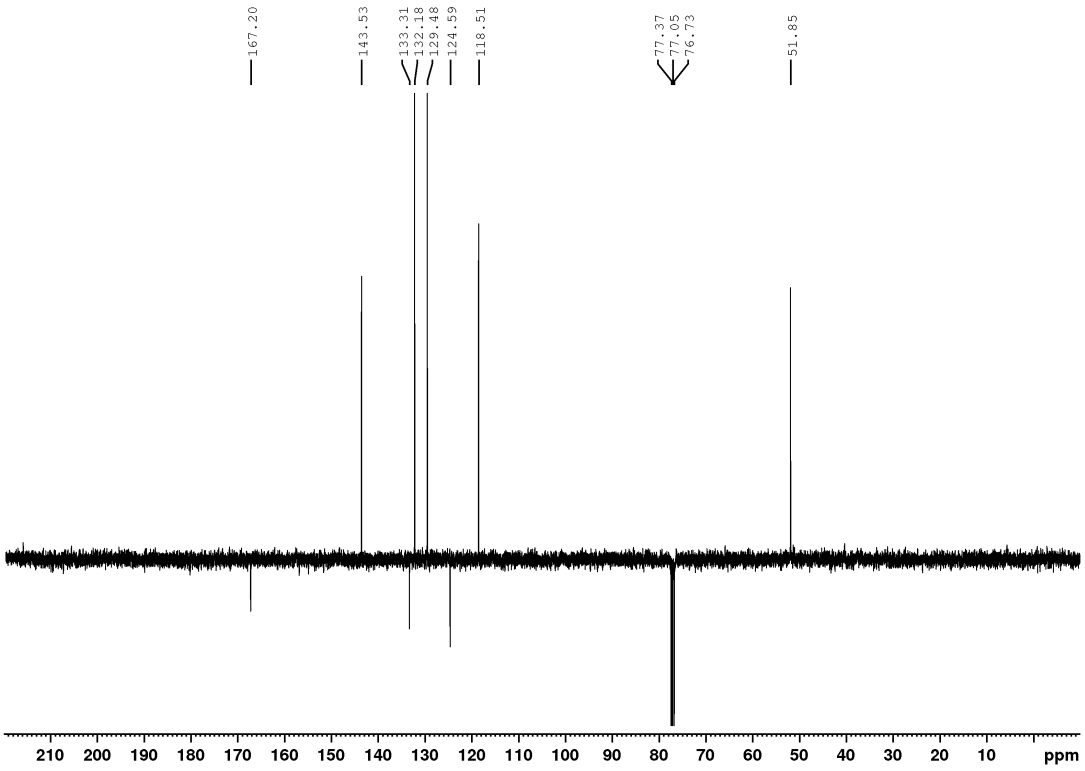

methyl (*E*)-3-(3-(methoxymethoxy)phenyl)acrylate **(35a)**

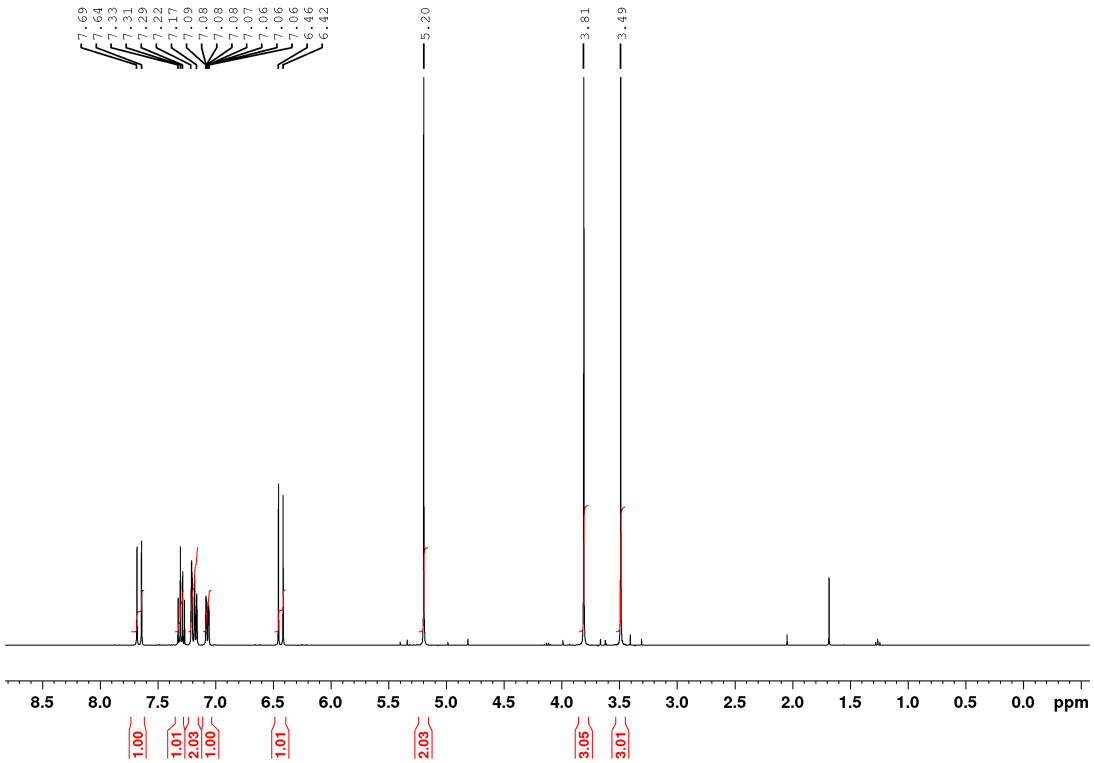

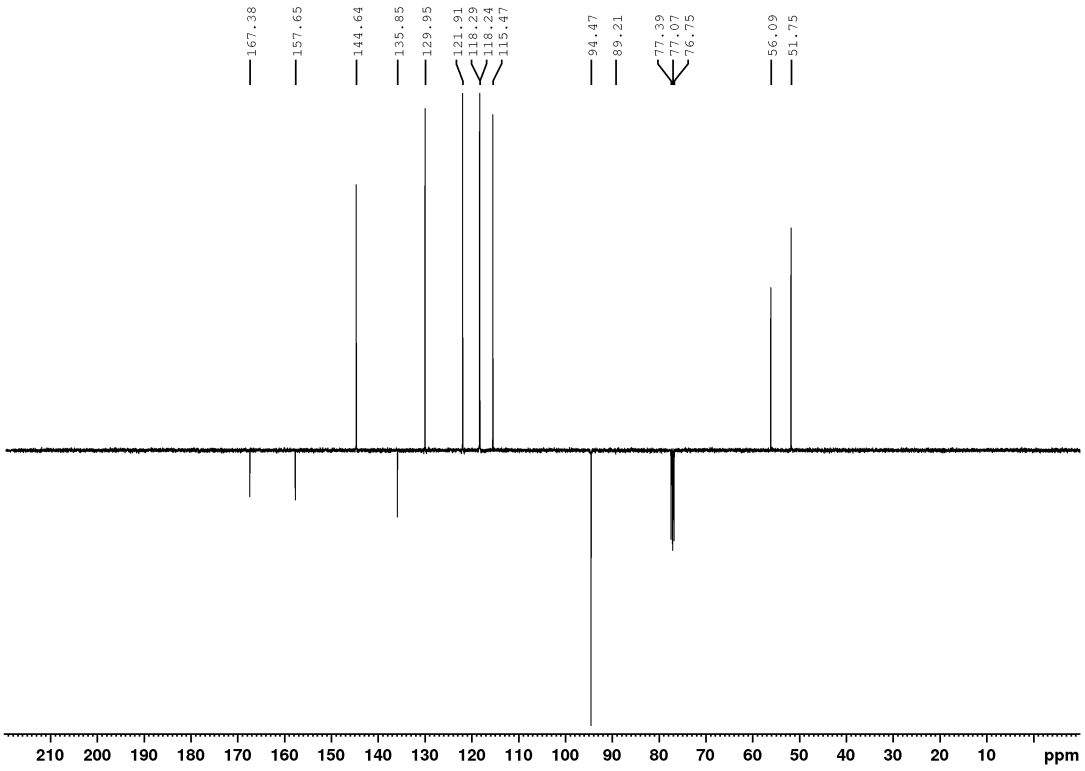

methyl (*E*)-3-(4-(methoxymethoxy)phenyl)acrylate **(35b)**

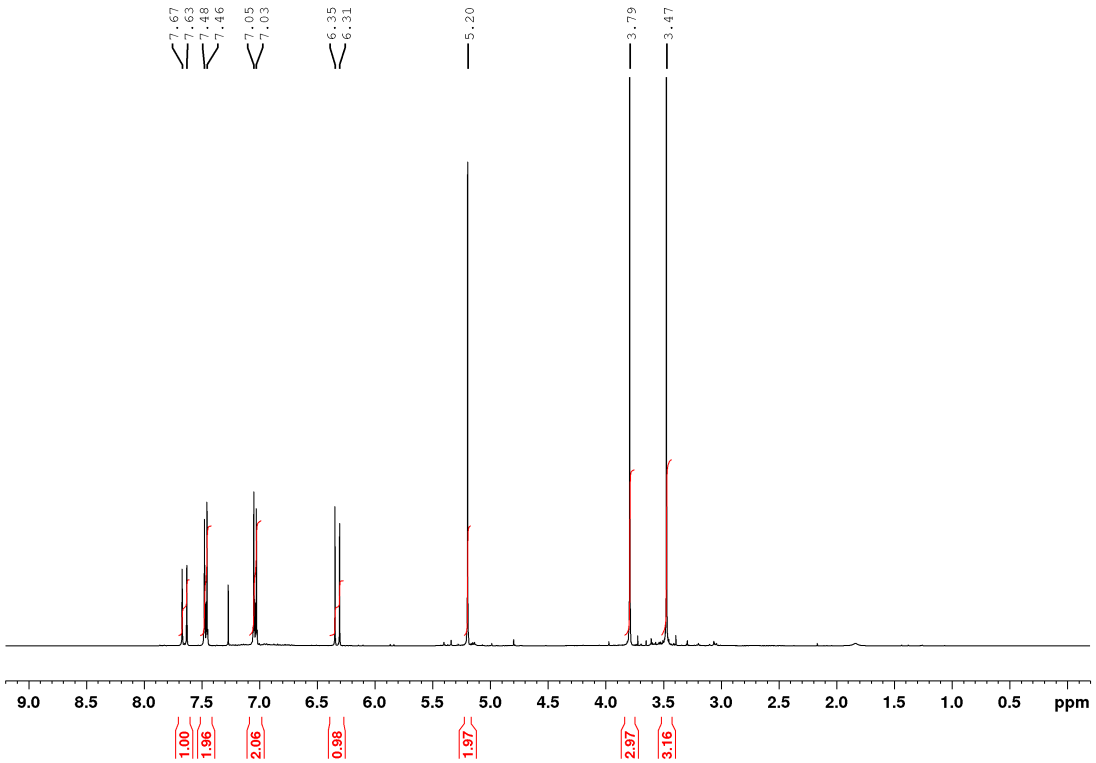

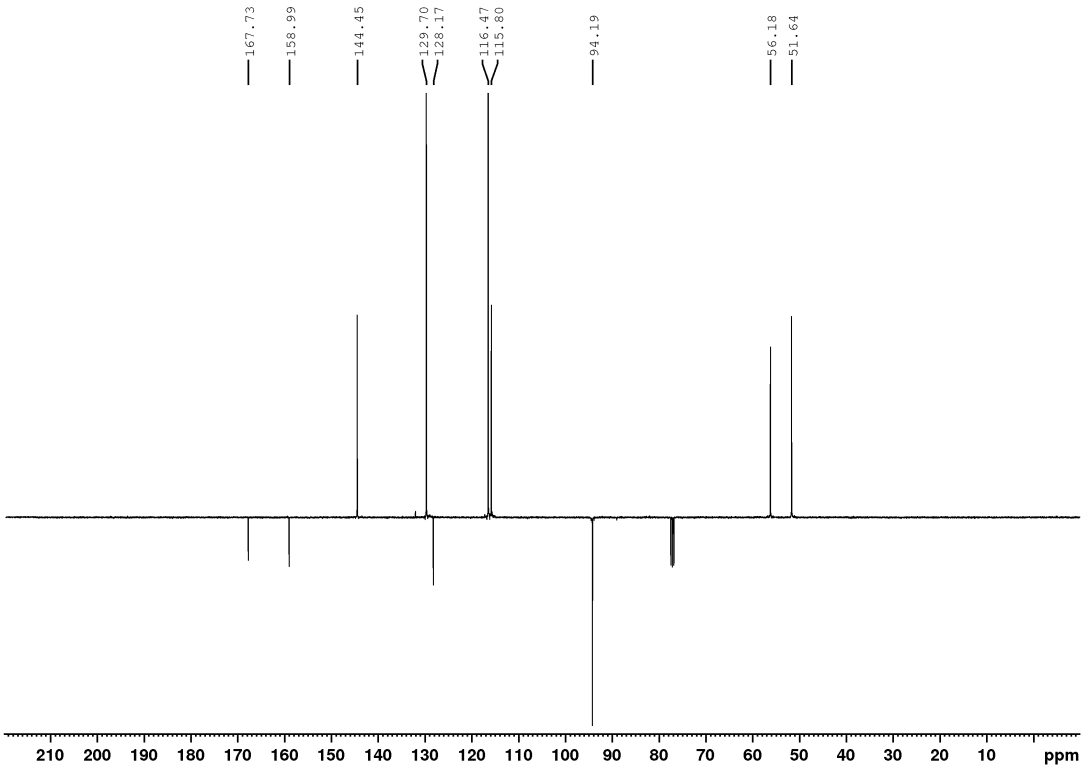

methyl 2-(3-(methoxymethoxy)phenyl)cyclopropane-1-carboxylate **(36a)**

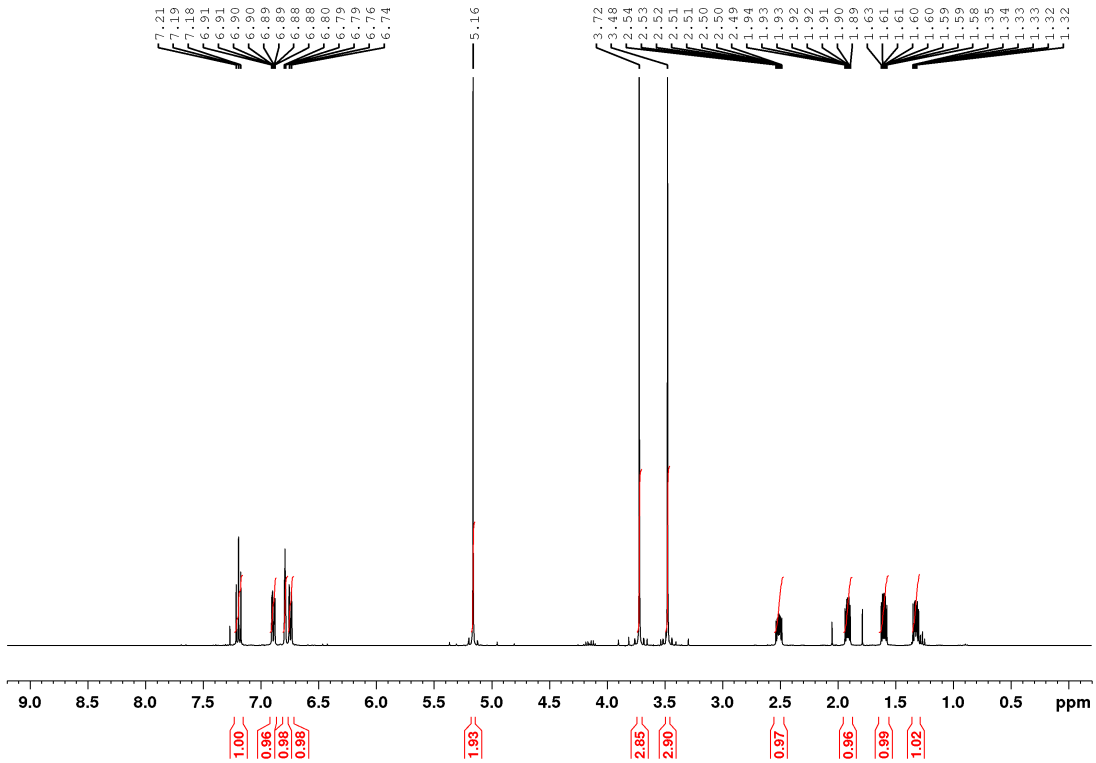

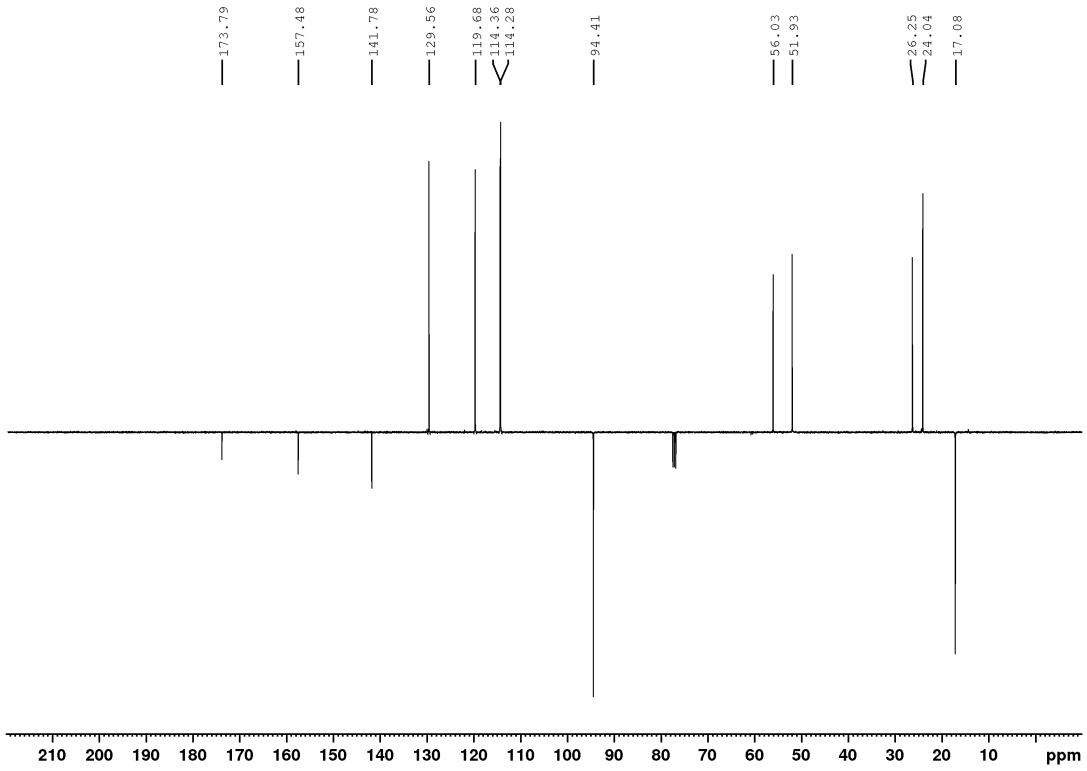

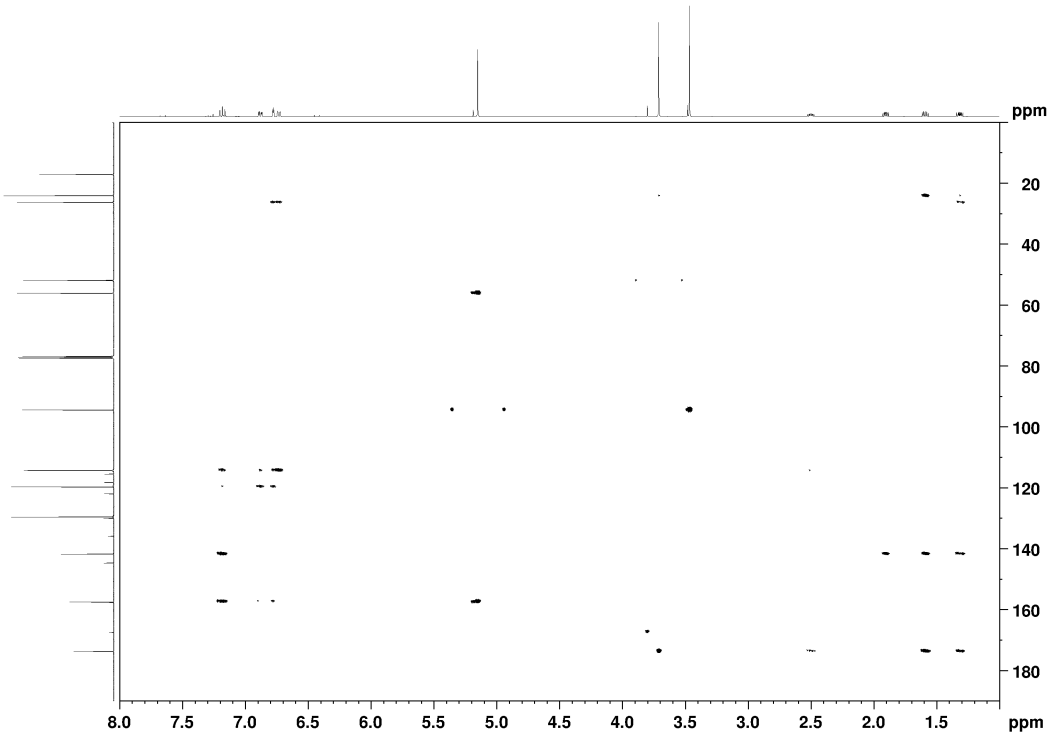
ppm
20
40
60
80
100
120
140
160
180
8.0
7.5
7.0
6.5
6.0
5.5
5.0
4.5
4.0
3.5
3.0
2.5
2.0
1.5
ppm

methyl 2-(4-(methoxymethoxy)phenyl)cyclopropane-1-carboxylate **(36b)**

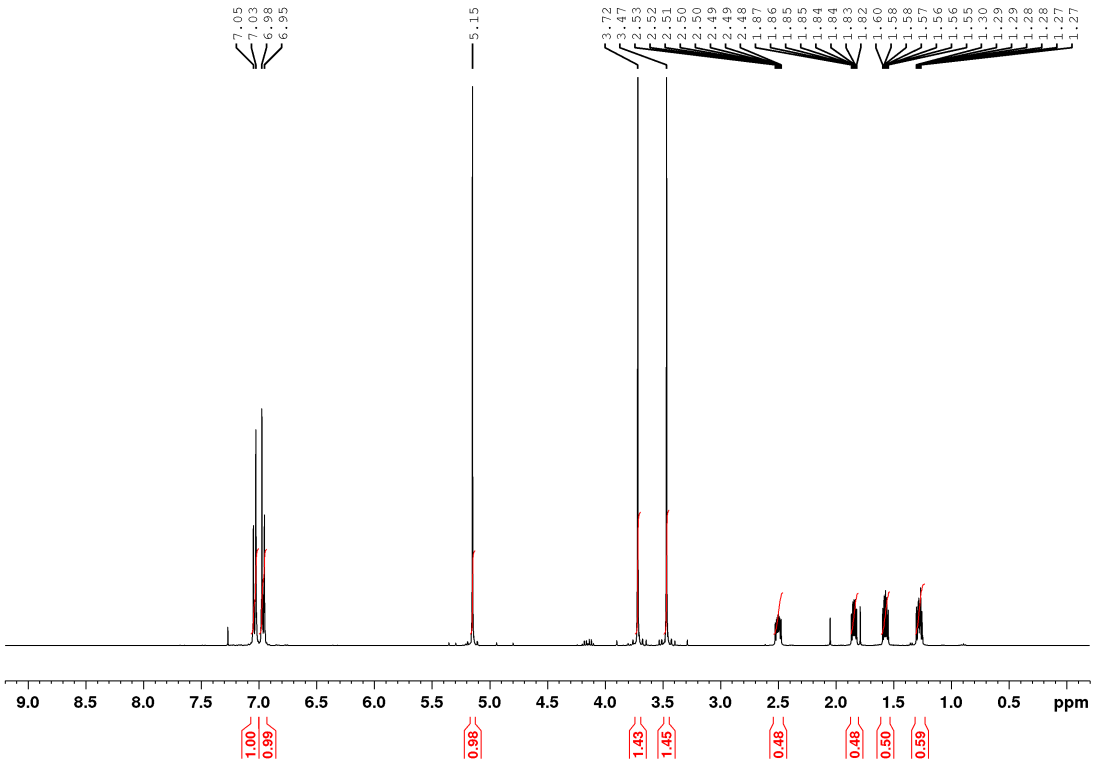

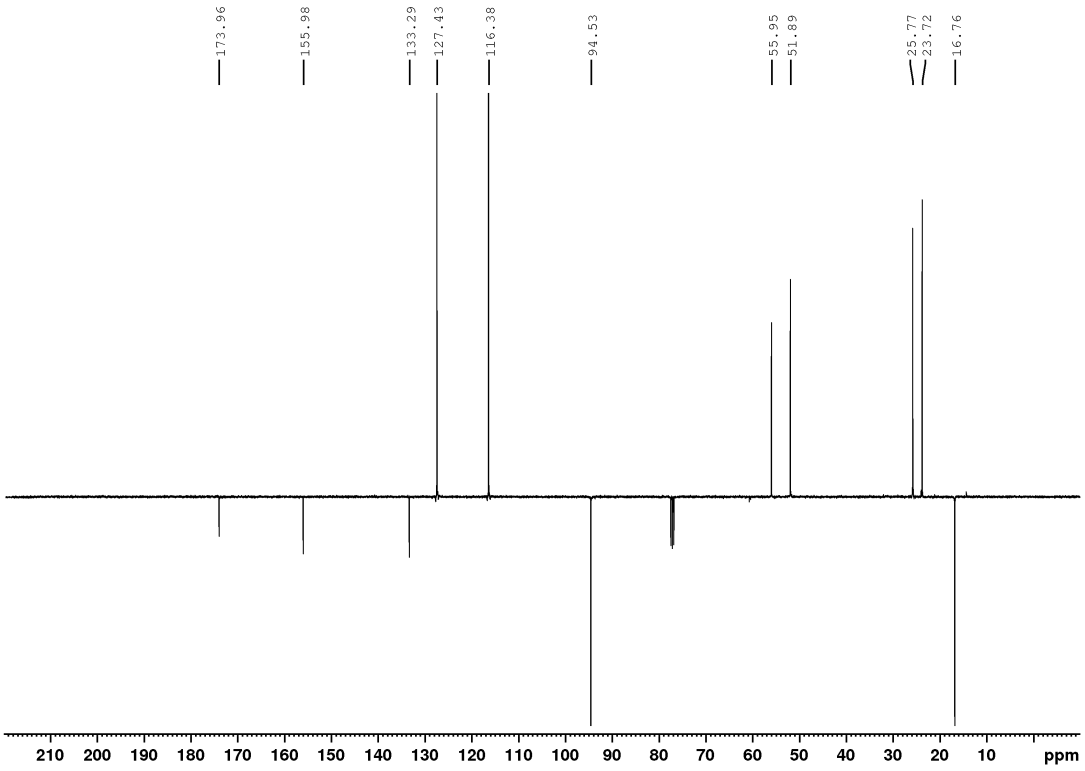

methyl 2-(3-bromophenyl)cyclopropane-1-carboxylate **(42a)**

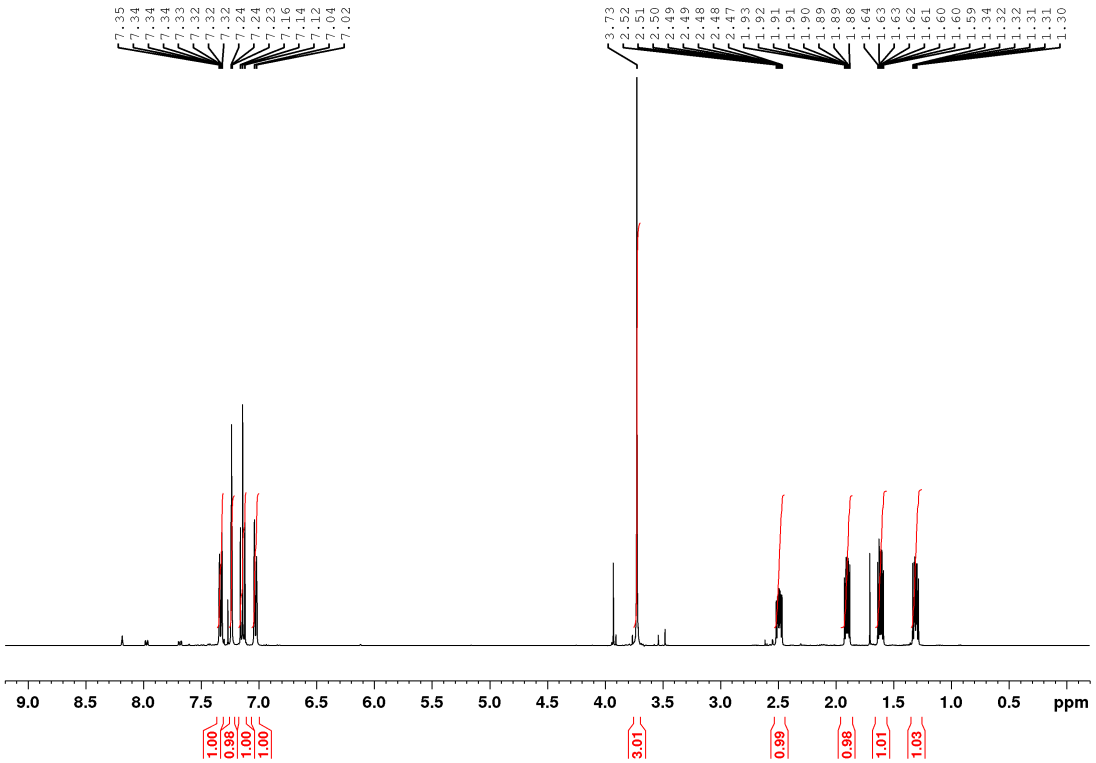

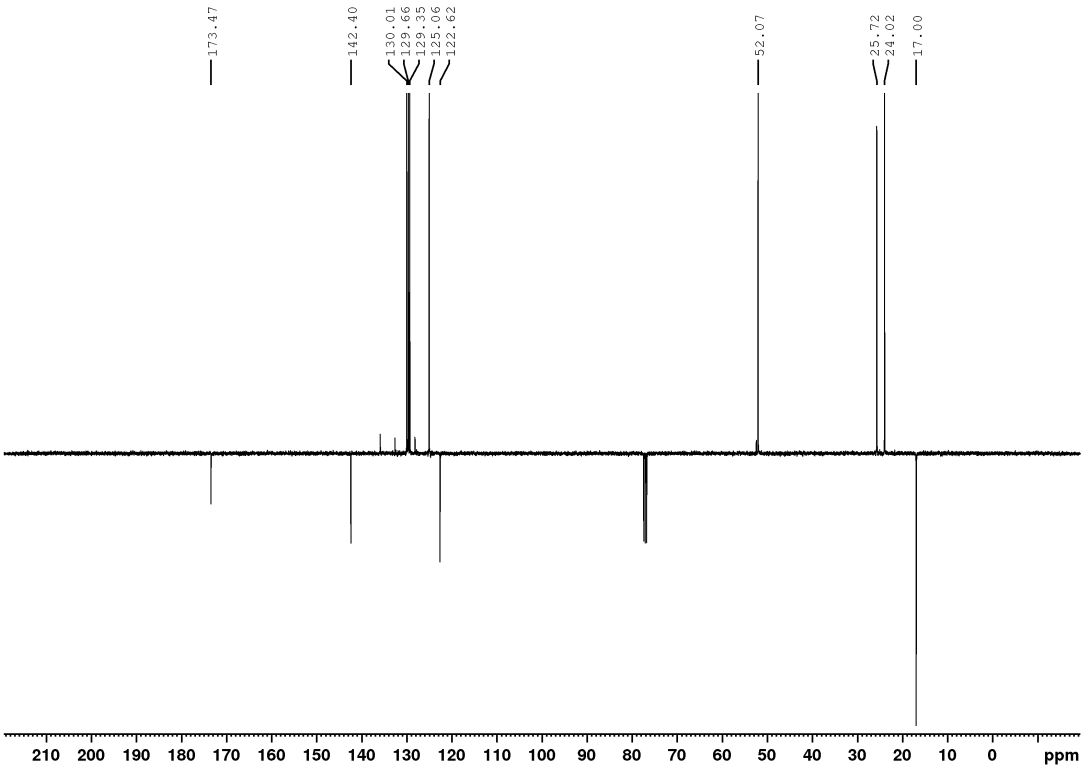

methyl 2-(4-bromophenyl)cyclopropane-1-carboxylate **(42b)**

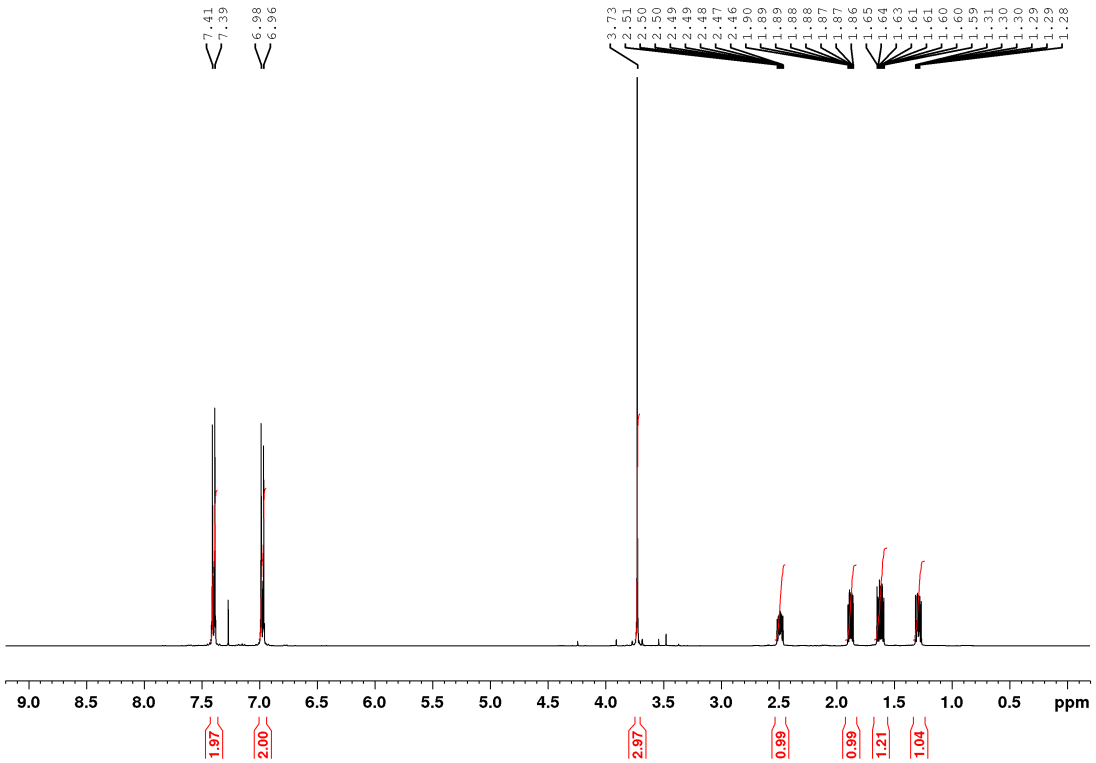

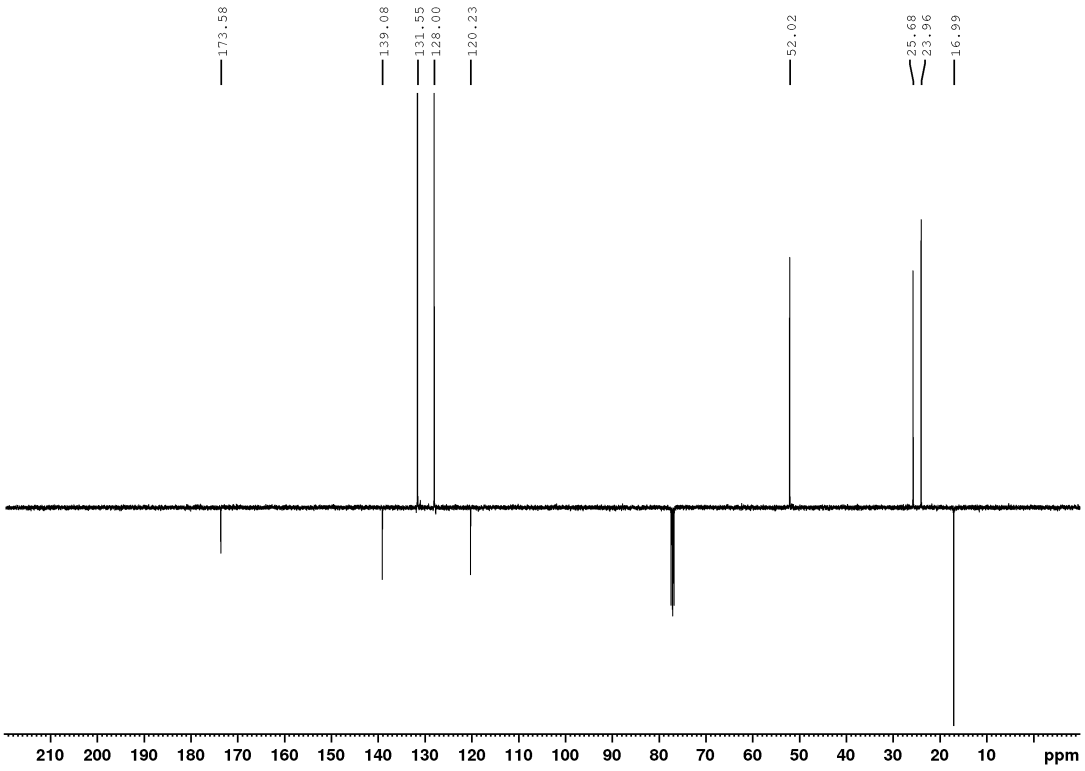

2-(3-(methoxymethoxy)phenyl)cyclopropane-1-carboxylic acid **(37a)**

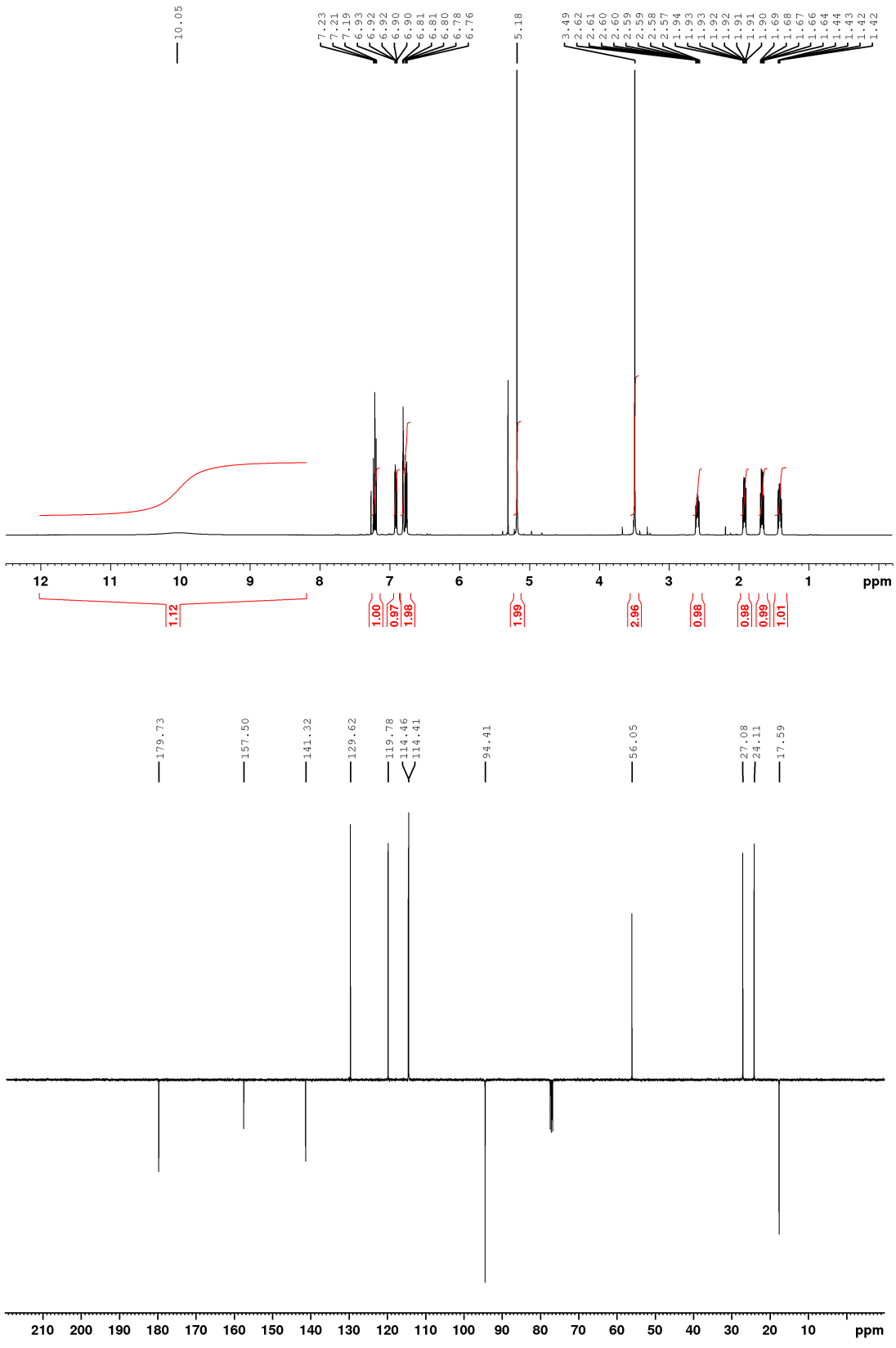

2-(4-(methoxymethoxy)phenyl)cyclopropane-1-carboxylic acid **(37b)**

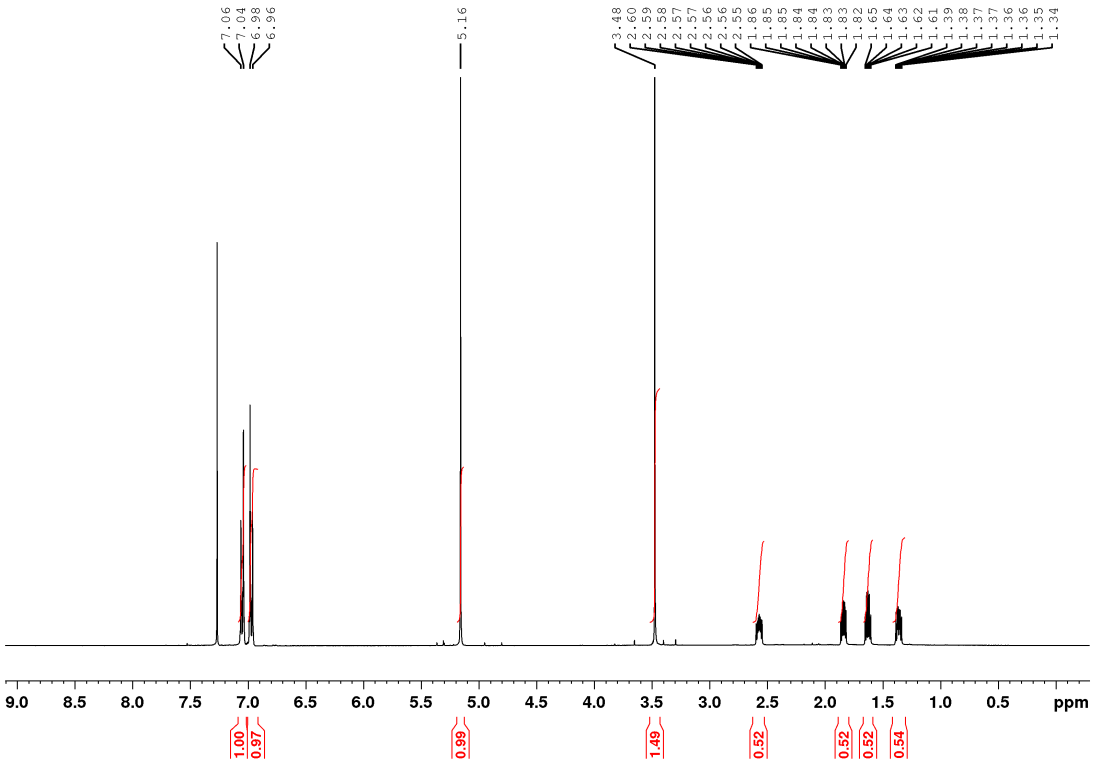

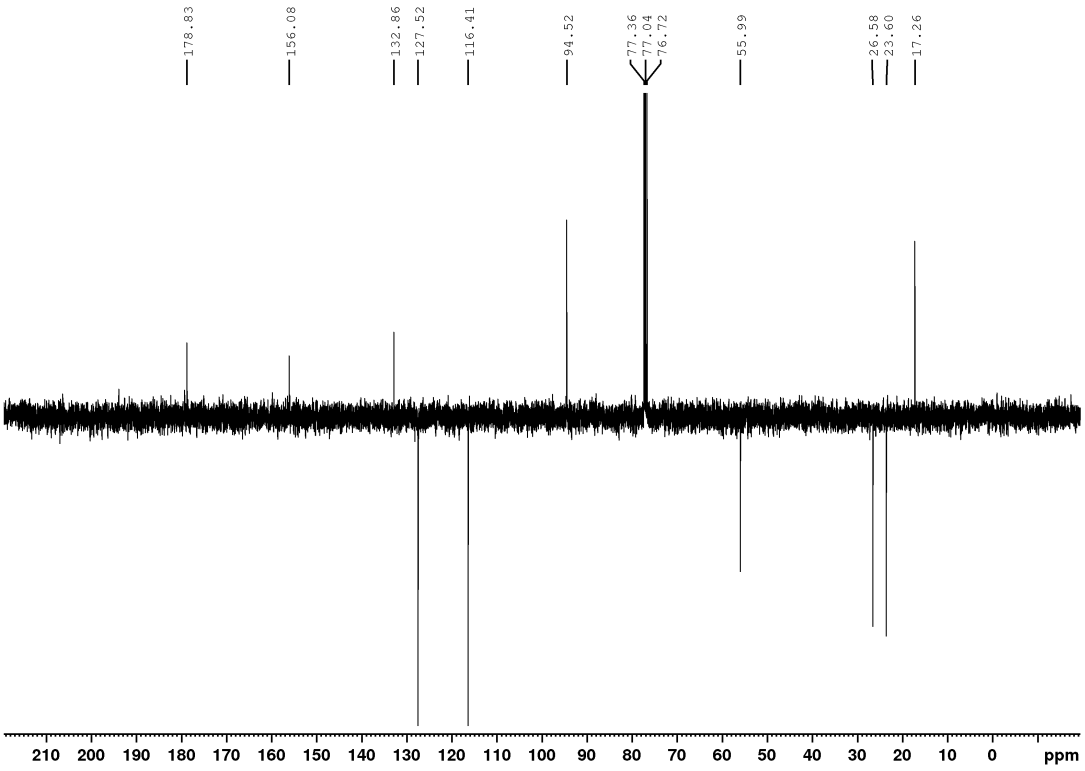

2-(3-bromophenyl)cyclopropane-1-carboxylic acid **(43a)**

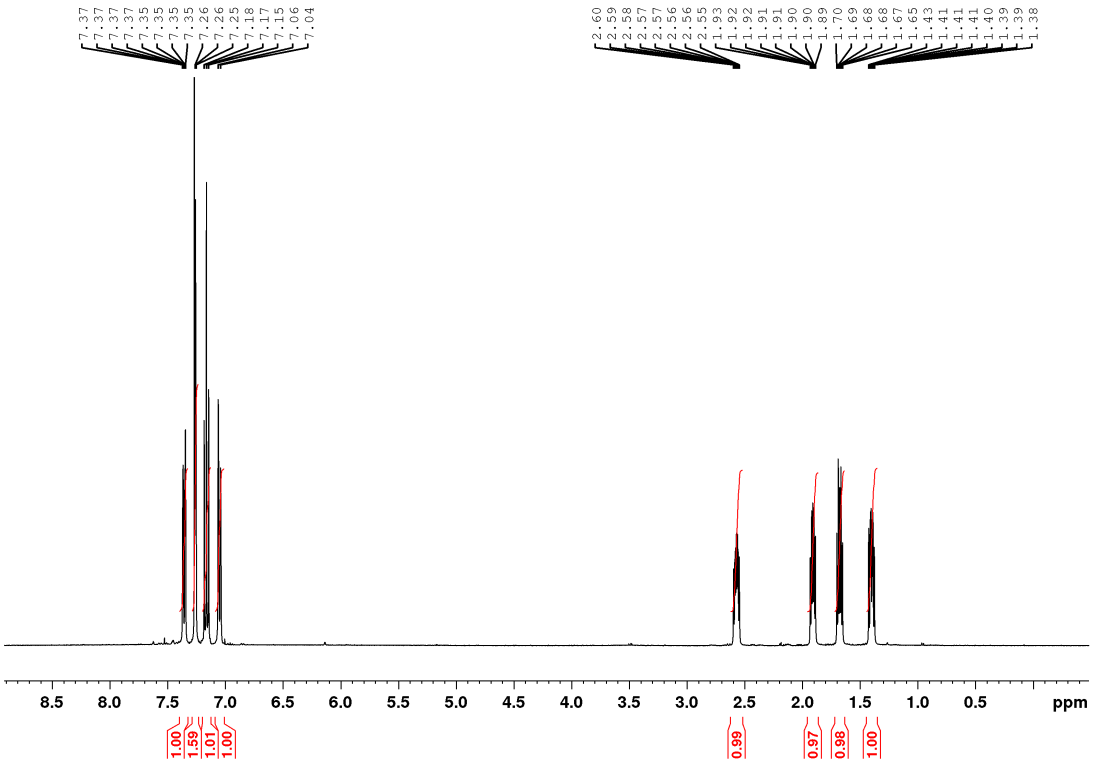

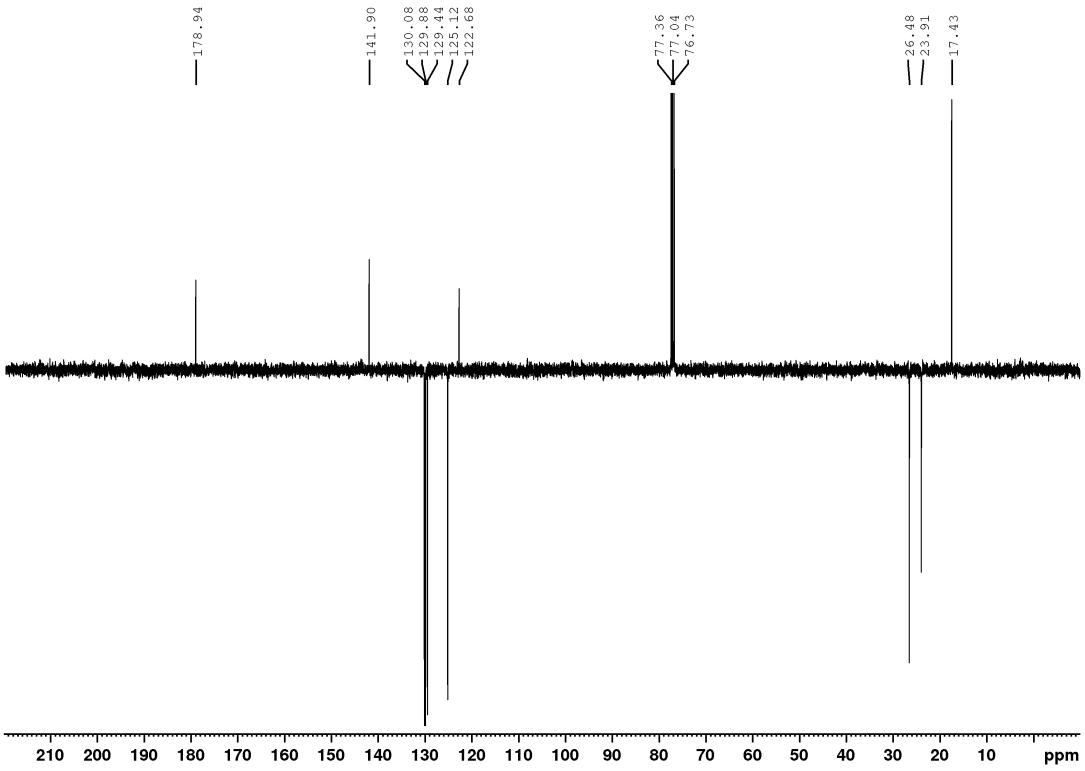

2-(4-bromophenyl)cyclopropane-1-carboxylic acid **(43b)**

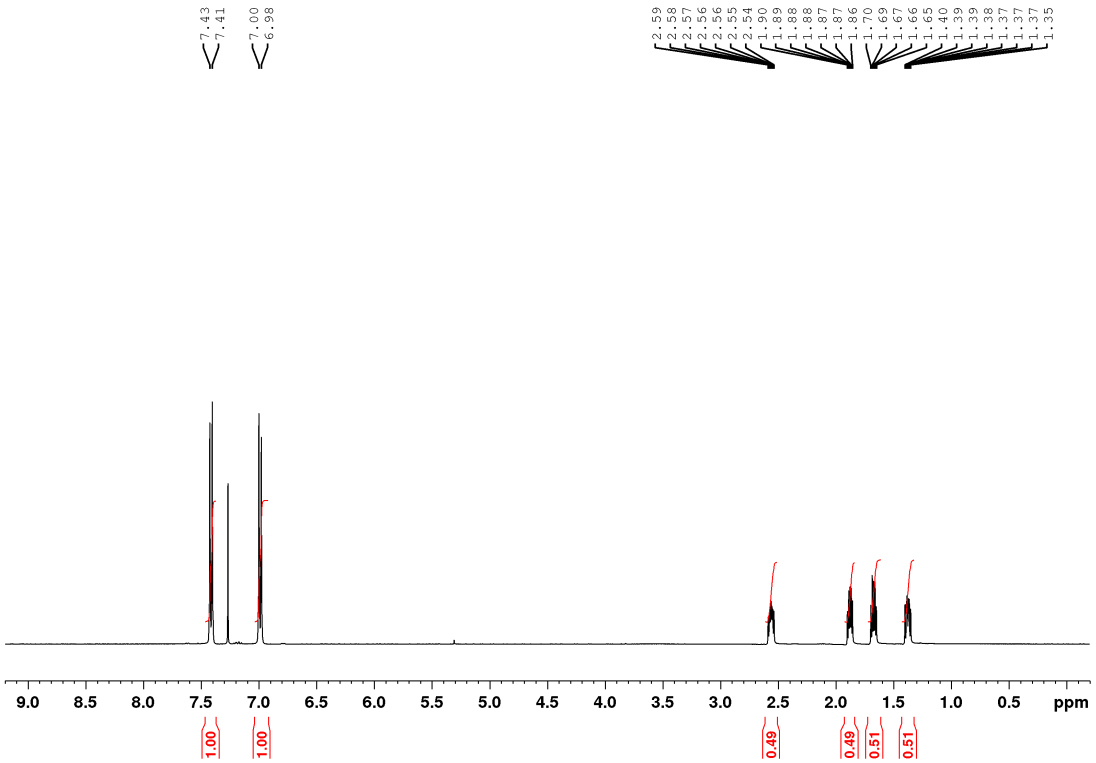

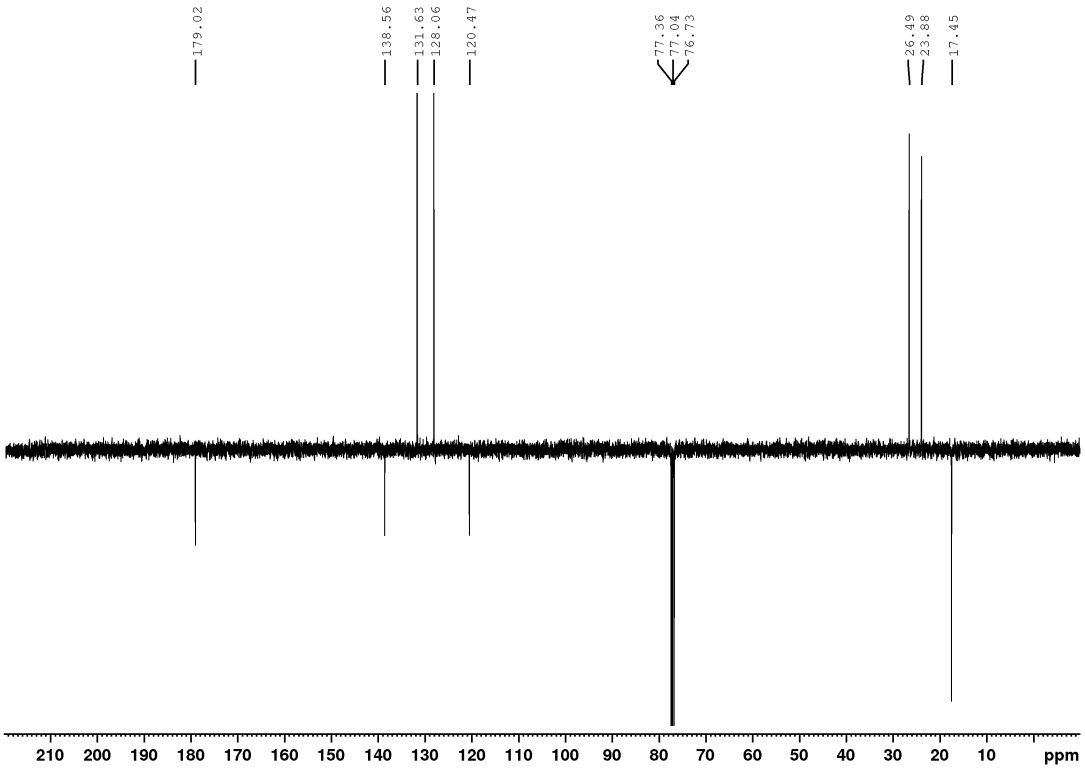

tert-butyl (2-(3-(methoxymethoxy)phenyl)cyclopropyl)carbamate **(38a)**

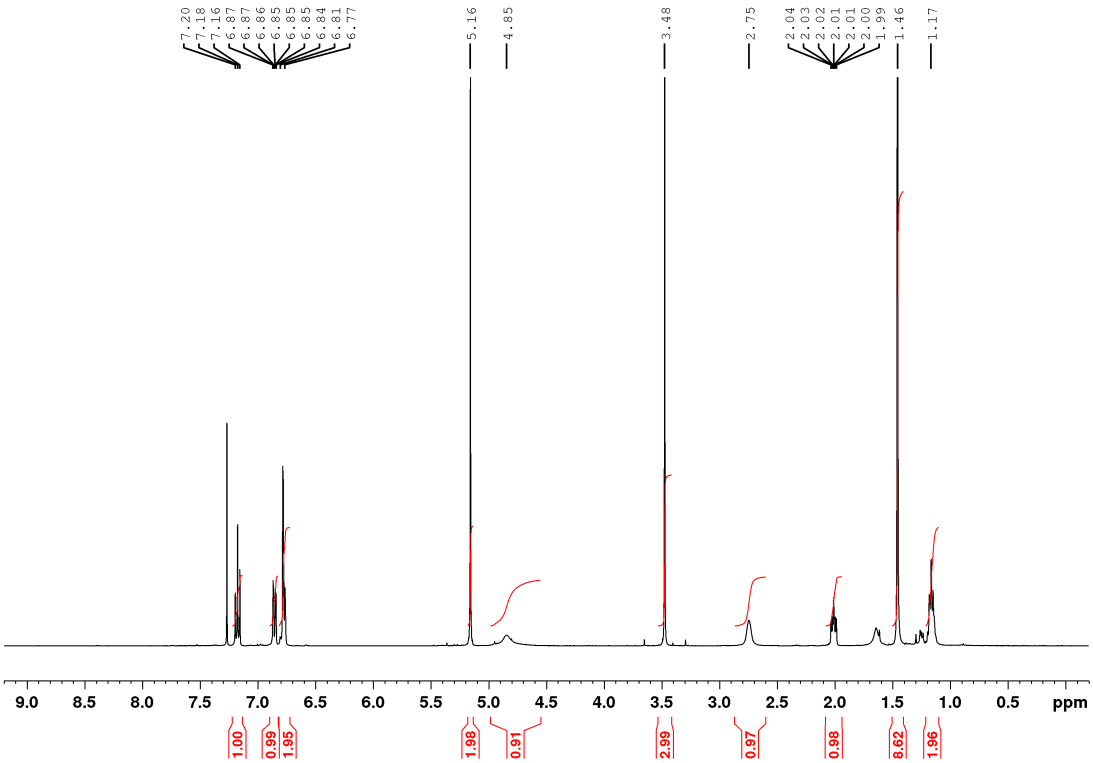

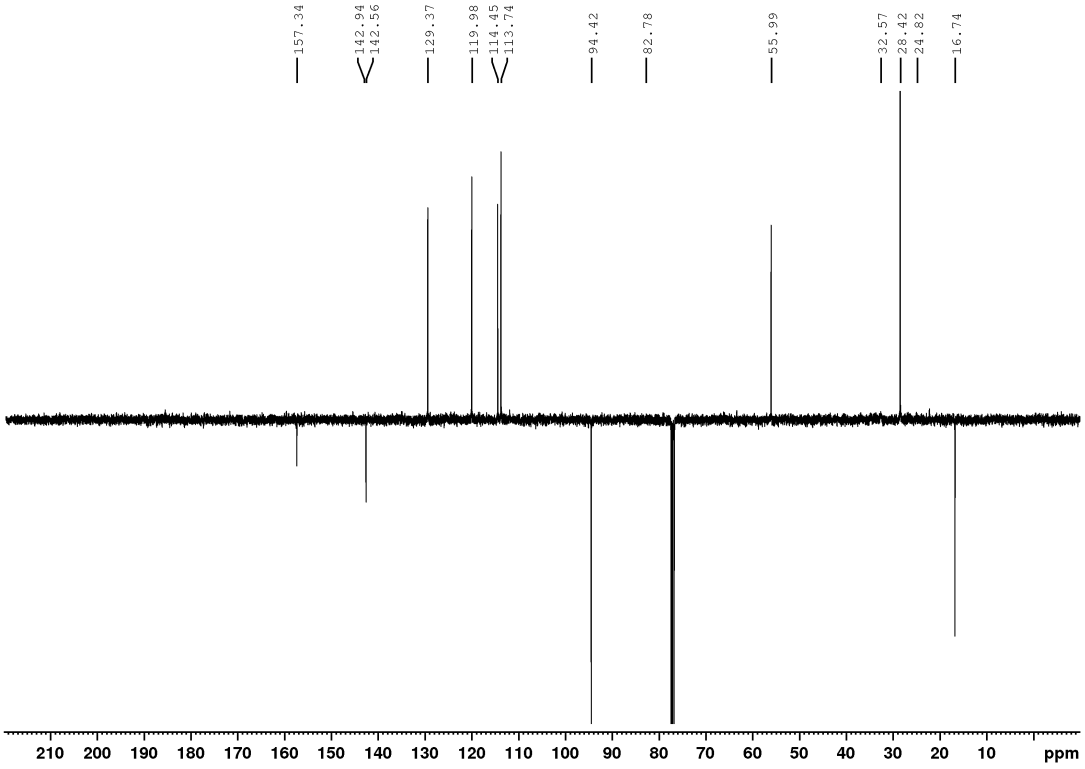

tert-butyl (2-(4-(methoxymethoxy)phenyl)cyclopropyl)carbamate **(38b)**

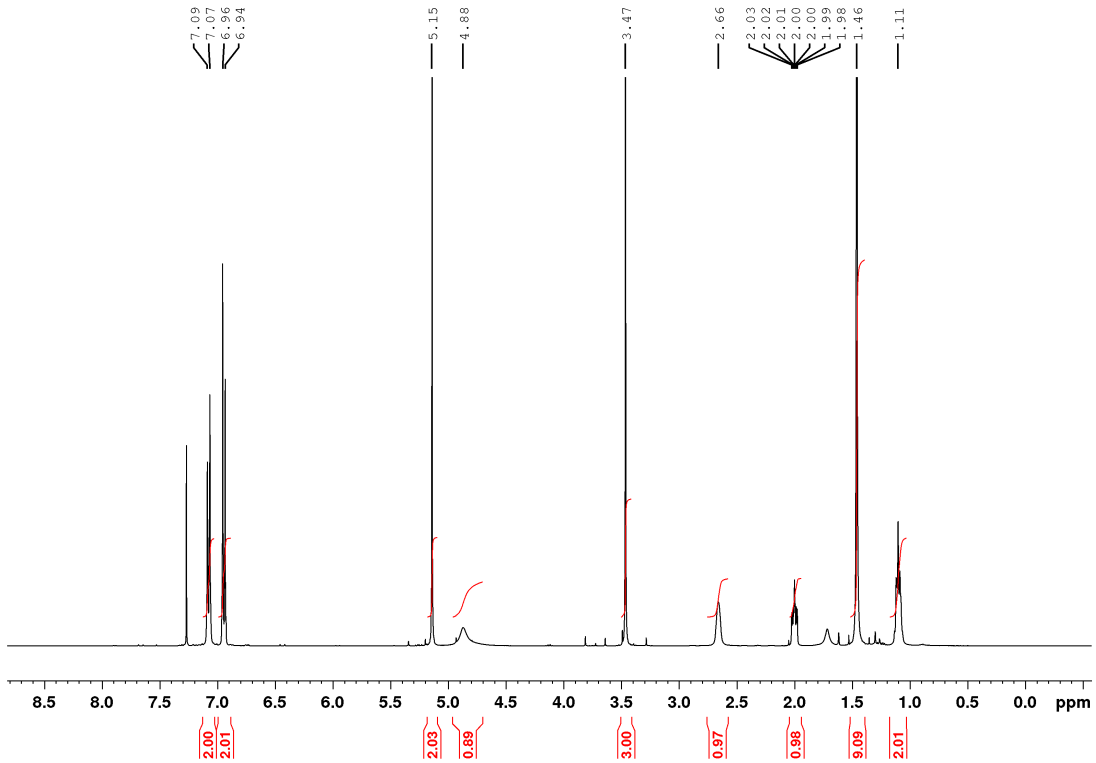

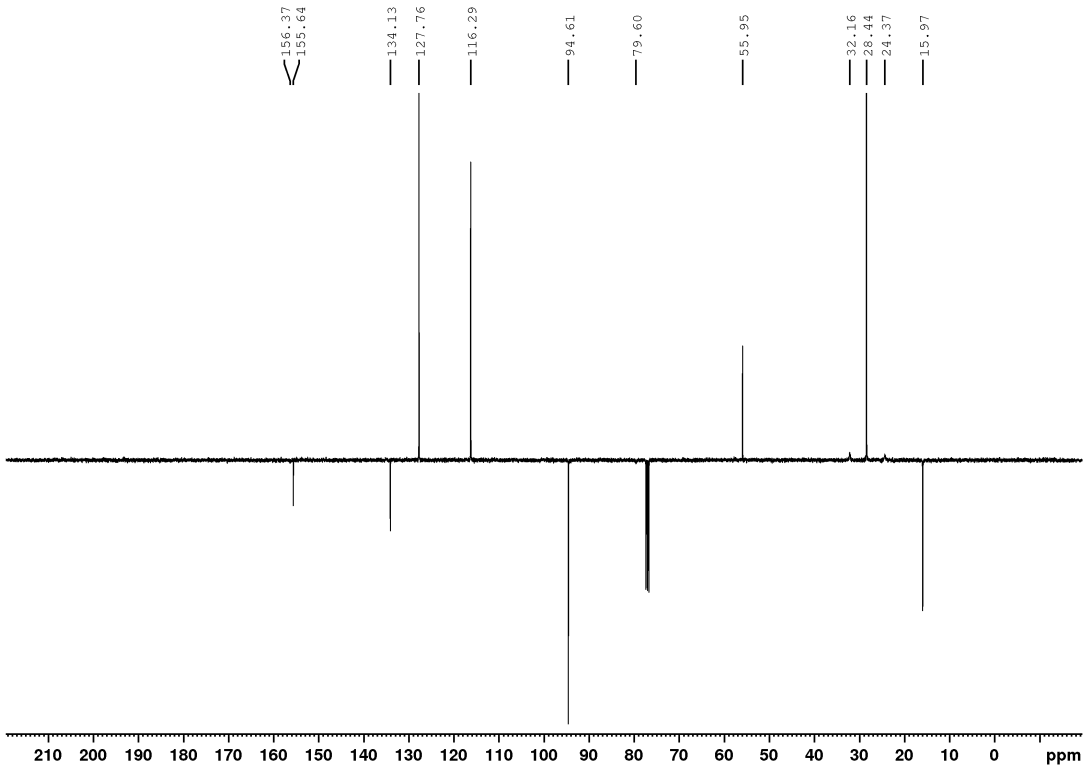

tert-butyl (2-(3-bromophenyl)cyclopropyl)carbamate **(44a)**

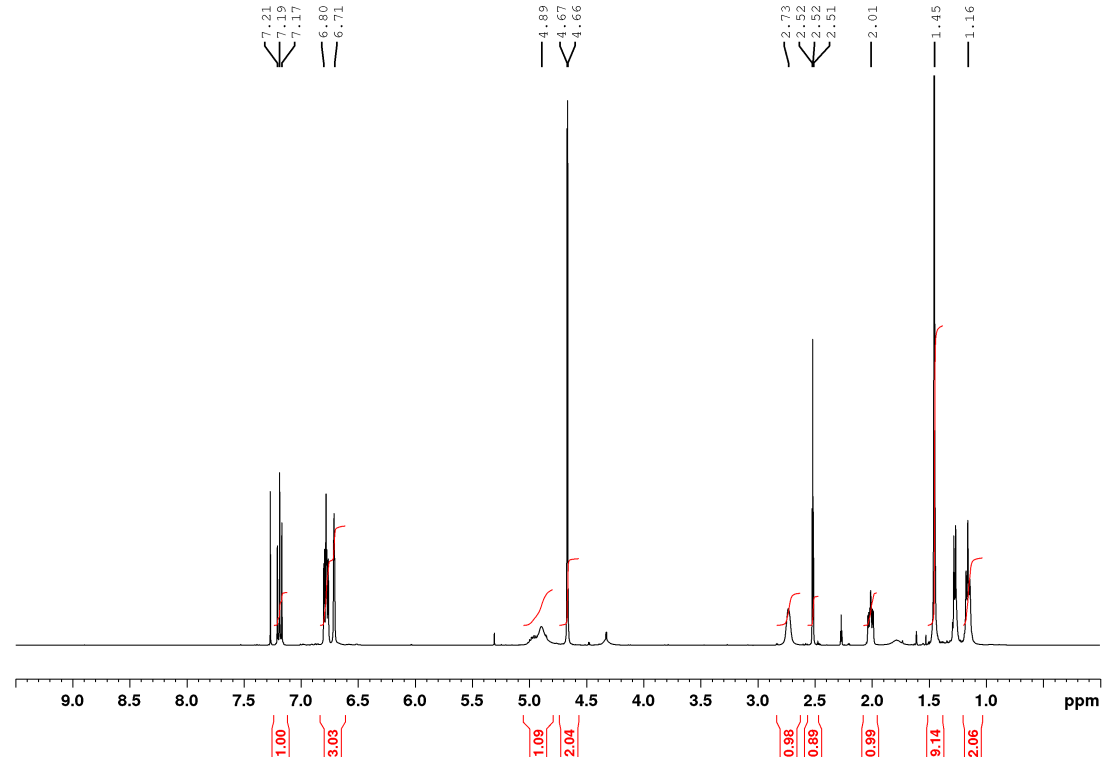

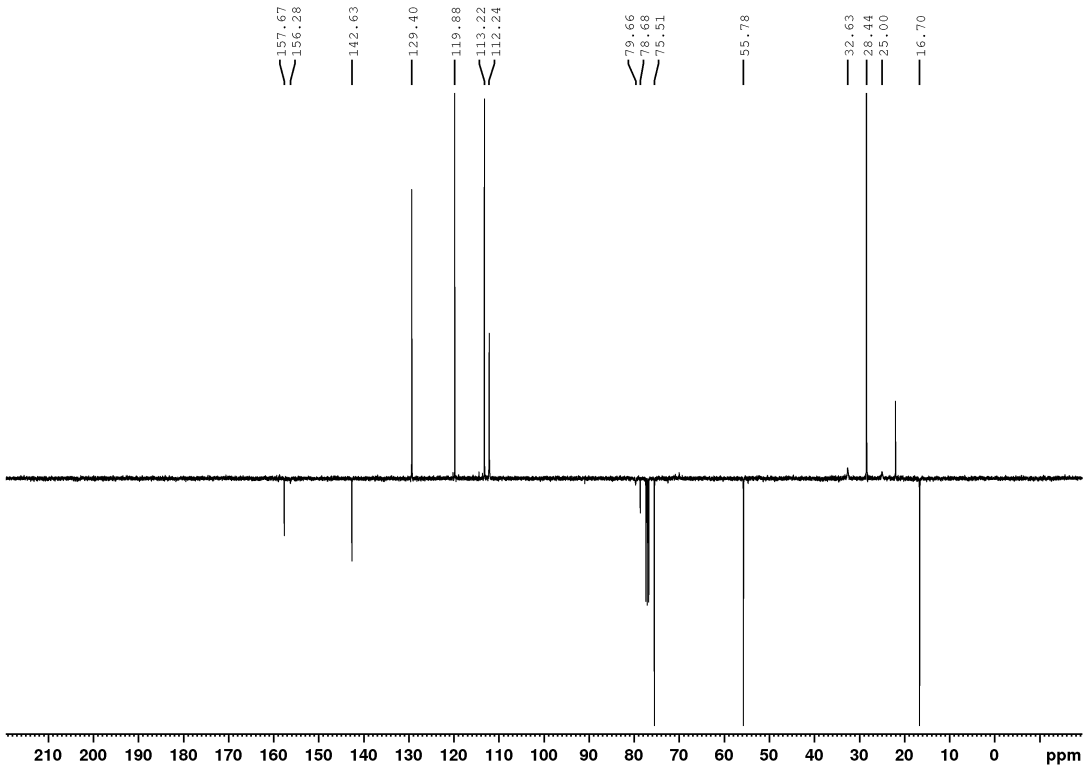

tert-butyl (2-(4-bromophenyl)cyclopropyl)carbamate **(44b)**

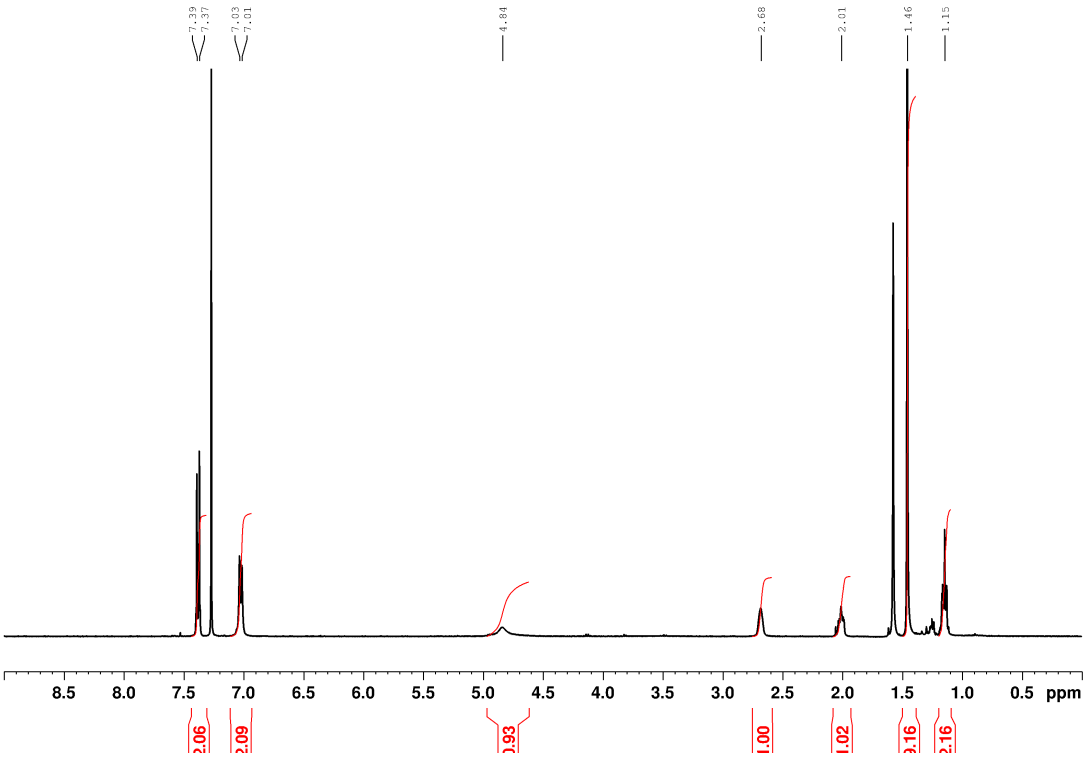

tert-butyl (2-(3-hydroxyphenyl)cyclopropyl)carbamate **(39a)**

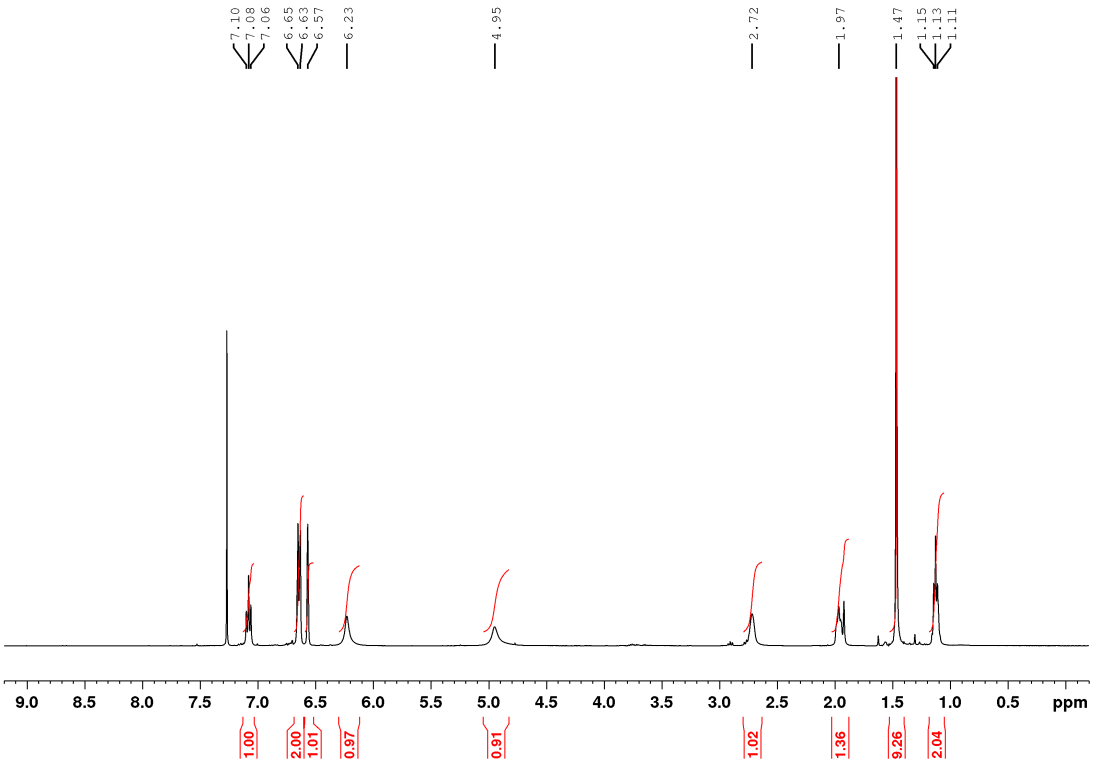

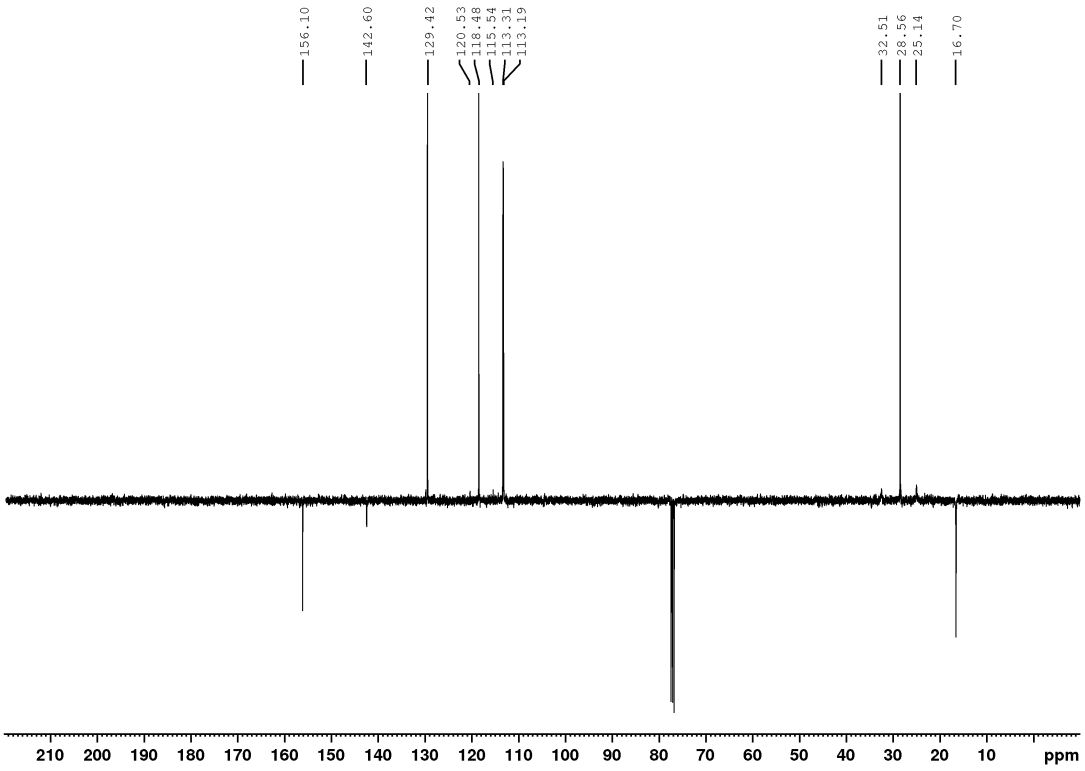

tert-butyl (2-(4-hydroxyphenyl)cyclopropyl)carbamate **(39b)**

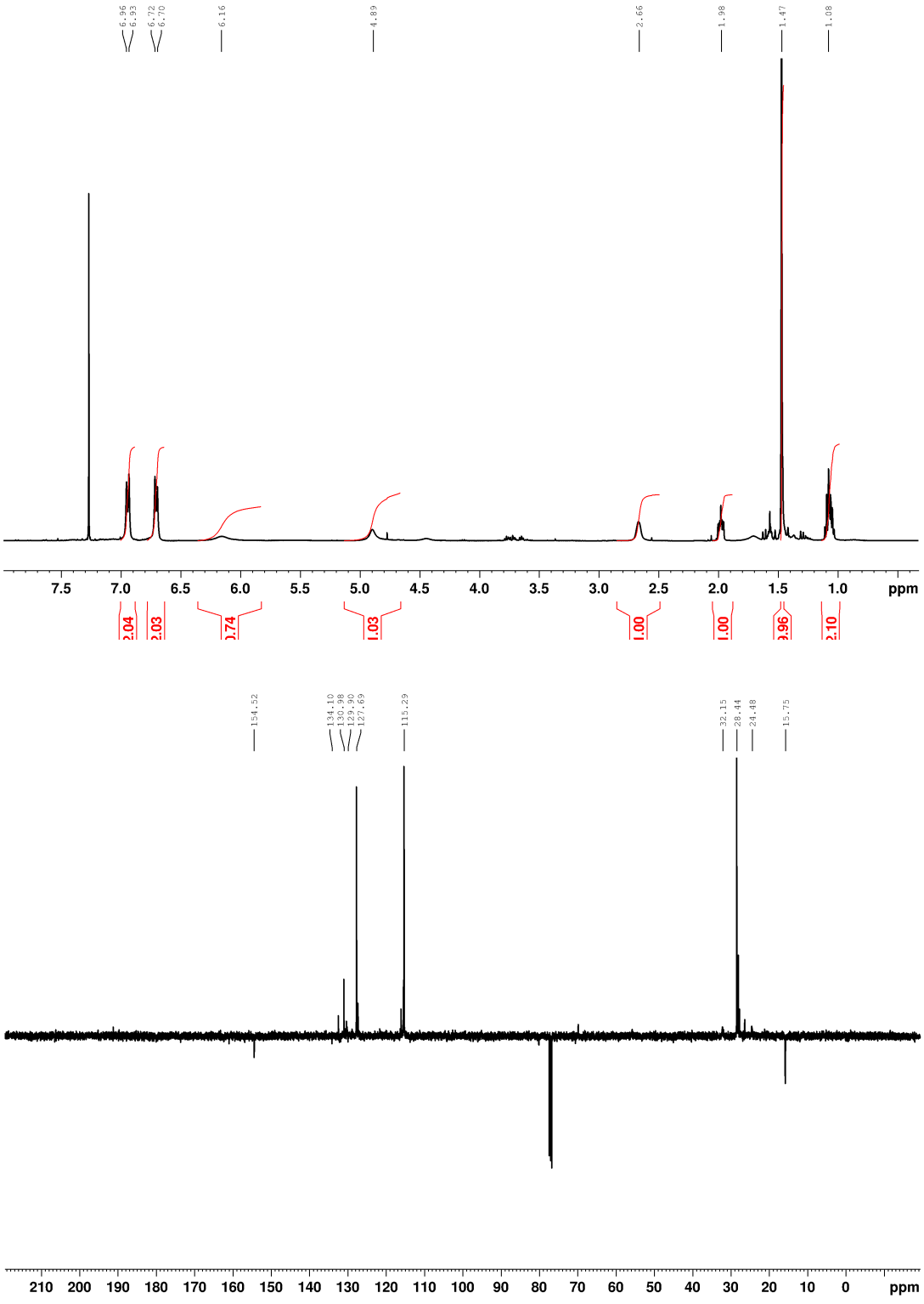

tert-butyl (2-(3-(prop-2-yn-1-yloxy)phenyl)cyclopropyl)carbamate **(45a)**

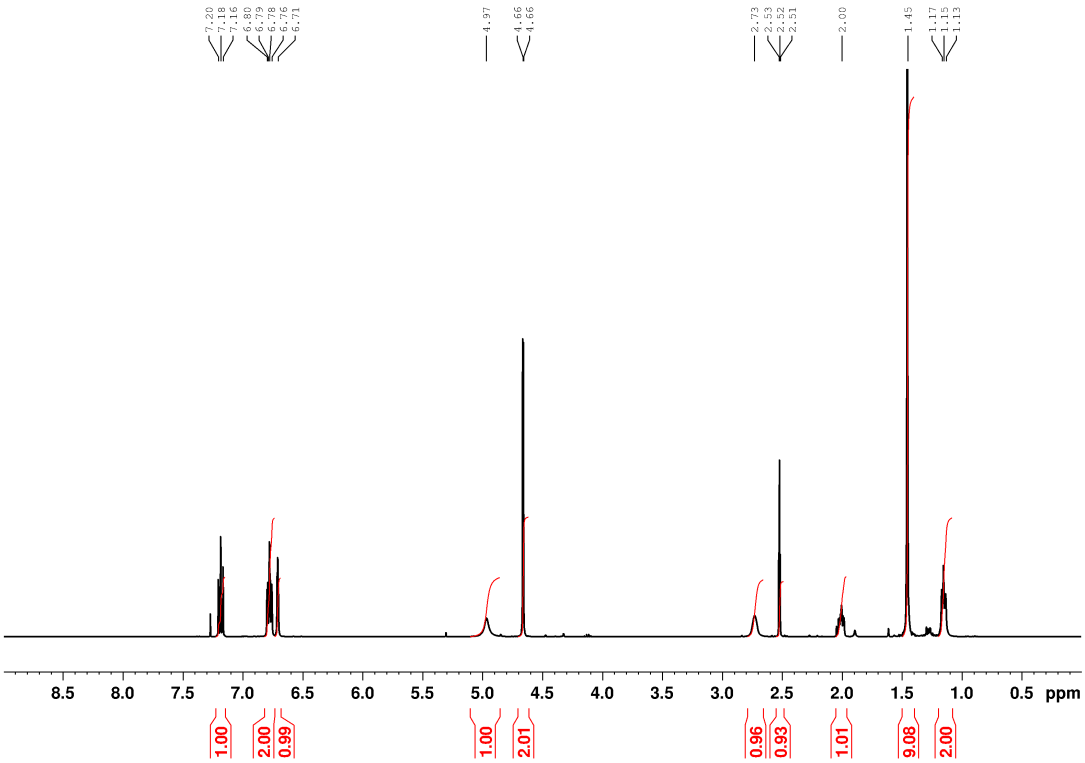

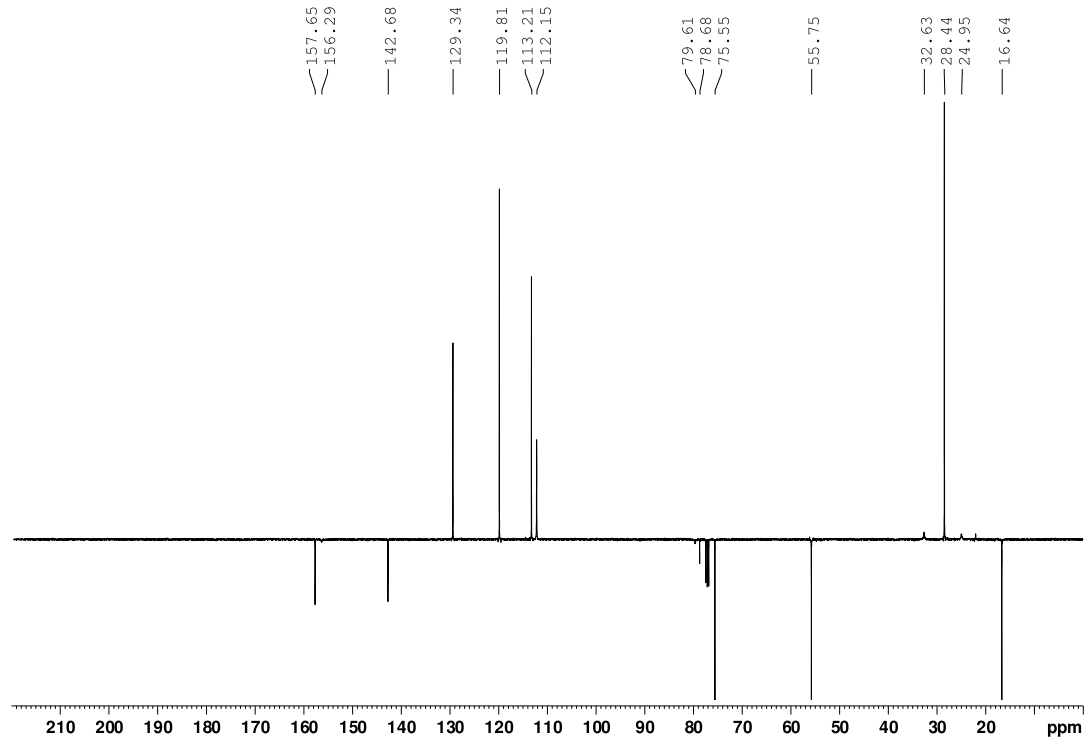

tert-butyl (2-(4-(prop-2-yn-1-yloxy)phenyl)cyclopropyl)carbamate **(45b)**

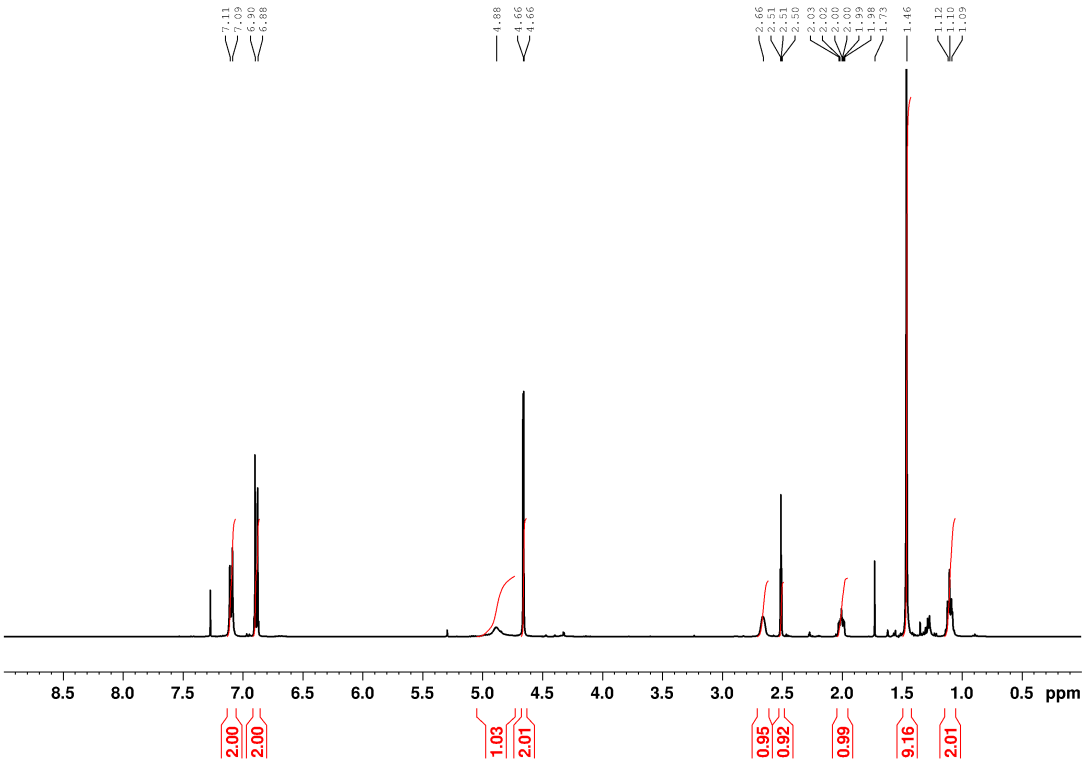

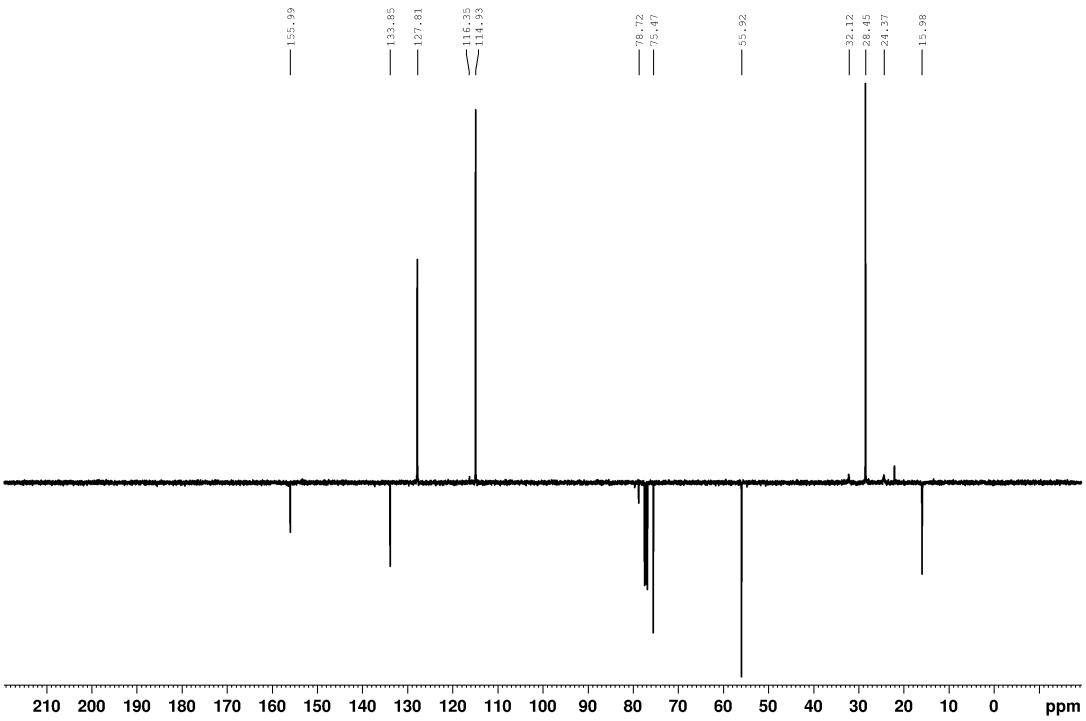

2-(3-(prop-2-yn-1-yloxy)phenyl)cyclopropan-1-amine **(probe 1)**

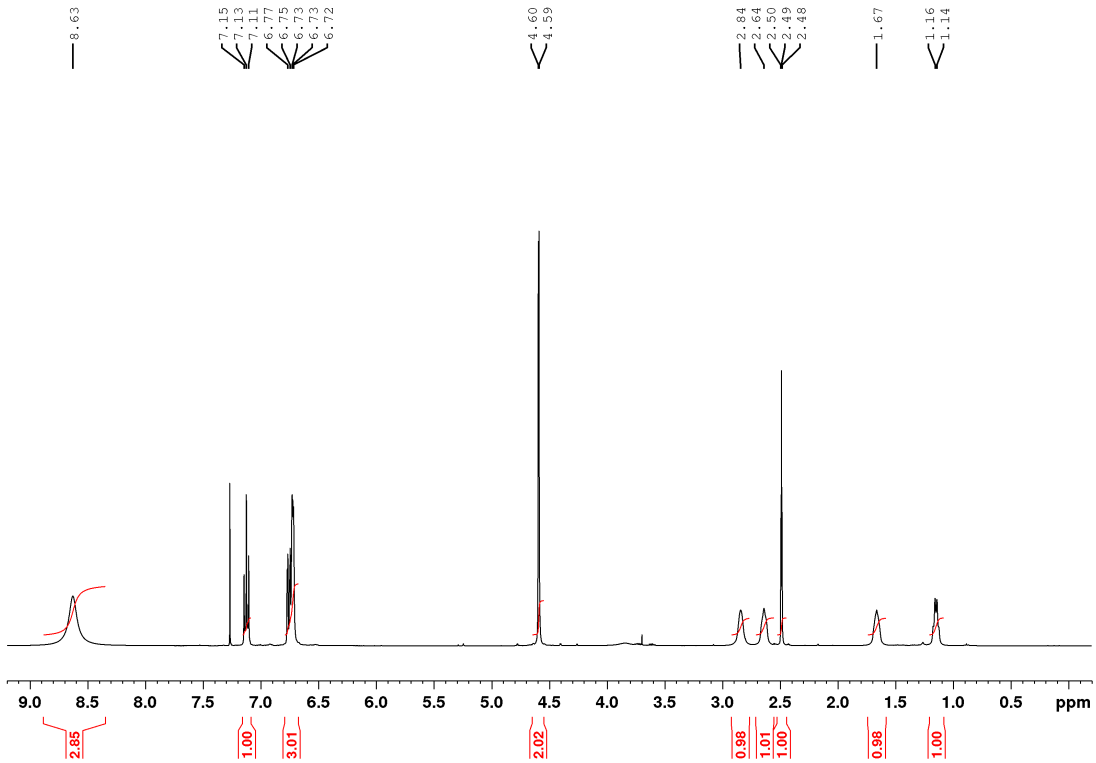

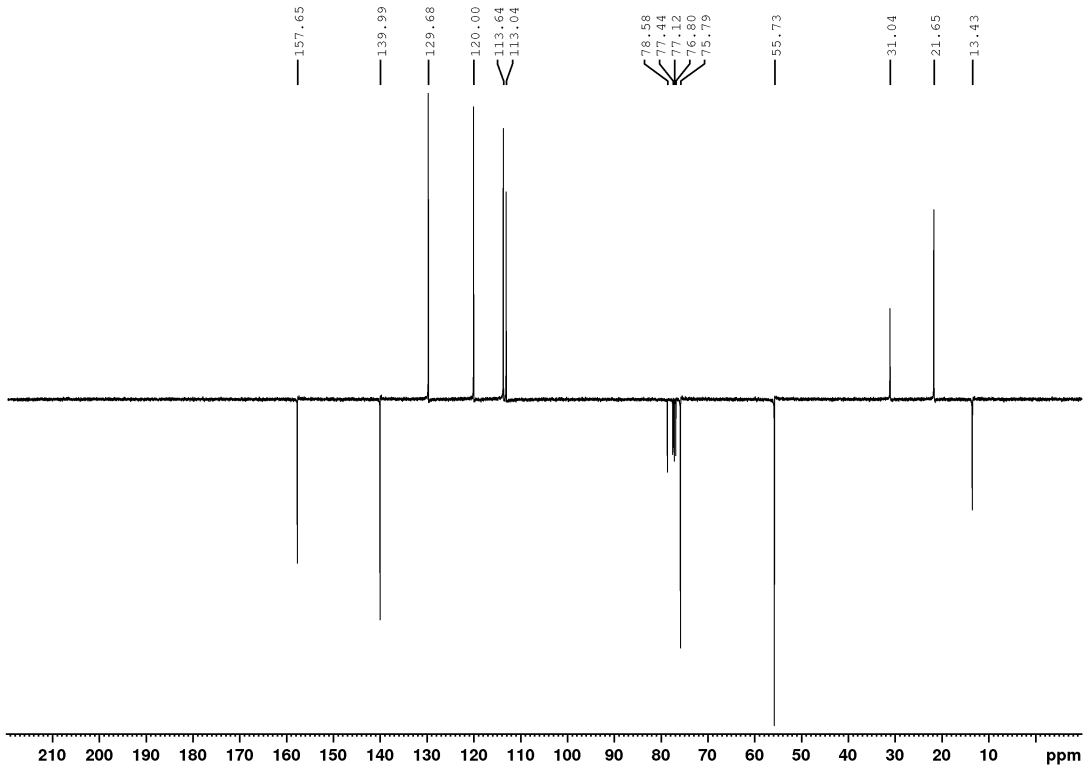

2-(4-(prop-2-yn-1-yloxy)phenyl)cyclopropan-1-amine **(probe 2)**

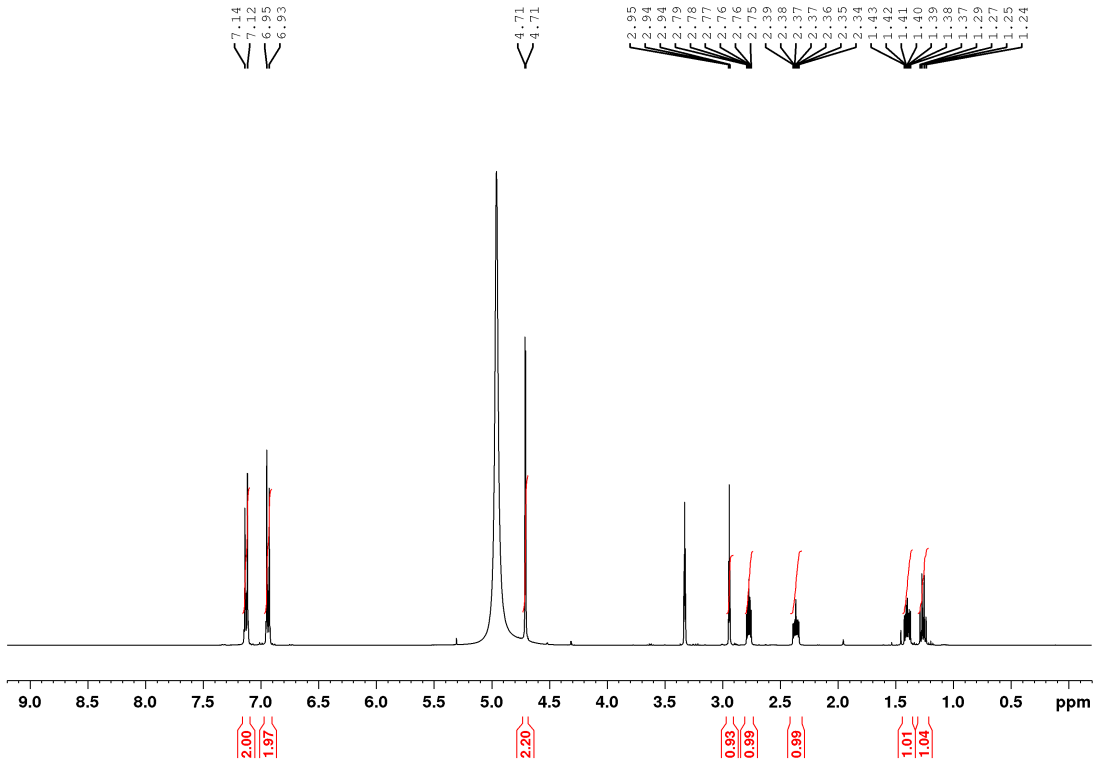

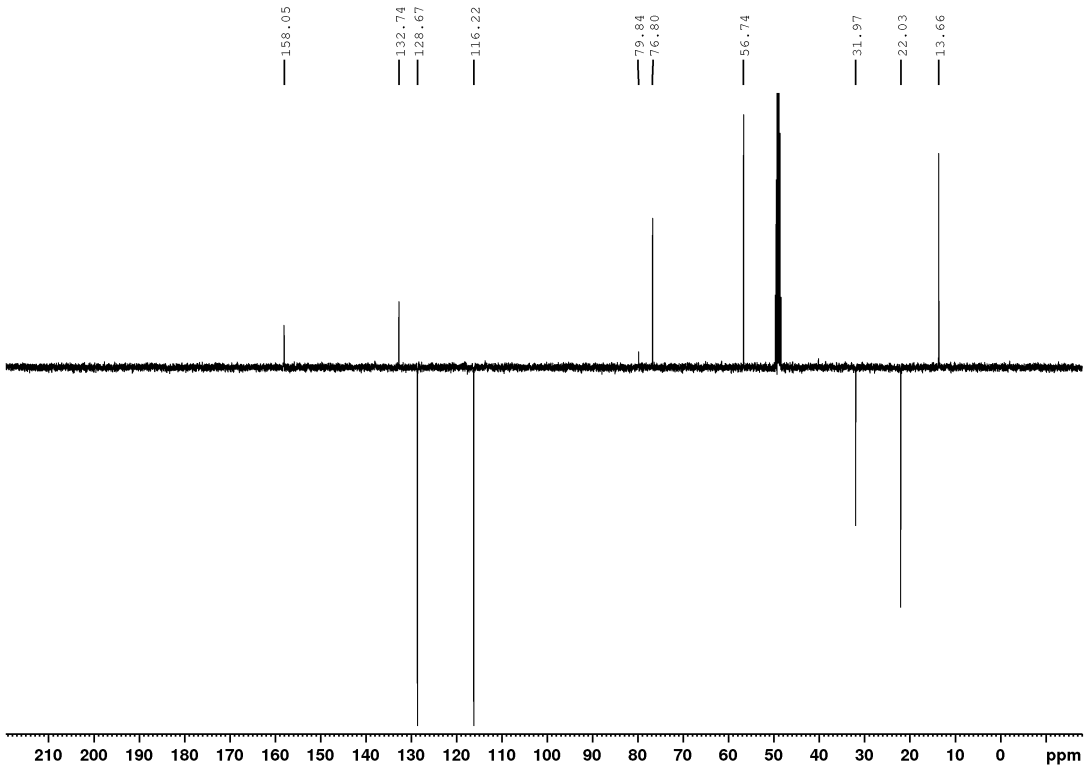

tert-butyl (2-(3-(3-bromopropoxy)phenyl)cyclopropyl)carbamate **(46a)**

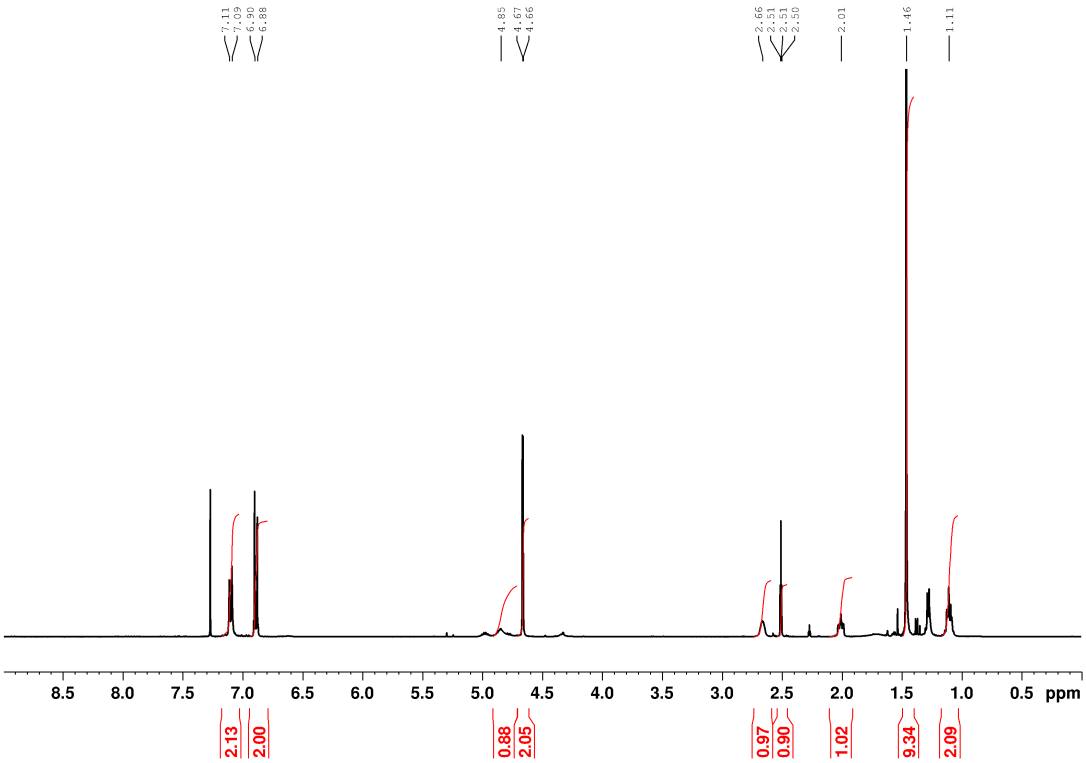

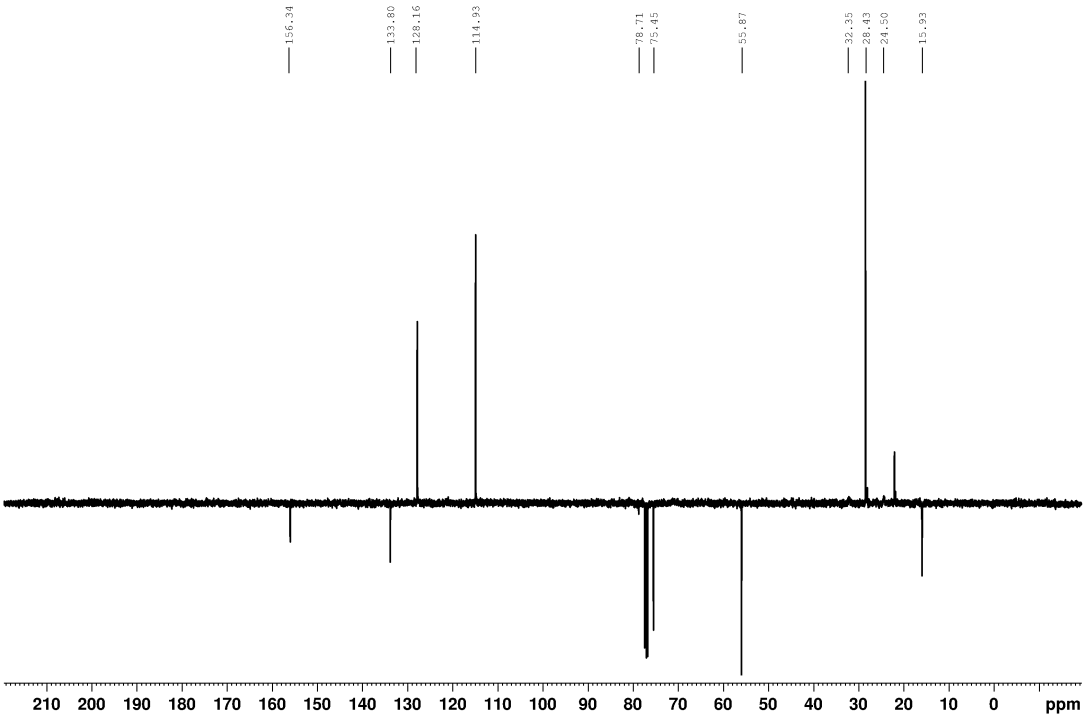

tert-butyl (2-(4-(3-bromopropoxy)phenyl)cyclopropyl)carbamate **(46b)**

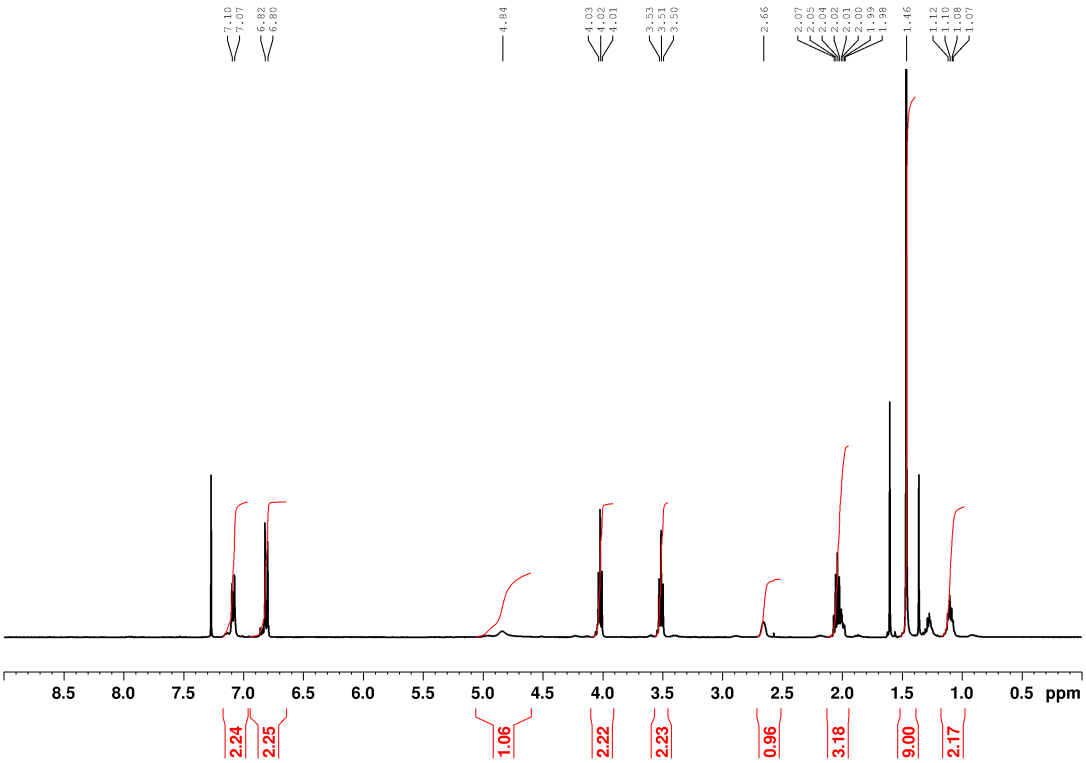

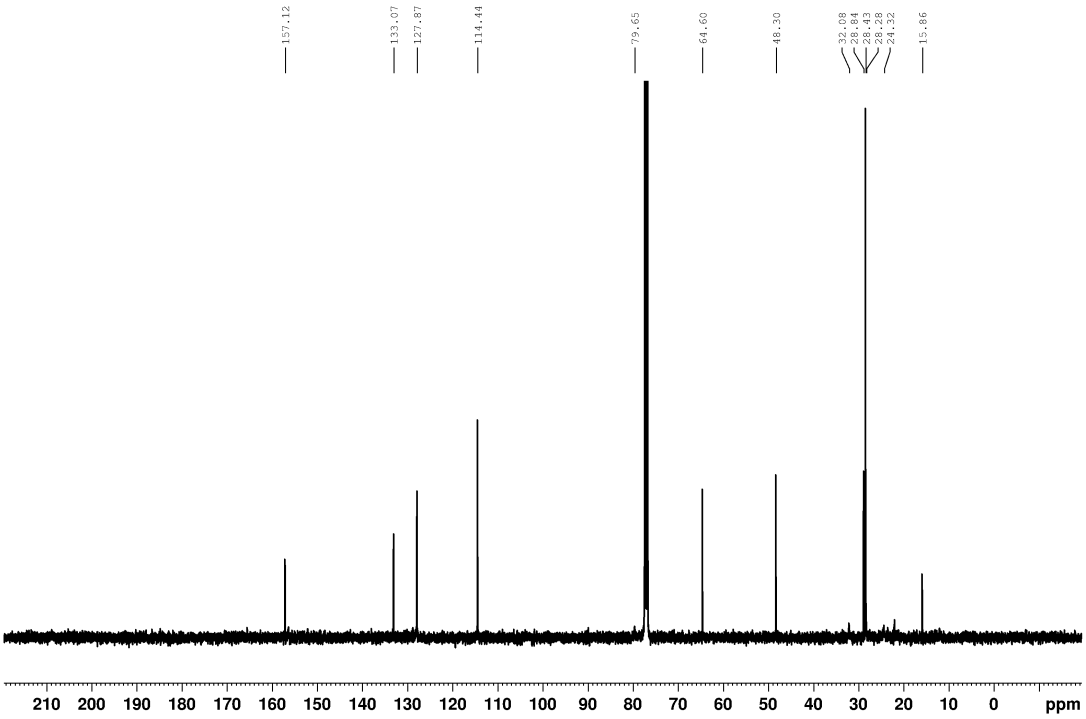

tert-butyl (2-(3-(3-azidopropoxy)phenyl)cyclopropyl)carbamate **(47a)**

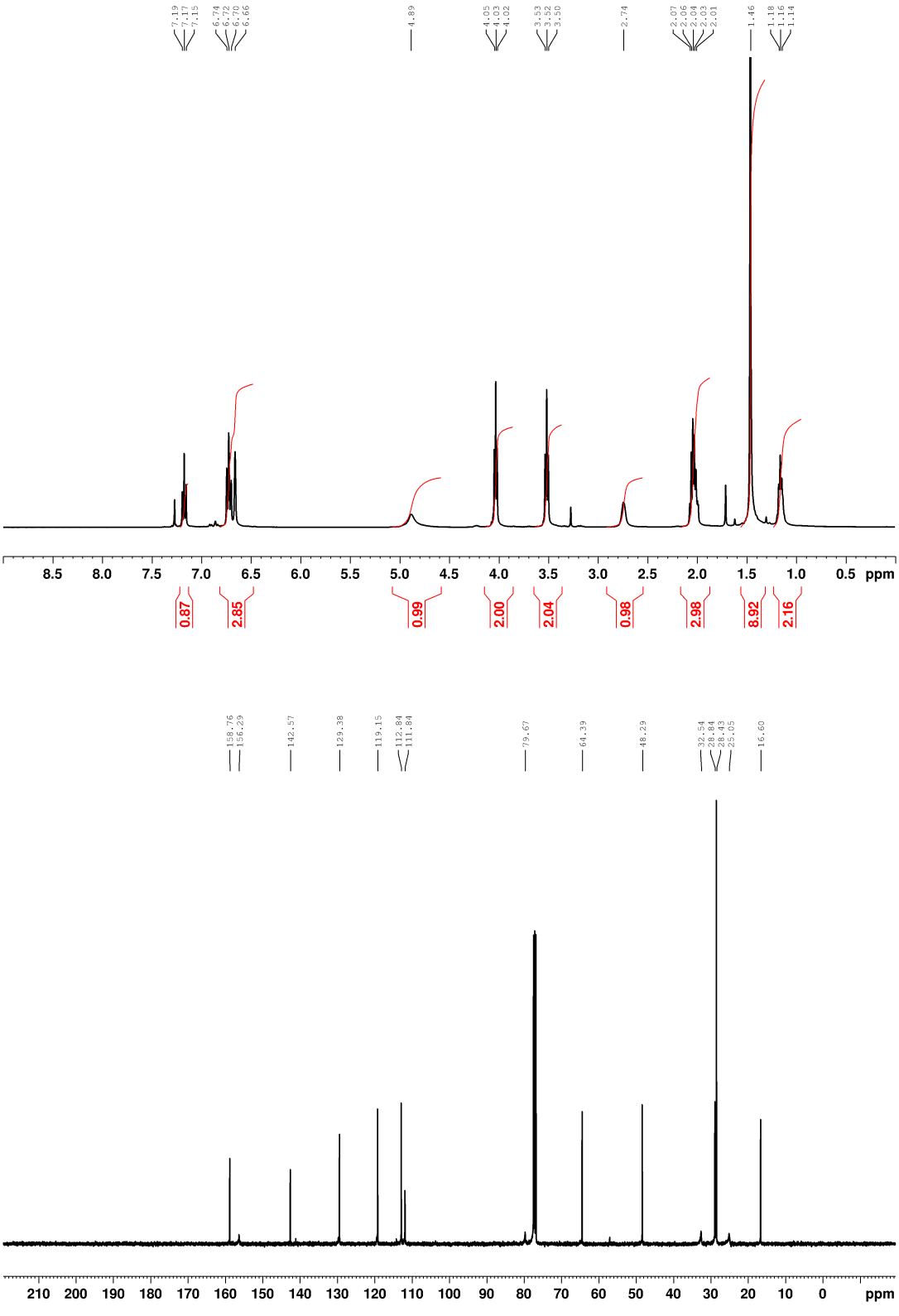

tert-butyl (2-(4-(3-azidopropoxy)phenyl)cyclopropyl)carbamate **(47b)**

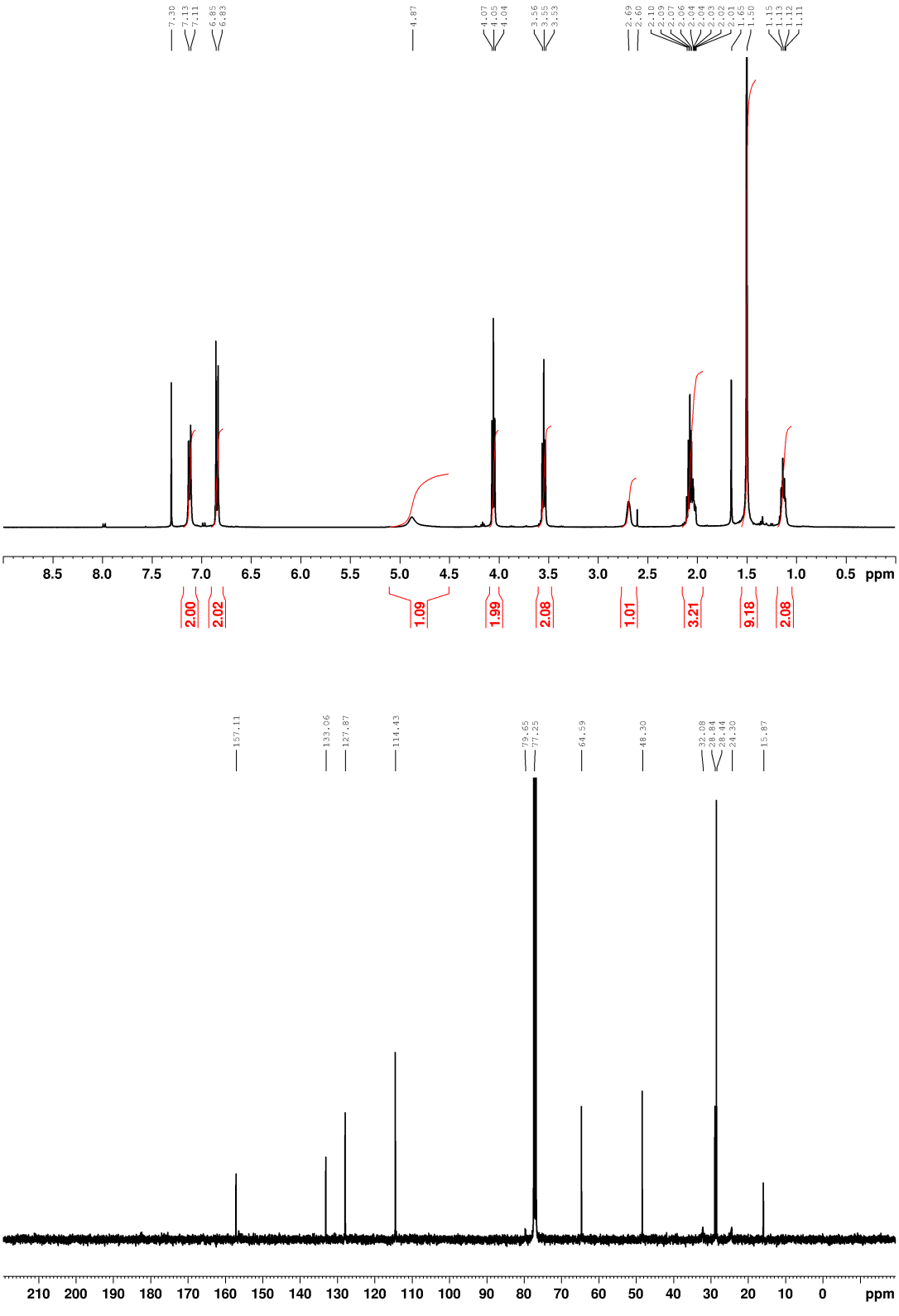

2-(3-(3-azidopropoxy)phenyl)cyclopropan-1-amine **(probe 3)**

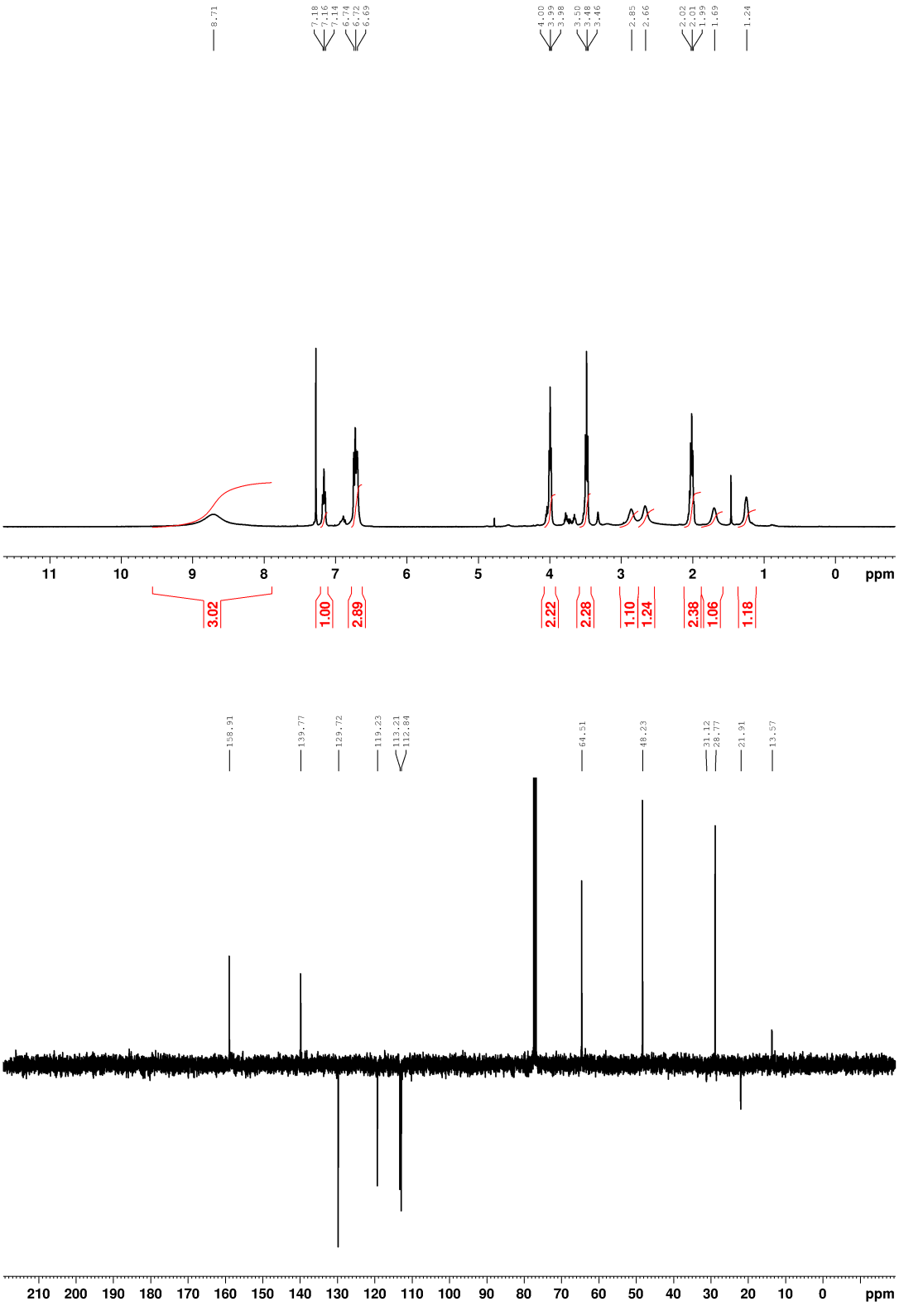

2-(4-(3-azidopropoxy)phenyl)cyclopropan-1-amine **(probe 4)**

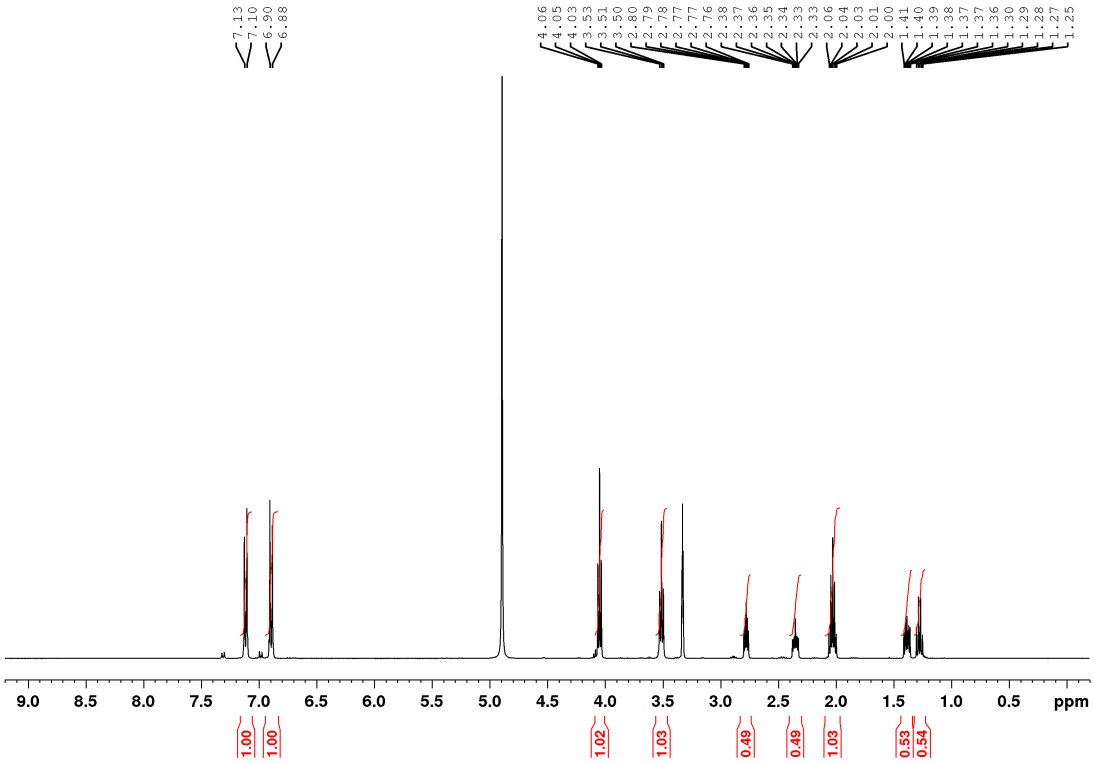

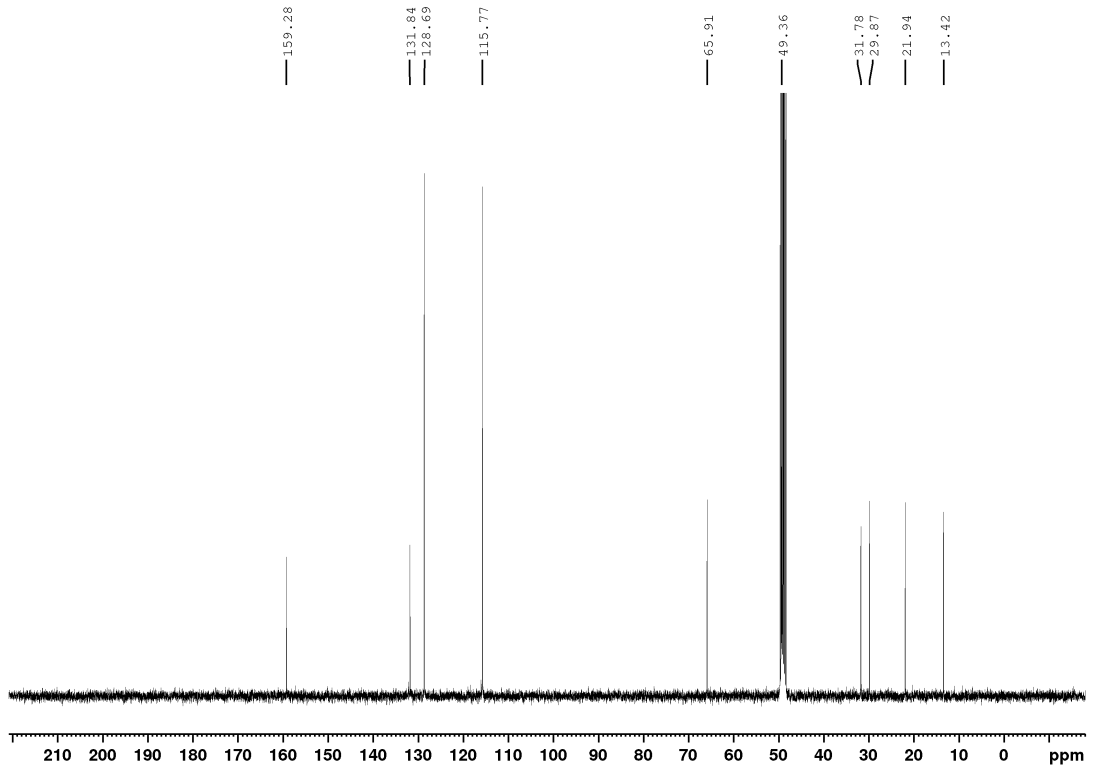

tert-butyl (2-(3'-(hydroxymethyl)-[1,1'-biphenyl]-3-yl)cyclopropyl)carbamate **(48a)**

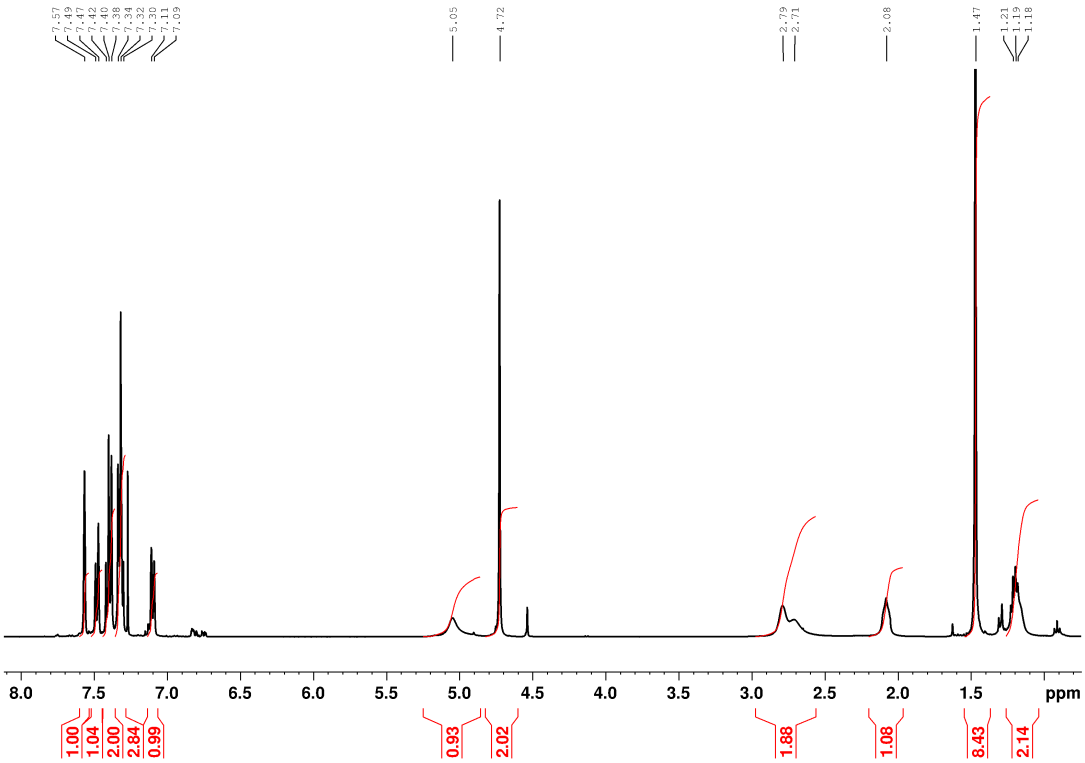

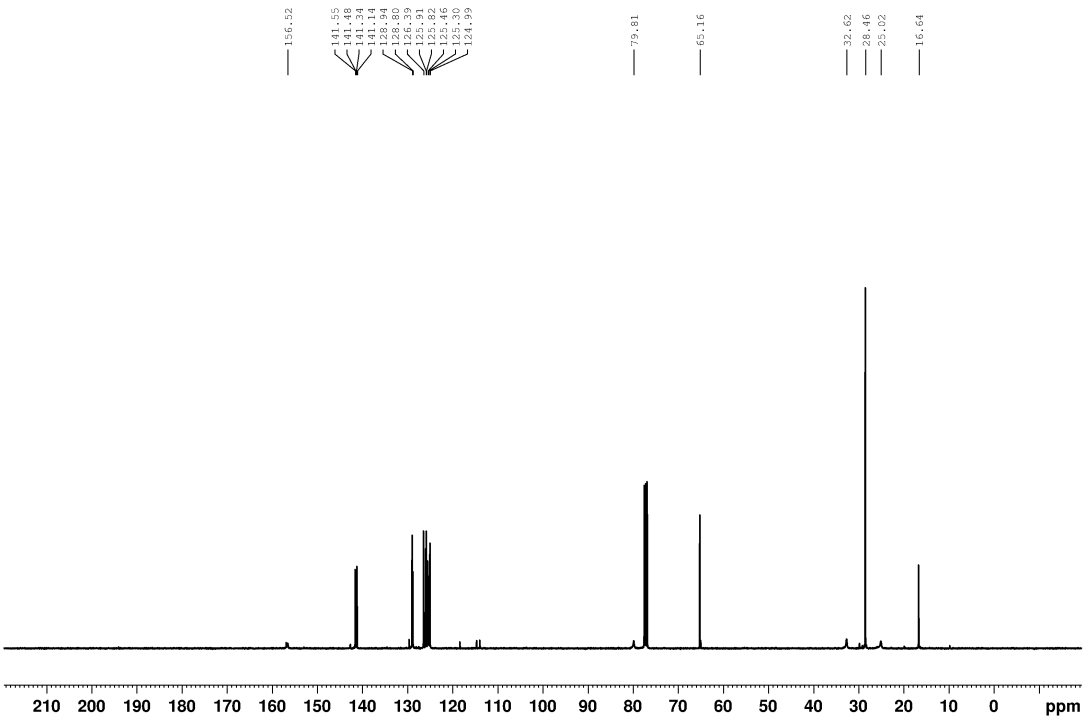

tert-butyl (2-(4'-(hydroxymethyl)-[1,1'-biphenyl]-3-yl)cyclopropyl)carbamate **(48b)**

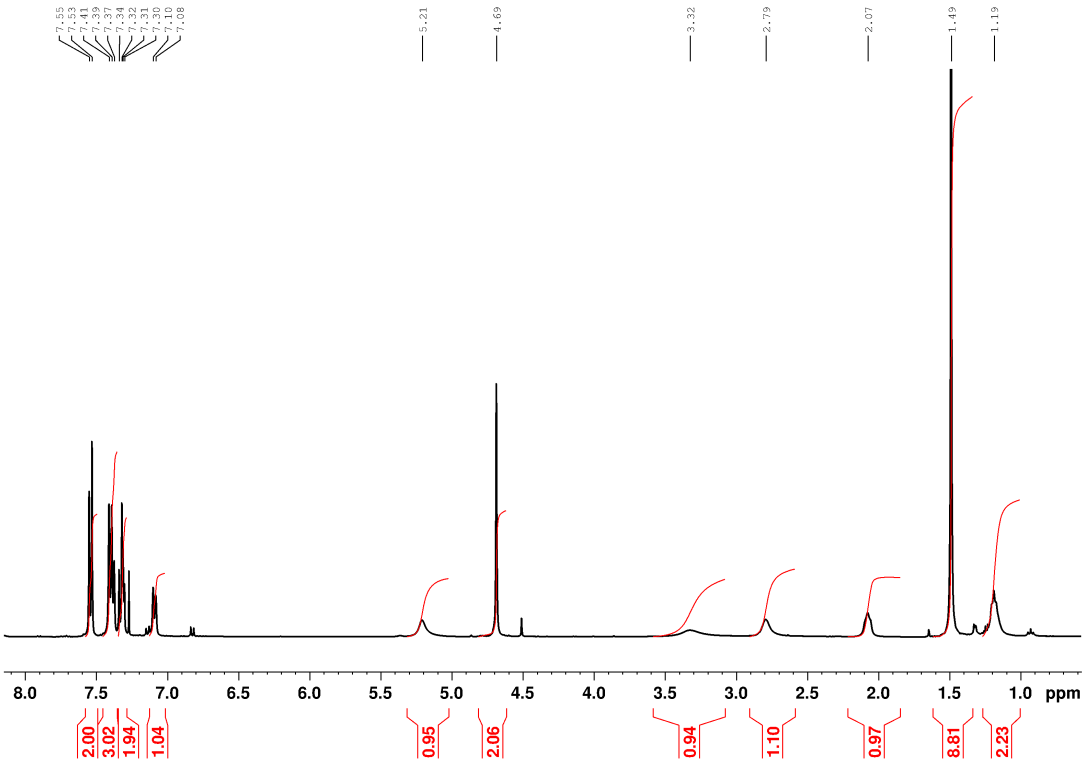

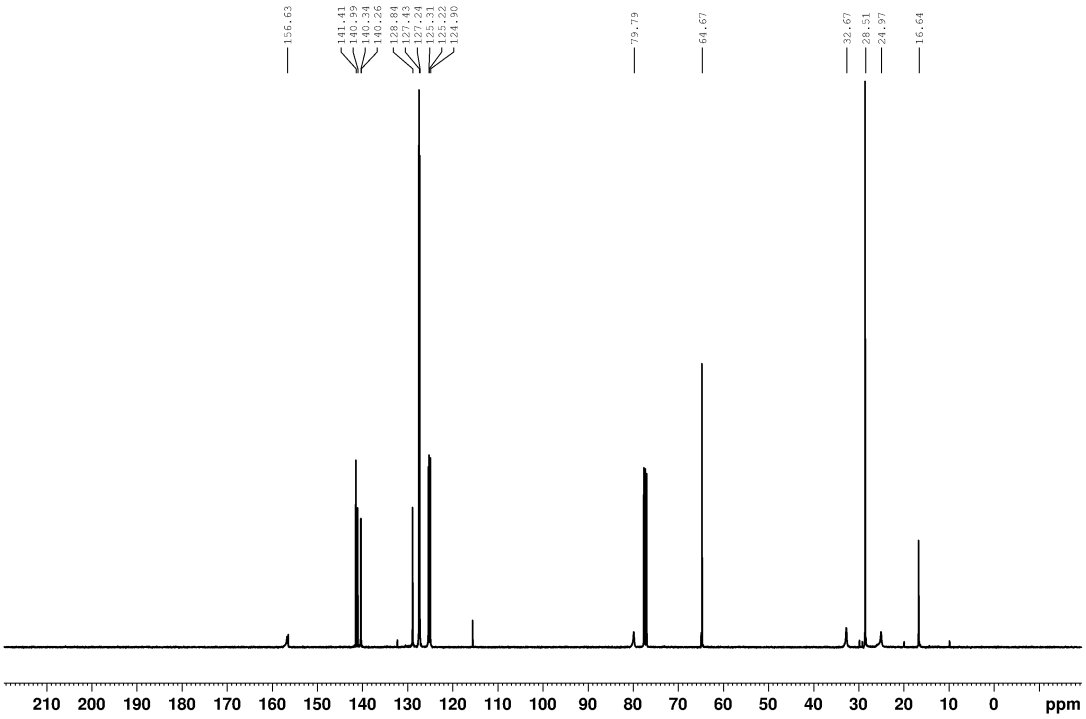

tert-butyl (2-(3'-(hydroxymethyl)-[1,1'-biphenyl]-4-yl)cyclopropyl)carbamate **(48c)**

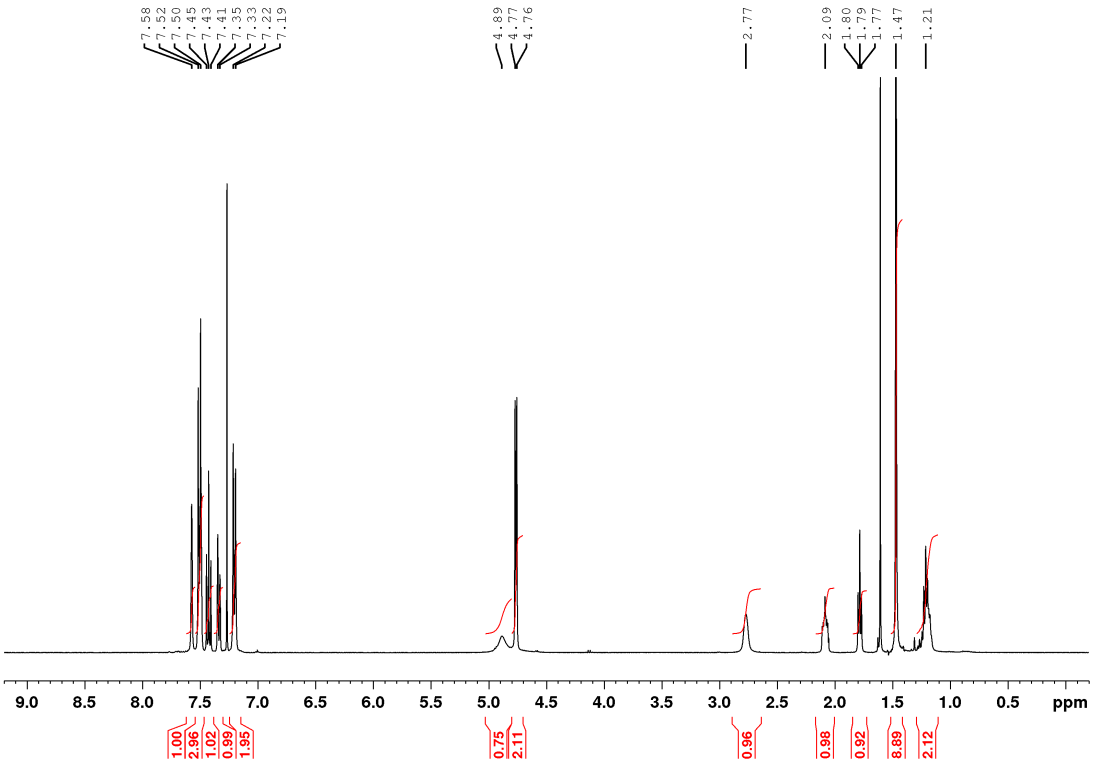

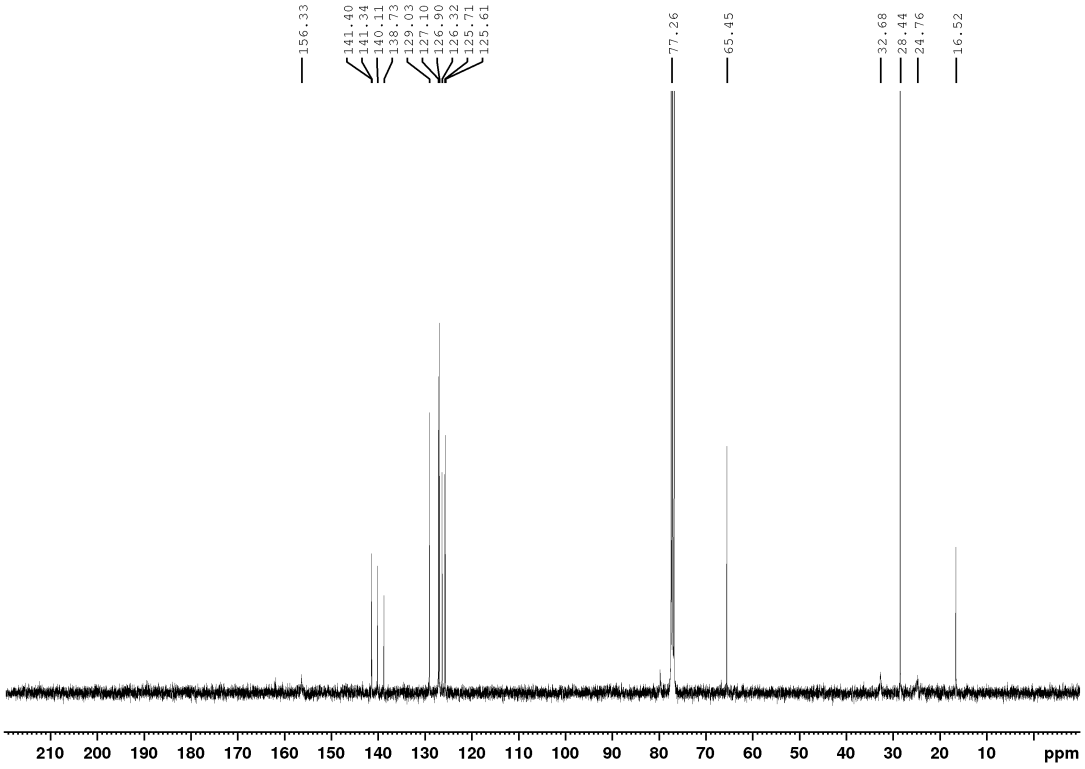

tert-butyl (2-(4'-(hydroxymethyl)-[1,1'-biphenyl]-4-yl)cyclopropyl)carbamate **(48d)**

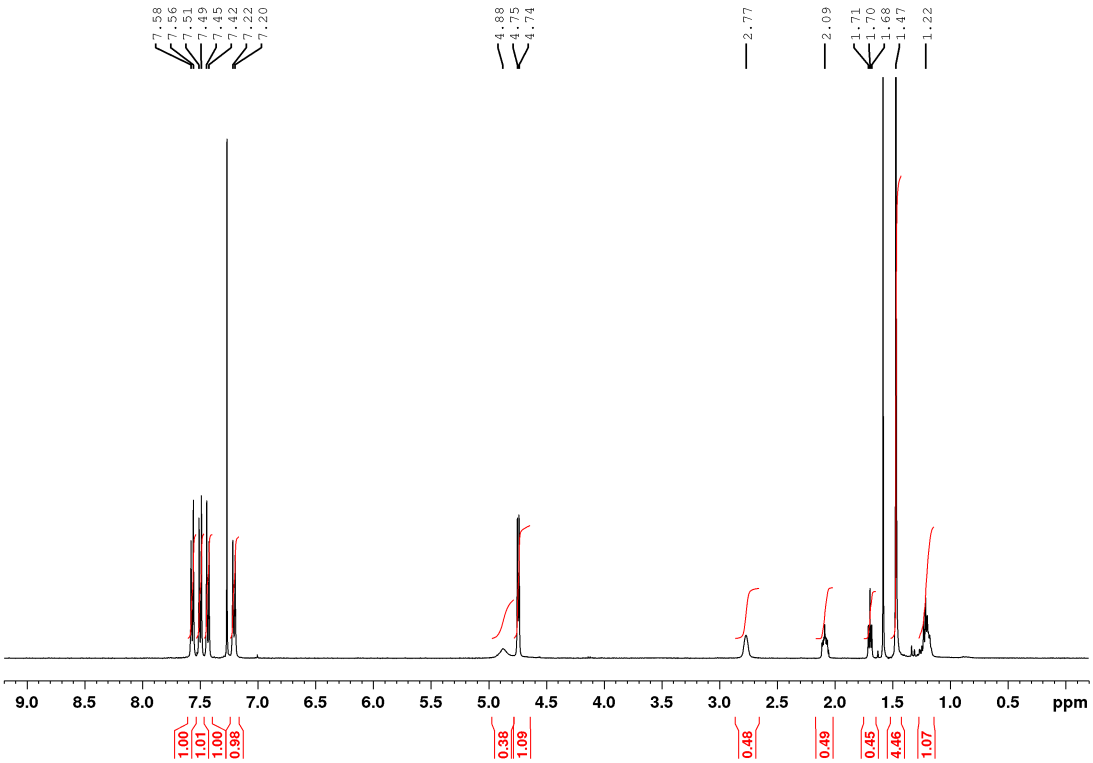

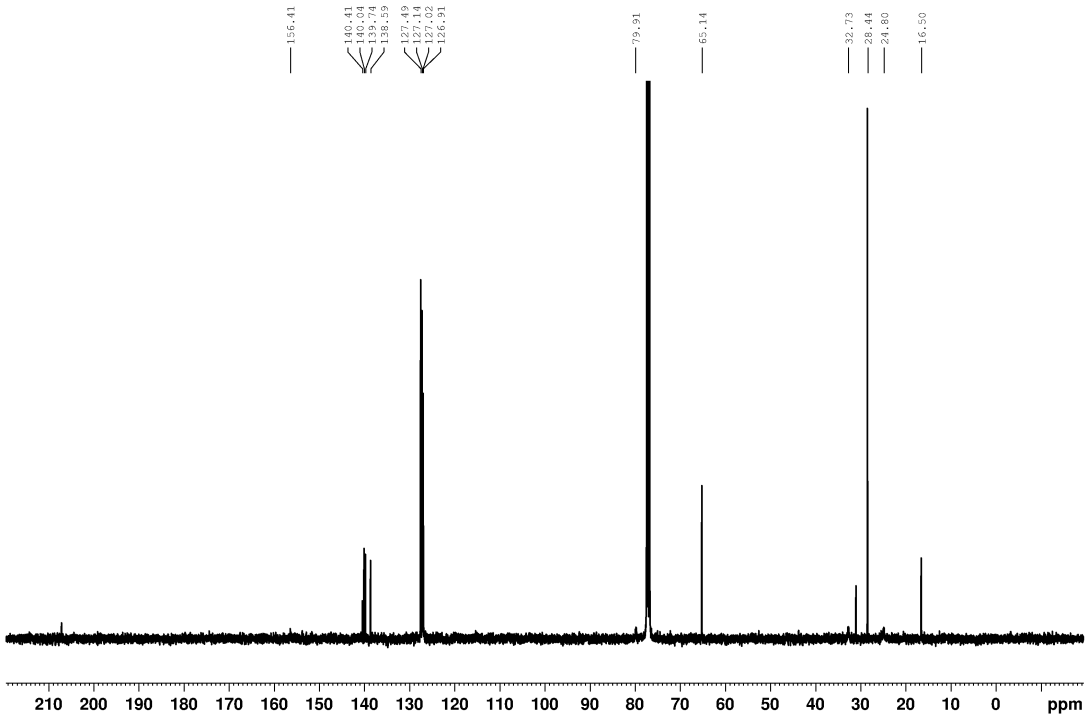

tert-butyl (2-(3'-(azidomethyl)-[1,1'-biphenyl]-3-yl)cyclopropyl)carbamate **(49a)**

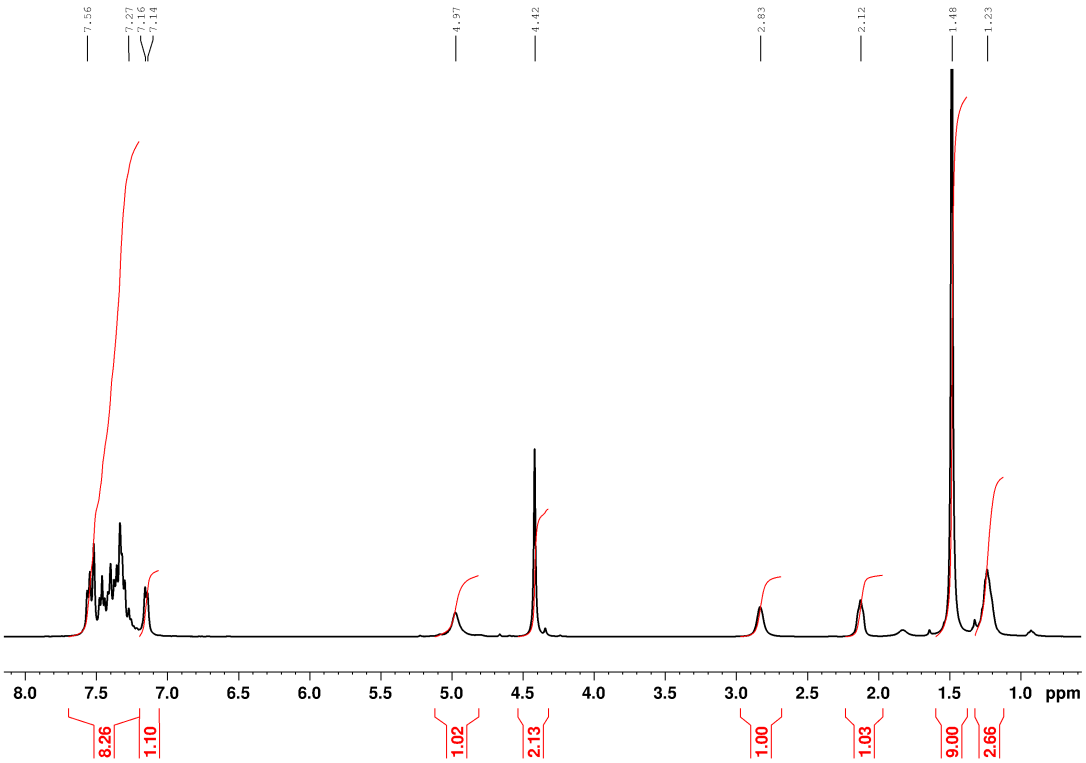

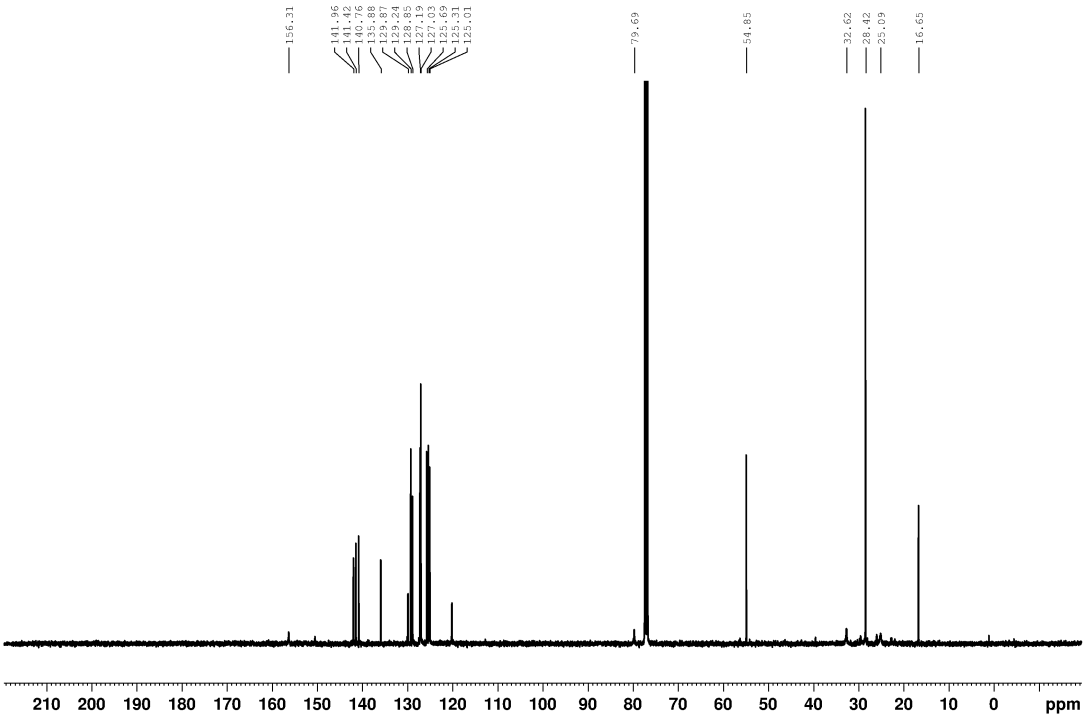

tert-butyl (2-(4'-(azidomethyl)-[1,1'-biphenyl]-3-yl)cyclopropyl)carbamate **(49b)**

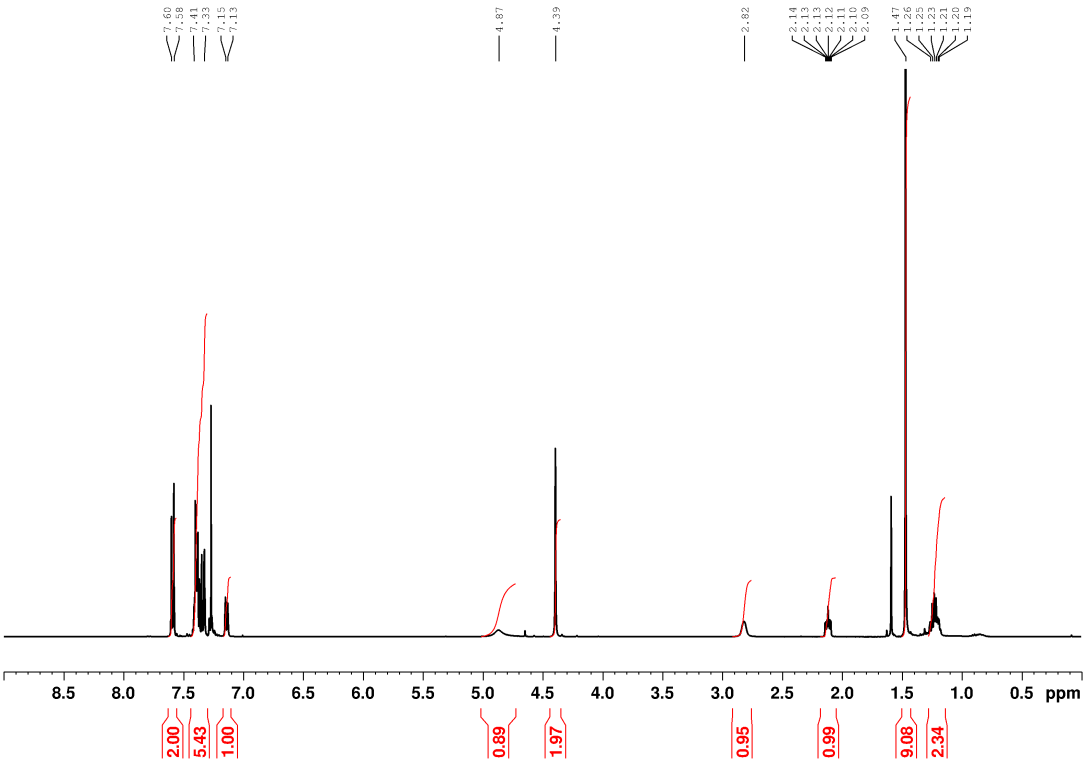

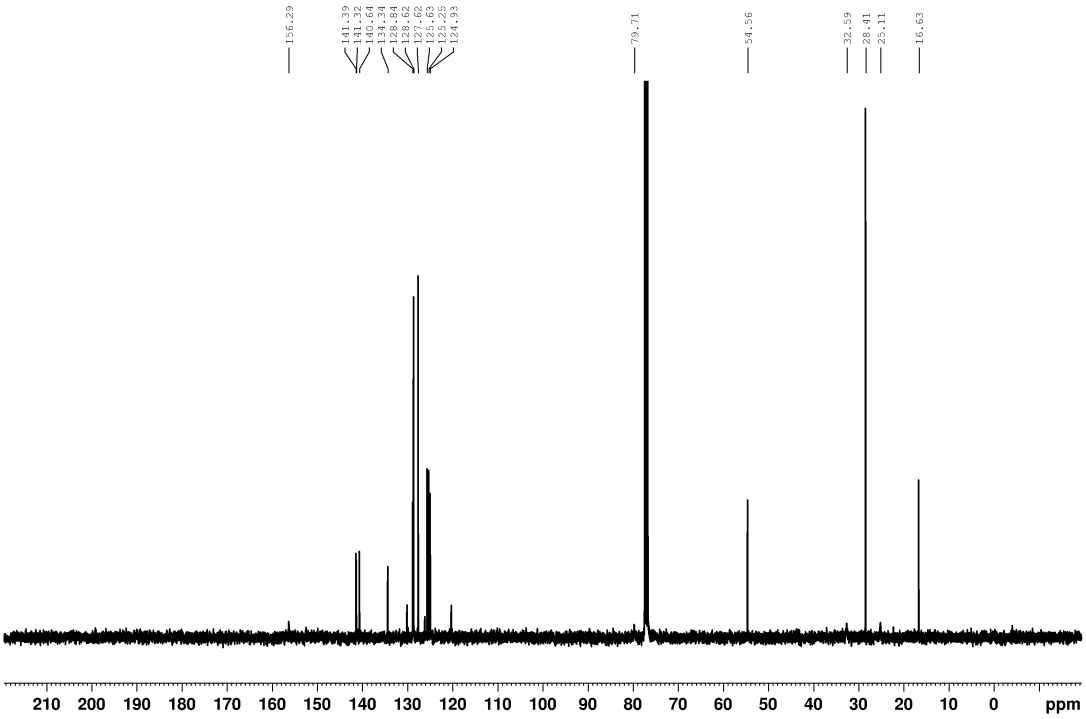

tert-butyl (2-(3'-(azidomethyl)-[1,1'-biphenyl]-4-yl)cyclopropyl)carbamate **(49c)**

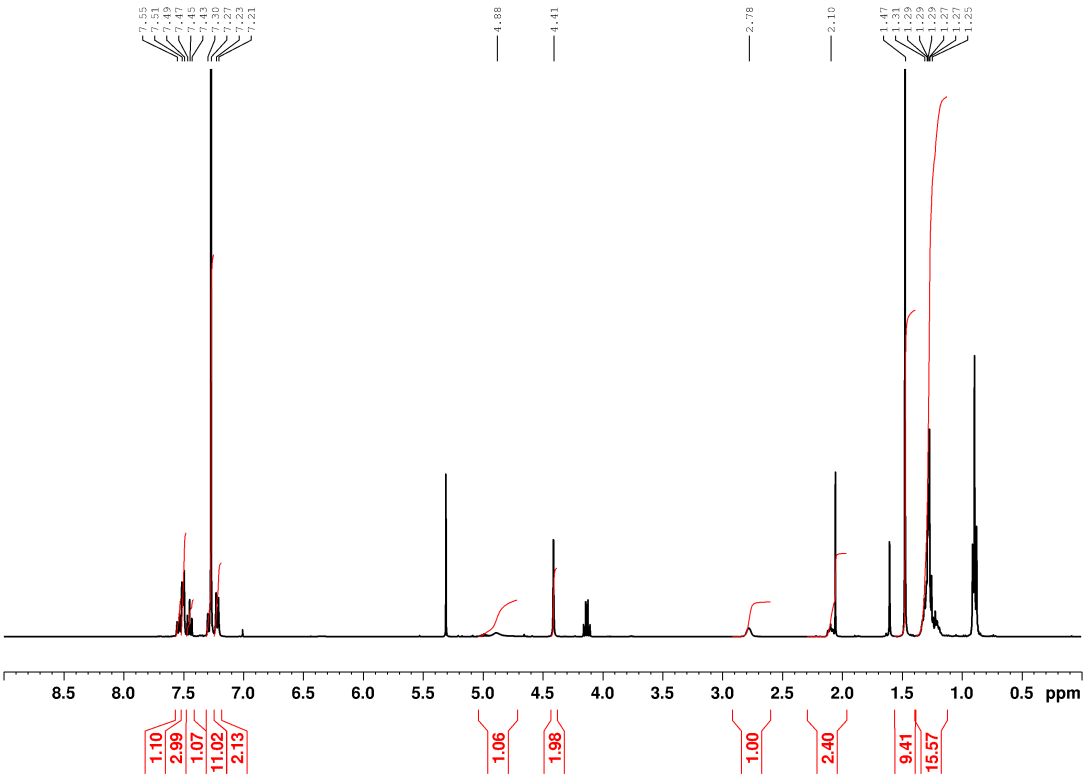

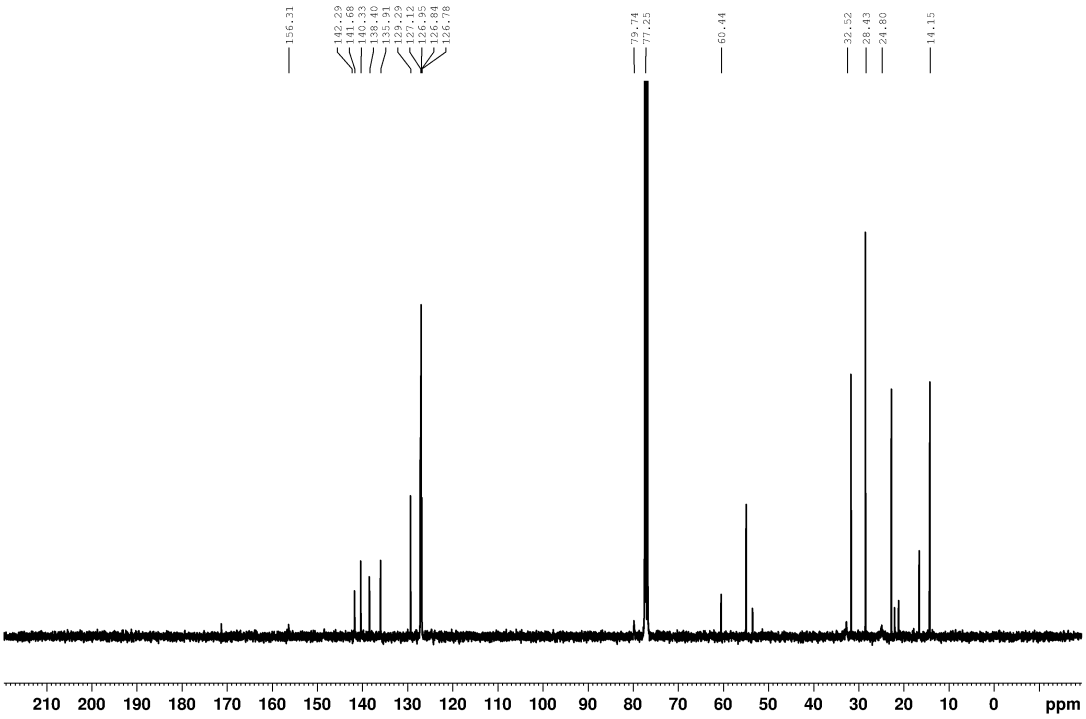

tert-butyl (2-(4'-(azidomethyl)-[1,1'-biphenyl]-4-yl)cyclopropyl)carbamate **(49d)**

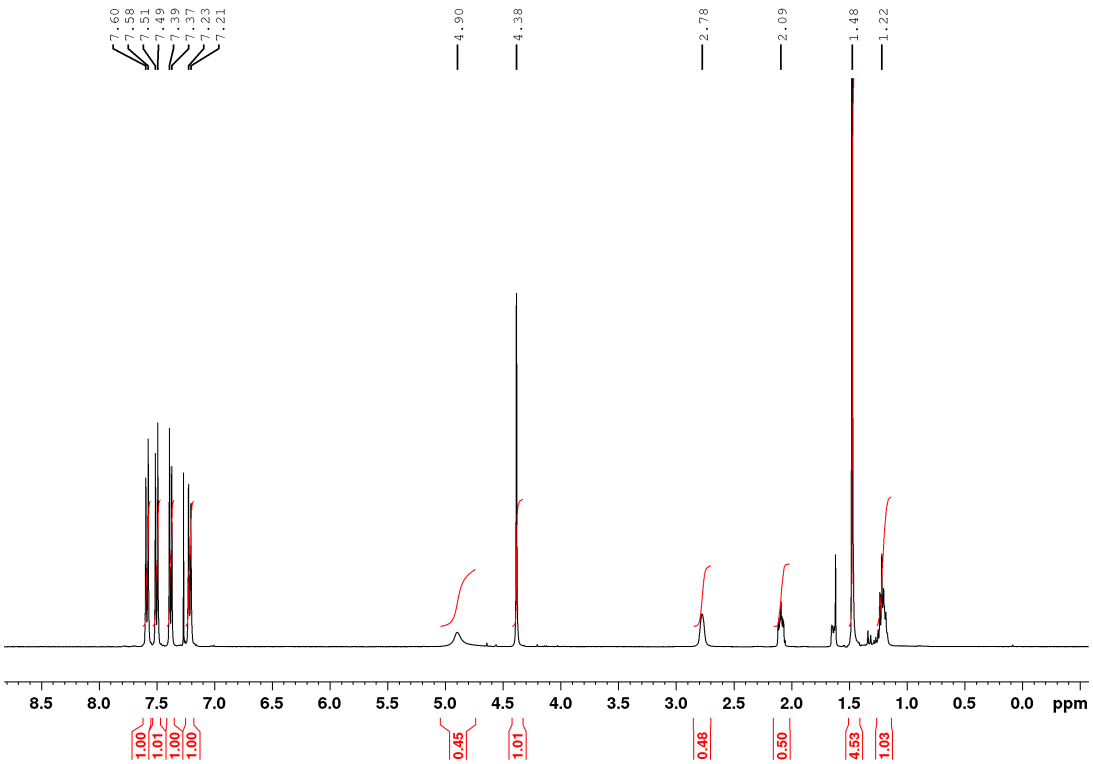

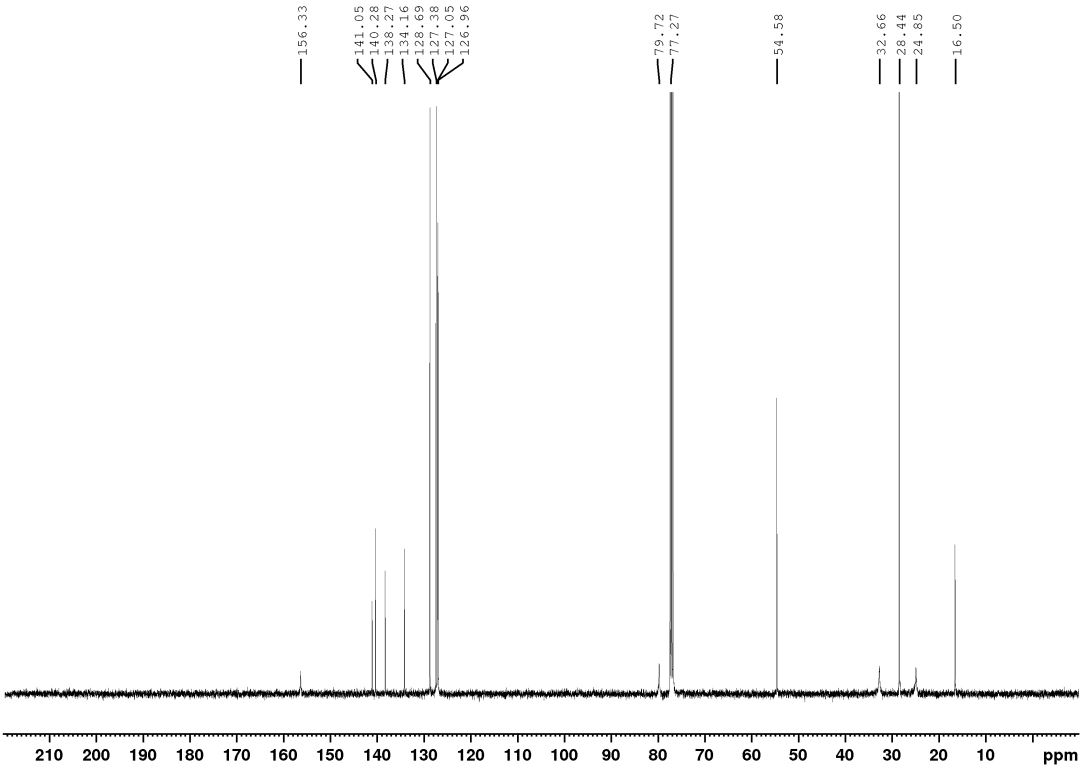

2-(3'-(azidomethyl)-[1,1'-biphenyl]-3-yl)cyclopropan-1-amine **(probe 5)**

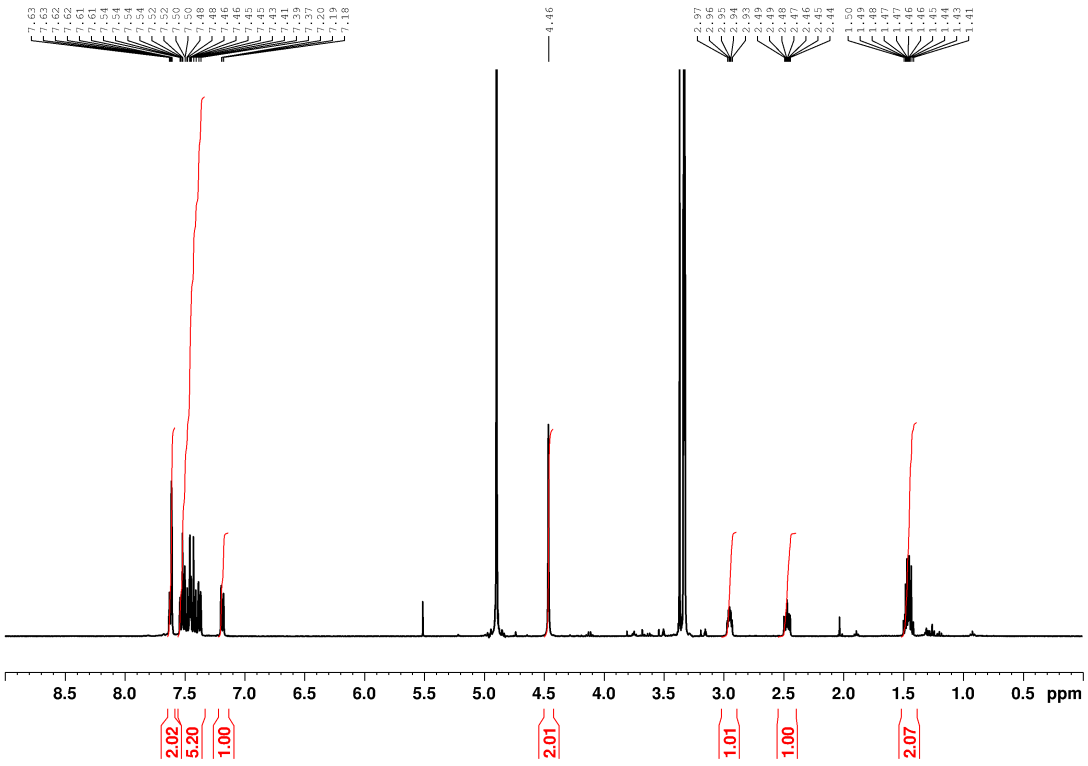

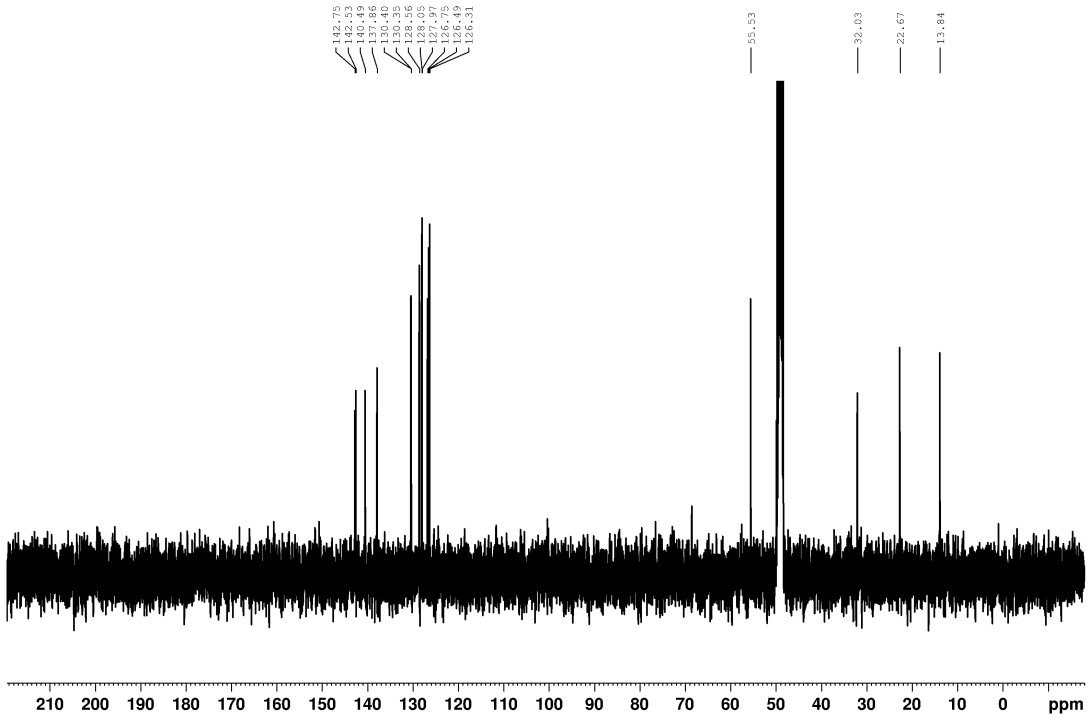

2-(4'-(azidomethyl)-[1,1'-biphenyl]-3-yl)cyclopropan-1-amine **(probe 6)**

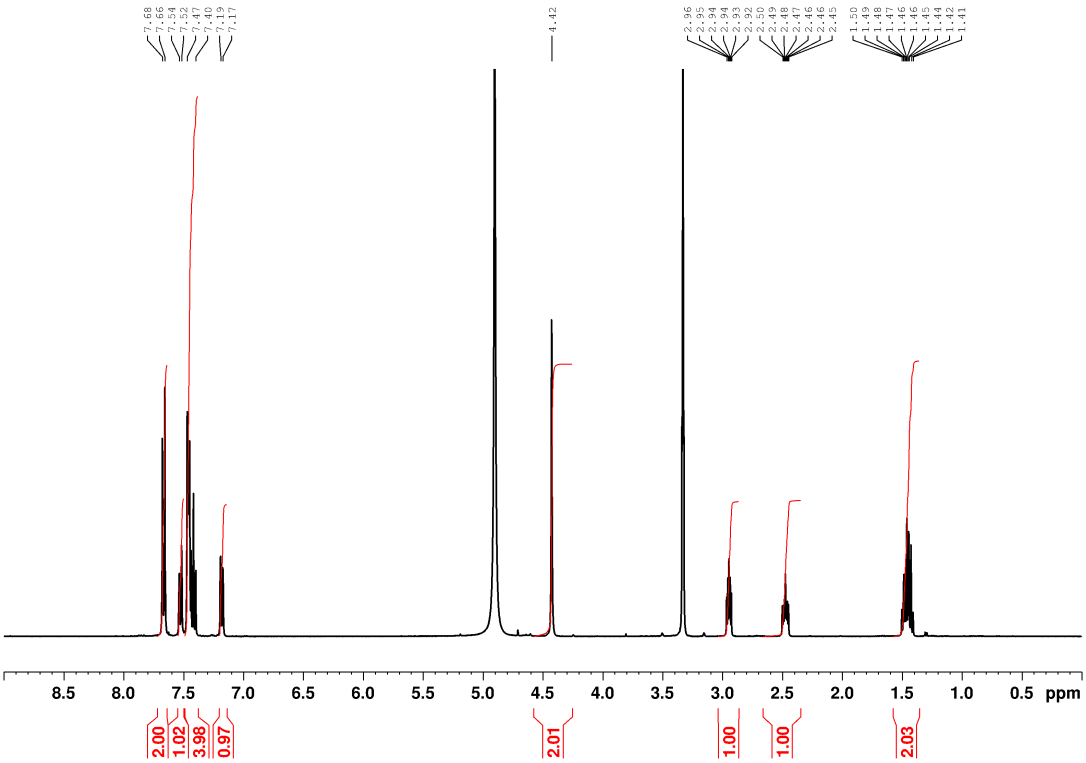

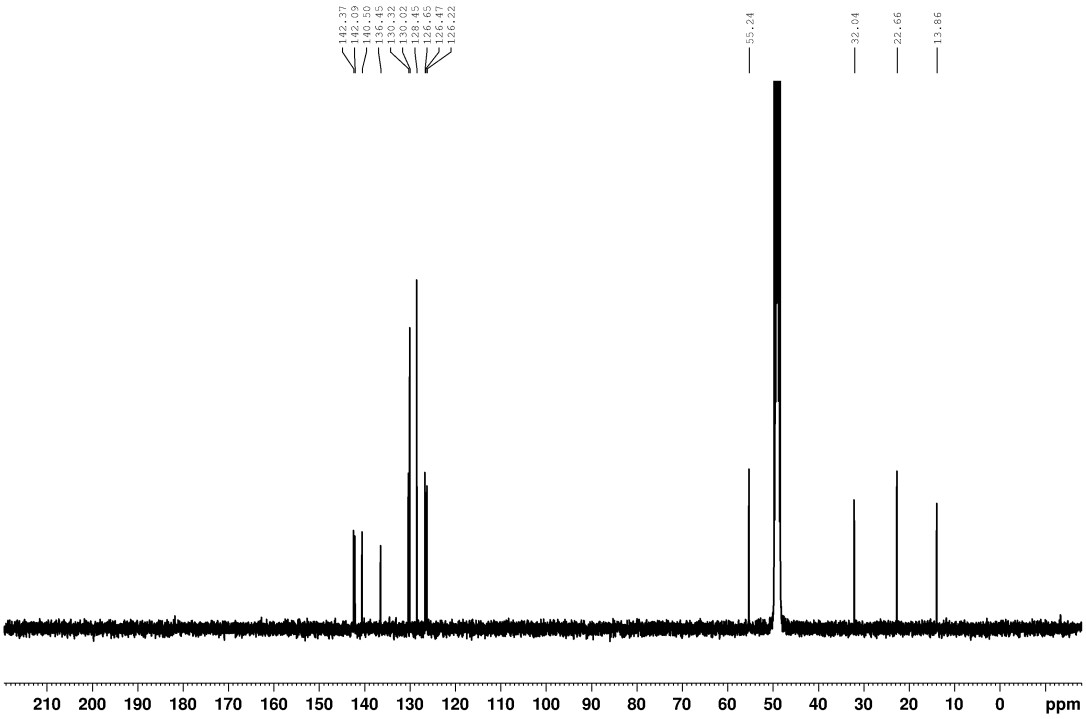

2-(3'-(azidomethyl)-[1,1'-biphenyl]-4-yl)cyclopropan-1-amine **(probe 7)**

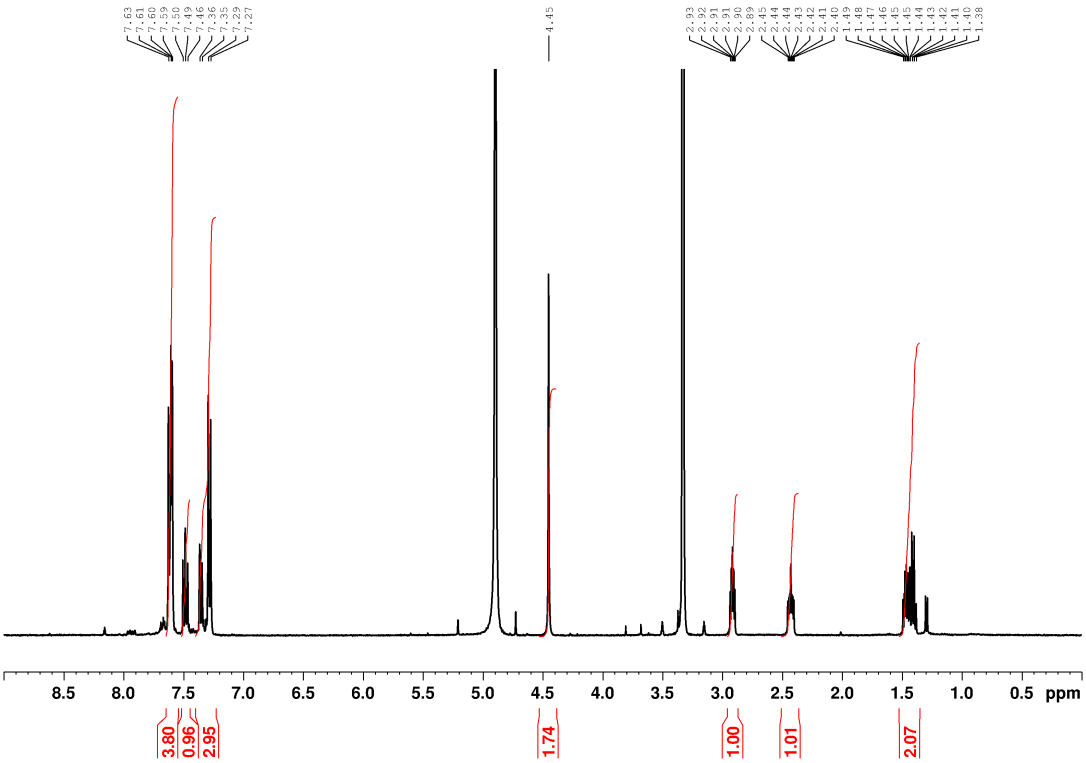

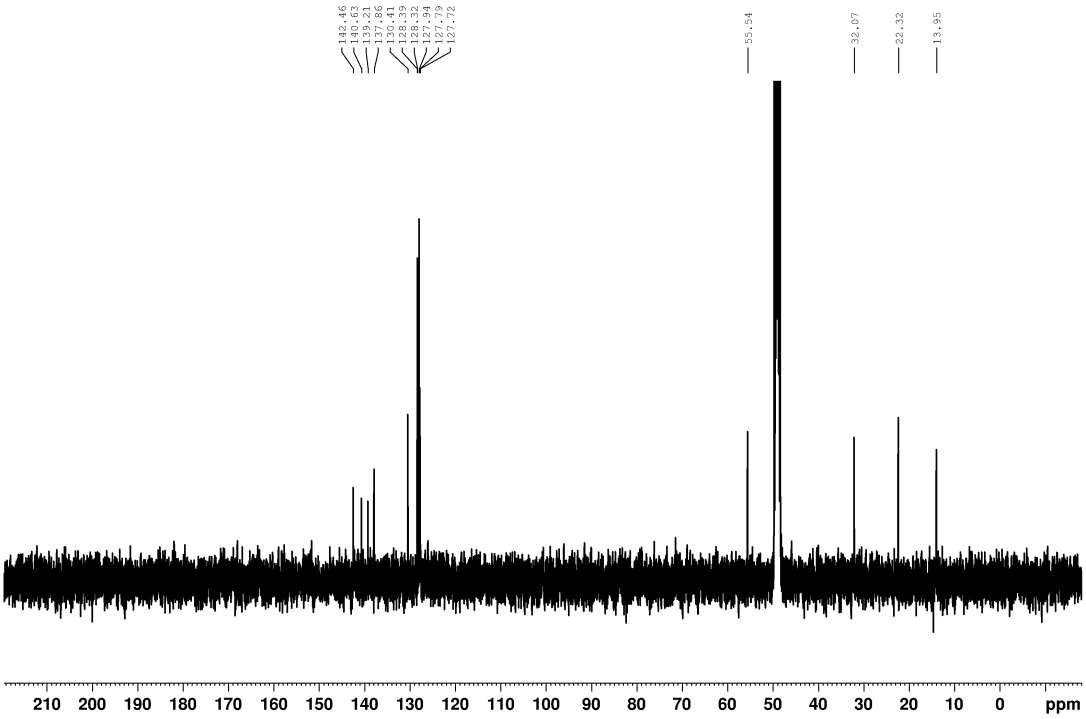

2-(4'-(azidomethyl)-[1,1'-biphenyl]-4-yl)cyclopropan-1-amine **(probe 8)**

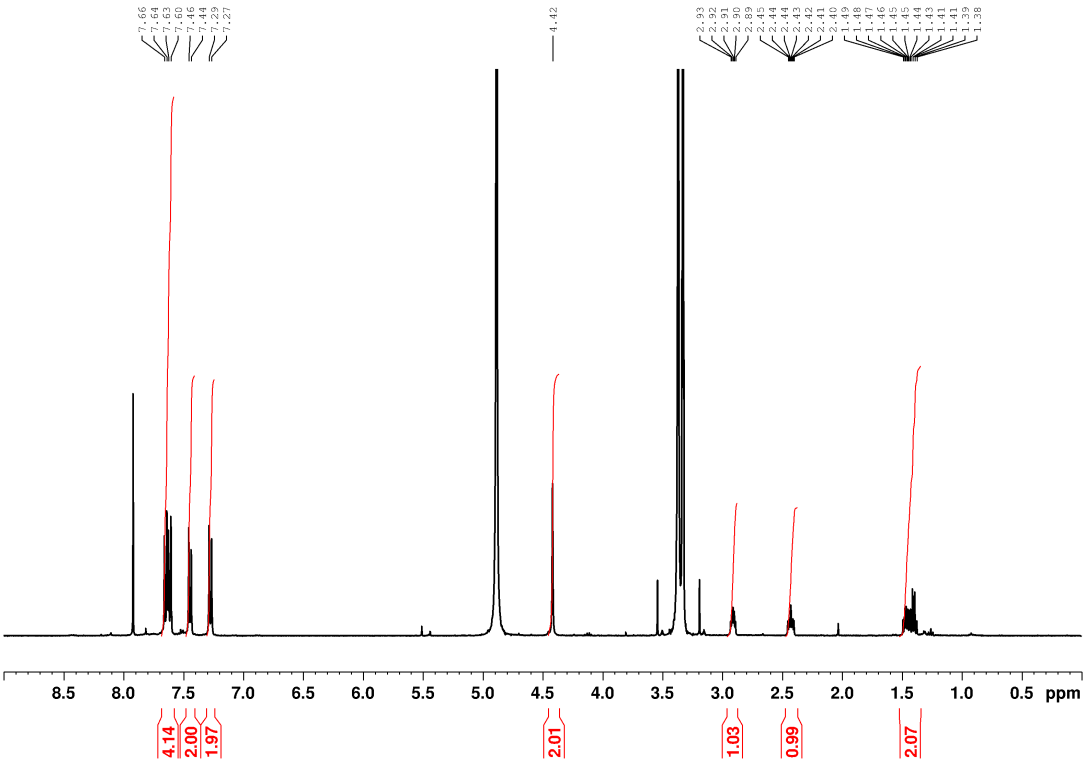

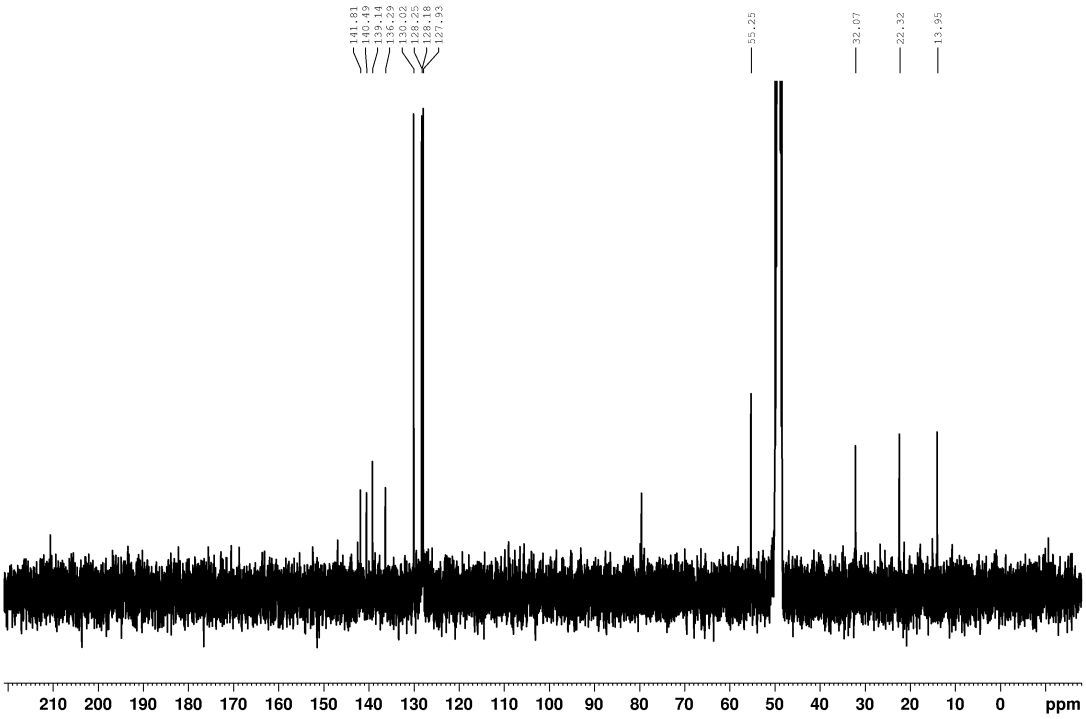

Chapter 9 Appendix B

(1 *R*, 2 *S*)-2-(4-bromophenyl)-N-((*R*)-1-phenylethyl)cyclopropane-1-carboxamide. **((1 *R*, 2 *S*) 50)**

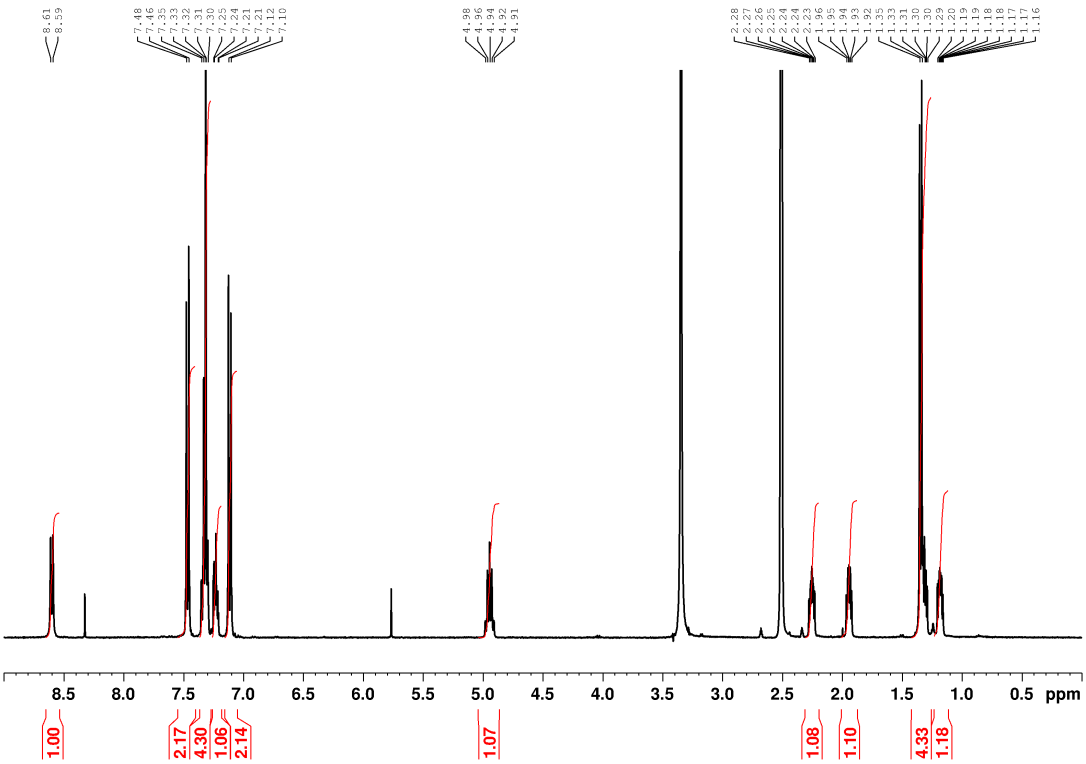

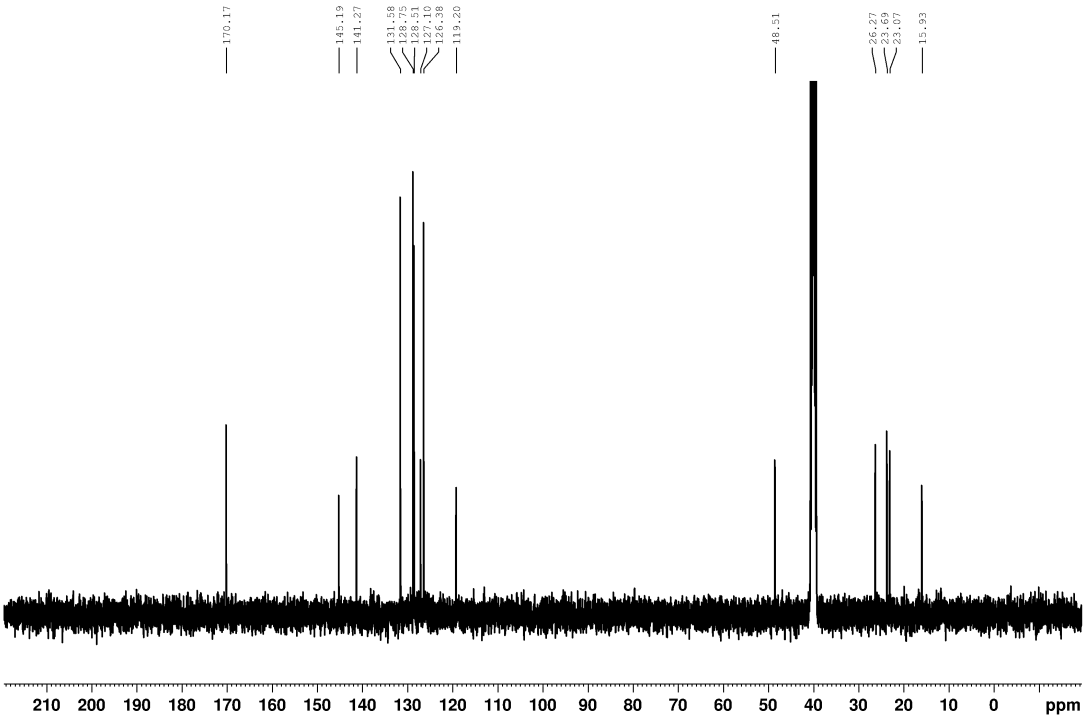

(1 *S*,2 *R*)-2-(4-bromophenyl)-N-((*R*)-1-phenylethyl)cyclo-propane-1-carbox-amide**, ((1 *S*, 2 *R*) 50)**

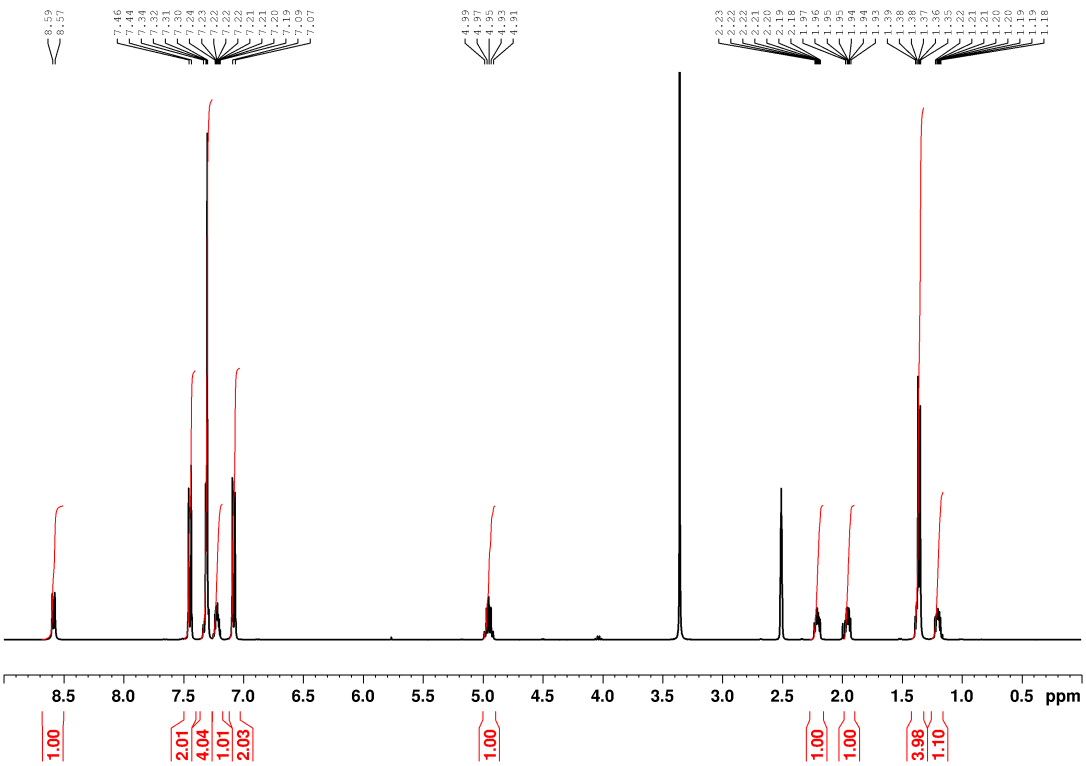

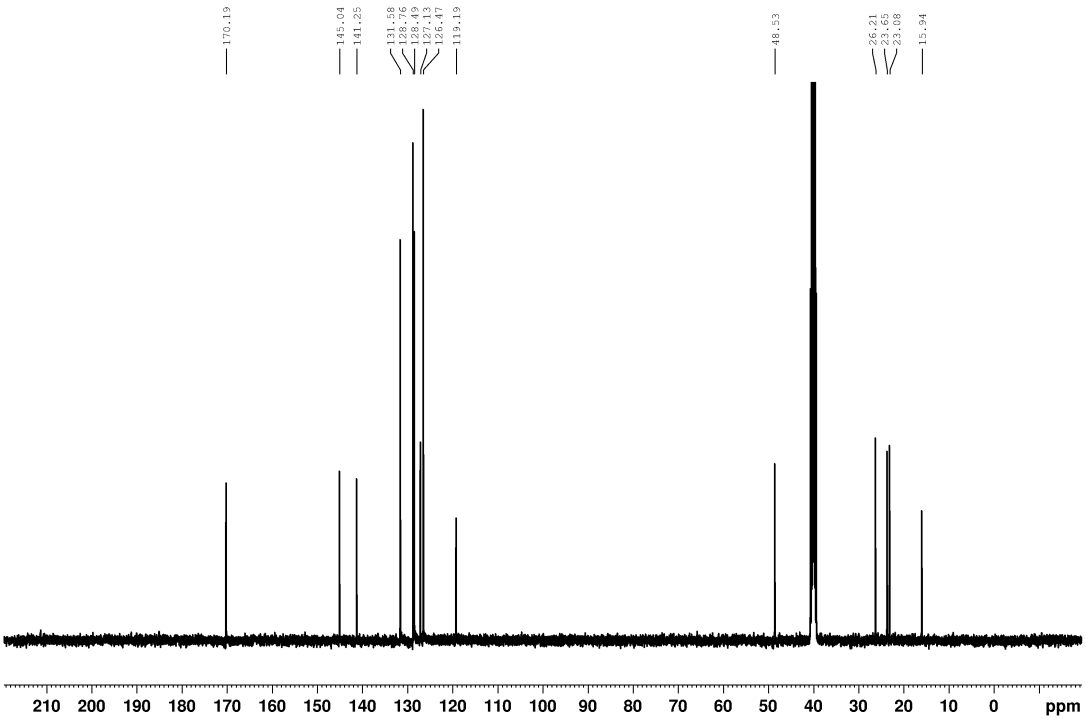

(1 *R*,2 *S*)-2-(4-bromophenyl)cyclopropane-1-carboxylic acid. **((1 *R*,2 *S*)-43b)**

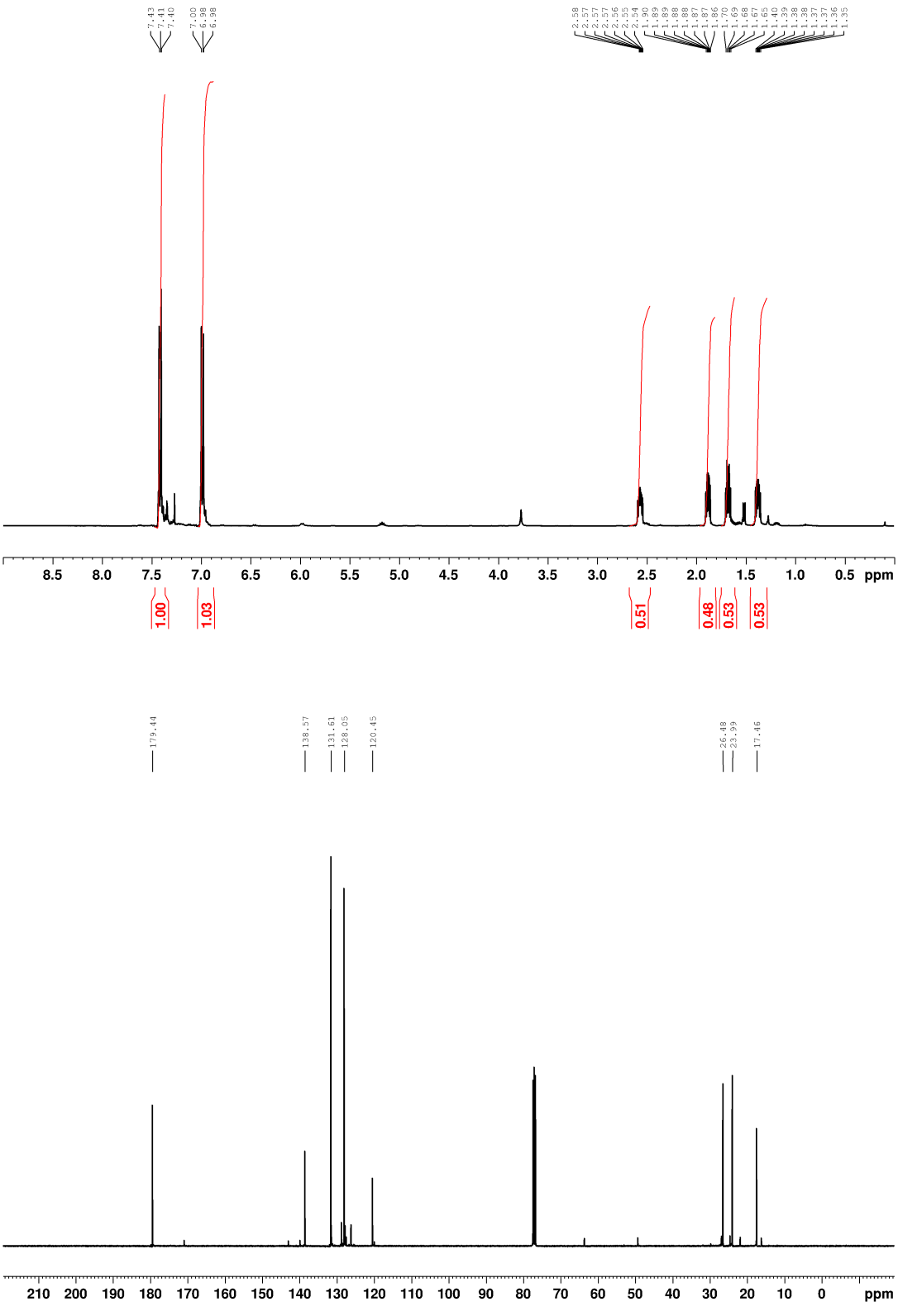

(1 *S*,2 *R*)-2-(4-bromophenyl)cyclopropane-1-carboxylic acid **((1 *S*,2 *R*)-43b)**

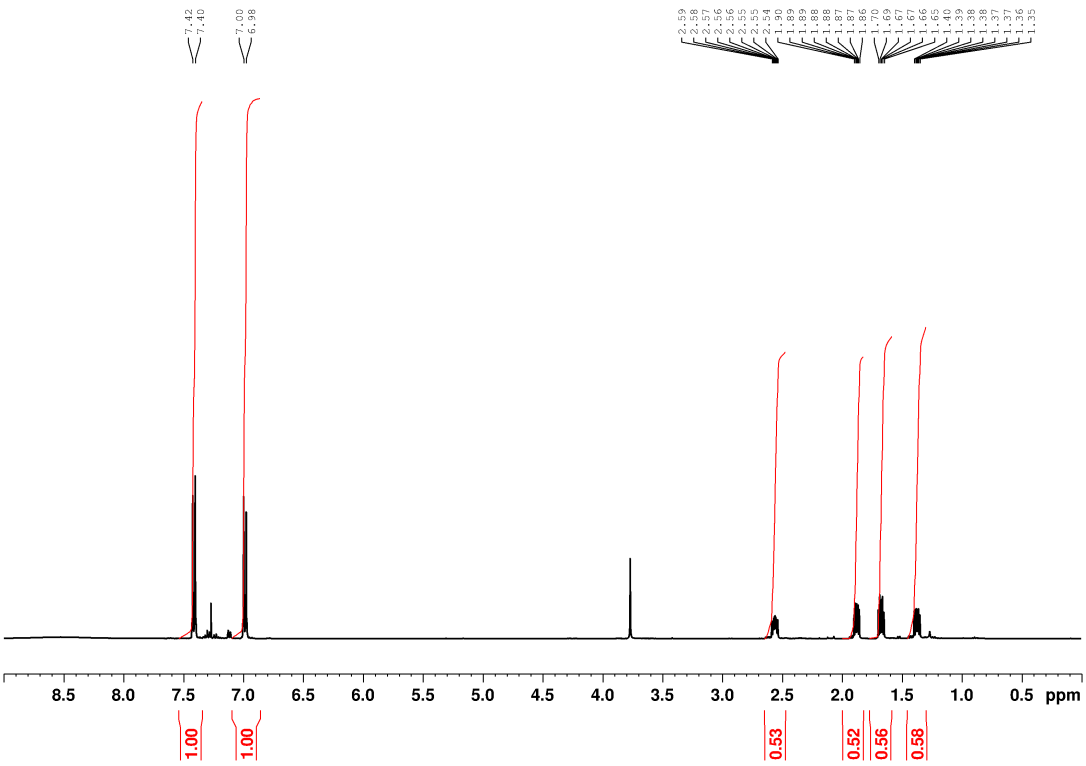

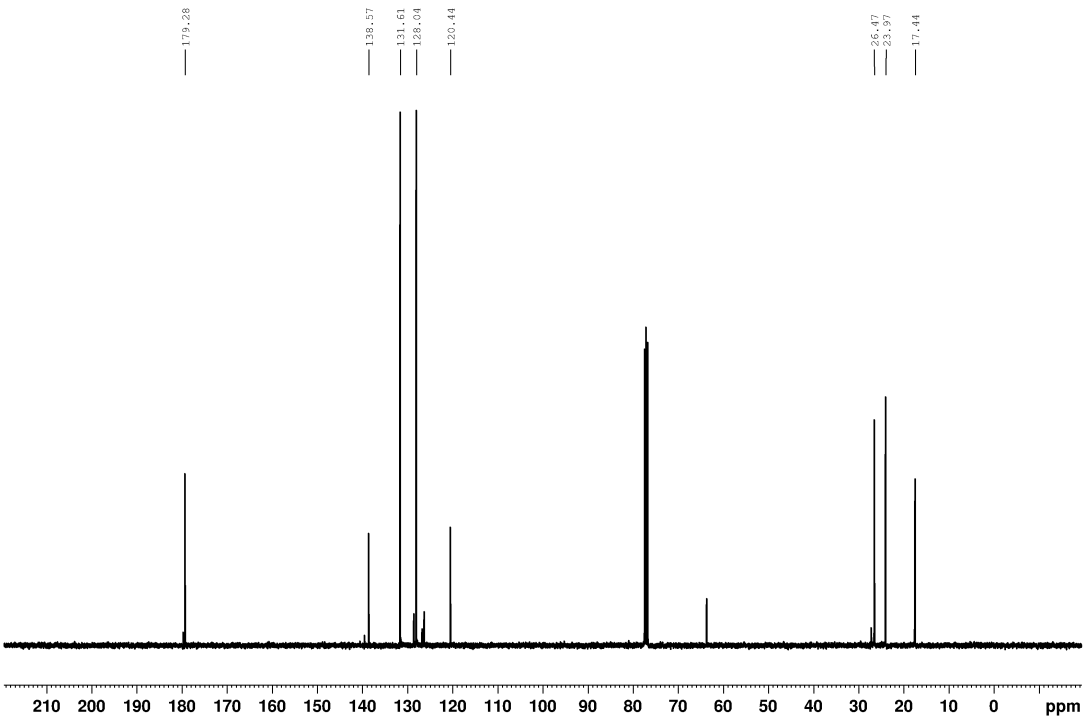

tert-butyl ((1 *R*,2 *S*)-2-(4-bromophenyl)cyclopropyl)carbamate **((1 *R*,2 *S*)-44b)**

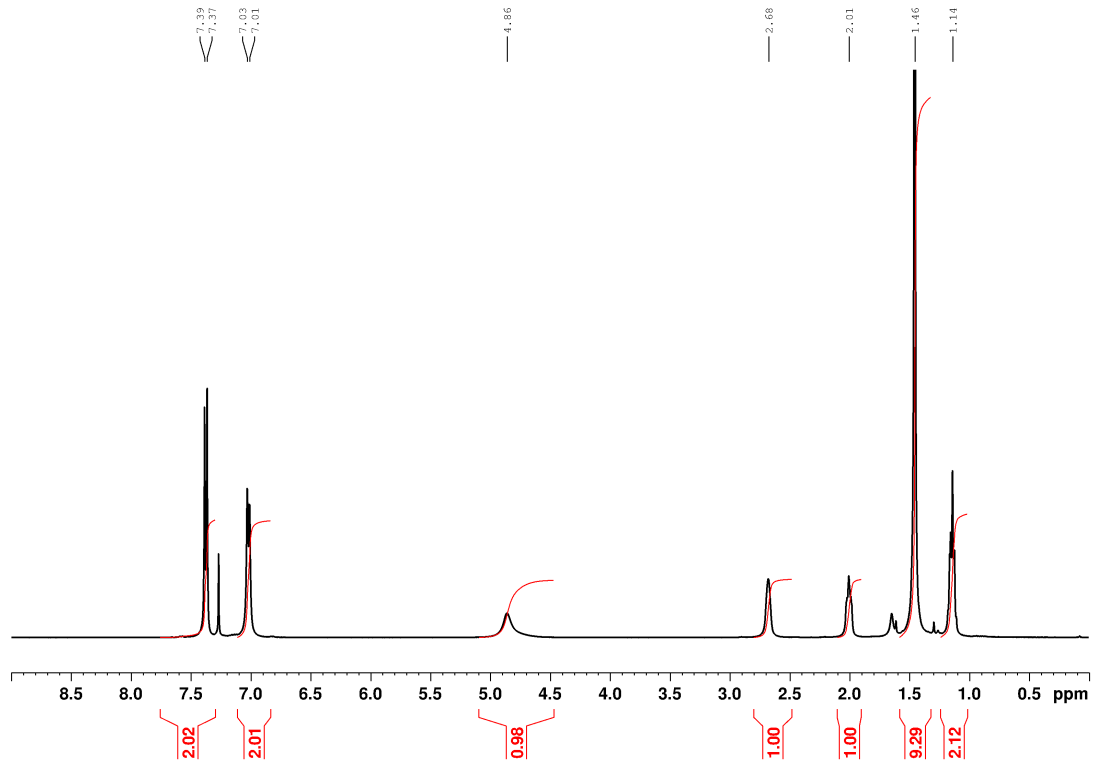

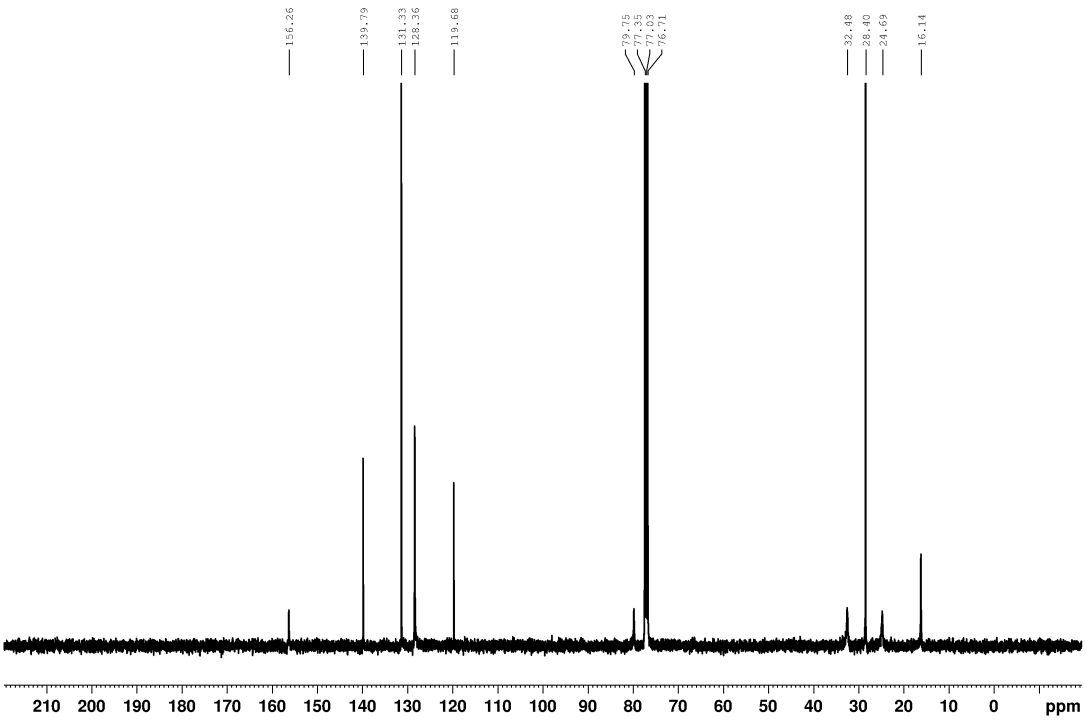

tert-butyl ((1 *S*,2 *R*)-2-(4-bromophenyl)cyclopropyl)carbamate **((1 *S*,2 *R*)-44b)**

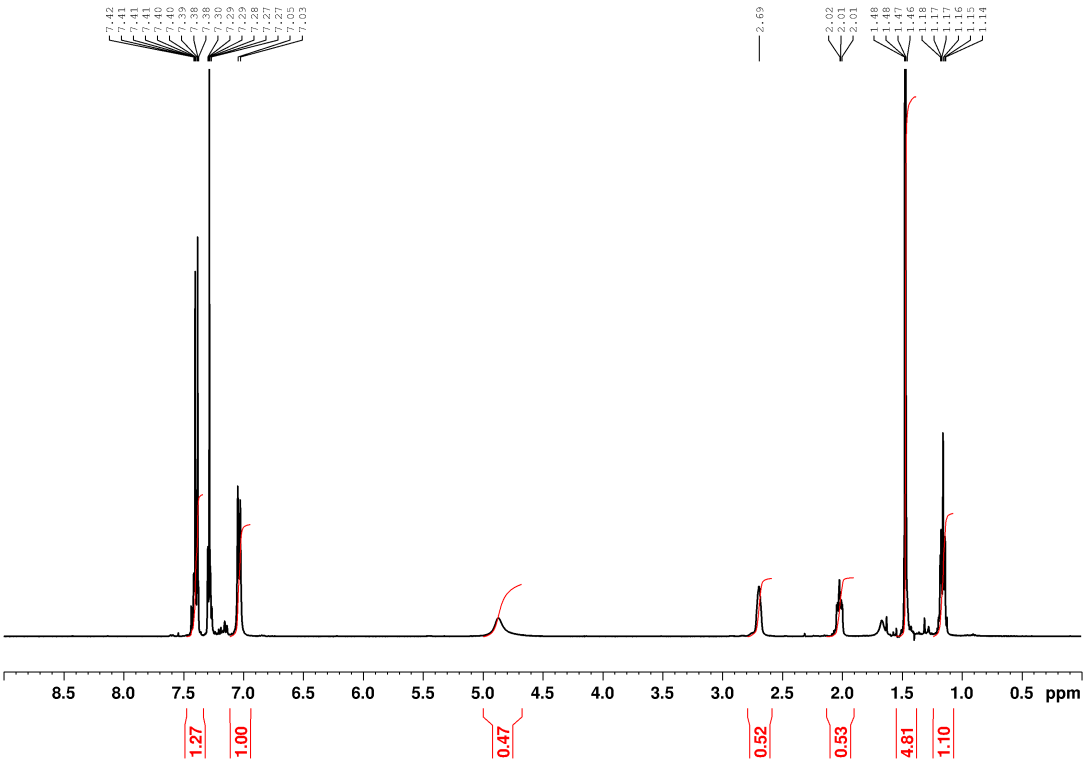

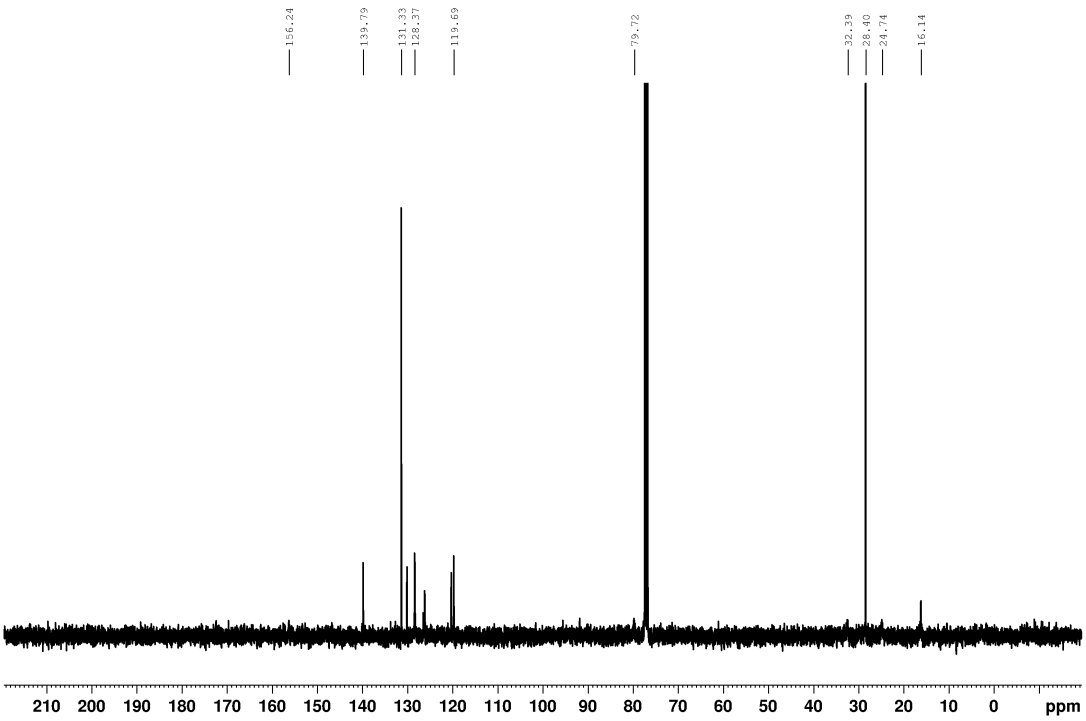

tert-butyl ((1 *R*,2 *S*)-2-(3'-(hydroxymethyl)-[1,1'-biphenyl]-4-yl)cyclopropyl)-carbamate **((1 *R*,2 *S*)-48b)**

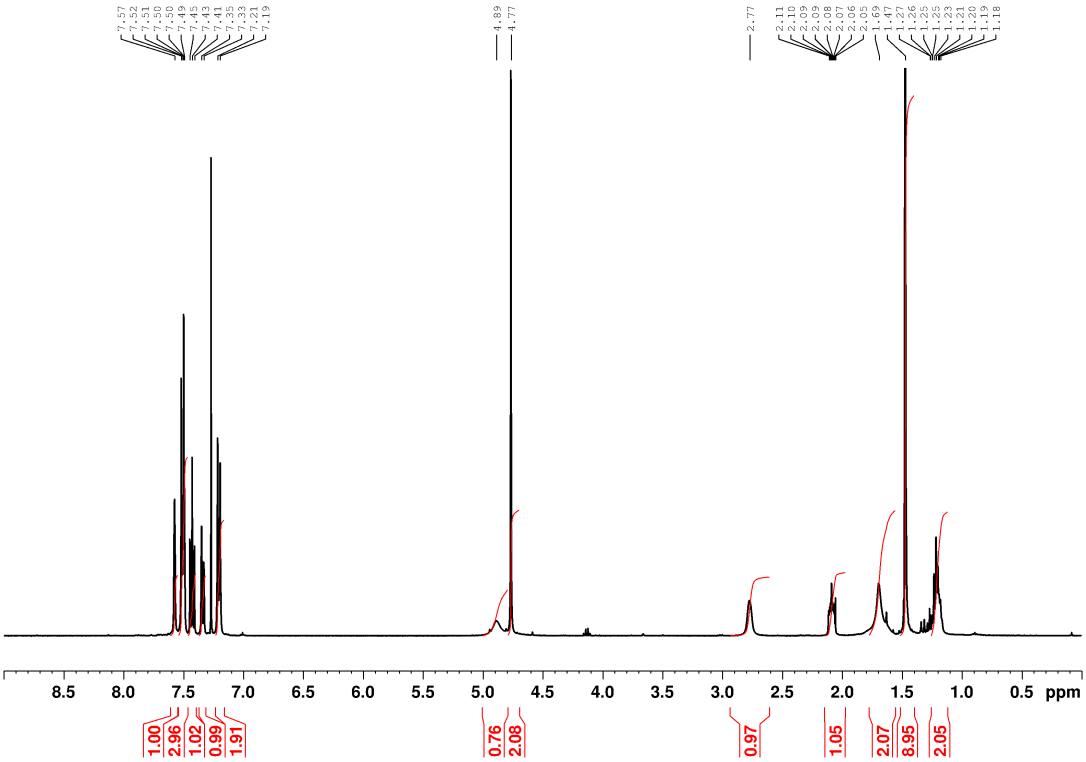

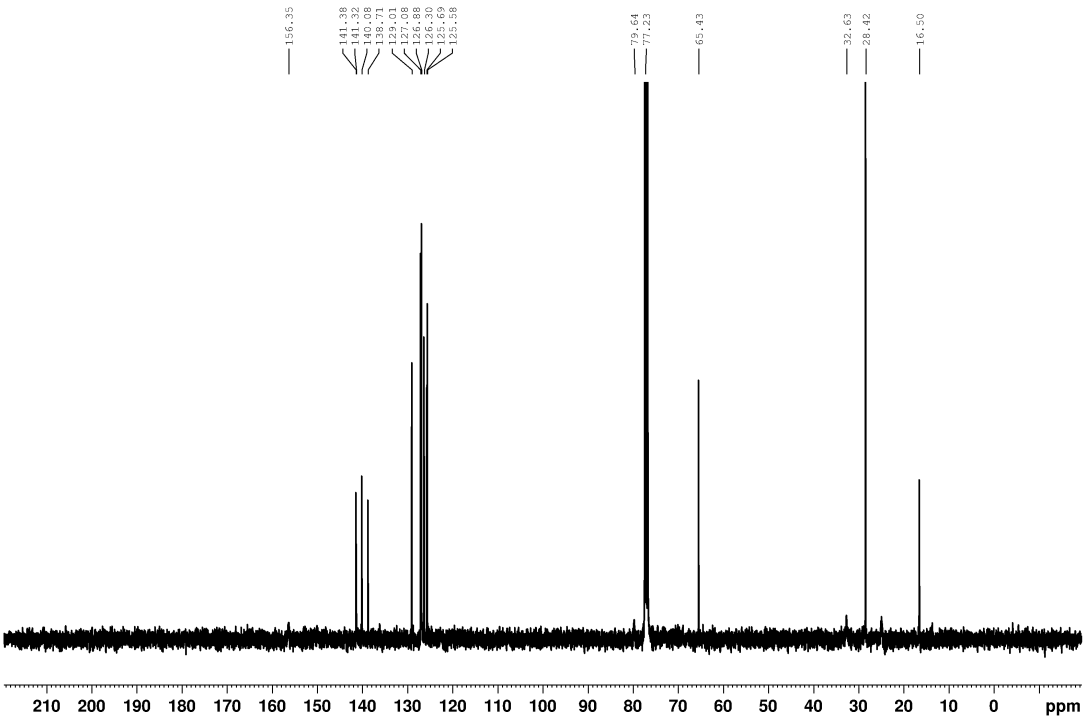

tert-butyl ((1 *S*,2 *R*)-2-(3'-(hydroxymethyl)-[1,1'-biphenyl]-4-yl)cyclopropyl)-carbamate **((1 *S*,2 *R*)-48b)**

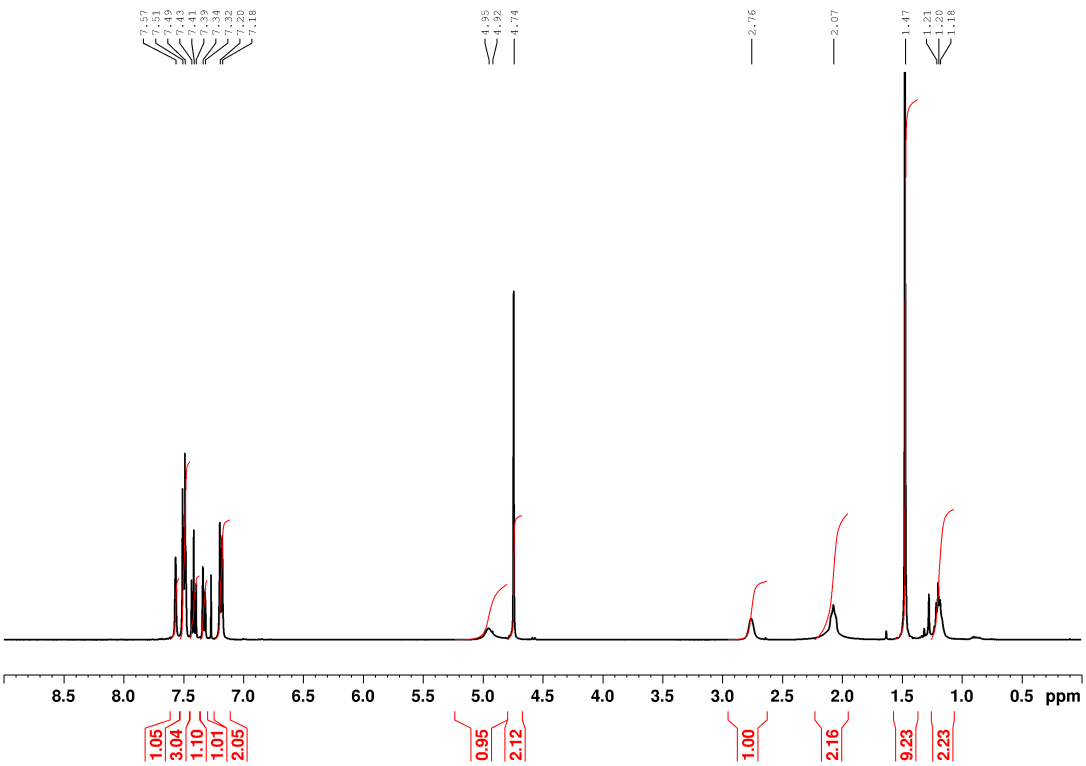

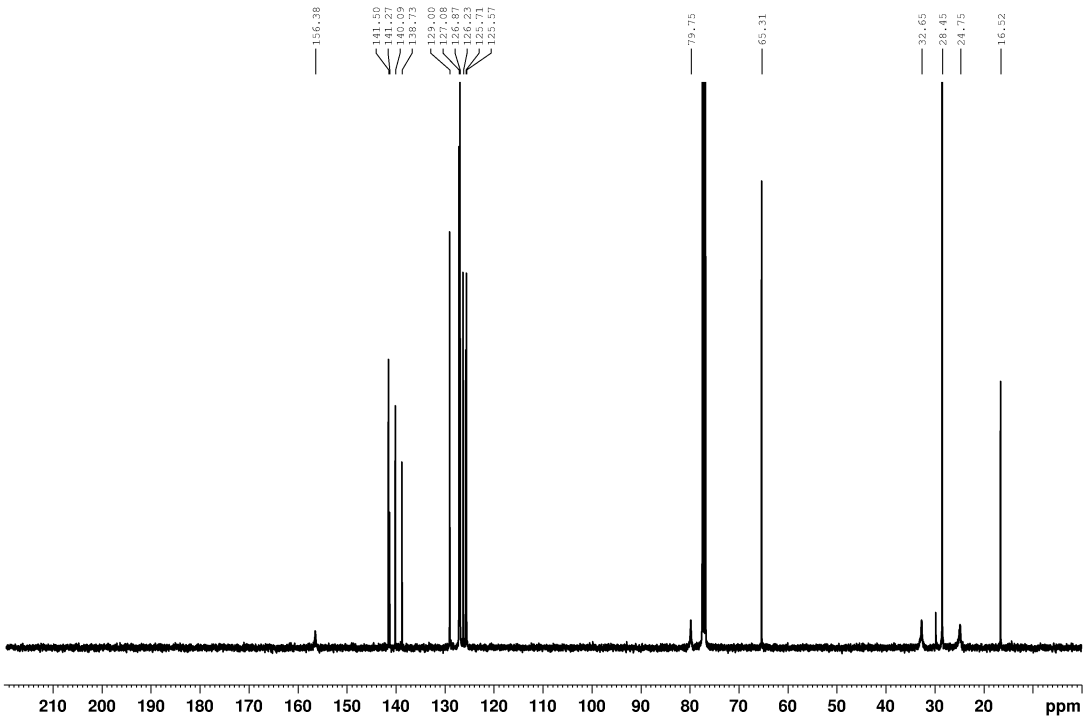

tert-butyl ((1 *R*,2 *S*)-2-(3'-(azidomethyl)-[1,1'-biphenyl]-4-yl)cyclopropyl)-carbamate **((1 *R*,2 *S*)-49b)**

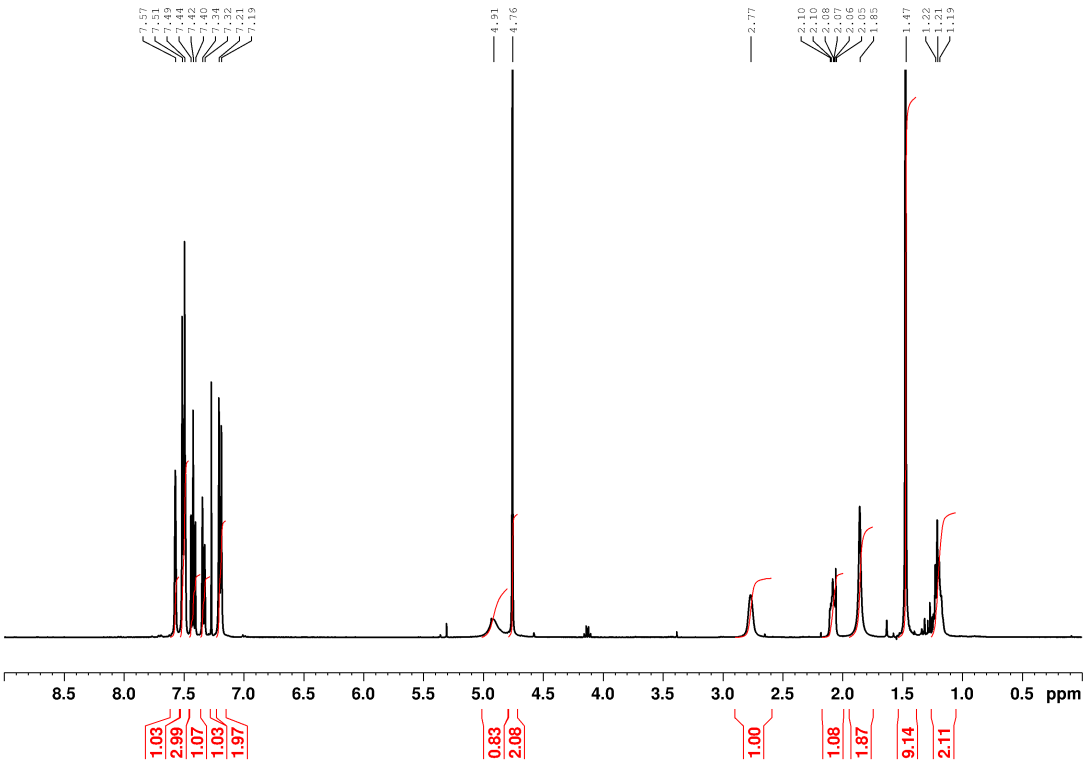

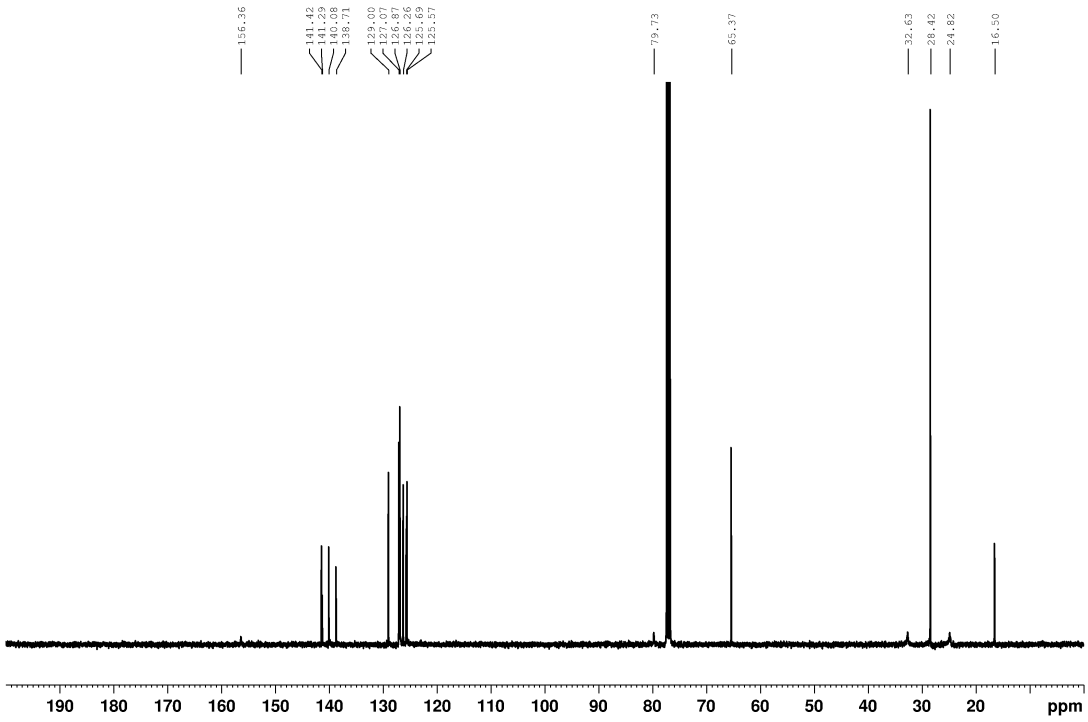

tert-butyl ((1 *S*,2 *R*)-2-(3'-(azidomethyl)-[1,1'-biphenyl]-4-yl)cyclopropyl)-carbamate **((1 *S*,2 *R*)-49b)**

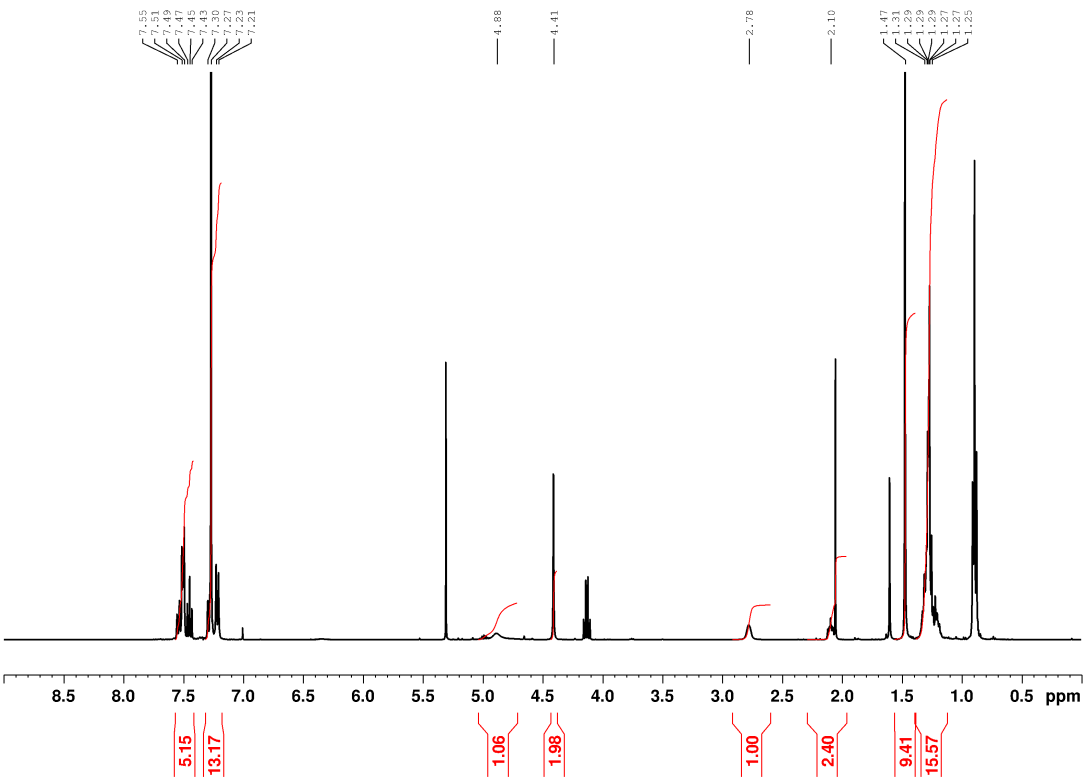

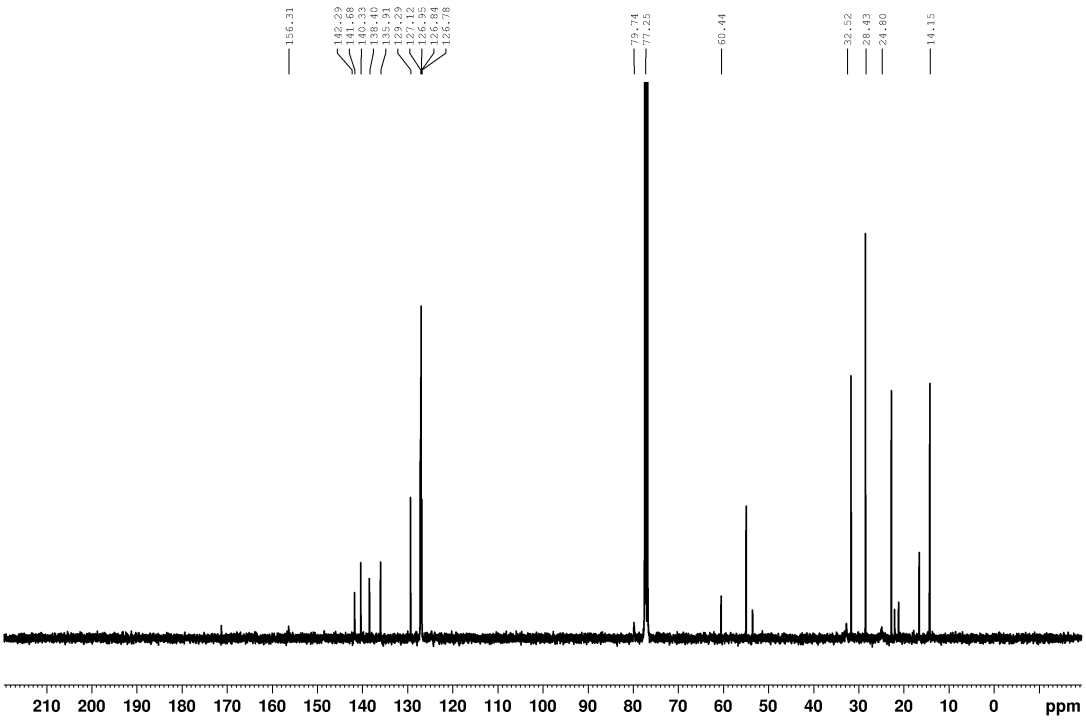

(1 *R*,2 *S*)-2-(3'-(azidomethyl)-[1,1'-biphenyl]-4-yl)cyclopropan-1-amine **((1 *R*,2 *S*)–probe 7)**

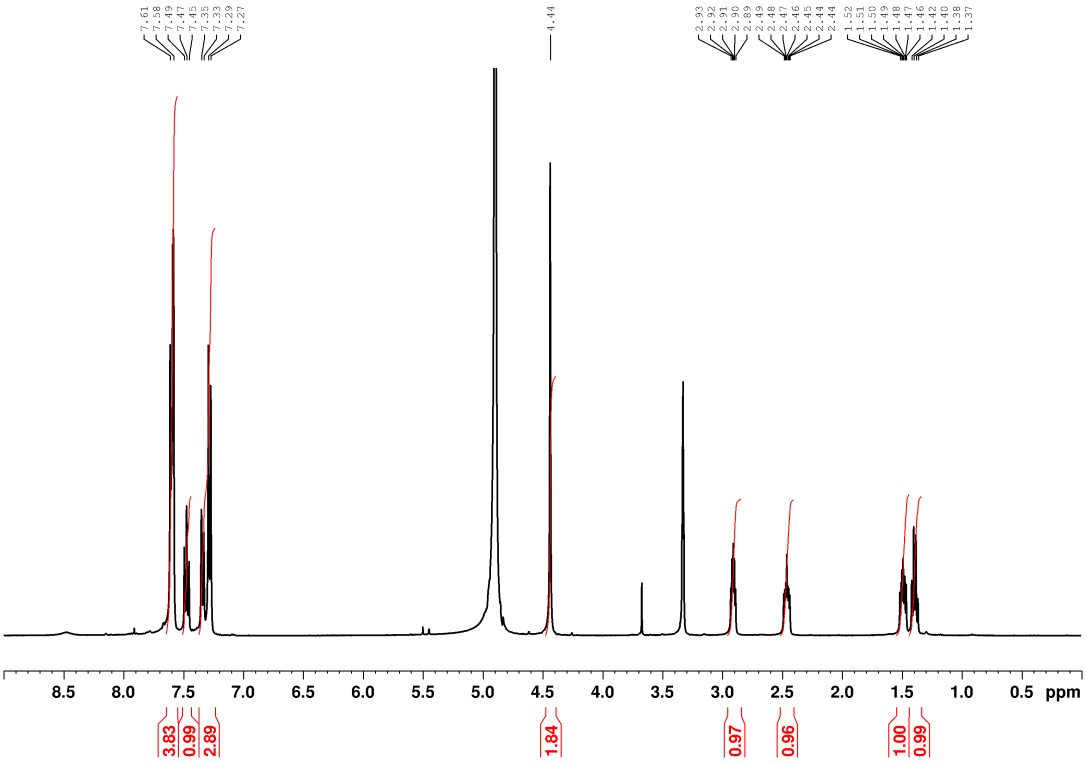

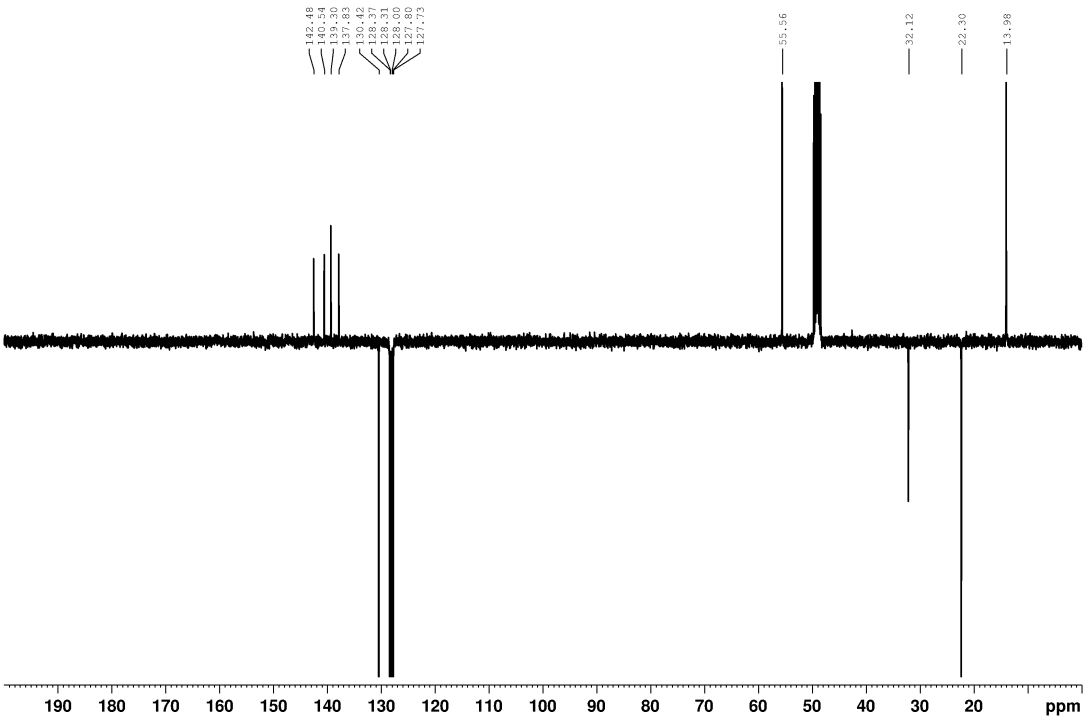

(1 *S*,2 *R*)-2-(3'-(azidomethyl)-[1,1'-biphenyl]-4-yl)cyclopropan-1-amine **((1 *S*,2 *R*)-probe 7)**

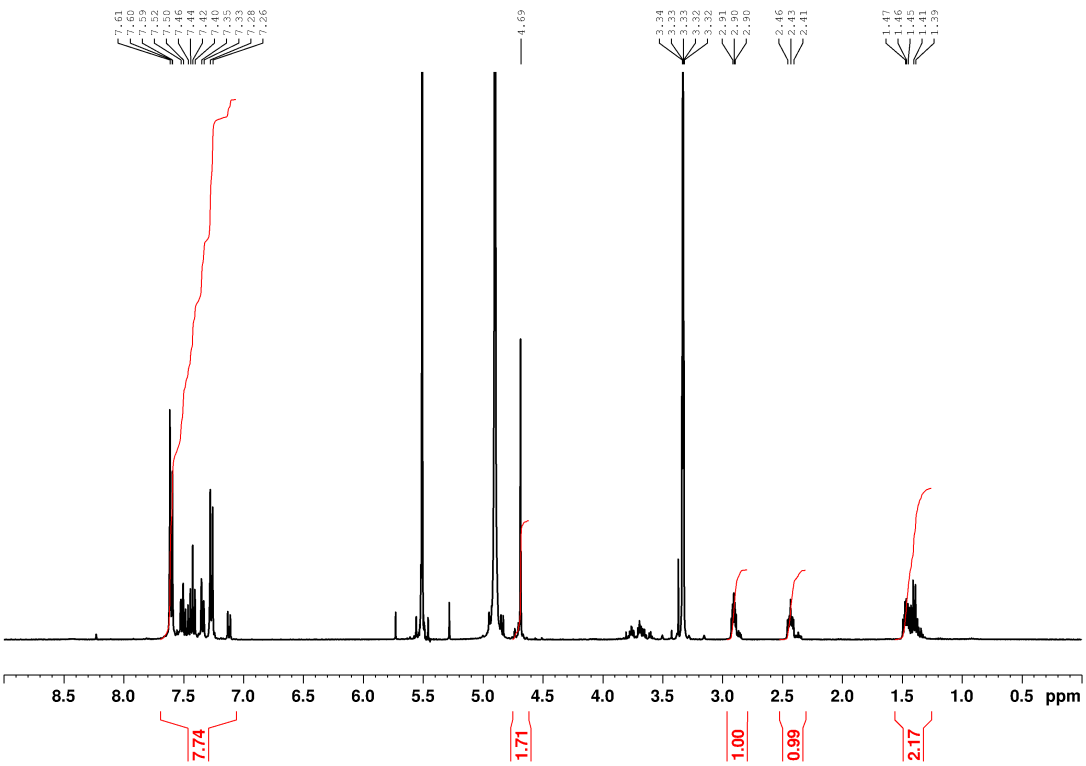

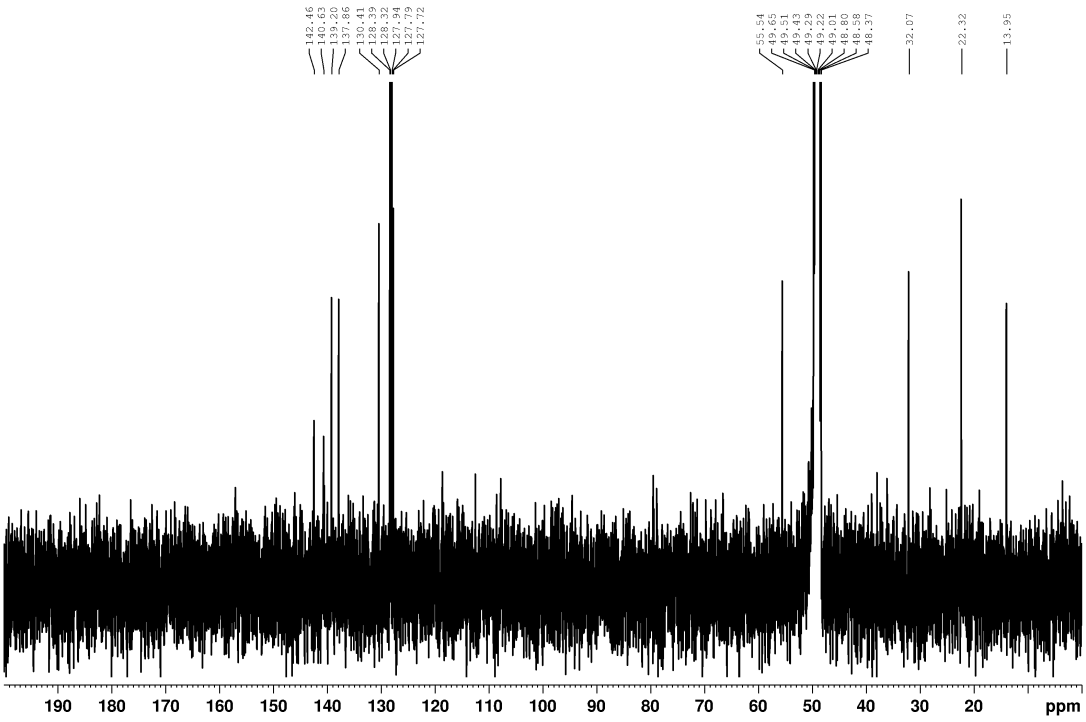

(*E*)-N-(2-(4-(3-azidopropoxy)phenyl)cyclopropyl)-1-(5-fluoro-2-methoxypyridin-3-yl)methanimine **(probe 9)**

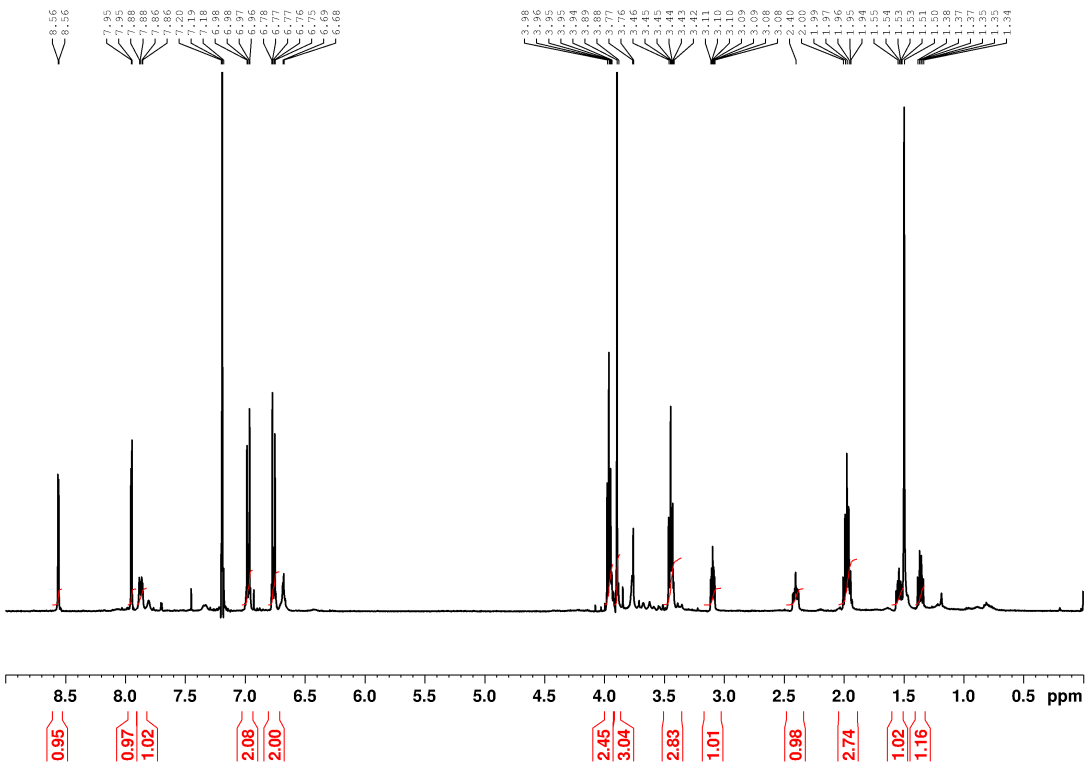

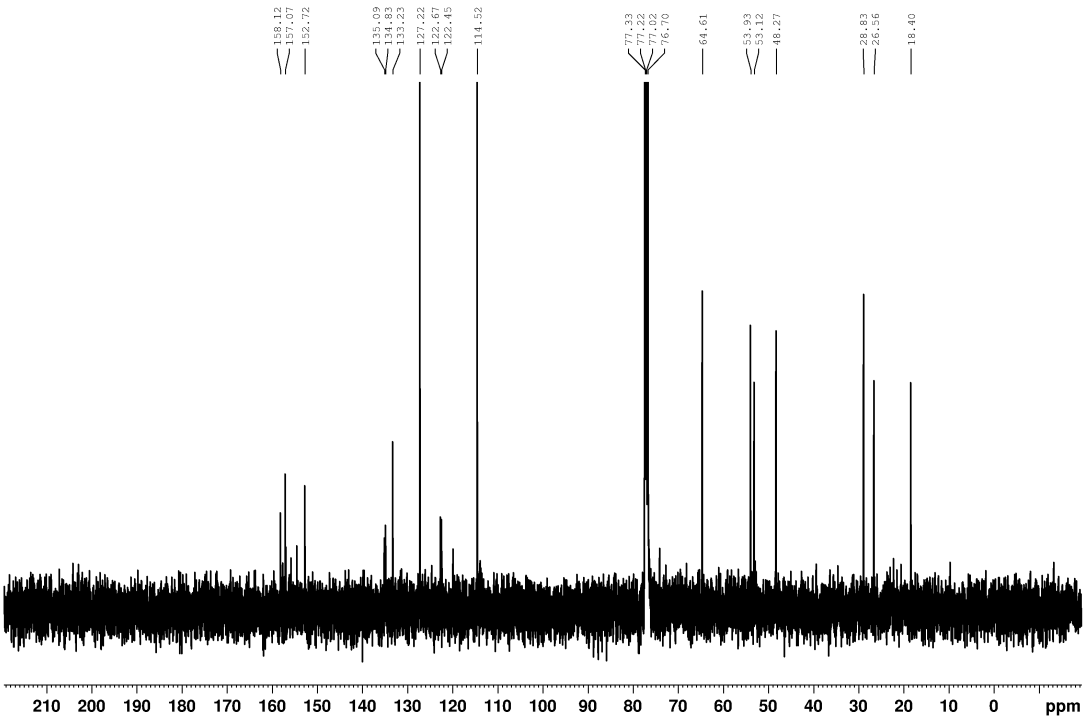

Chapter 10 Reference

1 K. N. Smitheman, C. D. Kamat, N. W. Johnson, C. L. Hann and R. G. Kruger, *Cancer Cell*, 2015, **28**, 57–69.
2 T. Suzuki and N. Miyata, *J. Med. Chem.*, 2011, **54**, 8236–8250.
3 M. T. Pedersen and K. Helin, *Trends Cell Biol.*, 2010, **20**, 662–671.
4 M. Rodriguez-Paredes and M. Esteller, *Nat Med*, 2011, 330–339.
5 S. RA, *JAMA*, 2011, **305**, 1484–1485.
6 B. Youngblood, J. S. Hale and R. Ahmed, *Immunology*, 2013, **139**, 277–284.
7 C. T. Foster, O. M. Dovey, L. Lezina, J. L. Luo, T. W. Gant, N. Barlev, A. Bradley and S. M. Cowley, 2010, **30**, 4851–4863.
8 M. A. Kerenyi, Z. Shao, Y. Hsu, G. Guo, S. Luc, K. O. Brien, Y. Fujiwara, C. Peng, M. Nguyen and H. Stuart, 2013, **3**, 1–23.
9 E. Metzger, M. Pavlovic, A. Jandausch, C. Jilg, D. Zhu, S. Ho, P. Galgoczy, C. Herz, M. Moser, D. Metzger, T. Gu, S. J. Arnold and R. Schu, , DOI:10.1038/ncomms4174.
10 M. N. Ahmed Khan, H. Tsumoto, Y. Itoh, Y. Ota, M. Suzuki, D. Ogasawara, H. Nakagawa, T. Mizukami, N. Miyata and T. Suzuki, *Med. Chem. Commun.*, 2015, **6**, 407–412.
11 D. Ogasawara, T. Suzuki, K. Mino, R. Ueda, M. N. A. Khan, T. Matsubara, K. Koseki, M. Hasegawa, R. Sasaki, H. Nakagawa, T. Mizukami and N. Miyata, *Bioorganic Med. Chem.*, 2011, **19**, 3702–3708.
12 E. Metzger, M. Wissmann, N. Yin, J. M. Müller, R. Schneider, A. H. F. M. Peters, T. Günther, R. Buettner and R. Schüle, *Nature*, 2005, **437**, 25–28.
13 R. D. Kornberg, *Science*, 1974, **184**, 868–871.
14 K. Luger, a W. Mäder, R. K. Richmond, D. F. Sargent and T. J. Richmond, *Nature*, 1997, **389**, 251–260.
15 L. Verdone, E. Agricola, M. Caserta and E. Di Mauro, *Briefings Funct. Genomics Proteomics*, 2006, **5**, 209–221.
16 Y. Arimura, H. Kimura, T. Oda, K. Sato, A. Osakabe, H. Tachiwana, Y. Sato, Y. Kinugasa, T. Ikura, M. Sugiyama, M. Sato and H. Kurumizaka, *Sci. Rep.*, 2013, **3**, 3510.
17 D. J. Tremethick, *Cell*, 2007, **128**, 651–654.
18 D. Rossetto, N. Avvakumov and J. Cote, *Epigenetics*, 2012, **7**, 1098–1108.
19 B. R. Shaw, T. M. Herman, R. T. Kovacic, G. S. Beaudreau and K. E. V. A. N. Holde, *Proc. Natl. Acad. Sci. United States Am.*, 1976, **73**, 505–509.
20 K. -i. Noma, *Science (80-.).*, 2001, **293**, 1150–1155.
21 N. A. Hathaway, O. Bell, C. Hodges, E. L. Miller, D. S. Neel and G. R. Crabtree, *Cell*, 2012, **149**, 1447–1460.
22 S. I. S. Grewal and D. Moazed, 2003, **301**, 798–803.
23 S. Kubicek and T. Jenuwein, *Cell*, 2004, **119**, 903–906.
24 B. Li, M. Carey and J. L. Workman, *Cell*, 2007, **128**, 707–719.
25 R. A. Copeland, M. E. Solomon and V. M. Richon, *Nat Rev Drug Discov*, 2009, **8**, 724–732.
26 H. D. Morgan, W. Dean, H. A. Coker, W. Reik and S. K. Petersen-Mahrt, *J. Biol. Chem.*, 2004, **279**, 52353–52360.
27 J. Kim and J. L. Workman, 2010, **1**, 738–740.
28 C. E. Berndsen and J. M. Denu, *Curr. Opin. Struct. Biol.*, 2008, **18**, 682–689.
29 O. D. Lau, A. D. Courtney, A. Vassilev, L. A. Marzilli, R. J. Cotter, Y.

Nakatani and P. A. Cole, *J. Biol. Chem.*, 2000, **275**, 21953–21959.
30 D. C. Montgomery, A. W. Sorum, L. Guasch, M. C. Nicklaus and J. L. Meier, *Chem. Biol.*, 2015, **22**, 1030–1039.
31 S. C. Hodawadekar and R. Marmorstein, *Oncogene*, 2007, **26**, 5528–5540.
32 I. V. Gregoretti, Y. M. Lee and H. V. Goodson, *J. Mol. Biol.*, 2004, **338**, 17–31.
33 H. J. Kim and S. C. Bae, *Am J Transl Res*, 2011, **3**, 166–179.
34 X. Zhou, P. A. Marks, R. A. Rifkind and V. M. Richon, *Proc. Natl. Acad. Sci. U. S. A.*, 2001, **98**, 10572–7.
35 B. W. Matthews, *Acc. Chem. Res.*, 1988, **21**, 333–340.
36 P. M. Lombardi, K. E. Cole, D. P. Dowling and D. W. Christianson, *Curr. Opin. Struct. Biol.*, 2011, **21**, 735–743.
37 M. J. Bottomley, P. Lo Lo Surdo, P. Di Di Giovine, A. Cirillo, R. Scarpelli, F. Ferrigno, P. Jones, P. Neddermann, R. De Francesco, C. Steinkuhler, P. Gallinari and A. Carfi, *J. Biol. Chem.*, 2008, **283**, 26694–26704.
38 A. Schuetz, J. Min, A. Allali-Hassani, M. Schapira, M. Shuen, P. Loppnau, R. Mazitschek, N. P. Kwiatkowski, T. A. Lewis, R. L. Maglathin, T. H. McLean, A. Bochkarev, A. N. Plotnikov, M. Vedadi and C. H. Arrowsmith, *J. Biol. Chem.*, 2008, **283**, 11355–11363.
39 A. Vaquero, M. B. Scher, H. L. Dong, A. Sutton, H. L. Cheng, F. W. Alt, L. Serrano, R. Sternglanz and D. Reinberg, *Genes Dev.*, 2006, **20**, 1256–1261.
40 J. L. Avalos, J. D. Boeke and C. Wolberger, *Mol. Cell*, 2004, **13**, 639–648.
41 M. T. Borra, M. R. Langer, J. T. Slama and J. M. Denu, *Biochemistry*, 2004, **43**, 9877–9887.
42 J. E. Brownell, J. Zhou, T. Ranalli, R. Kobayashi, D. G. Edmondson, S. Y. Roth and C. D. Allis, *Cell*, 1996, **84**, 843–851.
43 Y. Shi, F. Lan, C. Matson, P. Mulligan, J. R. Whetstine, P. A. Cole, R. A. Casero and Y. Shi, *Cell*, 2004, **119**, 941–953.
44 A. Karytinos, F. Forneris, A. Profumo, G. Ciossani, E. Battaglioli, C. Binda and A. Mattevi, *J. Biol. Chem.*, 2009, **284**, 17775–17782.
45 R. J. Klose, E. M. Kallin and Y. Zhang, *Nat Rev Genet*, 2006, **7**, 715–727.
46 Y. Shi, *Nat Rev Genet*, 2007, **8**, 829–833.
47 N. Mosammaparast and Y. Shi, *Annu. Rev. Biochem.*, 2010, **79**, 155–179.
48 S. M. Kooistra and K. Helin, *Nat Rev Mol Cell Biol*, 2012, **13**, 297–311.
49 H. Santos-Rosa, R. Schneider, A. J. Bannister, J. Sherriff, B. E. Bernstein, N. C. T. Emre, S. L. Schreiber, J. Mellor and T. Kouzarides, *Nature*, 2002, **419**, 407–411.
50 B. C. Smith and J. M. Denu, *Biochim. Biophys. Acta - Gene Regul. Mech.*, 2009, **1789**, 45–57.
51 D. R. Kipp, C. M. Quinn and P. D. Fortin, *Biochemistry*, 2013, **52**, 6866–6878.
52 T. Jenuwein, *Trends Cell Biol.*, 2017, **11**, 266–273.
53 K. Ahmad and S. Henikoff, *Mol. Cell*, 2002, **9**, 1191–1200.
54 F. Forneris, C. Binda, M. A. Vanoni, A. Mattevi and E. Battaglioli, *FEBS Lett.*, 2005, **579**, 2203–2207.
55 M. Yang, J. C. Culhane, L. M. Szewczuk, C. B. Gocke, C. A. Brautigam, D. R. Tomchick, M. Machius, P. A. Cole and H. Yu, *Nat Struct Mol Biol*, 2007, **14**, 535–539.
56 R. Baron, C. Binda, M. Tortorici, J. A. McCammon and A. Mattevi, *Structure*, 2011, **19**, 212–220.
57 F. Forneris, C. Binda, A. Dall'Aglio, M. W. Fraaije, E. Battaglioli and A.

Mattevi, *J. Biol. Chem.*, 2006, **281**, 35289–35295.
58 M. Yang, J. C. Culhane, L. M. Szewczuk, P. Jalili, H. L. Ball, M. Machius, P. A. Cole and H. Yu, *Biochemistry*, 2007, **46**, 8058–8065.
59 S. Mimasu, T. Sengoku, S. Fukuzawa, T. Umehara and S. Yokoyama, *Biochem. Biophys. Res. Commun.*, 2008, **366**, 15–22.
60 Y. Tsukada, J. Fang, H. Erdjument-Bromage, M. E. Warren, C. H. Borchers, P. Tempst and Y. Zhang, *Nature*, 2006, **439**, 811–816.
61 R. J. Klose, K. Yamane, Y. Bae, D. Zhang, H. Erdjument-Bromage, P. Tempst, J. Wong and Y. Zhang, *Nature*, 2006, **442**, 312–316.
62 P. A. C. Cloos, J. Christensen, K. Agger, A. Maiolica, J. Rappsilber, T. Antal, K. H. Hansen and K. Helin, *Nature*, 2006, **442**, 307–311.
63 B. D. Fodor, S. Kubicek, M. Yonezawa, R. J. O'Sullivan, R. Sengupta, L. Perez-Burgos, S. Opravil, K. Mechtler, G. Schotta and T. Jenuwein, *Genes Dev.*, 2006, **20**, 1557–1562.
64 J. R. Whetstine, A. Nottke, F. Lan, M. Huarte, S. Smolikov, Z. Chen, E. Spooner, E. Li, G. Zhang, M. Colaiacovo and Y. Shi, *Cell*, 2006, **125**, 467–481.
65 S. Pilotto, V. Speranzini, C. Marabelli, F. Rusconi, E. Toffolo, B. Grillo, E. Battaglioli and A. Mattevi, *Hum. Mol. Genet.*, 2016, **25**, 2578–2587.
66 M. Yang, C. B. Gocke, X. Luo, D. Borek, D. R. Tomchick, M. Machius, Z. Otwinowski and H. Yu, *Mol. Cell*, 2006, **23**, 377–387.
67 S. Y. Son, J. Ma, Y. Kondou, M. Yoshimura, E. Yamashita and T. Tsukihara, *Proc. Natl. Acad. Sci. U. S. A.*, 2008, **105**, 5739–5744.
68 C. Binda, P. Newton-Vinson, F. Hubálek, D. E. Edmondson and A. Mattevi, *Nat. Struct. Biol.*, 2002, **9**, 22–26.
69 Y. Chen, Y. Yang, F. Wang, K. Wan, K. Yamane, Y. Zhang and M. Lei, *Proc. Natl. Acad. Sci. U. S. A.*, 2006, **103**, 13956–13961.
70 L. Hudspith, F. Shmam, C. F. Dalton, A. Princivalle and S. M. Turega, *Org. Biomol. Chem.*, 2019, **17**, 8871–8877.
71 S. Ulrich, R. Ricken and M. Adli, *Eur. Neuropsychopharmacol.*, 2017, **27**, 697–713.
72 K. Cakir, S. S. Erdem and V. E. Atalay, *Org. Biomol. Chem.*, 2016, **14**, 9239–9252.
73 B. Karasulu, M. Patil and W. Thiel, *J. Am. Chem. Soc.*, 2013, **135**, 13400–13413.
74 C. Binda, S. Valente, M. Romanenghi, S. Pilotto, R. Cirilli, A. Karytinos, G. Ciossani, O. A. Botrugno, F. Forneris, M. Tardugno, D. E. Edmondson, S. Minucci, A. Mattevi and A. Mai, *J. Am. Chem. Soc.*, 2010, **132**, 6827–6833.
75 G. W. Langley, A. Brinkø, M. Münzel, L. J. Walport, C. J. Schofield and R. J. Hopkinson, *ACS Chem. Biol.*, 2016, **11**, 755–762.
76 R. Ueda, T. Suzuki, K. Mino, H. Tsumoto, H. Nakagawa, M. Hasegawa, R. Sasaki, T. Mizukami and N. Miyata, *J. Am. Chem. Soc.*, 2009, **131**, 17536–17537.
77 Y. C. Zheng, B. Yu, G. Z. Jiang, X. J. Feng, P. X. He, X. Y. Chu, W. Zhao and H. M. Liu, *Curr. Top. Med. Chem.*, 2016, **16**, 2179–2188.
78 S. Chandrasekhar, C. Narasihmulu, V. Jagadeshwar and K. V. Reddy, *Tetrahedron Lett.*, 2003, **44**, 3629–3630.
79 P. S. Coelho, E. M. Brustad, A. Kannan and F. H. Arnold, *Science (80-.).*, 2013, **339**, 307–310.
80 C. Binda, S. Valente, M. Romanenghi, S. Pilotto, R. Cirilli, A. Karytinos, G. Ciossani, O. A. Botrugno, F. Forneris, M. Tardugno, D. E. Edmondson and S. Minucci, 2010, 6827–6833.

81 S. Valente, V. Rodriguez, C. Mercurio, P. Vianello, B. Saponara, R. Cirilli, G. Ciossani, D. Labella, B. Marrocco, G. Ruoppolo, O. A. Botrugno, P. Dessanti, S. Minucci, A. Mattevi, M. Varasi and A. Mai, *ACS Med. Chem. Lett.*, 2015, **6**, 173–177.
82 D. Rotili, S. Tomassi, M. Conte, R. Benedetti, M. Tortorici, G. Ciossani, S. Valente, B. Marrocco, D. Labella, E. Novellino, A. Mattevi, L. Altucci, A. Tumber, C. Yapp, O. N. F. King, R. J. Hopkinson, A. Kawamura, C. J. Schofield and A. Mai, *J. Med. Chem.*, 2014, **57**, 42–55.
83 J. H. Kalin, M. Wu, A. V. Gomez, Y. Song, J. Das, D. Hayward, N. Adejola, M. Wu, I. Panova, H. J. Chung, E. Kim, H. J. Roberts, J. M. Roberts, P. Prusevich, J. R. Jeliazkov, S. S. Roy Burman, L. Fairall, C. Milano, A. Eroglu, C. M. Proby, A. T. Dinkova-Kostova, W. W. Hancock, J. J. Gray, J. E. Bradner, S. Valente, A. Mai, N. M. Anders, M. A. Rudek, Y. Hu, B. Ryu, J. W. R. Schwabe, A. Mattevi, R. M. Alani and P. A. Cole, *Nat. Commun.*, , DOI:10.1038/s41467-017-02242-4.
84 Y. C. Duan, Y. C. Ma, W. P. Qin, L. N. Ding, Y. C. Zheng, Y. L. Zhu, X. Y. Zhai, J. Yang, C. Y. Ma and Y. Y. Guan, *Eur. J. Med. Chem.*, 2017, **140**, 392–402.
85 C. Bailey, M. Romero, R. Han, J. Larson, O. Becher, D. Lee, M. Monje, V. Gopalakrishnan, W. Zaky and J. Chandra, *Neuro. Oncol.*, 2018, **20**, i102–i102.
86 H. P. Mohammad, K. N. Smitheman, C. D. Kamat, D. Soong, K. E. Federowicz, G. S. VanAller, J. L. Schneck, J. D. Carson, Y. Liu, M. Butticello, W. G. Bonnette, S. A. Gorman, Y. Degenhardt, Y. Bai, M. T. McCabe, M. B. Pappalardi, J. Kasparec, X. Tian, K. C. McNulty, M. Rouse, P. McDevitt, T. Ho, M. Crouthamel, T. K. Hart, N. O. Concha, C. F. McHugh, W. H. Miller, D. Dhanak, P. J. Tummino, C. L. Carpenter, N. W. Johnson, C. L. Hann and R. G. Kruger, *Cancer Cell*, 2015, **28**, 57–69.
87 T. Maes, C. Mascaró, I. Tirapu, A. Estiarte, F. Ciceri, S. Lunardi, N. Guibourt, A. Perdones, M. M. P. Lufino, T. C. P. Somervaille, D. H. Wiseman, C. Duy, A. Melnick, C. Willekens, A. Ortega, M. Martinell, N. Valls, G. Kurz, M. Fyfe, J. C. Castro-Palomino and C. Buesa, *Cancer Cell*, 2018, **33**, 495-511.e12.
88 T. Maes, E. Carceller, J. Salas, A. Ortega and C. Buesa, *Curr. Opin. Pharmacol.*, 2015, **23**, 52–60.
89 C. Buesa, T. C. P. Somervaille, M. Arevalo, J. Xaus, S. Gutierrez and R. Bullock, *Blood*, 2019, **134**, 3839.
90 P. Bose and M. Y. Konopleva, *Cancer Cell*, 2018, **33**, 342–343.
91 T. Maes, C. Mascaró, D. Rotllant, F. Cavalcanti, E. Carceller, A. Ortega, C. Molinero and C. Buesa, *Alzheimer's Dement.*, 2016, **12**, P1192–P1192.
92 P. Prusevich, J. H. Kalin, S. A. Ming, M. Basso, J. Givens, X. Li, J. Hu, M. S. Taylor, A. M. Cieniewicz, P. Y. Hsiao, R. Huang, H. Roberson, N. Adejola, L. B. Avery, R. A. Casero, S. D. Taverna, J. Qian, A. J. Tackett, R. R. Ratan, O. G. McDonald, A. P. Feinberg and P. A. Cole, *ACS Chem. Biol.*, 2014, **9**, 1284–1293.
93 S. Hazeldine, B. Pachaiyappan, N. Steinbergs, S. Nowotarski, A. S. Hanson, R. A. Casero and P. M. Woster, *J. Med. Chem.*, 2012, **55**, 7378–7391.
94 V. Sorna, E. R. Theisen, B. Stephens, S. L. Warner, D. J. Bearss, H. Vankayalapati and S. Sharma, *J. Med. Chem.*, 2013, **56**, 9496–508.
95 Y. Itoh, K. Aihara, P. Mellini, T. Tojo, Y. Ota, H. Tsumoto, V. R. Solomon, P. Zhan, M. Suzuki, D. Ogasawara, A. Shigenaga, T. Inokuma, H.

Nakagawa, N. Miyata, T. Mizukami, A. Otaka and T. Suzuki, *J. Med. Chem.*, 2016, **59**, 1531–1544.
96 Y. Itoh, D. Ogasawara, Y. Ota, T. Mizukami and T. Suzuki, .
97 T. Etani, T. Naiki, S. Nozaki, T. Nagai, K. Iida, R. Ando, N. Kawai, S. Takahashi, T. Suzuki and T. Yasui, *J. Urol.*, 2020, **203**, e135–e136.
98 R. Huisgen, *J. Heterocycl. Chem.*, 1986, **23**, 1899.
99 V. V Rostovtsev, L. G. Green, V. V Fokin and K. B. Sharpless, *Angew. Chemie Int. Ed.*, 2002, **41**, 2596–2599.
100 C. W. Tornøe, C. Christensen and M. Meldal, 2002, 3057–3064.
101 P. Wu and V. Fokin, *Catalytic Azide — Alkyne Cycloaddition : Reactivity and Applications*, 2007.
102 K. Sivakumar, F. Xie, B. M. Cash, S. Long, H. N. Barnhill and Q. Wang, 2010, 2596–2599.
103 T. Hsu, S. R. Hanson, K. Kishikawa, S. Wang, M. Sawa and C. Wong, *PNAS*, 2007, **104**, 1–6.
104 B. R. Buckley, M. M. P. Figueres, A. N. Khan and H. Heaney, *Synlett*, 2016, **27**, 51–56.
105 W. G. Lewis, F. G. Magallon, V. V Fokin and M. G. Finn, 2004, 9152–9153.
106 T. R. Chan, R. Hilgraf, K. B. Sharpless and V. V Fokin, 2004, **41**, 2002–2004.
107 V. O. Rodionov, S. I. Presolski, D. Dı, V. V Fokin and M. G. Finn, *J. AM. CHEM. SOC.*, 2007, 2210–2215.
108 E. V Soares, K. Hebbelinck and H. M. V. M. Soares, *Can. J. Microbiol.*, 2003, **49**, 336–343.
109 N. J. Agard, J. A. Prescher and C. R. Bertozzi, *J. AM. CHEM. SOC.*, 2004, **126**, 15046–15047.
110 J. A. Codelli, J. M. Baskin, N. J. Agard and C. R. Bertozzi, *J. AM. CHEM. SOC.*, 2008, 11486–11493.
111 A. J. Link and D. A. Tirrell, *J. Am. Chem. Soc.*, 2003, **125**, 11164–11165.
112 V. Hong, N. F. Steinmetz, M. Manchester and M. G. Finn, *Bioconjugate chem.*, 2010, **21**, 1912–1916.
113 Q. Wang, T. R. Chan, R. Hilgraf, V. V. Fokin, K. B. Sharpless and M. G. Finn, *J. Am. Chem. Soc.*, 2003, **125**, 3192–3193.
114 A. Salic and T. J. Mitchison, *Proc. Natl. Acad. Sci. U. S. A.*, 2008, **105**, 2415–2420.
115 H. I. Yoon, J. Y. Yhee, J. H. Na, S. Lee, H. Lee, S. W. Kang, H. Chang, J. H. Ryu, S. Lee, I. C. Kwon, Y. W. Cho and K. Kim, *Bioconjug. Chem.*, 2016, **27**, 927–936.
116 S. Miwa, A. Treumann, A. Bell, G. Vistoli, G. Nelson, S. Hay and T. Von Zglinicki, *Free Radic. Biol. Med.*, 2016, **90**, 173–183.
117 H. Benelkebir, C. Hodgkinson, P. J. Duriez, A. L. Hayden, R. A. Bulleid, S. J. Crabb, G. Packham and A. Ganesan, *Bioorganic Med. Chem.*, 2011, **19**, 3709–3716.
118 A. S. Thompson, G. R. Humphrey, A. M. DeMarco, D. J. Mathre and E. J. J. Grabowski, *J. Org. Chem.*, 1993, **58**, 5886–5888.
119 D. M. Z. Schmidt and D. G. McCafferty, *Biochemistry*, 2007, **46**, 4408–4416.
120 Y. Abe, H. Sasaki, T. Osaki, K. Kamiya, R. Kawano, N. Miki and S. Takeuchi, 2012, 956–958.
121 S. Li, L. Wang, F. Yu, Z. Zhu, D. Shobaki, H. Chen, M. Wang, J. Wang, G. Qin, U. J. Erasquin, L. Ren, Y. Wang and C. Cai, *Chem. Sci.*, 2017, **8**, 2107–2114.

122 Y. Takayama, K. Kusamori and M. Nishikawa, *Molecules*, , DOI:10.3390/molecules24010172.
123 B. Diniz, P. Thomas, B. Thomas, R. Ribeiro, Y. Hu, R. Brant, A. Ahuja, D. Zhu, L. Liu, M. Koss, M. Maia, G. Chader, D. R. Hinton and M. S. Humayun, *Investig. Ophthalmol. Vis. Sci.*, 2013, **54**, 5087–5096.
124 S. Mimasu, N. Umezawa, S. Sato, T. Higuchi, T. Umehara and S. Yokoyama, *Biochemistry*, 2010, **49**, 6494–6503.
125 B. Laurent and Y. Shi, *Methods Enzymol.*, 2016, **573**, 241–259.
126 M. A. Young, G. Ravishanker, D. L. Beveridge and H. M. Berman, *Biophys. J.*, 1995, **68**, 2454–2468.
127 S. C. Desbordes, D. G. Placantonakis, A. Ciro, N. D. Socci, G. Lee, H. Djaballah and L. Studer, *Cell Stem Cell*, 2008, **2**, 602–612.
128 R. Zhang, X. Qin, F. Kong, P. Chen and G. Pan, *Drug Deliv.*, 2019, **26**, 328–342.
129 L. M. Gaetke, H. S. Chow-Johnson and C. K. Chow, *Arch. Toxicol.*, 2014, **88**, 1929–1938.
130 S. Li, H. Cai, J. He, H. Chen, S. Lam, T. Cai, Z. Zhu, S. J. Bark and C. Cai, *Bioconjug. Chem.*, 2016, **27**, 2315–2322.
131 O. Mogck, M. Pons, V. Böhmer and W. Vogt, *J. Am. Chem. Soc.*, 1997, **119**, 5706–5712.
132 S. Parsons, H. D. Flack and T. Wagner, *Acta Crystallogr. Sect. B Struct. Sci. Cryst. Eng. Mater.*, 2013, **69**, 249–259.
133 A. Kumar and R. C. Rani Grace, eds. J. C. Lindon, G. E. Tranter and D. W. B. T.-E. of S. and S. (Third E. Koppenaal, Academic Press, Oxford, 2017, pp. 423–431.
134 C. Binda, M. Li, F. Hubalek, N. Restelli, D. E. Edmondson and A. Mattevi, *Proc. Natl. Acad. Sci. U. S. A.*, 2003, **100**, 9750–9755.
135 L. De Colibus, M. Li, C. Binda, A. Lustig, D. E. Edmondson and A. Mattevi, *Proc. Natl. Acad. Sci. U. S. A.*, 2005, **102**, 12684–12689.
136 A. K. Upadhyay, J. Wang and D. E. Edmondson, *Biochemistry*, 2008, **47**, 526–536.
137 X. Kong, S. Ouyang, Z. Liang, J. Lu, L. Chen, B. Shen, D. Li, M. Zheng, K. K. Li, C. Luo and H. Jiang, *PLoS One*, , DOI:10.1371/journal.pone.0025444.
138 K. Cakir, S. S. Erdem and V. E. Atalay, *Org. Biomol. Chem.*, 2016, **14**, 9239–9252.
139 A. H. Y. Tan, W. J. Tu, R. McCuaig, K. Hardy, T. Donovan, S. Tsimbalyuk, J. K. Forwood and S. Rao, *Front. Immunol.*, 2019, **10**, 1–17.
140 S. Ahmadi, L. Barrios Herrera, M. Chehelamirani, J. Hostaš, S. Jalife and D. R. Salahub, *Int. J. Quantum Chem.*, 2018, **118**, 1–34.
141 T. Benighaus and W. Thiel, *J. Chem. Theory Comput.*, 2009, **5**, 3114–3128.
142 A. Heyden, H. Lin and D. G. Truhlar, *J. Phys. Chem. B*, 2007, **111**, 2231–2241.
143 H. M. Senn and W. Thiel, *Angew. Chemie - Int. Ed.*, 2009, **48**, 1198–1229.
144 M. Prejanò, T. Marino and N. Russo, *Front. Chem.*, 2018, **6**, 1–9.
145 A. G. Leach, L. L. Olsson and D. J. Warner, *Medchemcomm*, 2013, **4**, 180–186.
146 M. R. A. Blomberg, T. Borowski, F. Himo, R. Z. Liao and P. E. M. Siegbahn, *Chem. Rev.*, 2014, **114**, 3601–3658.
147 H. Hirao, *J. Phys. Chem. A*, 2011, **115**, 9308–9313.
148 M. A. Iron and J. Gropp, *Phys. Chem. Chem. Phys.*, 2019, **21**, 17555–

17570.
149 M. Orio, D. A. Pantazis and F. Neese, *Photosynth. Res.*, 2009, **102**, 443–453.
150 S. Tsuzuki and T. Uchimaru, *Phys. Chem. Chem. Phys.*, 2020, **22**, 22508–22519.
151 A. Siiskonen and A. Priimagi, *J. Mol. Model.*, 2017, **23**, 1–9.
152 A. D. Becke, *J. Chem. Phys.*, 1993, **98**, 1372–1377.
153 K. K. Pandey, P. Patidar, P. K. Bariya, S. K. Patidar and R. Vishwakarma, *Dalt. Trans.*, 2014, **43**, 9955–9967.
154 J. N. Harvey, *Phys. Chem. Chem. Phys.*, 2007, **9**, 331–343.
155 Y. Wang, P. Verma, X. Jin, D. G. Truhlar and X. He, *Proc. Natl. Acad. Sci. U. S. A.*, 2018, **115**, 10257–10262.
156 H. S. Yu, X. He, S. L. Li and D. G. Truhlar, *Chem. Sci.*, 2016, **7**, 5032–5051.
157 F. Neese, *Wiley Interdiscip. Rev. Comput. Mol. Sci.*, 2012, **2**, 73–78.
158 R. Franke and B. Hannebauer, *Phys. Chem. Chem. Phys.*, 2011, **13**, 21344–21350.
159 A. Schäfer, C. Huber and R. Ahlrichs, *J. Chem. Phys.*, 1994, **100**, 5829–5835.
160 A. D. Becke, *Phys. Rev. A, Gen. Phys.*, 1988, **38**, 3098–3100.
161 J. P. Perdew, *Phys. Rev. B. Condens. Matter*, 1986, **33**, 8822–8824.
162 A. Klamt, *Wiley Interdiscip. Rev. Comput. Mol. Sci.*, 2011, **1**, 699–709.
163 Y. Zhao and D. G. Truhlar, *Theor. Chem. Acc.*, 2008, **120**, 215–241.
164 US. Pat., 030 552, 2012.
165 EP. Pat., 067 053, 2016.
166 K. Luger, a W. Mäder, R. K. Richmond, D. F. Sargent and T. J. Richmond, *Nature*, 1997, **389**, 251–260.
167 J. Ding, Z. M. Zhang, Y. Xia, G. Q. Liao, Y. Pan, S. Liu, Y. Zhang and Z. S. Yan, *Br. J. Cancer*, 2013, **109**, 994–1003
168 N. J. Yang and M. J. Hinner, *Mol. Bio.*, 2015, **1266**, 29–53.
169 M. E. Daub, H. Jung, B. J. Lee, J. Won, M.-H. Baik and T. P. Yoon, J*. Am. Chem. Soc.*, 2019, **141**, 9543–9547
170 R. Dondi, E. Yaghini, K. M. Tewari, L. Wang, F. Giuntini, M. Loizidou, A. J. MacRobert and I. M. Eggleston, *Org. Biomol. Chem*., 2016, **14**, 11488–11501.
171 S. López, I. Gracia, M. T. García, J. F. Rodríguez and M. J. Ramos, *ACS Omega*, 2021, **6**, 6163–6171.
172 O. Mitsunobu and M. Yamada, Bull. *Chem. Soc.* Jpn., 1967, **40**, 2380–2382.